The discovery of small molecule modulators of soluble guanylate cyclase aided by surface plasmon resonance

---

A thesis submitted in accordance with the requirements

for the degree of

Doctor of Philosohy

by

Filipa Mota

June 2014

UCL

I, Filipa Mota confirm that the work presented in this thesis is my own. Where information has been derived from other sources, I confirm this has been indicated in the thesis.

Abstract

Soluble guanylate cyclase is a multidimeric enzyme that regulates cardiovascular homeostasis and is the receptor for nitric oxide in the brain. The enzyme is the known target for a new agonist drug used for the treatment of pulmonary hypertension. Whilst drug discovery has been successful for the finding of small molecules that activate the enzyme, the currently available inhibitors lack selectivity as they act through oxidation of a heme prosthetic group in the enzyme, which is conserved amongst other hemeproteins. Nonetheless, it has been suggested that inhibition of soluble guanylate cyclase by small molecules could be useful in the treatment of neurological conditions such as Parkinson’s Disease. In this thesis, new activators of soluble guanylate cyclase have been identified by virtual screening, and a new class of inhibitors has been designed and synthesised. The synthetic routes developed are efficient and take advantage of microwave-assisted organic synthesis. The drug-target interaction was characterised using a biophysical technique based on surface plasmon resonance, which allows the detection of label-free binding between small molecules and biological macromolecules. The biophysical assay has been developed using different constructs of soluble guanylate cyclase and validated through binding of the natural ligands ATP and GTP. The instrument and assay design were validated using the well-defined interaction between natriuretic peptides and the extracellular domain of natriuretic peptide type-C. Additional biochemical characterisation of the ligands allowed discrimination between activators and inhibitors. This combination of biophysical and biochemical techniques allowed the identification of the catalytic domain of soluble guanylate cyclase as the target for binding of the new class of synthesised inhibitors and has given insight into the functional groups necessary for activity and binding to the enzyme.

Contents

Table of figures 7

Table of tables 12

Table of equations 13

List of abbreviations 14

Chapter 1: General Introduction 18

1.1. Target-based drug discovery 19

1.1.1. The druggable genome 20

1.1.2. Small molecules and drug likeness 21

1.1.3. Chemical probes 22

1.1.4. Assay development 22

1.1.5. Compound screening 33

1.1.6. Medicinal chemistry 34

1.2. Understanding and predicting protein-ligand interactions 37

1.2.1. Intermolecular interactions 38

1.2.2. Molecular modelling 41

1.3. The guanylate cyclase protein family 44

1.3.1. Natriuretic peptide receptors 46

1.3.2. Soluble guanylate cyclase 47

1.4. Project aims and thesis overview 57

Chapter 2: Validation of a SPR assay using NPR-C 60

2.1. Introduction 61

2.1.1. NPR-C agonists 61

2.1.2. SPR assay design 62

2.1.3. Solubility measurements 66

2.2. Results and Discussion 67
2.2.1. SPR assay 67
2.2.2. Solubility Measurements 82
2.3. Summary 84
Chapter 3: Discovery and characterisation of drug-like sGC activators 86
3.1. Introduction 87
3.1.1. The binding mode of sGC activators 87
3.1.2. SPR assay design 87
3.2. Results and Discussion 88
3.2.1. Screening for sGC activators 88
3.2.2. Biophysical assay development 92
3.2.3. Binding of nucleotides 94
3.2.4. ATP and GTP binding site competition 96
3.2.5. Binding of activators 98
3.3. Summary 102
Chapter 4: Discovery and characterisation of small molecule inhibitors of sGC 103
4.1. Introduction 104
4.2. Results and discussion 106
4.2.1. Compound screening 106
4.2.2. The synthesis of substituted quinoxalines 109
4.2.3. Synthesis of hit compound 41 110
4.2.4. Biochemical characterisation of synthesised compound 41 114
4.2.5. Characterisation of the binding of compound 41 to sGC 114
4.2.6. Docking studies 118
4.3. Summary 122
Chapter 5: Design, synthesis and characterisation of small molecules as potential sGC inhibitors 124

5.1. Introduction 125

5.1.1. Design rationale for analogues of compound 41 125

5.2. Results and discussion 126

5.2.1. Replacement of phenols 126

5.2.2. Replacement of the nitro group 128

5.2.3. Synthesis of mono-substituted quinoxalines 137

5.2.4. Improved synthesis of mono-substituted quinoxalines by Buchwald – Hartwig aryl amination 138

5.2.5. Asymmetrically substituted quinoxalines 142

5.2.6. Removal of the *NH* linker 147

5.2.7. The role of superoxide dismutase in the biochemical assay 149

5.3. Summary 151

Chapter 6: General conclusions 153

6.1. Future work 156

Chapter 7: Experimental methods 158

7.1. General methods 159

7.1.1. SPR 159

7.1.2. Biochemical assay for sGC activity 160

7.1.3. Chemistry 160

7.2. Chapter 2 methods 160

7.2.1. SPR 160

7.2.2. Solubility measurements 162

7.3. Chapter 3 Methods 163

7.3.1. Protein expression and purification 163

7.3.2. SPR 163

7.4. Chapter 4 methods 164

7.4.1. Virtual screening 164

7.4.2. Particulate guanylate cyclase assay 165

7.4.3. Synthesis 166

7.4.4. SPR 167

7.4.5. Molecular modelling 167

7.5. Chapter 5 methods 168

7.5.1. General methods 168

7.5.2. Synthesis 170

Bibliography........ 211

Appendix I: Publications 228

Table of figures

Figure 1. The pipeline of drug discovery. 19

Figure 2. General concept of an immunoassay.. 23

Figure 3. General setup of the SPR detection system. 25

Figure 4. Difference of light resonance angle at the sensor chip surface as a result of biomolecular interactions by SPR.. 26

Figure 5. General overview of a sensorgram. 27

Figure 6. One-to-one interaction model at the surface in a flow cell. 29

Figure 7. The sensor chip. 30

Figure 8. Examples of available Biacore sensor chip chemistries. 32

Figure 9. Schematic representation of the disciplines integrating medicinal chemistry. 35

Figure 10. Catalytic mechanism of guanylate cyclase activity. 44

Figure 11. Natriuretic peptide receptors and soluble guanylate cyclase domain structure and signaling pathway. 45

Figure 12. Chemical structures of small molecules used in the treatment of Parkinson's Disease and sGC inhibitor ODQ. 50

Figure 13. Schematic representation of the structural organisation of sGC domains. 51

Figure 14. Overview of sGC catalytic domain heterodimer crystal structure (PDB ID: 3uvj). 53

Figure 15. Chemical structures of known sGC activators. 55

Figure 16. Mechanism of action of sGC activator cinaciguat **6**. 56

Figure 17. Chemical structures of NPR-C lead agonists and antagonist M372049 (**15**). 62

Figure 18. Protein immobilisation through amine coupling using EDC and NHS. 65

Figure 19. General setup for equilibrium solubility measurements. 67

Figure 20.Sensorgrams showing the immobilisation of NPR-C. 69

Figure 21. Sensorgrams showing CNP binding to NPR-C. 71

Figure 22. Regeneration conditions scouting. 73

Figure 23. Single-cycle kinetics of CNP (a) and ANP (b). 75

Figure 24. Sensorgrams of M372049 (**15**) binding to NPR-C.. 77

Figure 25. Ranking of NPR-C agonists binding to NPR-C. 78

Figure 26. Examples of NPR-C agonist binding sensorgrams. 81

Figure 27. Sensorgram of concentration-dependent (1.2 to 150 µM) binding of compound **13**. 82

Figure 28. Chemical structure of sildenafil **20**. 83

Figure 29. Solubility calibration curves for sildenafil 20 and compounds **12** and **13**. 83

Figure 30. Pipeline Pilot protocol. 89

Figure 31. Biochemical activation of sGC by selected compounds. 91

Figure 32. Sensorgrams of nucleotides binding to the catalytic domain of sGC. 95

Figure 33. Fitting curves for ATP (a) and GTP (b) binding to the catalytic domain of sGC. 96

Figure 34. Proposed mechanism for ATP and GTP competition measured by SPR. 97

Figure 35. GTP and ATP competition assay 97

Figure 36. Binding response of selected compounds to sGC measured by SPR. 99

Figure 37. Sensorgrams for binding of YC-1 (**5**) (a, b) and cinaciguat **6** (c, d) to catalytic domain and full-length sGC, repectively. 100

Figure 38. Correlation between compound binding to full length and catalytic domain sGC (a) and between compound binding to catalytic domain and clogP (b). 101

Figure 39. Chemical structures of inhibitors of sGC activity 105

Figure 40. Schematic representation of different mechanisms for inhibition of sGC activity. 105

Figure 41. Chemical structure of lamotrigine **34** and analogues **35** and **36**. 107

Figure 42. Chemical structure of diethylamine NONOate (DEA/NO). 107

Figure 43. Chemical structures of virtually screened substructures and hit compounds. 108

Figure 44. Spectroscopic characterisation of compound **41**.. 113

Figure 45. Comparison of biochemical activity between commercial and synthesised compounds **41**. 114

Figure 46. Sensorgrams of compound **44** binding to different immobilised constructs of sGC. 116

Figure 47. Dose-response plots of compound **41** binding to sGC. 118

Figure 48. Cartoon representation of the catalytic domain of sGC (pdb entry 3uvj).. 119

Figure 49. Superimposition of the binding poses of compound **41** in the pseudosymmetric site of sGC.. 120

Figure 50. Highest ranking docking pose of compound **41** into the pseudosymmetric site of sGC. .. 121

Figure 51. Substructures of compounds analogues of compound **41** to be synthesised. 126

Figure 52. Chemical structure of the Bcl-XL inhibitor ABT-737. 129

Figure 53. ^{1}H NMR of compound **75**. 133

Figure 54. Reductive pathways involved in the metabolism of nitroaromatics. 135

Figure 55. Superimposition of compounds **41** and **66** binding to the pseudosymmetric site of sGC. 136

Figure 56. LC-MS spectrum of compound **78**.. 138

Figure 57. ^{1}H NMR of compound **80**. 141

Figure 58. Monitoring the purification of compound **89** by liquid chromatography and mass spectrometry. 146

Figure 59. Docking of compounds **92** and **96** into the pseudosymmetric site of sGC. 149

Figure 60. The activity of compounds **41**, **73**, **74**, **87**, and **89** in the presence and absence of SOD. . 150

Figure 61. Chemical structure of the SOD mimetic Tempol **100**. 151

Figure 62.Schematic representation of the inhibition of sGC activity through binding of a small molecule to an allosteric site on the catalytic domain of the enzyme. 155

Figure 63. Chemical structures of most potent sGC inhibitors. 156

Table of schemes

Scheme 1. Pd-catalysed synthesis of a substituted *N^2,N^3*-diphenylquinoxaline-2,3-diamine.[121] 110

Scheme 2. S_NAr mechanism for the synthesis of compound **41**. 111

Scheme 3. Synthesis of 2,3-dichloroquinoxalines. 129

Scheme 4. Proposed mechanism for DMF catalysed chlorination with thionyl chloride.................. 130

Scheme 5. Synthesis of 2,3-dichloro-N-methylquinoxaline-6-carboxamide **64**. 131

Scheme 6. Proposed mechanism for nitro reduction with $NaBH_4$ and $SnCl_2$. 132

Scheme 7. Synthesis of compound **78.** 137

Scheme 8. Proposed mechanism for Buchwald-Hartwig cross-coupling reaction. 140

Scheme 9. Synthesis of compounds **79** and **80**. 141

Scheme 10. Proposed mechanism for the nitration of 2,3,-dichloro-6-nitroquinoxaline. 143

Scheme 11. Synthesis of 2,3-dichloro-6,7-dinitroquinoxaline **83**. 143

Scheme 12. Synthetic route to compound **87**. 144

Scheme 13. Synthesis of 4-(3-(2-morpholinophenylamino)-6,7-dinitroquinoxalin-2-ylamino)phenol **89**. 145

Scheme 14. Demethylation of 1,2-bis(3-methoxyphenyl)ethane-1,2-dione **91**................................ 147

Scheme 15. Synthesis of 2,3-diphenylquinoxalines. 148

Table of tables

Table 1. Relative specificity and strength of intermolecular interactions. 38

Table 2. The USP definition of solubility. 66

Table 3. Kinetics of natriuretic peptides and antagonist binding to NPR-C. 74

Table 4. SAR of NPR-C small molecule agonists. 79

Table 5. Calculated solubility of sildenafil **20** and compounds **12** and **13**. 84

Table 6. Chemical structures of sGC activators. 90

Table 7. pH scouting for sGCcat immobilisation. 93

Table 8. Biochemical activity of hit compounds **40** and **41**. 109

Table 9. Reaction conditions for the synthesis of compound **41**. 112

Table 10. Calculated equilibrium dissociation constants for compound **41**. 117

Table 11. Possible interactions between compound **41** and sGC and their respective distances obtained by docking. 122

Table 12. SAR of compounds where p-phenols have been substituted. 128

Table 13. SAR of compounds where the nitro group has been substituted. 134

Table 14. Characterisation of compounds **78 - 80**. 142

Table 15. SAR of 2,3-diphenylquinoxalines. 148

Table of equations

Equation 1. Binding capacity of the SPR surface. 33

Equation 2. Tanimoto Coefficiency. 34

Equation 3. Arrhenius equation. 36

Equation 4. Total energy in an additive force field. 41

Equation 5. Model for one-to-one binding interaction. 115

Equation 6. Model for non stoichiometric binding interaction. 115

List of abbreviations

ADME	Absorption, Distribution, Metabolism, Excretion
ANP	Atrial Natriuretic Peptide
ATP	Adenosine Triphosphate
cAMP	3’,5’-cyclic adenosine monophosphate
cGMP	3’,5’-cyclic guanosine monophosphate
CI	Chemical ionisation
CNP	C-type Natriuretic Peptide
DCM	Dichloromethane
DEA/NO	Diethylamine NONOate
DMF	Dimethyl Formamide
DMSO	Dimethyl Sulfoxide
DNA	Deoxyribonucleic Acid
DTT	Dithriothreitol
EDC	1-Ethyl-3-(3-dimethylaminopropyl)carbodiimide
EDHF	Endothelium-derived Hyperpolarizing Factor
EI	Electron Ionisation
ES	Electrospray Ionisation
FDA	US Food and Drug Administration
FP	Fluorescence Polarisation
GC	Guanylate Cyclase
GOLD	Genetic Optimisation for Ligand Docking
GPCR	G-Protein Coupled Receptor
GTP	Guanosine Triphosphate
HBS	HEPES Buffered Saline
HEPES	2-[4-(2-hydroxyethyl)piperazin-1-yl]ethanesulfonic acid

H-NOX	Heme Nitric Oxide/Oxygen binding
HPLC	High Performance Liquid Chromatography
HRMS	High Resolution Mass Spectrometry
HSQC	Heteronuclear Single Quantum Coherence
HTS	High Throughput Screening
IC_{50}	Half-maximal Inhibitory Concentration
ITC	Isothermal Calorimetry
IUPAC	International Union of Pure and Applied Chemistry
K_a	Association rate constant
K_d	Dissociation rate constant
K_D	Equilibrium dissociation constant
LC-MS	Liquid Chromatography – Mass Spectrometry
LRMS	Low Resolution Mass Spectrometry
m/z	Mass to charge ratio
MACCS	Molecular Access System
MM	Molecular Mechanics
MOE	Molecular Operating Environment
NHS	N-Hydroxysuccinimide
NMP	N-methyl-2-pyrrolidone
NMR	Nuclear Magnetic Resonance
NO	Nitric Oxide
NOS	Nitric Oxide Synthase
NP	Natriuretic Peptide
NPR	Natriuretic Peptide Receptor
NPR-C	Natriuretic Peptide Receptor C
NTP	Nucleotide Triphosphate

PBS	Phosphate Buffered Saline
PD	Parkinson’s Disease
PDB	Protein Data Bank
PDE	Phosphodiesterase
pGC	particulate Guanylate Cyclase
pI	Isoelectric Point
ppm	Parts per million
PSA	Polar Surface Area
QM	Quantum Mechanics
QSAR	Quantitative Structure Activity Relationships
R_{max}	Maximal Response
rt	Room temperature
RU	Response Unit
SAR	Structure-Activity Relationship
sGC	soluble Guanylate Cyclase
sGCcat	Catalytic domain of soluble guanylate cyclase
SOD	Superoxide Dismutase
SPR	Surface Plasmon Resonance
TIR	Total Internal Reflection
TLC	Thin Layer Chromatography
USP	United States Pharmacopeia

Acknowledgments

I would like to thank the Medical Research Council UK for funding my PhD research.

Thank you to my supervisor, Prof. David Selwood, for his valuable support and mentorship during the course of this PhD, and the past and current members of the Selwood group: Matt Gooding, Paul Gane, Lorcan Browne, Justin Warne, David Steadman, Kiri Stevens, and Ioanna Sevastou, for the numerous scientific discussions, support, coffee and cakes. A special thank you to my “science mum” Edith Chan.

I would also like to thank my secondary supervisor, Prof. Adrian Hobbes, and Prof. John Garthwaite, Kate Hampden-Smith, Rey Selvarajah and Charles Allerston for their support and intellectual input in the development of this project.

There are many people I would like to thank for making the past three years so enjoyable: my flatmates Elizabeth, Katie, and Gabija; my travel buddies (too many to name) for giving me the best excuse to leave the lab every now and then; all my friends and family who took some time to visit me in London for bringing me a piece of home; and all those who supported me from a distance. Thank you to Evan and my more-than-Goodenough friends for keeping me sane during the writing up period.

A special thanks to Cris, Hugo, João, Tiza, Delfim, and Carlos, who were always there. Thank you to Víctor, for his encouragement, support, and Barcelona.

Finally, my deepest gratitude goes to my mum, Maria Albertina Mota. Obrigada por tudo.

Chapter 1: General Introduction

1. General introduction

1.1. Target-based drug discovery

As scientific and technological advances are made every day there is an implicit expectation that these will in some way improve our lives, whether it is to make us live longer, happier, or more comfortable. On one hand, population is growing and life expectancy is increasing, so we are becoming more efficient at postponing death; on the other hand, diseases such as cancer, heart diseases, Alzheimer's and other cardiovascular and neurological diseases still present our biggest fears. Whether medical conditions are genetic, environmental or lifestyle induced, biomedical research has allowed the discovery of the molecular mechanisms that underlie a great number of diseases, providing for a better comprehension of how the human body works and fails, which in turn provides the possibility to devise new treatments.

In the past, drug development would start with the identification of a lead compound with useful activity, which would then be modified to develop a clinically useful drug. Research into the drug target and mechanism of action often took place many years after discovery of the drug. Current state of the art technology allows for a rational drug design, which starts with the identification of a biomolecular target. Target-based drug discovery focusses on finding modulators of the activity of a specific biological macromolecule which can be associated with a disease model. The basic requirements for this approach to drug discovery are a druggable target and a bioassay, which usually allow a library of compounds to be screened for binding and/or activity. Once a hit compound has been identified, drug design aims at optimizing drug-target interactions in order to obtain an improved compound with greater activity, which can then undergo development in order to improve its absorption and bioavailability, reduce its toxicity and side effects (Figure **1**).

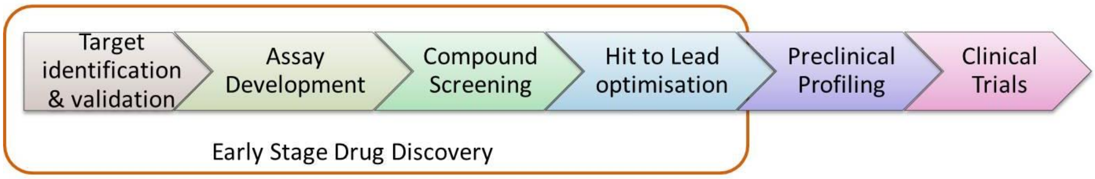

Figure 1. The pipeline of drug discovery.

1.1.1. The druggable genome

The "druggable genome" is represented by the ~ 30,000 genes in the human genome that express proteins able to bind drug-like molecules. Approximately half of these proteins remain functionally unclassified. Hopkins *et al*. analysis of known molecular targets concluded that only 130 protein families represent the known drug targets and nearly half of these targets fall into just six gene families: G-protein-coupled receptors (GPCRs), serine/threonine and tyrosine protein kinases, zinc metallopeptidases, serine proteases, nuclear hormone receptors and phosphodiesterases (PDEs).[1]

The effective number of drug targets has been estimated by analytical methods, leading to a controversy in numbers, as it primarily depends on the definition one gives to "the druggable genome".[2-4] Overington *et al.* analysed the US FDA's Orange Book for primarily small-molecule drugs, and the Center for Biologics Evaluation and Research (CBER) website for biological drugs, concluding that all current drugs with a known mode of action act through 324 distinct molecular drug targets, out of which 226 are human-genome-derived proteins, and the remainder are bacterial, fungal, or other pathogenic organism targets. 60 % of drug targets are located at the cell surface, compared to only ~ 22 % of all proteins in the human genome. Another interesting result of this analysis is the relatively constant rate of target innovation, with an average rate of first-against target drugs of 5.3 new drugged targets per year over the period of 20 years (from 1985 to 2005).[5]

It is possible that technological advances will aid the expansion of druggable targets. So far, drug discovery projects targeting enzymes have been the most successful, followed by GPCRs.[1] Most drugs achieve their activity by competing for a binding site on a protein with an endogenous small molecule. Their success might be explained by a well-defined active site and generally better understood mode of action. Nonetheless, enzyme modulators are also easier to identify by biochemical assays since a direct activation/inhibition can usually be measured by enzymatic turnover. It is predicted that modern biophysical assays which detect direct binding of a small-molecule to a protein will facilitate high-throughput screening (HTS) for non-enzymes, such as scaffolding proteins or transcription factors. Their lack of obvious binding pockets and/or involvement in protein –protein interactions which involve larger contact areas makes them a more challenging target.[6]

"The druggable genome" is therefore a term that leaves some ambiguity and is only as big as the creativity of drug designers. Drug discovery seems to follow a trend, as exemplified by the great number of drugs targeting kinases following approval of the Brc-Abl kinase inhibitor imatinib.[7] Although targeting an enzyme known to be druggable, or with a precedent of druggability in its protein family is somehow safe, it limits innovation and a "trial and error" approach may be necessary to realize how big the druggable genome actually is.

1.1.2. Small molecules and drug likeness

Orally available drugs are generally small organic molecules, the majority of which follow a set of "rules" or "trends" in their chemical structure and physicochemical properties. An analysis performed in 1997 of a dataset of 3 000 drugs led to the implementation of "the rule of 5" as a set of characteristics required for a small molecule orally available drug. Lipinski's rule of 5 states that "*poor absorption or permeation are more likely when there are more than 5 H-bond donors (expressed as the sum of OHs and NHs); the Molecular weight is over 500; the Log P is over 5 (or MLogP is over 4.5); there are more than 10 H-bond acceptors (expressed as the sum of Ns and Os")*.[8] A separate analysis by Veber suggested polar surface area (PSA) and the number of rotatable bonds as properties to take into consideration as well.[9] Yet, drug likeness is much more than this set of rules which are focused on oral bioavailability. Drugs that act on the central nervous system and drugs which are not intended for oral absorption will have other characteristics. Overington's analysis identified a total of 1 204 small-molecule drugs, out of which only 73 % pass the rule of 5.[5]

Despite the perception that the rule of 5 would lead to smaller and more lipophilic drugs to be designed a 50-year retrospective analysis of molecules published in the *Journal of Medicinal Chemistry* (*American Chemical Society*) has concluded that the mean and median values of a wide range of physical properties of molecules have risen. A decrease of 2 % in clogP in the period between 2000 and 2004 was observed, possibly as a result of the rule of 5 implementation, but it rose again afterwards.[10]

1.1.3. Chemical probes

Not all small molecules are designed to be drugs. Binding of a small molecule with appropriate physical and chemical properties and high affinity to a certain protein does not necessarily make it a potential drug as that target must be associated with a disease condition. Nonetheless, many small-molecules can be used as valuable biochemical tools to study signalling pathways *in vivo* and *in vitro*. These tools are also called chemical probes.

Frye postulated five principles of a quality chemical probe:[11]

- Molecular profiling. In vitro potency and selectivity data which associates with cellular or in vivo profile.
- Mechanism of action. Sufficient mechanistic data versus its intended molecular target, which includes dose-dependency in either a cell-based assay or a cell-free assay that recapitulates a physiological function of the target.
- Identity of the active species. Sufficient data to attribute assay results to its intact structure or a well-characterised derivative.
- Proven utility as a probe. Sufficient cellular activity data to confidently address at least one hypothesis about the role of the molecular target in a cell’s response to its environment.
- Availability to the academic community with no restrictions in use.

1.1.4. Assay development

1.1.4.1. Biochemical Assays

Most assays used in the early stages of drug discovery are performed *in vitro* and are optimised to be able to test a large number of compounds in a relatively easy and automated manner, using cheaper technology than that required for *in vivo* tests. Immunoassays, for example, are routinely employed to measure the activity of small molecules against enzymes. These require an antibody to specifically bind an antigen and commonly have some form of label attached that can easily be detected by means of radiation, fluorescence, or luminescence for example. [12]

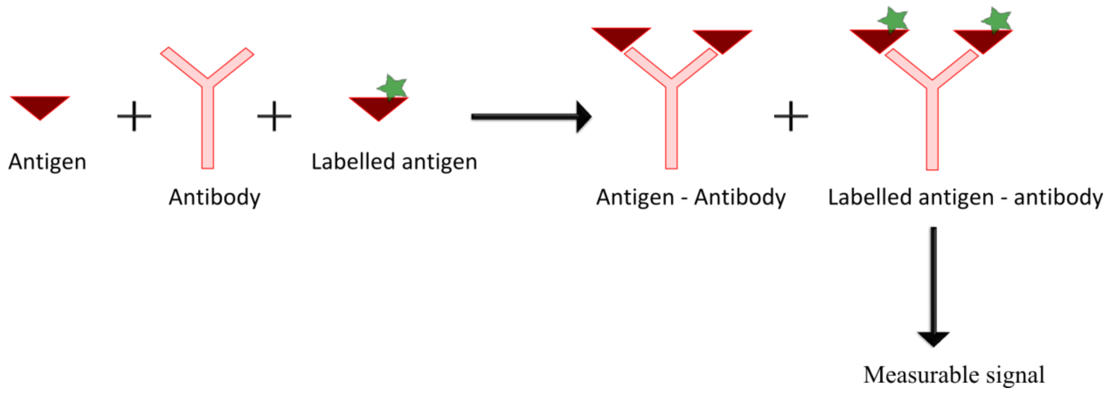

Figure 2. General concept of an immunoassay. An antigen can be quantified by reacting with a specific antibody and an added labelled antigen which will complete for antibody binding. The labelled antigen – antibody complex can then be measured. Less label measured in the assay indicates a higher amount of unlabelled antigen present.

1.1.4.2. Biophysical Assays

Biophysical assays allow the detection of direct binding of a small molecule to its target, and can deliver a fast way of compound screening as well as providing information regarding binding sites. Many techniques exist which use different physical phenomenon to measure drug-target interactions. Some will be briefly described as follows, and detailed attention will be given to surface plasmon resonance, the technique employed in the research presented in this thesis.

Isothermal titration calorimetry (ITC) detects small changes in temperature caused by the absorption or release of heat upon molecular interactions, allowing for thermodynamics measurements to be made.[13] The technique produces very accurate values for binding affinity, stoichiometry and enthalpy changes. However, it often requires high amounts of protein.

A technique based on fluorescence called *fluorescence polarisation* (FP) quantifies bound ligand by detecting the change in size of the protein-ligand complex. For FP measurements, samples are excited with plane polarized light (horizontally or vertically, depending on the equipment) at the excitation wavelength of the fluorophore. Emitted light is simultaneously measured in the parallel and the perpendicular planes, relative to the excitation source. When a rigid and entirely immobile fluorophore is excited by plane-polarized light, it emits light in orientations that depend on the angle between the orientations of the absorbing and emitting dipoles. If the molecule rotates it will no longer be aligned. The speed at which the ligand tumbles relative to the lifetime of its excited state will determine whether rotation of a molecule can be detected – with other conditions constant, the speed of tumbling is inversely related to molecular volume. A large molecule is therefore likely to retain the same orientation during the interval between absorbing and emitting a photon, whereas a smaller one is more likely to re-orient.[14]

Nuclear magnetic resonance (NMR) is also a powerful technique which can be used not only for molecule characterisation but also for the description of binding events by monitoring changes in protein signals as a consequence of ligand interactions. For example, $^{15}N - {}^{1}H$ *HSQC* (heteronuclear single quantum coherence) spectrums can be obtained in the presence and absence of ligand; each peak corresponds to H-N pairs in the protein and can be used to monitor changes in the chemical environment of backbone NH, allowing not only detection of ligand binding but also providing binding site information if a residue resolved map of the protein is available. Another example of a recent NMR development is *target immobilised NMR screening* (TINS), which uses a single sample of immobilised protein to screen an entire fragment library.[15]

Surface Plasmon Resonance (SPR)

Surface Plasmon Resonance (SPR) is a biophysical technique that detects direct binding between two molecules, including proteins, nucleic acids, lipids, whole cells and small molecules. It can provide a wide range of information regarding the biomolecular interactions, from the specificity of the interaction to affinity and kinetics. SPR is now recognised as a valuable tool to screen and characterise small molecules that modulate the activity of a range of targets, including kinases and G protein-coupled receptors (GPCRs).[16-18] The microfluidics system of the biosensor allows the injection of an analyte (small molecule, hormone, protein) over an immobilised ligand (protein, nucleic acid, etc.) and the optical detector measures the direct binding between the two entities based on the difference in refractive index near the surface that occurs as the compound binds, thus allowing a real-time and label-free measurement of compound binding to the target (Figure **3**). Added benefits of using SPR-based assays include the ability to screen fragments (fragment-based drug design) and the use of separate domains of proteins, which may provide information about the location of the binding site.[19] Further studies with mutated constructs may also allow additional characterisation of the binding mode when crystal structures are not available.

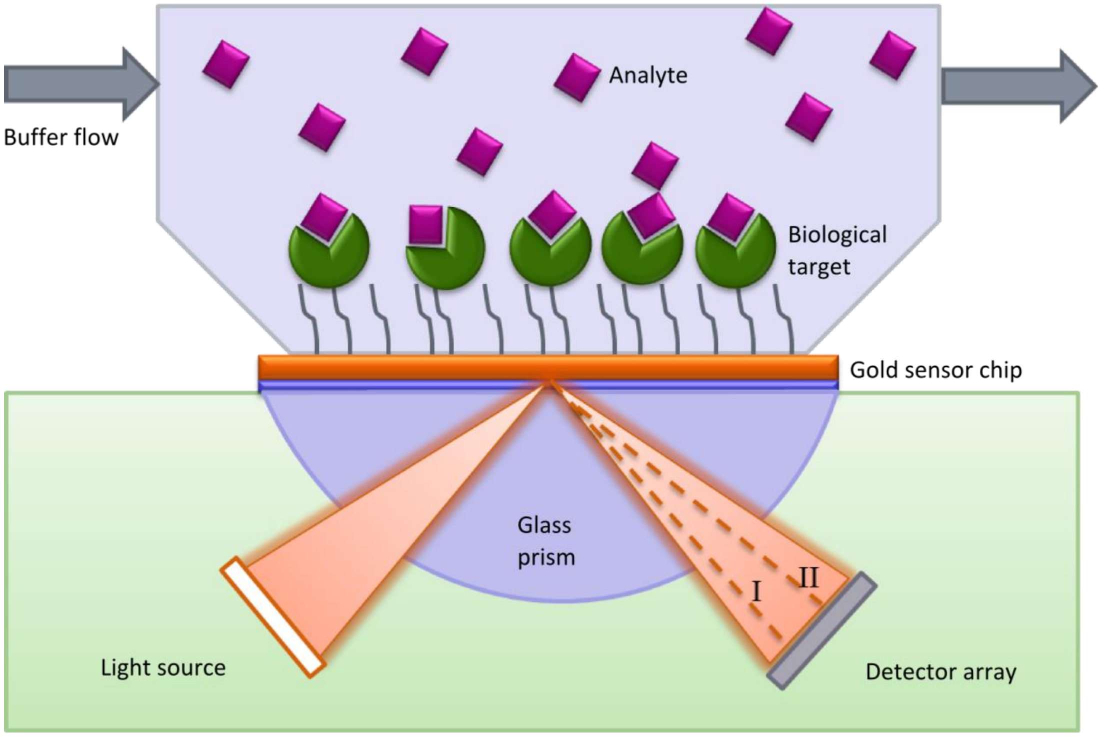

Figure 3. General setup of the SPR detection system.

The principles of SPR:

Surface plasmons are a form of electromagnetic energy and represent electron density fluctuations in a conducting metal that can be regarded as equivalent to photons in the case of light. The underlying principles of SPR are total internal reflection (TIR) and evanescence electric field. TIR occurs when light propagates between two different media of different refractive index. Above a critical incidence angle the light is no longer refracted but propagates back. When this happens, an electric field intensity called “evanescence wave” is formed and when the interface is coated with a thin metal film of gold the components of the evanescent field induce electromagnetic surface plasmon waves in the metal. The generated evanescence wave penetrates into the sample cell allowing the detection of refractive index properties to a distance of about 1 μm from the surface. Interactions at the surface of the sensor chip cause a change of the solute concentration and therefore of the refractive index of the medium. The resulting change in the detected light angle (Figure **4**) is converted into a response signal, where a shift in resonance angle of approximately 10^{-4} degrees corresponds to 1 response unit (RU). An increase in response units also directly correlates to an increase in mass at the surface. In the case of protein, this has been determined as 1 RU being equivalent to 1 pg/mm^2.[20-21]

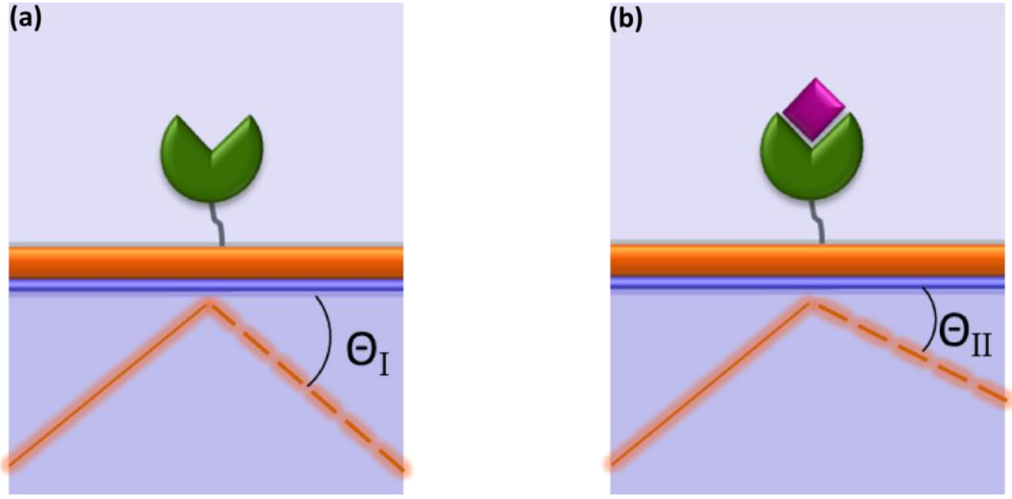

Figure 4. Difference of light resonance angle at the sensor chip surface as a result of biomolecular interactions by SPR. (a) Sensor surface before binding of analyte to the immobilised target; (b) Sensor surface upon binding of analyte to the immobilised target. Where Θ_I and Θ_{II} correspond to the detected light angle.

Qualitative information obtained from SPR assays:

The SPR response can be used for simple binding/no-binding assays in which the purpose is to determine whether or not there is an interaction between a given analyte and the immobilised macromolecule. This kind of assay is usually employed for compound screening, to check for compound specificity, or to determine the location of binding sites if different protein domains or mutants are immobilised.

Quantitative analysis

- *Kinetics*

The kinetics of an interaction consist of the rate at which a complex is formed (*association*, K_a) and the rate at which it decays (*dissociation*, K_d); and can be determined from the information in a sensorgram, the plot of response units over time. The concept is that association takes place as the sample passes over the sensor surface and the response in the sensorgram increases; and dissociation starts when the sample is replaced by buffer and the response decreases (Figure **5**).

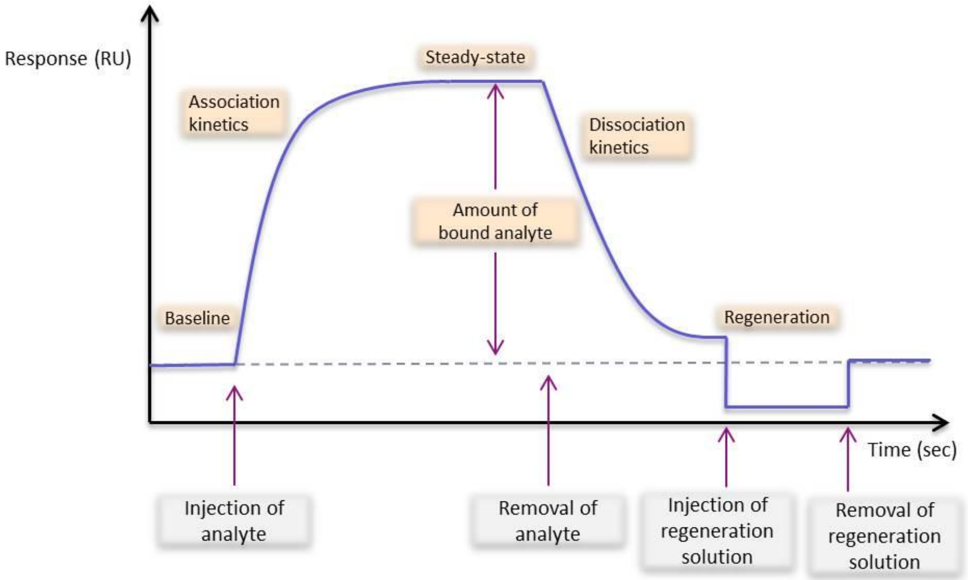
Response (RU)
Steady-state
Association kinetics
Dissociation kinetics
Amount of bound analyte
Baseline
Regeneration
Time (sec)
Injection of analyte
Removal of analyte
Injection of regeneration solution
Removal of regeneration solution

Figure 5. General overview of a sensorgram. Injection of an analyte increases the signal response from the baseline until the binding reaches equilibrium, after which the injection of the analyte stops and the response signal decrease as the analyte dissocates form the surface. Injection of a regeneration buffer removes any bound material and the signal returns to baseline.

When performing kinetics studies, one may encounter mass transport limitations: the amount of analyte that binds to the ligand depends on the amount of analyte that effectively reaches the surface where the ligand is bound. The analyte concentration on the surface may be depleted and a gradient generated through the liquid layer – this is called diffuse mass transport. In any assay it is necessary to establish efficient mass transfer between the bulk and the surface. For example, mass transport limitations cause both the association and dissociation phases to exhibit slower kinetics, which has direct effects on the information retained from the sensorgram. Therefore, one must account for these limitations when analysing the data and include mass transport in the fitting model if necessary.

Two types of kinetics assays can be applied. The conventional approach is to inject the analyte at different concentrations with regeneration of the surface between every analysis cycle – this is called *multicycle kinetics*. More recently, another technique has been used in which the regeneration step is absent and the sensorgram consists of a titration from low to high concentration of analyte – *single-cycle kinetics*.

- *Affinity*

The affinity of an analyte to the ligand is time-independent and defines how strongly bound the complex is. Affinity determines how much complex is formed at equilibrium – steady state where association balances dissociation. Affinity can be determined from kinetic measurements as for a simple 1:1 interaction, the equilibrium constant K_D is the ratio of the kinetic rate constants, K_d/K_a. When the association and dissociation rates are too fast to determine accurately, affinity can be determined by using the binding information at equilibrium if saturation can be observed, and it yields the equilibrium constant K_D.

- *Thermodynamics*

Kinetics or affinity measurements can be performed at different temperatures, allowing an analysis of the variation of kinetics and affinity constants with temperature and an assessment of thermodynamic parameters from the data.[22]

One-to-one interaction model

Assuming a one-to-one interaction between a soluble analyte and an immobilised ligand, Figure **6** summarises the kinetics of the model system: Molecule B is immobilised to the sensor surface, molecule A is transported to the surface in the thin layer flow cell, and the concentration of complex AB is measured; A_0 represents molecule A in the eluent stream and A_s at the sensor surface. k_m and k_{-m} describe the flux of molecules to the sensor surface and out from the sensor surface; k_a and k_d are the kinetic association and dissociation constants, respectively, and k_f and k_r are the resulting forward and reverse rate constants that determine the overall rate of the AB complex formation at the surface. The kinetic and concentrations parameters calculated by the Biacore software are based on this model.[23]

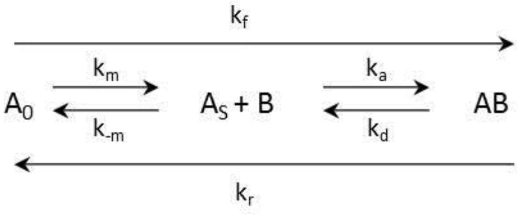

Figure 6. One-to-one interaction model at the surface in a flow cell. Where B is immobilised at the sensor surface; A is present in the flow system; k_m and k_{-m} are mass transport rate constants; k_a and k_d are the rate constants for the reaction between A and B, and k_f and k_r are the overall rate constants in the system.

As mentioned above, the signals at steady-state equilibrium can be used for assay of equilibrium-binding constants, whilst the association and dissociation phases can be used for kinetic analysis, and may also yield equilibrium-binding constants under proper conditions. If a simple one-to-one interaction model applies, then kinetic analysis can usually be easily performed, yielding the association rate (k_{on} or k_a) and the dissociation rate (k_{off} or k_d). Nevertheless, more complex binding interactions often take place for instance due to heterogeneity of the surface, mass transport limitations, conformational changes or multivalent binding. When binding kinetics data cannot be fitted to a simple model or falls outside the detection range of the instrument, steady-state binding data can usually be used to determine the equilibrium constant, $K_{D.}$ For an accurate determination of K_D it is desirable that a range of analyte concentration be used, ranging from well below K_D up to 10-fold K_D. If high concentrations do not lead to saturation of the steady-state response this indicates that weaker interactions are taking place, such as binding to nonspecific binding sites.

The sensor chip

The sensor chip is constructed from a thin layer of gold coated with a covalently bound matrix of carboxymethylated dextran, a flexible carbohydrate polymer that forms a surface layer of approximately 100 nm on the most commonly used sensor chip CM5, and provides a means for attachment of molecules (Figure **10**).

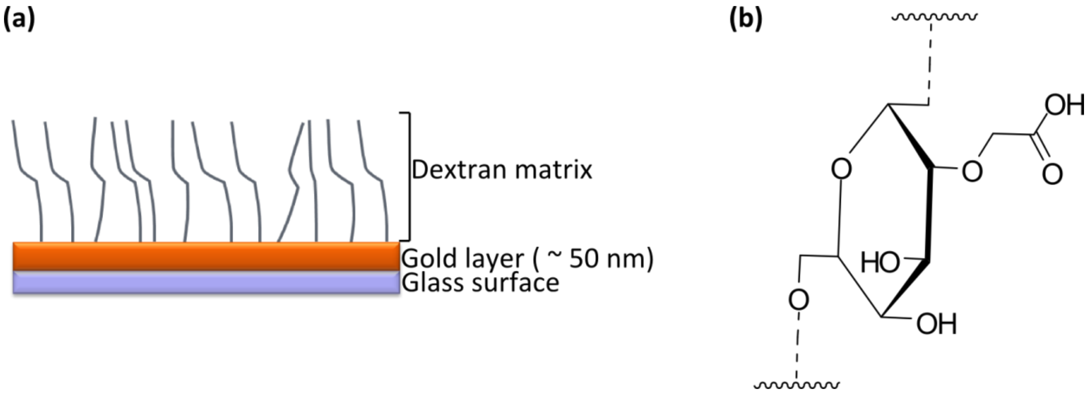

Figure 7. The sensor chip. (a) setup of a sensor chip; (b) carboxylated dextran unit.

The dextran matrix is the environment in which the interaction being studied will occur, and gives important properties to the sensor surface. The negative carboxyl groups allow electrostatic concentration of positively charged molecules from solution, enabling efficient immobilisation from dilute ligand solutions. It provides a defined chemical basis for immobilisation of biomolecules using well defined chemistries, and its hydrophobic environment is favourable to most solution-based biomolecular interactions. In addition, the dextran matrix extends the region where interactions take place to encompass a surface layer with a thickness of the same order of magnitude as the penetration depth of the evanescent wave.[24]

The CM-series sensor chips, which contain the carboxymethylated dextran matrix, permit molecule attachment using a variety of chemical methods, exploiting common functional groups on the protein such as amino, thiol, and aldehyde groups. Additionally, antibodies may also be attached that rely on the specific binding immobilised antibody and the antigenic epitope on the ligand (Figure **8a–c** and **f**). In addition to CM5 chips mentioned above, other CM chips are available with modified matrixes. CM4 chips have a CM-dextran with lower carboxymethylated level than CM5 and are used for low immobilisation levels and reduced non-specific binding. CM3 chips have a shorter dextran matrix and used for large ligand molecules and particles. If higher binding capacity and higher signal to noise is needed, for instance for confident measurements of low molecular weight compounds, a CM7 chip can be used, with a higher degree of carboxylation and a denser matrix than CM5.

For tagged proteins, different immobilisation procedures can be applied. The SA sensor chip carries a dextran matrix to which streptavidin has been covalently attached, therefore preparing the surface for high affinity capture of biotinylated ligands (Figure **8d**); polyhistidine-tagged ligands can be captured onto a NTA sensor chip which has a dextran matrix with immobilised nitrilotriacetic acid. The NTA molecule chelates metal ions, leaving coordination sites free that can bind to polyhistidine tags on recombinant proteins (Figure **8e**). There are additional modified chips available that allow experiments with lipid vesicles and liposomes, and even membrane-associated molecules (Figure **8g**).

Assay Design

- *Immobilisation*

The available sensor chips provide a variety of means for immobilisation as their surface allows for chemical derivatisation.[25] The carboxymethylated dextran matrix can be modified so that proteins can be covalently attached by taking advantage of the functional groups on their amino acid side chains.

Amine coupling is the most frequently used immobilisation chemistry and can occur through lysine residues and the protein N-terminus (Figure **8a**). Cysteines can be bound to the CM-dextran through their free thiol groups, either by formation of disulphide bridges or by covalent reactions with maleimides. Since free thiols are relatively rare, these approaches can lead to site-directed, and thus oriented, immobilisation of the target (Figure **8b**). Carbohydrate molecules and glycoproteins such as antibodies can be immobilised through aldehyde coupling on a hydrazine-activated surface. The aldehyde groups may be native or introduced by oxidation of cis-diols.

After immobilisation of a target onto a sensor chip, the immobilization level of the surface (measured as a difference in response units) dictates its binding capacity, R_{max}.[24]

$$R_{max} = \frac{analyte\ Mw}{ligand\ Mw} \times RL\ \times S$$

Equation 1. Binding capacity of the SPR surface. Where RL is the immobilisation level, S is the stoichiometric ratio, Rmax is the maximal response for a certain analyte.

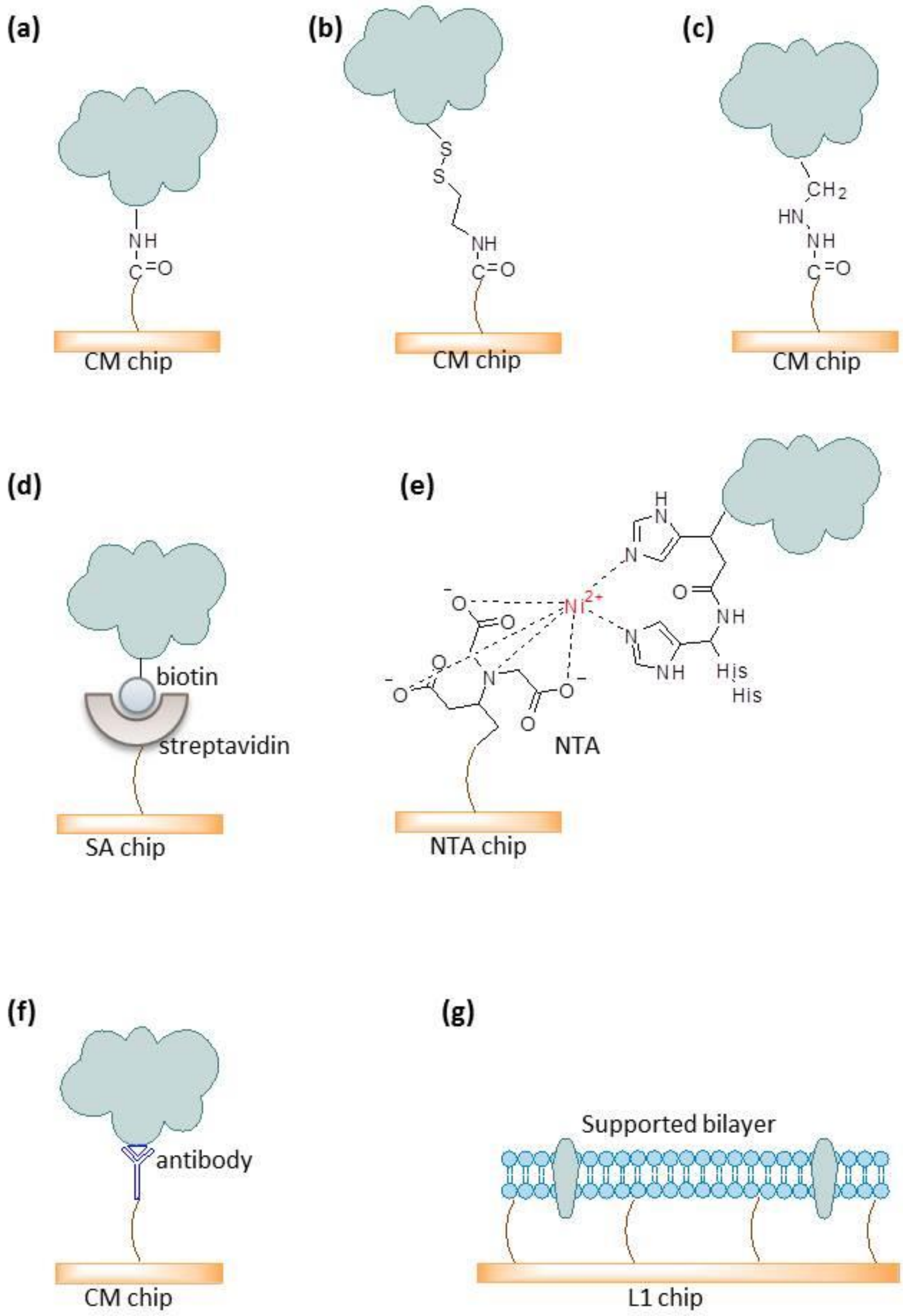
(a)
NH
C=O
CM chip
(b)
S
S
NH
C=O
CM chip
(c)
CH2
HN
NH
C=O
CM chip
(d)
biotin
streptavidin
SA chip
(e)
H
N
N
Ni2+
O
O
NH
N
NH
His
His
O
O
N
O
O
O
NTA
NTA chip
(f)
antibody
CM chip
(g)
Supported bilayer
L1 chip

Figure 8. Examples of available Biacore sensor chip chemistries. (a) covalent immobilisation through amine coupling; (b) covalent immobilisation through thiol coupling; (c) covalent immobilisation through aldehyde coupling; (d) capturing through streptavidin – biotin interaction; (e) capturing through NTA – Ni^{2+} - poly-histidine tag interaction; (f) capturing through antibody – antigen interaction; (g) capture of lipid vesicles and liposomes through interaction with immobilised lipophilic residues.

- *Surface Regeneration*

Surface regeneration consists of the injection of a buffer that will remove any bound analyte from the surface to leave it intact for the following cycle of sample injection. Optimal conditions are specific for the ligand-analyte configurations, although for protein surfaces the most commonly used conditions are low pH (10 mM glycine-HCl at pH 1.5 – 3) and ethylene glycol at concentrations up to 100 % for highly hydrophobic interactions. Sodium chloride can also be used at a concentration of 1 M to disrupt mostly ionic interactions. Regeneration is a critical part of the binding assay since conditions that are too mild lead to analyte remaining and a possible carry-over effect, whilst harsh conditions might denature the immobisiled protein. Regeneration of the surface is not always necessary if the circumstances are such that the analyte dissociates fast enough and all analyte may be removed within a reasonable time by simply washing with buffer.

- *Assay conditions and instrument specifications*

Depending on the instrument used, conditions such as temperature and automation of the assay can be varied. The work presented here was performed using a Biacore T200. This instrument supports the use of 96 and 384-well microplates, allowing medium-high throughput screening; the temperature can be set between 4 and 45 °C, and it can detect weak binding interaction in the low milimolar (mM) range. The instrument specifications do not set a lower limit of molecular weight detection for organic molecules. The recommended working ranges for association rate constant (k_a) are between 10^3 to 10^9 $M^{-1}s^{-1}$ for proteins and 10^3 to 5 x 10^7 $M^{-1}s^{-1}$ for low molecular weight molecules. Dissociation rate constants (k_d) of 10^{-5} to 1 s^{-1} are within the typical working range. When setting up an assay, all injection times can be specified, such as contact and dissociation between the two molecules, regeneration and conditioning steps.[26]

1.1.5. Compound screening

A commonly used technique in drug discovery is the screening of large libraries of compounds in order to identify those structures which are most likely to bind to a drug target. These libraries can be both physical and assessed by means of a biological or biophysical assay, as described above, or virtual databases of known structures which are computationally screened. If a biologically active compound for a certain target is already known it is possible to search these virtual libraries for similar compounds – this process is called a similarity search. The common way of characterizing these molecules is by attributing to them a chemical fingerprint, which is simply a list of binary values (0 or 1).

The molecular access system (MACCS) keys fingerprint for a given structure is based on a set of questions about the chemical structure, such as “are there fewer than 3 oxygens?” or “is there a ring of size 4?”. The result of this is a list of binary values- either true (1) or false (0) and it characterises the molecule. Once the molecules have been represented by such a code a Tanimoto coefficient (Equation **2**) can be used as a measure of similarity. Compounds that have a Tanimoto coefficient value > 0.85 are generally considered similar to each other.[27]

The positive hits obtained in a virtual screen are not always active but provide a means of filtering virtual libraries and usually make experimental screening methods more efficient by providing compounds that are more likely to be biologically active.

$$T = \frac{Nab}{Na + Nb - Nab}$$

Equation 2. Tanimoto Coefficiency. Where Na represents the number of features in molecule A, Nb is the number of features in B, and Nab is the number of features common to both A and B.

1.1.6. Medicinal chemistry

The International Union of Pure and Applied Chemistry (IUPAC) defines medicinal chemistry as “a chemistry-based discipline, also involving aspects of biological, medical and pharmaceutical sciences. It is concerned with the invention, discovery, design, identification and preparation of biologically active compounds, the study of their metabolism, the interpretation of their mode of action at the molecular level and the construction of structure-activity relationships.”[28]

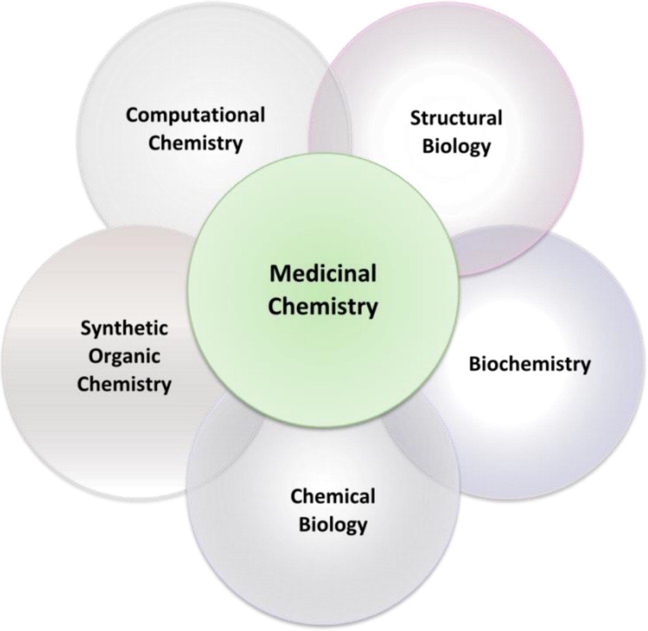

Figure 9. Schematic representation of the disciplines integrating medicinal chemistry.

As represented in Figure **9**, medicinal chemistry combines techniques from various fields, including structural biology, biochemistry, chemical biology, synthetic chemistry, and computational chemistry to design and synthesise biologically active molecule, as well as characterising their biological activity and binding interactions to the target.

Small molecule hits from a drug discovery screen are commonly optimised using medicinal chemistry. Firstly, the synthesis of a hit obtained from a virtual screen or a commercial library must be investigated and the bioactivity of the synthesised compound assessed. Hit to lead optimisation can take place by synthesising analogue compounds which can provide insight into the binding mode and functional groups necessary for activity. Understanding the binding interactions between a drug and its target can consequently lead to an improved design of drugs to be synthesised. A successful drug design is expected to result in compounds with improved biological activity and/or physico-chemical properties. Synthetic routes are expected to be easily modified, so that a range of analogue compounds can be synthesised, employing modern techniques and reagents which are able to provide faster, cleaner, and more efficient chemistry.

1.1.6.1. Microwave assisted organic synthesis

Microwave-assisted organic synthesis allows for faster reaction times and can be applied to most types of reactions. It is easily reproducible, safe, and evidently allows for the synthesis of multiple compounds to be performed in a much shorter time span than thermally driven reactions. A basic understanding of the physics behind this process might also allow for an improved synthesis.

A microwave is a form of electromagnetic energy that falls within a frequency of 300 to about 300 000 megahertz (MHz). Within this region only molecular rotation is affected, not molecular structure. Microwaves couple directly with the molecules in a reaction mixture, leading to a rapid increase in temperature, via two fundamental mechanisms: Dipole rotation and Ionic conductance. Dipole rotation refers to the alignment of polar molecules with the electric field component of the radiation and it is the sympathetic agitation of the molecules that generates heat. Ionic conductance occurs when free ions or ionic species are present in the substance being heated. Heat generation is due to frictional losses, which depends on the size, charge, and conductivity of the ions as well as on their interactions with the solvent.[29]

Microwave energy is transferred by dielectric loss. The dielectric loss factor (Ɛ'') and the dielectric constant (Ɛ') of a material are two determinants of the efficiency of heat transfer to the sample. Their quotient (Ɛ''/ Ɛ') is the dissipation factor (tan δ), high values of which indicate ready susceptibility to microwave energy. The Arrhenius equation can be used to explain how microwaves increase the rate of reaction. A reaction rate constant (k) is dependent on the frequency at which molecules collide, and on whether the molecules are properly oriented when they collide (A); and the fraction of those molecules that have the minimum energy required to overcome the activation energy barrier ($e\text{-}^{Ea/RT}$). [29]

$$k = Ae^{-Ea/RT}$$

Equation 3. Arrhenius equation. Where: k is the rate constant; A is the pre-exponential factor and represents the total number of collisions (leading to a reaction or not) per second; T is the temperature; R is the universal gas constant; and E_a is the activation energy.

Microwave energy will affect the temperature parameter of the equation. An increase in temperature causes the molecules to move about more rapidly and consequently leads to a greater number of more energetic collisions. Generally, the reaction rate for a microwave-assisted synthesis doubles for every 10 °C increase in the reaction temperature of a heat-driven reaction.[30]

When developing a new method for microwave synthesis the four most important factors to consider are: solvent, temperature, time and power. Most microwave reactions are performed in closed systems rather than at atmospheric pressure. This allows solvents to be heated up to temperatures that are four times their respective boiling point. The choice of solvent is a critical step: the more polar a reaction mixture is the greater its ability to couple with the microwave energy, resulting in a faster rise in internal temperature; thus, if the reactants are “non-absorbing” the solvent must be polar. A starting point for deciding the temperature of the reaction is 10 °C above the temperature used in conventional methods, if known. For reactions performed under reflux, the temperature can be set to 50 °C above the boiling point. Deciding on how long to run a microwave reaction for depends on the type of reaction being performed, but a good starting point for pressurized reactions is 5-10 min. the amount of power being applied is also important: whilst a low power level might not provide successful results, excessive power may cause decomposition. 50 watt is generally good for high-absorbance solvents, and 150 watt for medium absorbers. If the system is struggling to reach the desired temperature the power should be increased. As the reaction reaches its set temperature, the power is reduced so that the mixture does not bypass that temperature point. The fast reaction times and small scale in which microwave reactions can be performed provide an easy technique for development and optimisation of the method.[29-30]

1.2. Understanding and predicting protein-ligand interactions

Drug targets have binding sites into which drugs can fit and bind. Most drugs bind to their targets by means of intermolecular interactions, which can be experimentally determined by analysis of 3D structures or hypothesised by means of theoretical studies using computational methods.

1.2.1. Intermolecular interactions

There are several ways in which a drug might interact with its target. The different types of intermolecular bonding interactions differ in their bond strengths and depend on the structure of the drug and the functional groups that are present

The actual absolute strengths of the interactions vary depending on the molecules involved Table **1** shows the relative strength of some intermolecular interactions and a range of their average strength. The strength of covalent bonds is > 80 kcal/mol.[31]

Table 1. Relative specificity and strength of intermolecular interactions.

Interaction	**Specificity**[31]	**Strength**[31-32]
Hydrogen bonding	High	0.25 – 40 kcal/mol
Halogen bonding	High	1 – 40 kcal/mol
Electrostatic	Low	5 – 10 kcal/mol
π – stacking	Moderate	5 – 7 kcal/mol
Hydrophobic	Low	1.5 – 2 kcal/mol
Van der Waals	Low	< 1 kcal/mol

Each drug may use one or more of these, but not necessarily all of them. Once a lead compound is known one must determine which parts of the molecule are important for biological activity and which are not. In some cases, x-ray crystallography may be used to solve the structure of the compound bound to the target site and then studied using molecular modelling software to identify binding interactions and possibly improve these by changing the structure of the molecule.

1.2.1.1. Ionic interactions

Ionic or electrostatic interactions take place between groups having opposite charges. These interactions are stronger in hydrophobic environments than in polar ones. If an ionic interaction is possible between a drug and a protein, this is likely to be the most important initial interaction as the drug enters the binding site.[32]

1.2.1.2. Hydrogen bonds

Hydrogen bonds vary in strength and occur between an electron-rich heteroatom, which contains a lone pair of electrons, and an electron-deficient hydrogen which is usually linked to an electronegative atom such as oxygen or nitrogen. Both CO and NH groups from a protein can form hydrogen bond interactions. The functional group donating the hydrogen to the bond is called a hydrogen bond donor, whilst the group that interacts with the hydrogen is called hydrogen bond acceptor. The bond distance is typically between 2.6 and 3.2 Å and the angle between the donor-hydrogen and the acceptor is generally above 150 °.[33]

1.2.1.3. Halogen bonds

Halogens are commonly added to drugs to provide hydrophobic bulk and/or improve ADME properties (absorption, distribution, metabolism, excretion). It has been observed that in some cases the organic halides Cl, Br, and I can interact with protein electronegative atoms such as O, S, and N. The small size and high electronegativity of fluoride prevents it from making halogen bonds. The strength of halogen bonds is similar to that of hydrogen bonds.[33]

1.2.1.4. Orthogonal multipolar interactions

This type of interaction is characterised by a close orthogonal contact between two dipolar functional groups. For example, it has been observed that the CF_3 group of the abl kinase inhibitor nilotinib forms one interaction orthogonal to an amide besides two further contacts to the imidazole NH of a histidine as well as an isoleucine side chain.[34]

1.2.1.5. Hydrophobic interactions

In a protein-ligand interaction, the amount of protein hydrophobic surface buried upon ligand binding is the structural parameter that better correlates with binding affinity. Hydrophobic interactions involve the displacement of ordered layers of water molecules that surround hydrophobic regions of the molecule.[35] This type of interaction is the only listed that is entropy driven.[31]

1.2.1.6. Cation – π interactions

An ion – dipole interaction can occur when a charged or ionic group in one molecule interacts with a dipole in a second molecule. An aromatic ring can interact with an ionic group such as a quaternary ammonium ion if the positive charge of the ammonium group distorts the π electron cloud of the ring to produce a dipole moment where the face of the aromatic ring is electron-rich and the edges are electron-deficient. These interactions can be strong on the surfaces of proteins and have rarely been found buried within proteins.[36]

1.2.1.7. Van de Waals interactions

Van der Waals interactions involve interactions between hydrophobic regions of different molecules. The electronic distribution in neutral regions is never completely even and there can be areas of high and low electron densities leading to temporary dipoles. The dipole in one molecule can induce dipoles in a neighbouring molecule, leading to weak interactions between the two molecules.

1.2.1.8. Repulsive interactions

Forms of repulsion include proximity and identical charges: if molecules come too close to each other their molecular orbitals start to overlap and repel each other; similarly, two positively or negatively charged groups are also repelled.

1.2.2. Molecular modelling

The use of molecular modelling comes from a need to represent 3D molecular structures such as proteins and DNA in a way that is easy to visualise and therefore easier to understand. In medicinal chemistry, molecular modelling is mostly used to study drug-target interactions, allowing the prediction of binding sites and the more stable binding modes. These studies can be performed using the x-ray crystal structure of the target or a modelled structure based on homologous proteins with determined structure. 3D visualisations of molecular interactions are only made possible through the use of complex mathematical equations that follow the laws of classical and quantum physics. The computational methods used in molecular modelling can be split into molecular mechanics and quantum mechanics.

1.2.2.1. Molecular and Quantum mechanics

Molecular mechanics (MM) applies classical physics to calculate force fields, a set of parameters and mathematical equations involved in how molecules associate. The “force field” is therefore a MM equation and its associated atom types, and different force fields, are designated for different purposes.

The basic form of the total energy in a force field includes the energies involved in both bonded (covalent) and non-bonded interactions, where bonded energies result from bond stretching, angle bending and torsion, and non-bonded interaction include electrostatic and Van der Waals interactions (Equation **4**). This is a very simplistic representation of a force field and non-bonded interactions often value in additional factors such as partial covalent bonds including hydrogen bonds, halogen bonds, aromatic bonds, and hydrophobic interactions.

$$E_{total} = \underbrace{E_{strength} + E_{angle} + E_{torsion}}_{\textbf{Bonded interactions}} + \underbrace{E_{VdW} + E_{electrostatic}}_{\textbf{Non-bonded interactions}}$$

Equation 4. Total energy in an additive force field. The total energy equals the sum of the energies involved in bonded interactions and non-bonded interactions.

MM ignores electrons, calculating the energy of the system from the nuclear positions. This method is suitable for energy minimization and conformational analysis. Quantum mechanics (QM) uses quantum physics to calculate the properties of a molecule by considering the interactions between the electrons and the nuclei of the molecule. QM methods can be subdivided into two broad categories: *ab initio* and semi-empirical. *ab initio* calculations are extremely computationally demanding and do not use any stored parameters or data, being restricted to small molecules and suitable for measuring molecular properties such as molecular orbital energies and coefficients. If calculations consider valence electrons only and/or experimental data they can be massively reduced and can be carried out on larger molecules. These are known as semi-empirical methods. MM and QM provide the basis for molecular dynamics studies, structure alignment and docking analysis.

1.2.2.2. Docking

Molecular dynamics is a program designed to mimic the movement of atoms within a molecule and can be carried out on a molecule to generate different conformations, which on energy minimisation give a range of stable conformations.

Genetic and evolutionary algorithms are algorithms programmed to work as biological evolution. In molecular modelling, these are designed to produce different binding conformations and to carry on an evolutionary process which selects the most stable conformations.

Docking is the process of fitting a molecule into a binding site based on steric and/or chemical complementarity. It is used to predict the binding modes and affinities of compounds when they interact with their target and can be used to analyse large libraries of compounds and/or optimise binding for great ligand affinity. Most approaches consider the protein to be rigid and allow the ligand to be flexible. Different algorithms are available for protein-ligand docking and commonly used programs are DOCK, FlexX, and GOLD.[37]

The molecular modelling software employed in this project was GOLD 5.1 (from the Cambridge crystallographic data centre) and MOE (from chemical computing group).

GOLD software

GOLD (Genetic Optimisation for Ligand Docking) is a genetic algorithm for docking flexible ligands into protein binding sites.

Docking programs usually employ a scoring function to rank ligands according to their theoretical affinity. The Goldscore fitness function is optimised for the prediction of ligand binding positions rather than the prediction of binding affinities, although some correlation may be found. This function is made up of four components:

- Protein-ligand hydrogen bond energy (*external H-bond*)
- Protein-ligand van der Waals (vdw) energy (*external vdw*)
- Ligand internal vdw energy (*internal vdw*)
- Ligand torsional strain energy (*internal torsion*)

Ligand intramolecular hydrogen bond energy (internal H-bond) may be added. The fitness score is taken as the negative of the sum of the component energy terms, so that larger fitness scores are better. GOLD optimises the fitness score by using a genetic algorithm. Briefly, a population of possible docking solutions is set up at random; each solution is encoded as a “chromosome” containing information about the mapping of ligand H-bond atoms onto complementary protein H-bond atoms, mapping of hydrophobic points on the ligand onto protein hydrophobic points, and the conformation around flexible ligand bonds and protein OH groups; each chromosome is assigned a fitness score and the chromosomes within the population are ranked according to fitness.[38]

MOE software

MOE (Molecular Operating Environment) is a molecular graphics software which also performs molecular modelling functions. It has been optimised for structure-based drug design, allowing scaffold replacement, docking, conformation analysis, and ligand optimisation in pocket. MOE is also used for pharmacophore discovery, quantitative structure activity relationships (QSAR), homology modelling and macromolecular simulation.[39] Aditionally, it provides a series of applications for medicinal chemistry which allow a clear visualisation of non-bonded interaction and protein-ligand interaction diagrams, as well as the building of surfaces to define binding site topology.[40-41] The "Ligand:Protein interaction diagrams" function of MOE provides schematic 2D representations of key interactions between proteins and ligands, which aids the analysis of docking studies.[42]

1.3. The guanylate cyclase protein family

The macromolecular targets explored in this thesis belong to the guanylate cyclase protein family. Guanylate cyclases (guanylyl cyclases, GCs) are a family of homologous enzymes that exist as a number of isoforms, some of which are membrane-bound, also called particulate guanylate cyclases (pGC), while others are soluble (sGC). Both sGC and pGCs catalyse the conversion of guanosine triphosphate (GTP) into the second messenger 3',5'-cyclic guanosine monophosphate (cGMP) and pyrophosphate (PPi) (Figure **10**). Although sGC and pGCs share a homologous catalytic domain the mechanisms by which they are activated are different: pGCs are stimulated by small peptide hormones, whilst sGC is the human receptor for nitric oxide (NO). GTP binds to a single catalytic site in sGC and two catalytic sites on pGC.[43-44]

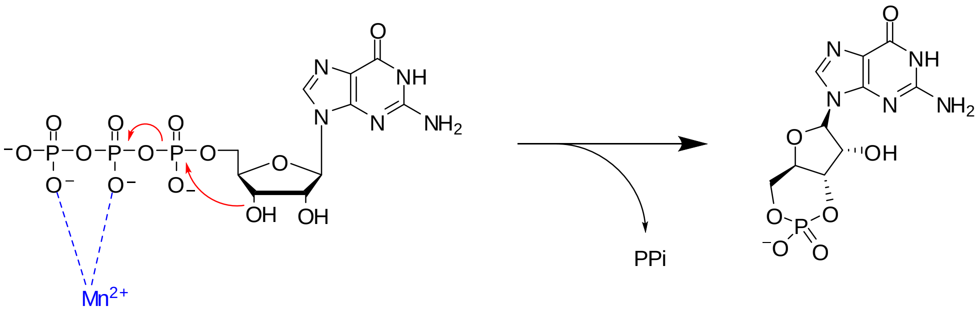

Figure 10. Catalytic mechanism of guanylate cyclase activity.

Membrane- bound guanylate cyclases, GC-A and GC-B, are members of the natriuretic peptide receptor family and are also called natriuretic peptide receptor-A (NPR-A) and natriuretic peptide receptor-B (NPR-B), respectively. A third receptor for natriuretic peptides, NPR-C, lacks the GC domain.[45] Figure **11** summarises the signalling pathways of GCs. Natriuretic peptides bind to the extracellular domain of pGCs, catalysing the conversion of GTP into cGMP at the intracellular GC domain. Nitric oxide synthase (NOS) catalyses the production of NO from L-arginine. NO binds to the heme nitric oxide/oxygen (H-NOX) domain of sGC, leading to the formation of cGMP at the GC domain.[46] cGMP is a substrate for cGMP-dependent protein kinases[47], PDEs[48], and gated channels[49].

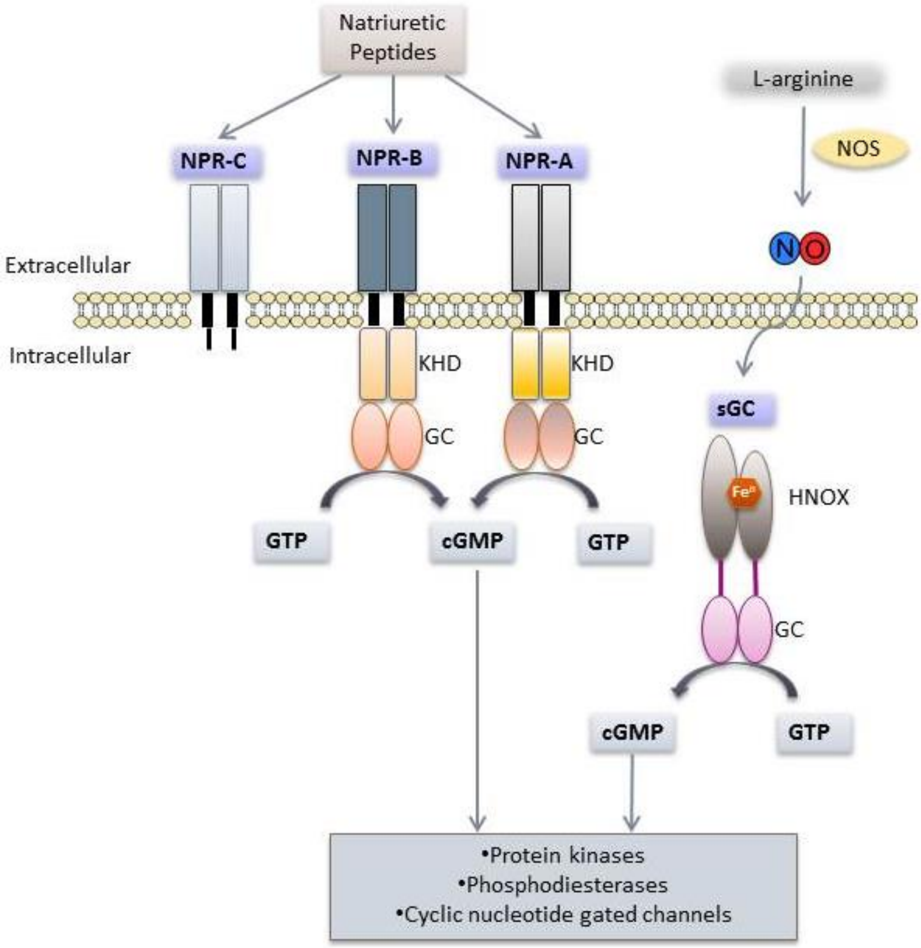
Natriuretic Peptides
L-arginine
NOS
NPR-C
NPR-B
NPR-A
N O
Extracellular
Intracellular
KHD
KHD
GC
GC
sGC
Fe
HNOX
GTP
cGMP
GTP
GC
cGMP
GTP
•Protein kinases
•Phosphodiesterases
•Cyclic nucleotide gated channels

Figure 11. Natriuretic peptide receptors and soluble guanylate cyclase domain structure and signaling pathway. NOS: nitric oxide synthase; KHD: Kinase homology domain; GC-guanylate cyclase domain; HNOX: hydrogen and nitric oxide exchange domain.

1.3.1. Natriuretic peptide receptors

Natriuretic peptides (NPs) are structurally related hormones/paracrine factors that regulate vascular homeostasis, fat metabolism and long bone growth. The family of mammalian natriuretic peptides is formed by natriuretic peptides type-A (ANP), type-B (BNP) and type-C (CNP). ANP was the first to be discovered and related to the promotion of sodium and water excretion via a cGMP signalling pathway.[50] ANP acts mainly as a cardiac hormone released from the atria which upon cleavage of proANP into the mature peptide enters the coronary sinus and is distributed to its target organs via the circulation. BNP is actively produced by the ventricles and unlike ANP, it is not stored in granules but rather transcribed as needed in response to cardiac stress states. Levels of both ANP and BNP are elevated in patients with congestive heart failure. CNP differs from both ANP and BNP as it acts in a paracrine manner. It is the most highly expressed natriuretic peptide in the brain but is also expressed in chondrocytes and endothelial cells. CNP is not stored in granules and its secretion is increased by growth factors and sheer stress. Its expression in neointimal vascular smooth cells is increased in response to vascular injury.[45, 51]

NPR-A binds natriuretic peptides at a stoichiometry of 2:1 with a rank preference of ANP>> BNP>>CNP. NPR-B is the most active NPR in the failed heart and preferentially binds CNP. NPR-C is a non-GC receptor that binds all three NPs.[45, 52]

1.3.1.1. CNP/NPR-C signalling

NPR-C was initially thought to function solely as a clearance receptor for the degradation of NPs. It was later found to play an important role in the cardiovascular systems and its activation has been linked to the smooth muscle hyperpolarisation induced by CNP in resistance arteries, where the natriuretic peptide acts as an endothelium-derived hyperpolarizing factor (EDHF).[53]

NPR-C is coupled to an inhibitory heterotrimeric G protein, Gi, and both the α and βγ subunits of this protein mediate a number of important physiological effects. It presents a 37 aminoacid cytoplasmatic domain that is composed of Gi activator sequences but its structure does not resemble the traditional heptahelical G protein-coupled receptor with seven transmembrane spanning domains. The 17 aminoacid sequence in the middle region of the 37 aminoacid intracellular domain (R469-R485) has been identified as the functionally relevant G_i activator sequence.[54] CNP is a 22 residues peptide circularised by a disulphide bond between C6-C22. The peptide binds into a V-shaped cleft formed from the homodimer of the receptor.

Activation of NPR-C in vascular smooth muscle cells activates a potassium conductance which leads to hyperpolarisation and relaxation. CNP activation of NPR-C has also been shown to inhibit adenylyl cyclase activity leading to a reduction in intracellular cAMP levels in cardiac myocytes.[54] CNP does not circulate in the blood stream to any great extent, except in disease state. CNP mRNA is increased in response to shear stress, pro-inflammatory cytokines and lipopolysaccharides, and plasma levels of CNP are elevated in inflammatory cardiovascular pathologies.[55]

CNP is likely to maintain a substantial cytoprotective, anti-atherogenic influence on the blood vessel wall and loss of endothelium-derived CNP may be an important contributor to the pathogenesis of inflammatory cardiovascular diseases such as atherosclerosis and restenosis. The observation that CNP responses are accentuated in the absence of endothelium-derived NO leads to the hypothesis that CNP might compensate for deficiencies in NO and show anti-atherogenic activity.[53]

Studies performed in rat isolated mesenteric arteries showed that blockade of NPR-C inhibits CNP- and EDHF- dependent responses, corroborating the role of CNP as an EDHF. NPR-C antagonism inhibits the smooth muscle hyperpolarisation associated with EDHF-dependent dilation in these arteries, suggesting that the CNP/NPRC signalling might be an important target for the treatment of cardiovascular diseases.[56]

1.3.2. Soluble guanylate cyclase

sGC domains are conserved within species and have been suggested to be acquired by the animal lineage via transfer from bacterial sources.[57] GC catalytic domains are homologues to the C1 and C2 domains in adenylate cyclase, which converts ATP into 3’,5’-cyclic adenosine monophosphate (cAMP) and diphosphate.

1.3.2.1. The NO-sGC-cGMP signalling

NO can be viewed as both a cytotoxic agent and a vital signalling molecule. The identification of this diatomic gas as an endothelium-derived relaxation factor rendered it of great importance in biological studies.[58] NO can easily diffuse through cell membranes into target cells and bind to a prosthetic heme group in sGC, leading to a conformational change that increases the rate of GTP conversion into cGMP.

The NO-sGC-cGMP signalling has an important role in regulating blood flow, and in the perfusion and function of many organs and tissues. Increased levels of cGMP lead to smooth muscle relaxation, inhibition of platelet aggregation and anti-inflammatory effects. Reduced bioavailability or responsiveness to NO contributes to the development of cardiovascular, pulmonary and hepatic diseases. In contrast, aberrant signalling has also been linked to vascular disorders such as hypertension, atherosclerosis and coronary heart diseases and has also been shown to occur during sepsis and neurodegenerative disorders.[59-60]

Signalling in the cardiovascular system

In the vasculature, cGMP is generated by both cytosolic sGC and pGCs. cGMP has a key role in the control of vascular tone and blood pressure. Indeed, its primary action is the relaxation of vascular smooth muscle and vasodilation.[61] Reciprocal regulation of the NO-sGC-cGMP and NP-pGC-cGMP pathways is evident, such that one cGMP generating system may compensate for the dysfunction of the other. For instance, reduced NO-sGC-cGMP signalling in patients with cardiovascular risk factors and atherosclerosis may be compensated for by increased pGC-derived cGMP.[62]

cGMP has also been related to endothelial and VSM growth, endothelial permeability, and anti-inflammatory actions. The increase in endothelial permeability mediated by cGMP may be involved in ischemia/reperfusion injury. Both NPs- and NO- derived cGMP have anti-inflammatory activity: whilst NPs prevent immune cell activation, sGC activity appears to play an important role in modulating leukocyte adhesion. Moreover, vascular activity of cGMP has been correlated to a range of cardiovascular conditions, from systemic and pulmonary hypertension to coronary artery disease and atherosclerosis, as well as erectile dysfunction. Thus, modulation of sGC activity is of profound interest in this field and may have great potential for therapeutic applications.[63]

Signalling in the nervous system

In the brain, sGC acts as a neurotransmitter receptor. The rapid on- and off-kinetics and the desensitization profile of activity, combined with variations in the rate of cGMP breakdown, provide fundamental mechanisms for shaping cellular cGMP responses and is important in decoding NO signals under physiological and pathological conditions.[64]

NO-sGC-cGMP signalling has also been implicated in the modulation of synaptic transmission and to act in long-term potentiation, one of the major cellular mechanisms that underlie the processes of learning and memory[65]

Moreover, involvement of cGMP in early differentiation events of embryonic stem cells has been proposed. In rats, high cGMP levels promote neural stem cells differentiation to neurons whilst reduced cGMP levels promote differentiation to non neuronal (mainly glial) cells, which consequently leads to impaired cognitive function. Restoring cGMP levels with sildenafil normalizes neural stem cells differentiation.[66]

sGC and Parkinson’s disease

NO can mediate neurotoxicity and cause neuronal cell death. The neurotransmitter is associated with pathogenic mechanisms involved in multiple neurodegenerative diseases, including Parkinson’s Disease (PD). Such mechanisms include excitotoxicity, DNA damage, and protein modifications such as nitrosylation and nitration.[67]

Recent research has suggested the involvement of NO in PD is due to activation of sGC. PD is associated with loss of dopaminergic stimulation to a part of the brain called the striatum. Disruption of striatal NO-sGC-cGMP signalling cascades result in profound changes in behavioural, electrophysiological, and molecular responses to pharmacological manipulations of dopamine and glutamate transmission.[68]

The dopaminergic neurons are responsive for motor control. Therefore, the most common symptoms of PD are movement associated including tremors, rigidity, and postural unsteadiness. In extreme cases cognitive issues may also arise, leading to memory impairment and dementia. Drugs used in the treatment of PD are shown in Figure **12**. Conventional treatment of PD is based on dopamine replacement with the pro-drug levodopa **1** (L-DOPA) in combination with an inhibitor of its peripheral conversion to dopamine (carbidopa **2** or benserazide **3**). This is however only a symptomatic treatment and leads to progressive loss of efficacy with time.[69] Thus, alternative treatments are being explored that target alternative neurotransmitter systems.

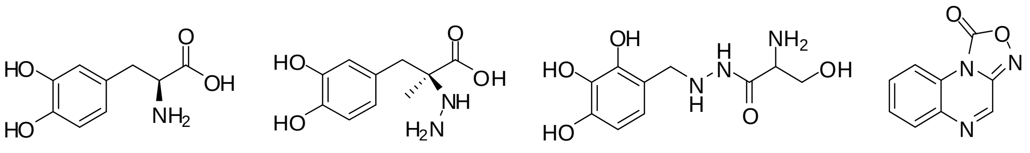

L-DOPA Carbidopa Benserazide ODQ

1 **2** **3** **4**

Figure 12. Chemical structures of small molecules used in the treatment of Parkinson's Disease and sGC inhibitor ODQ.

Studies performed in animal models of PD with a potent sGC inhibitor, ODQ **4**, have shown that the enzyme could be a new drug target for restoring basal ganglia dysfunction and attenuating motor symptoms associated with PD. ODQ **4** reversed the characteristic elevations in striatal cGMP levels and reduced the increase in spontaneous firing observed in the dopamine-depleted striatum.[68] NO-sGC-cGMP signalling is thus a new target for non-dopamine treatment for PD.

1.3.2.2. Structure and regulation of sGC

sGC is generally found as a heterodimer composed of a β-subunit (70 kDa) and a larger α-subunit (77 kDa). The best characterized isoform is the α_1/β_1 protein, but α_2 and β_2 subunits have also been identified. Each subunit is composed of multiple domains, as represented in Figure **13**. The H-NOX of sGC is located at the N-terminus, but only the β-subunit presents a prosthetic heme group. PAS-like domains are present in both subunits and are thought to direct preferential heterodimer formation. A coiled-coil (CC) bundle is followed by the C-terminal catalytic domain where turnover of GTP into cGMP occurs.[70] GTP binds to the β-subunit through its purine ring and the cofactor Mg^{2+}, which stabilises the β and γ phosphates, binds to acidic residues in the α-subunit.[71]

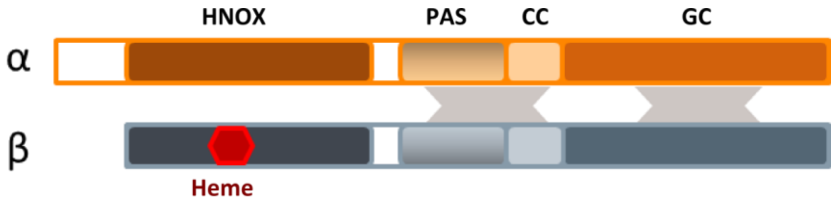

Figure 13. Schematic representation of the structural organisation of sGC domains. Adapted from [71]

The heme group on sGC does not bind O_2 and CO is only a very weak activator. The binding of NO and CO, and discrimination of O_2 by sGC has been the subject of great discussion and extensively studied using physical-chemical methods. Elucidation of the sGC mechanism depends on the understanding of the sGC heme environment and the structural changes induced by NO and CO binding to the sGC heme co-factor. UV-vis spectroscopy showed that the β_1-subunit (1 – 385) contains a five-coordinate, high-spin ferrous heme. Through site-directed mutagenesis and spectroscopic approaches it was demonstrated that the heme in sGC is coordinated to the proximal Histidine-105 in the β_1 subunit. Raman characterization of the heme domain showed that in addition to the relatively weak Fe-His bond and relatively negative polarity of the distal heme pocket, the lack of hydrogen bond formation between a distal residue and oxygen in heterodimeric sGC may significantly contribute to the stability of the enzyme under physiological conditions. [72-73] The CO-sGC complex on the other hand, was determined to be a six-coordinate with the Fe-His bond intact and CO bound on the distal side of the heme.[74]

More recent studies have been focused on the desensitization and conformational changes associated with sGC activation, which might involve S-nitrosation. For instance, hydrogen-deuterium exchange mass spectrometry (HDX-MS) has recently been used to map NO-induced changes in sGC surface accessibility to develop a model of the conformational changes that control sGC activity.[75]

The mechanism for sGC regulation by NO is controversial and has been suggested to involve both NO binding to the heme and a second NO binding site. The non-heme binding site seems to mediate vasodilation by acute NO signals, whereas the tight NO-heme complex mediates resting tone in the vasculature. NO has been proposed to act at the non-heme site of the enzyme in the presence of ATP and GTP, suggesting the presence of several allosteric nucleotide-binding sites that regulate NO-heme dynamics and thereby catalytic activity.[70]

Whilst the crystal structure of the full length sGC remains unknown, structures of the catalytic domain heterodimer and β-homodimer have been determined (PDB entries 3uvj and 2wz1, respectively).[71] Earlier analysis of the crystal structure of the catalytic domain of a sGC (CYC12) from the unicellular green algae *"Chlamydomonas reinhardtii"*, which shares 40 to 50 % identity with the soluble and membrane-bound GC catalytic domains, has shown that it resembles that of adenylate cyclase which was expected due to the sequence and functional similarity between them. The structure of the GC catalytic domain differs from that of adenylate cyclases primarily in the elements that connect strands and helices, and in the less-conserved C-terminal subdomains. It has been suggested that the difficulty in crystallizing GC domains in comparison to structurally-related adenylate cyclase may be due to an increased intrinsic flexibility in the GC domain.[76]

In the catalytic domain of sGC, the α- and β-subunits come together to form a head-to-tail dimer (Figure **14**). The monomers are highly similar and consist of seven β-sheets and five α-helices. The crystal structure has revealed a suble but possible important difference in the monomers. An extended β4-β5 hairpin in the α-subunit points away from the β-subunit, whilst in other cyclase structures it has been shown to be involved in interdomain contacts.[71]

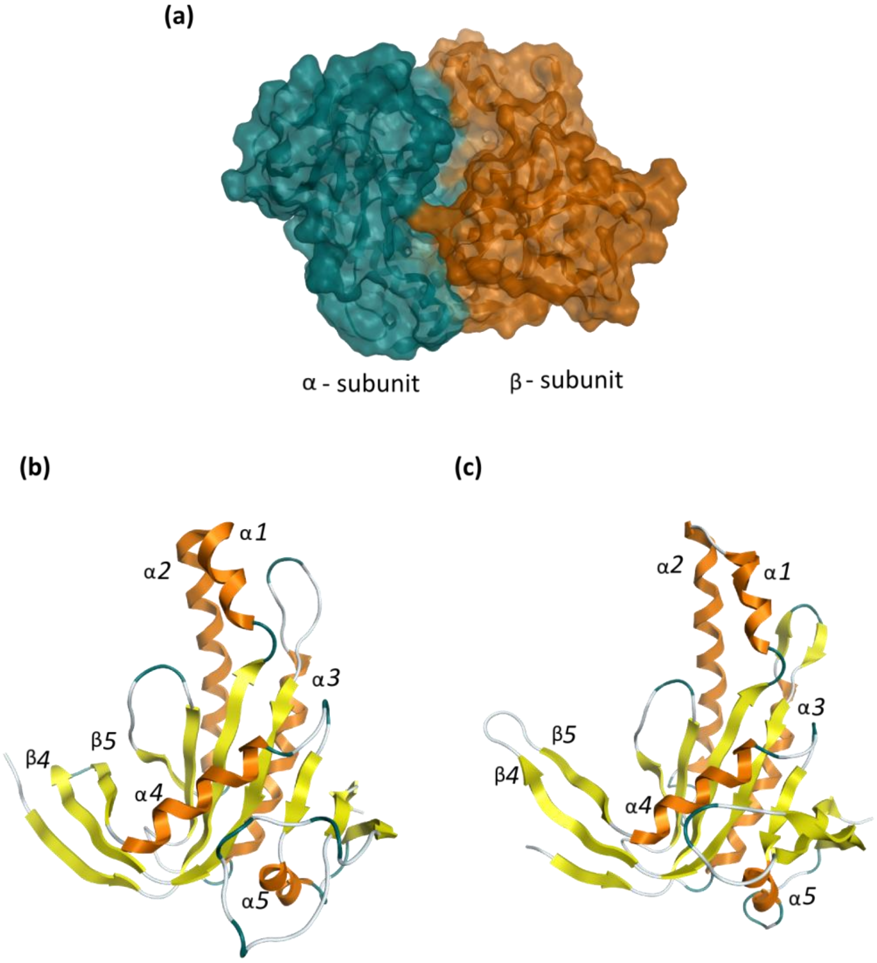

Figure 14. Overview of sGC catalytic domain heterodimer crystal structure (PDB ID: 3uvj). a) Heterodimer of sGCα and sGCβ catalytic domains; b) Architecture of the α-subunit of the GC catalytic domain; c) Architecture of the β-subunit of the GC catalytic domain. Adapted from [71]

The catalytic domain of human sGC possesses two well-defined binding sites, one site responsible for catalysis and one allosteric binding site (also referred to as the pseudosymmetric site), which is thought to be able to accommodate small molecules that control enzyme activity in a manner similar to forskolin in the binding pocket of adenylyl cyclase.[71, 77] It has also been proposed that ATP binds to both sites in sGC and inhibits sGC activity via competition with GTP, highlighting the potential for allosteric regulation of the enzyme.[59, 78-79]

1.3.2.3. Chemical biology tools for sGC

The first two chemical biology tools available to study sGC activity were YC-1 (**5**) and ODQ **4**, a stimulator and an inhibitor, respectively. There are currently two compound classes known to activate sGC by different mechanisms, one that acts in the absence of NO by replacing the heme moiety, such as cinaciguat (BAY 58-2667, **6**) and a second class of compounds such as the benzylindazole derivative YC-1 (**5**) which is thought to bind to an allosteric site and act synergistically with NO to increase cGMP production.[80-81] The inhibitor ODQ **4** acts by oxidizing sGC, leading to the formation of an NO-insensitive form of the enzyme.

sGC activators

Small molecules known to activate sGC are represented in Figure **15**. YC-1 – like sGC stimulators are heme-dependent: they stimulate sGC directly and enhance the sensitivity of the reduced enzyme to low levels of bioavailable NO. Some of these compounds are BAY 41-2272 (**7**), riociguat (BAY 63-2521, **8**), and CFM-1571 (**9**). Conversely, heme-independent compounds do not modulate NO signalling but activate the oxidized or heme-free enzyme via binding to the heme pocket and include the compounds cinaciguat **6** and HMR-1766 (**10**).

The activity of YC-1 (**5**) in the NO-sGC-cGMP pathway was first discovered in human platelets, where the compound shows an antiplatelet effect.[82] It was then shown to act synergistically with NO to increase intracellular cGMP levels in vascular smooth muscle cells where it exerts vasorelaxation.[83] YC-1 (**5**) increases the maximal catalytic rate and sensitizes the enzyme towards its gaseous activators by binding to an allosteric site on sGC molecules, thereby reducing the ligand dissociation rate from the heme group.[84-85] It was discovered that YC-1 (**5**) not only activates sGC, but also affects cGMP metabolism, as it inhibits both cGMP breakdown in aortic extracts and the activity of PDE isoforms 1 – 5 in vitro. Thus, YC-1 (**5**) is a highly effective vasodilator - It combines the functions of a classical nitrovasodilator with PDE inhibition of vasoconstriction. However, it shows relatively low potency and low selectivity.[86-87]

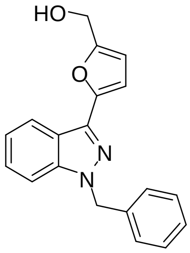

YC-1

5

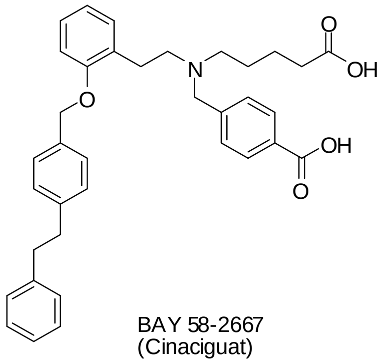

BAY 58-2667
(Cinaciguat)

6

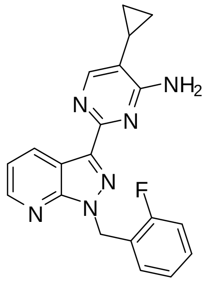

BAY 41-2272

7

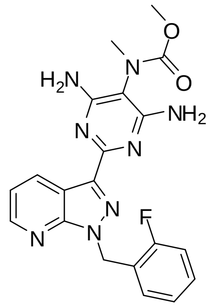

BAY 63-2521
(Riociguat)

8

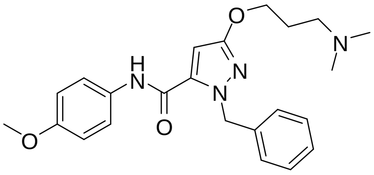

CFM 1571

9

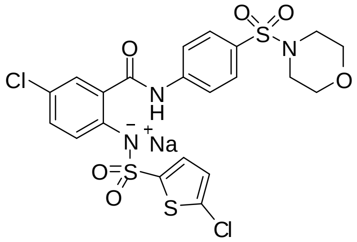

HMR 1766
(Ataciguat)

10

Figure 15. Chemical structures of known sGC activators.

YC-1 (**5**) paved the way to the design and discovery of other stimulators such as the compound BAY 41-2272 (**7**). The residues cysteine-238 and cysteine-243 region in the α1-subunit of sGC had been suggested as the target for this new type of stimulators.[88] Structure-activity relationship (SAR) data for BAY 41-2272 (**7**) revealed that several structurally related compounds relax aortic rings and reveal a long-lasting blood pressure lowering affect in rats, showing that these compounds could be valuable for the treatment of cardiovascular diseases.[89] The activity of sGC stimulators in animal models demonstrated potential therapeutic use in a range of diseases from hypertension to heart failure, artherosclerosis, restenosis, thrombosis and erectile dysfunction. Optimization of BAY 41-2272 (**7**) lead to the discovery of riociguat **8**, an sGC activator which has recently been FDA-approved for the treatment of pulmonary arterial hypertension (PAH) and persistent/recurring chronic thromboembolic pulmonary hypertension (CTEPH).[90]

The sGC activator cinaciguat **6** resulted from the optimization of a hit obtained in the screening of more than 900 000 compounds in a cell-based assay for cGMP. In contrast to the sGC stimulators which act synergistically with NO, cinaciguat **6** shows only an additive effect when combined with different concentrations of NO-donors. The mechanistic model proposed for the cinaciguat **6**-induced enzyme activation shows that the sGC prosthetic heme **11** is replaced by the compound. The 2.3 Å crystal structure of the H-NOX•cinaciguat complex of the cyannobacteria *Nostoc* (PDB entry 3l6j) has provided insights into the molecular mechanisms of sGC activation by a heme mimetic.[91] As represented in Figure **16**, at a basal state the heme group is coordinated to a histidine residue. Upon NO binding, the histidine bond is broken, leading to the conformational change necessary for enzyme activation. Cinaciguat **6** either displaces the heme or binds to the apoenzyme, activating the enzyme without NO.[80]

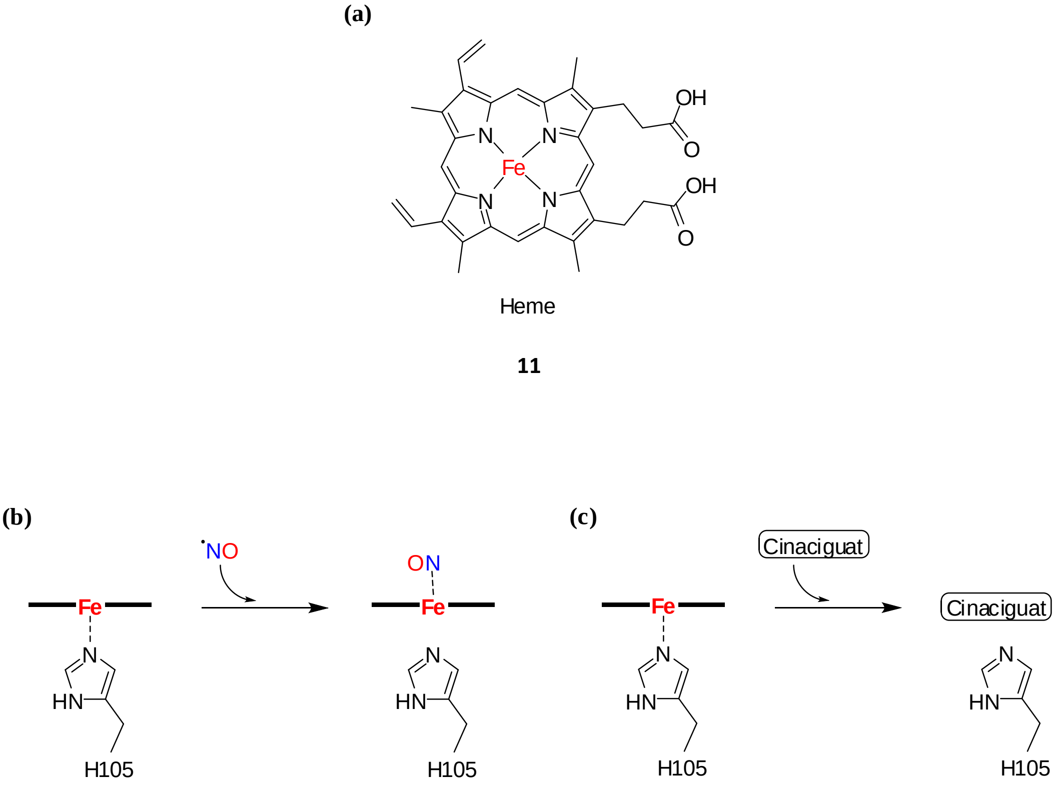

Figure 16. Mechanism of action of sGC activator cinaciguat 6. a) chemical structure of the heme in sGC; b) activation of sGC via binding of NO to the distal face of the 5-coordinated heme leads to breakage of the proximal Fe-Histidine bond; c) activation of sGC by cinaciguat 6 requires displacement of the heme such that cinaciguat 6 can now occupy the heme pocket. Adapted from Martin, F et al.[80]

During oxidative stress, common to vascular disease, sGC is desensitized and degraded upon heme loss; cinaciguat **6** activates sGC, protecting heme-oxidised sGC from degradation. Phase II clinical trials (COMPOSE programme) for acute heart failure with cinaciguat **6** were terminated due to an excess of hypotension and recruitment difficulties.[92]

sGC inhibitors

As discussed above, a great effort has been put towards the development of small molecules activators of sGC. Conversely, the availability of GC inhibitors is scarce and the available compounds act on the heme domain, rendering the enzyme unresponsive to its natural ligand, NO. ODQ **4** is one such compound and despite not being specific to the heme of sGC it has been widely used to study the function of the NO-sGC-cGMP signal transduction pathway and was a valuable tool to distinguish signal transduction events mediated by sGC from those involving other nucleotide cyclases.[93] ODQ **4** reacts with the ferrous heme of sGC to yield ferric heme, therefore not affecting the catalytic domain of sGC.[94]

Current sGC inhibitors show poor selectivity and bioavailability, as they can oxidise other heme-containing proteins such as haemoglobin.

1.4. Project aims and thesis overview

The nitric oxide receptor sGC is a known druggable target and small molecules successfully manipulate its activity by different mechanisms. Drugs can activate the enzyme either through interaction with its heme site or binding to an allosteric site, showing important responses in cardiovascular and pulmonary diseases. On the other hand, inhibition of the enzyme has shown promising results in neurodegenerative diseases and sepsis, using potent inhibitors which oxidise the heme on sGC making it unresponsive to NO. Although many advances have been made in the characterisation of NO-sGC-cGMP signalling pathways in the cardiovascular and pulmonary systems, its role and implications in the nervous system is not completely understood.

The aim of this project was to discover and characterise small molecules capable of inhibiting sGC activity through a mechanism different from that of ODQ **4**, through binding to the catalytic domain of sGC rather than the heme domain, with the view that such compounds could be used as a tool to further study the implication of sGC in neurological diseases such as PD. The approach followed for the discovery of small molecule inhibitors of sGC would include compound screening, organic synthesis, molecular modelling, and biochemical and biophysical characterisation of the compounds' activities and binding to sGC through a newly developed SPR assay.

Chapter **1** gives an overview of target-based drug discovery and the techniques being currently employed in the search of small molecule drugs. Moreover, the target of this thesis, soluble guanylate cyclase, is introduced.

A new assay was developed for assessing binding of small molecules to sGC. Thus, the SPR instrument used and the assay design approach were firstly validated using the well characterised extracellular domain of NPR-C in chapter **2**. Binding kinetics and affinity of natriuretic peptides type-A and type-C and a known antagonist could be determined and compared to literature data. This system would also be used to characterise a subset of small molecules designed as NPR-C agonists, and their binding strength analysed alongside activity data obtained *in vitro*.

In chapter **3**, the development of an SPR assay for sGC is described. This assay was validated through the characterisation of ATP and GTP binding, as well as the observation of binding competition between the nucleotides. Furthermore, the assay was used to evaluate the binding of cinaciguat **6**, YC-1 (**5**) and a new subset of sGC activators discovered through screening of a small library of YC-1- related compounds synthesised in the Selwood laboratory. The assay was developed to allow detection of binding of small molecules to the full length sGC and a construct of its catalytic domain, thus providing information regarding the domain to which the molecules bind in the enzyme.

The search for sGC inhibitors started with the screening of commercially available compounds using a radioimmunoassay to characterise their activity *in vitro*. A hit compound was selected and fully characterised for biochemical activity and binding affinity using SPR. Molecular modelling studies were carried out and a possible binding mode was investigated (Chapter **4**).

Chapter **5** presents a series of compounds analogues of the hit compound. Their design, synthesis, and characterisation with regards to sGC inhibition and binding is described.

A general discussion and conclusions can be found in chapter **6.**

Experimental methods for all chapters and spectroscopic characterisation of synthesised compounds are presented in Chapter **7**.

Chapter 2: Validation of a SPR assay using NPR-C

2. Validation of a SPR assay using NPR-C

2.1. Introduction

SPR was the biophysical technique used to characterise the interactions between small molecules and sGC. The technique had never been used with sGC, thus a new assay had to be developed. In order to validate the instrument and the assay design, a different assay was initially designed using NPR-C as target. The binding of peptides to NPR-C has been extensively characterised before, and it was therefore possible to compare SPR results with published data using different biophysical techniques.

2.1.1. NPR-C agonists

Endothelium derived CNP has been attributed cytoprotective and anti-atherogenic functions and it is now established as crucial in the regulation of vascular tone, smooth muscle relaxation, activation of leukocytes and platelets and protection against ischaemia-reperfusion injury.[95] The finding that many of the vasoprotective effects of CNP are mediated by NPR-C established this signal transduction mechanism as a target for the treatment of cardiovascular diseases. Thus, synthetic agonists of NPR-C would serve as tools for unravelling the role of CNP/NPR-C regulated pathways and could also be viewed as potential therapeutic agents.

Research at the Selwood and Hobbs groups has led to the design, synthesis, and functional characterisation of novel small molecule drug-like compounds that mimic the cytoprotective activity of CNP *in vitro* and *in vivo*.[96] Chemical biology tools used to study the activity of NPR-C are shown in Figure **17**.

This drug design process started with a pharmacophore search targeting key interaction between CNP and NPR-C of a number of databases, and guided synthesis of new compounds followed. Evaluation of the potency of these molecules was first assessed using a cell-based screening assay that measured inhibition of Ca^{2+} influx in primary mesenteric artery smooth muscle cells in response to Angiotensin II. Compounds **12** (EC_{50} = 1.8 µM) and **13** (EC_{50} = 2.8 µM) from a bromo-quinoline series showed the best activity in rat isolated mesenteric arteries and were identified as lead agonists for NPR-C. Further modifications obtained by Suzuki coupling resulted in similarly active compounds, exemplified by compound **14** (EC_{50} = 4.8 µM).

An additional assay was however required, to confirm direct binding of compounds to the receptor. In this Chapter, a SPR-based assay is described, which characterises the binding of a subset of compounds to NPR-C. The assay was developed with the extracellular domain of NPR-C and validated through the characterisation of binding of its natural ligands ANP and CNP, which show similar binding affinities to NPR-C in the picomolar range, as well as the nanomolar antagonist M372049 (compound **15**).[56, 97]

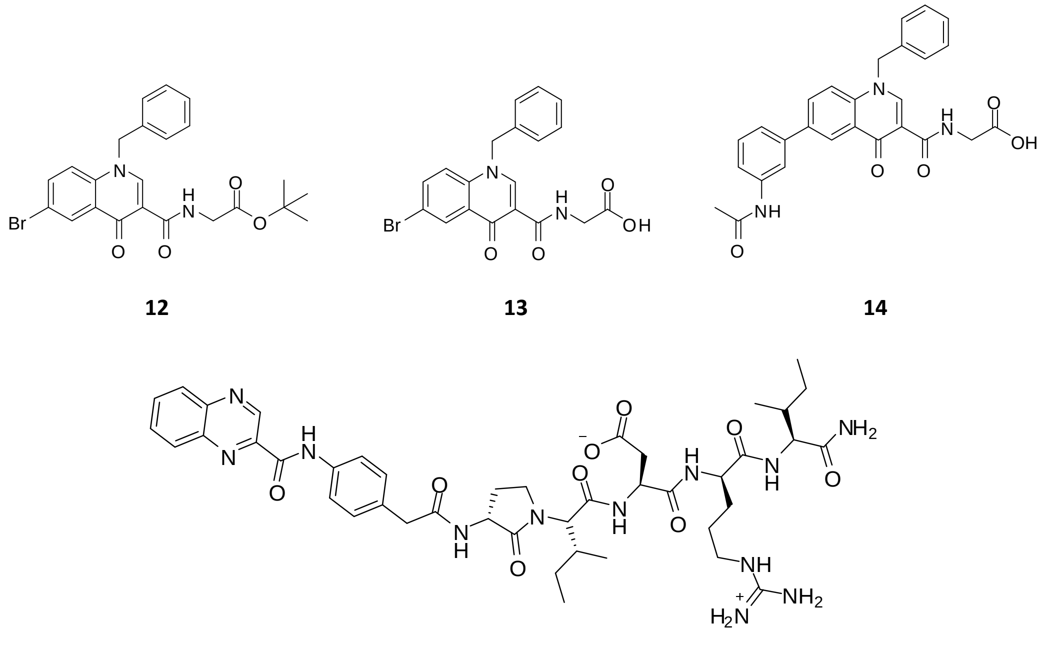

12 **13** **14**

15

Figure 17. Chemical structures of NPR-C lead agonists and antagonist M372049 (15).

2.1.2. SPR assay design

The SPR assay presented here has the advantage of detecting direct binding between the compounds and the receptor, without the need to label any of the interactants or perform competition assays.

In principle, there are two major binding experiments that can be performed by SPR to characterise drug binding: high-resolution studies give information regarding the kinetics of a drug, whilst ranking studies provide qualitative information about binding strength and are used to compare binding between compounds. The SPR signals at a single concentration are divided by the molecular weight of the compound and multiplied by 100 to give a normalised response that can be used for comparative purposes.

The homodimeric extracellular domain of NPR-C presents a number of exposed lysines, suggesting it might be possible to immobilise the protein to a chip through amine coupling. The basic steps for the assay development and key points to consider are:

- Determination of optimal pH for protein immobilisation.
- Assess if enough protein can be immobilised to give a response within the detection limits of the system and good signal to noise when analysing small molecules.
- Observation of binding with a natural ligand.
- Investigation of optimal surface regeneration conditions.
- Perform binding affinity and kinetics studies with CNP and ANP.
- Perform binding affinity and kinetics studies with antagonist compound **15.**
- Assess binding with lead compound **13**.
- Characterisation of the binding of a subset of small molecules and how do these relate to activity.

2.1.2.1. Immobilisation through amine coupling

Immobilisation of macromolecules is usually performed from dilute ligand solutions (10 – 200 µg/mL) in 10 mM buffer, generally sodium acetate. The carboxyl groups are activated with 1-ethyl-3-(3-dimethylaminopropyl)carbodiimide (EDC) and N-hydroxysuccinimide (NHS) to form an activated ester, followed by covalent attachment of ligand by its primary amines (lysines and N-terminus). The remaining esters are deactivated with ethanolamine

(Figure **18**). In order for the reaction with the activated ester to take place the molecule to be immobilised must be uncharged and brought in close proximity to the surface by a process called preconcentration – this is achieved by electrostatic attraction between the opposite charges of the amino groups in the target and the remaining carboxyl groups in the dextran. The optimal reaction rate of the EDC/NHS chemistry proceeds around pH 8 and no reaction occurs below pH 3.5. Therefore, the buffer pH for coupling must be optimised experimentally, as it needs to be lower than the isoelectric point (pI) of the protein, so that some amines are charged and attracted to the carboxylated dextran, and higher than 3.5 to enable efficient covalent attachment. Most proteins can be immobilised using a buffer pH between 4 and 5.5.

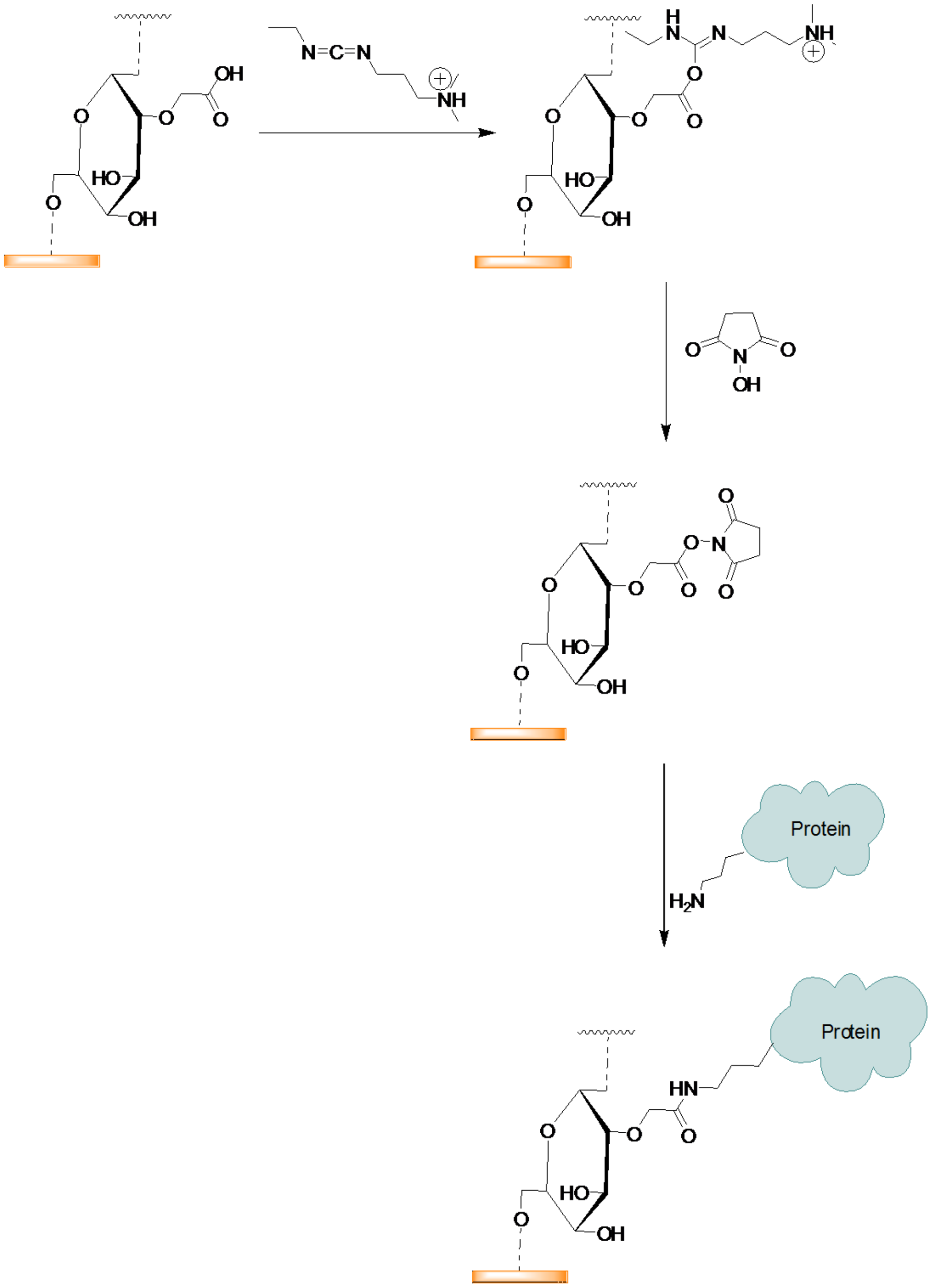

OH
O
O
HO
OH
N=C=N
NH
H
N
N
NH
Protein
H2N
HN

Figure 18. Protein immobilisation through amine coupling using EDC and NHS. The carboxyl groups at the sensor surface are activated by EDC and NHS, after which the protein can be covalently bound through the primary amines in lysine residues and the N-terminus.

2.1.3. Solubility measurements

A common problem associated with small molecule assays is that organic molecules will have different levels of solubility, which may limit their use in certain assay buffers. Generally, libraries of compounds are stored as high concentration stock solutions in dimethyl sulfoxide (DMSO), and these are diluted in the assay buffer to give a low final percentage of DMSO concentration. The Biacore system tolerates low levels of DMSO, as do most proteins. However, some compounds may still not be soluble in buffers containing only up to 5% DMSO and may give false results in the SPR assay if assay plates and sensorgrams are not correctly examined.

The U.S. Pharmacopeia (USP) uses seven different expressions to define solubility, from very soluble to practically insoluble (Table **2**).[98]

Table 2. The USP definition of solubility.

Description forms (solubility definition)	Parts of solvent required for one part of solute	Solubility range (mg/ml)	Solubility assigned (mg/ml)
Very soluble (VS)	<1	>1000	1000
Freely soluble (FS)	From 1 to 10	100–1000	100
Soluble	From 10 to 30	33–100	33
Sparingly soluble (SPS)	From 30 to 100	10–33	10
Slightly soluble (SS)	From 100 to 1000	1–10	1
Very slightly soluble (VSS)	From 1000 to 10,000	0.1–1	0.1
Practically insoluble (PI)	>10,000	<0.1	0.01

Previous studies with the NPR-C agonists described here had suggested a difference in solubility between the most active compounds **12** and **13**, which could have an influence in the biological results obtained. An assay was developed to determine the equilibrium/thermodynamic solubility of compounds as shown in Figure **19**. The protocol is based on the traditional shake flask method and uses LC-MS as the analytical tool to determine the concentration of the compounds in a saturated solution at equilibrium. The diode array detector is used to quantify the compound by peak integration and the MS trace is used to confirm peak identity.

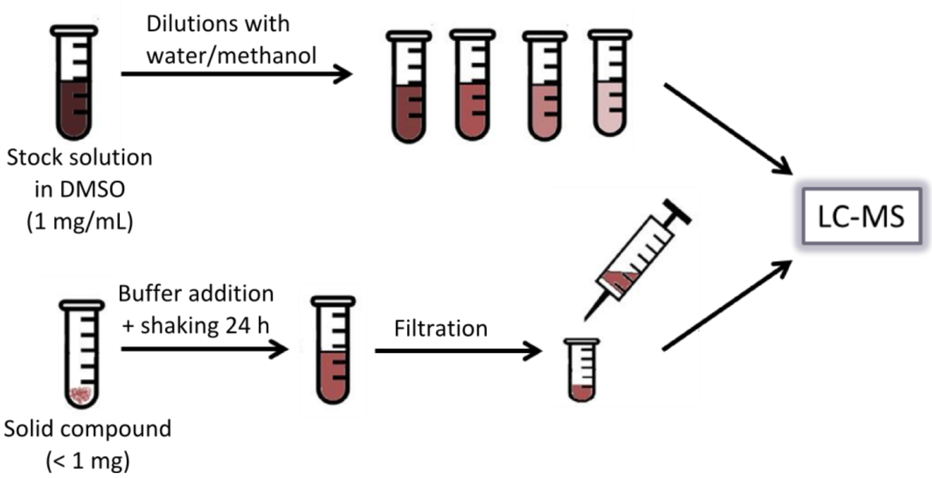
Dilutions with water/methanol
Stock solution in DMSO (1 mg/mL)
LC-MS
Buffer addition + shaking 24 h
Filtration
Solid compound (< 1 mg)

Figure 19. General setup for equilibrium solubility measurements. A stock solution is made up in DMSO to a concentration of 1mg/mL and diluted with water:methanol for the generation of a calibration curve by LC-MS: the MS trace is used to confirm peak identity and the UV-DAD for peak quantification. Aqueous buffer is added to a sample of solid material (0.6 to 0.9 mg) and the solution is shaken for 24 h, filtered to remove undissolved compound, and the concentration of the sample solution is quantified by LC-MS using the calibration curve.

2.2. Results and Discussion

2.2.1. SPR assay

2.2.1.1. Immobilisation

The calculated pI of the extracellular domain of NPR-C is 5.9. Protein solutions of 30 µg/mL were prepared in 10 mM sodium acetate buffers of different pH: 4, 4.5, 5, and 5.5. The protein was brought into contact with the sensor chip surface using a contact time of 2 min, after which it was washed off injecting a short pulse of 50 mM NaOH (Figure **20a**). It was observed that the lower the pH of the sample the higher the amount of preconcentrated protein. Generally, the preconcentration step must give a relative response two times higher than the targeted immobilisation level, since not 100 % of the biomolecules attracted to the surface will be successfully immobilised. At pH 5 and 5.5 the relative response obtained was only 7.6 and 5.1 kRU, respectively. Therefore, the conditions for immobilisation were decided as 30 µg/mL NPR-C in 10 mM sodium acetate pH 4.5, which gave a preconcentration of 11.7 kRU.

The sensor chips used in the Biacore T200 are made of four flow cells where interactions can occur. Generally, they are used as pairs and one is used as a reference and the other is the active flow cell, where the interactions in the reference flow cell can be either unmodified or chemically modified as in the active flow cell, but without addition of the biomolecule to be immobilised. This cell is used to control non-specific binding to the surface as well as bulk responses obtained from changes in the refractive index of the samples injected. In this case, the reference cell was chemically modified with amine coupling reagents, in a process called blank immobilisation (Figure **20b**). Treatment of the active flow cell (Figure **20c**) starts with preconcentration of NPR-C at the surface so the system estimates the amount of sample to be injected to reach the aimed immobilisation level (1); the surface is then washed with 50 mM NaOH to remove any protein aggregated at the surface (2); the carboxyl groups of the dextran matrix are activated with a mixture of EDC and NHS (3) and then serial injections of the NPR-C sample are performed until the aimed immobilisation level is reached (4); blocking of any remaining activated esters is performed with ethanolamine (5).

(a) pH scouting

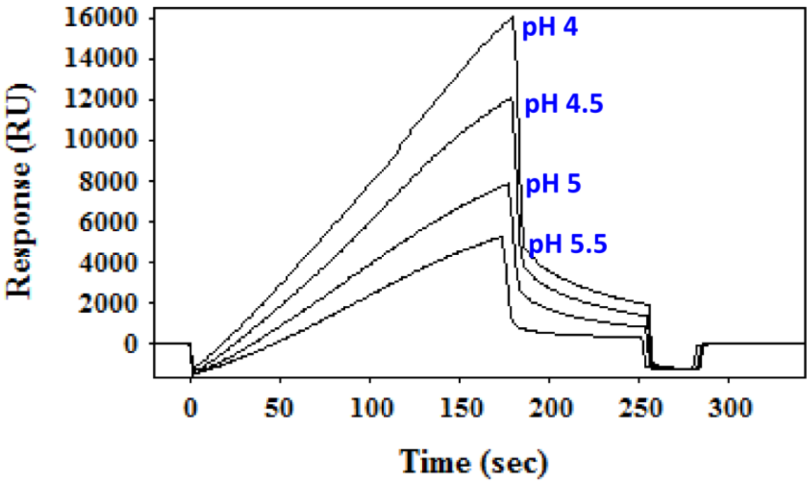

(b) Reference flow cell

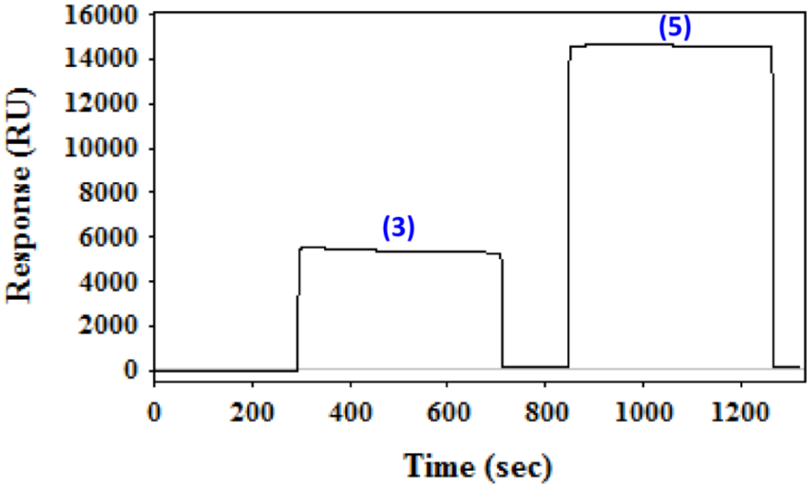

(c) Active flow cell

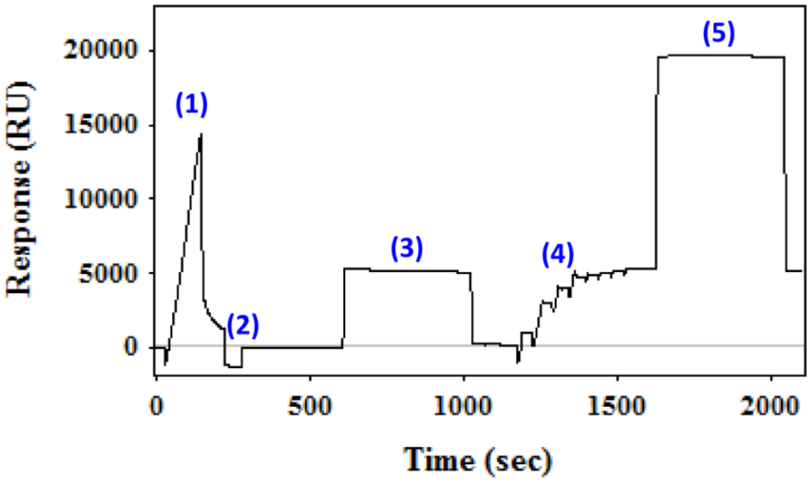

Figure 20.Sensorgrams showing the immobilisation of NPR-C. (a) pH scouting; (b) blank immobilisation on reference flow cell; (c) Amine coupling immobilisation in active flow cell; where: 1) NPR-C pre-concentration; 2) wash with NaOH; 3) EDC/NHS activation; 4) binding of NPR-C; 5) blocking with ethanolamine.

2.2.1.2. Surface testing

In order to assess if NPR-C remains active after immobilisation, a test was performed using a high concentration of CNP. First, a blank injection was performed using the assay buffer, followed by a 500 nM CNP injection, both using a contact time of 60 sec followed by 120 seconds of undisturbed dissociation. The sensorgrams in Figure **21** have been zeroed so that the response in RU in the y-axis is relative to the baseline before injection and the time in the x-axis starts from zero at the time of injection. Figure **21a** shows the bulk response obtained in the reference flow cel (fc1), where the blue line corresponds to the binding of CNP and the orange to the blank sample. The evaluation software allows the subtraction of the response obtained in the reference flow cell (fc1) (Figure **21a**) from the active flow cell (fc2) (Figure **21b**), and a reference subtracted sensorgram such as the one in Figure **21c** is generally used throughout the whole thesis, unless stated otherwise. The blank sample serves also as a negative control for binding, which can be subtracted from the sensorgram if a bulk response is observed. The resulting sensorgram is therefore a double-referenced sensorgram, to represent a more realistic binding which excludes the bulk response and noise given by the assay buffer.

If all binding sites of NPR-C were accessible the R_{max} for CNP would be 91 RU. The double-referenced binding response obtained with CNP gave 72 RU, which indicates 80 % of the binding sites are accessible and occupied.

(a) Reference flow cell (fc1)

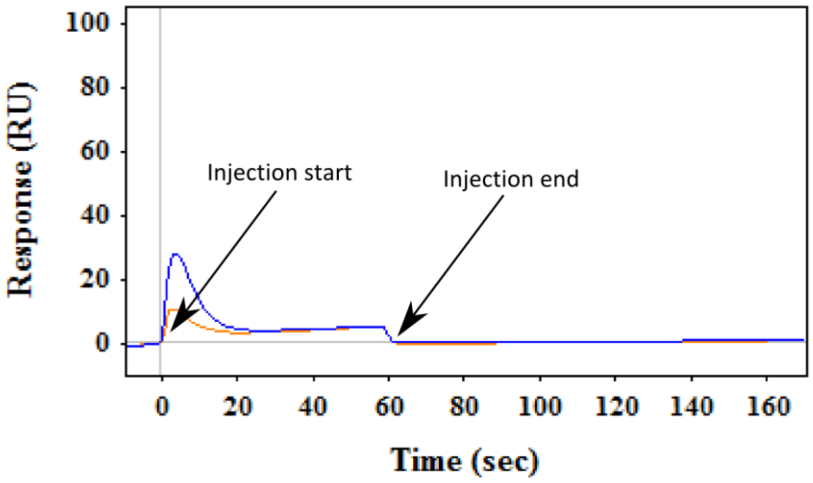

(b) Active flow cell (fc2)

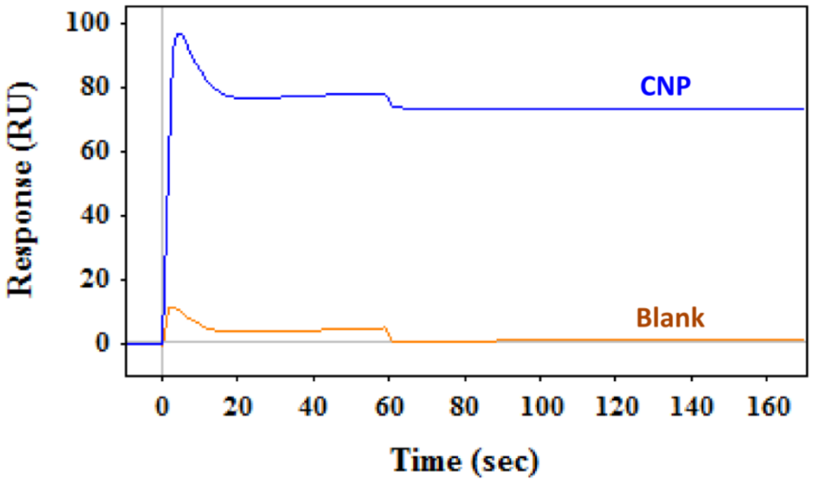

(c) Reference subtracted (fc2 - fc1)

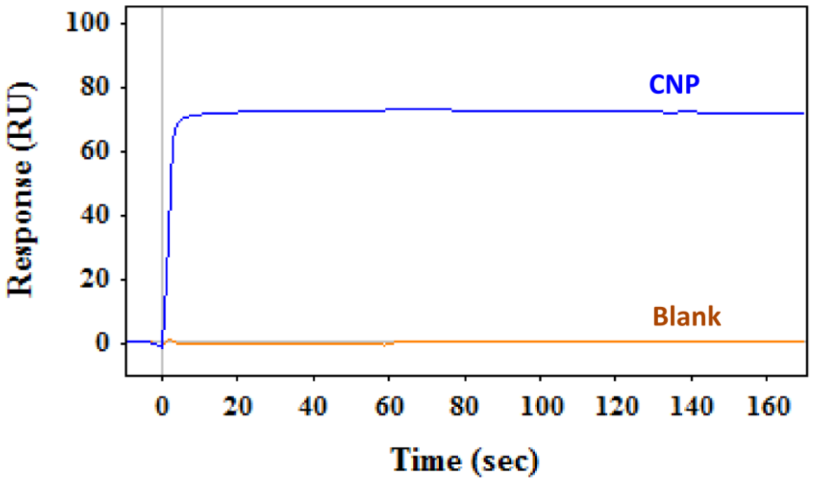

Figure 21. Sensorgrams showing CNP binding to NPR-C. (a) Reference flow cell; (b) Active flow cell; (c) Reference subtracted sensorgram.

2.2.1.3. Surface regeneration

Regeneration of the surface is not always necessary. If the analyte dissociates quickly enough, all analyte may be removed within a reasonable time simply by washing the surface the assay buffer. This is evident by observation of the sensorgram, since the response returns to baseline after the sample injection.

CNP shows a very slow dissociation from NPR-C, after 10 min of buffer flow no decrease in response units was observed. Thus, regeneration of the surface was necessary for it to be reused. Regeneration scouting of the NPR-C surface was performed by testing six repeated cycles of CNP binding at 1 nM and regeneration. The results are summarised in Figure **22**. The solutions tested were 10 mM glycine-HCl at pH 1.5, 2, and 3, 50 mM NaOH, and 1 M NaCl. The results were assessed in terms of trends in analyte response and baseline level. Glycine-HCl solutions failed to successfully regenerate the surface (Figure **22a–c**). As a general trend, these solutions failed to remove bound CNP as shown by an increase in baseline level and decrease in CNP binding. 50 mM NaOH damaged the NPR-C surface, CNP did not bind after a first contact of the protein with NaOH and the baseline level decreased, indicating these conditions were too harsh for regeneration (Figure **22d**). The use of 1 M NaCl as a regeneration solution showed the best results as CNP binding remained constant, and only a small increase in the baseline level was observed (Figure **22e**). This was therefore the solution chosen for regeneration of the NPR-C surface.

(a) Glycine-HCl pH 3

(b) Glycine-HCl pH 2

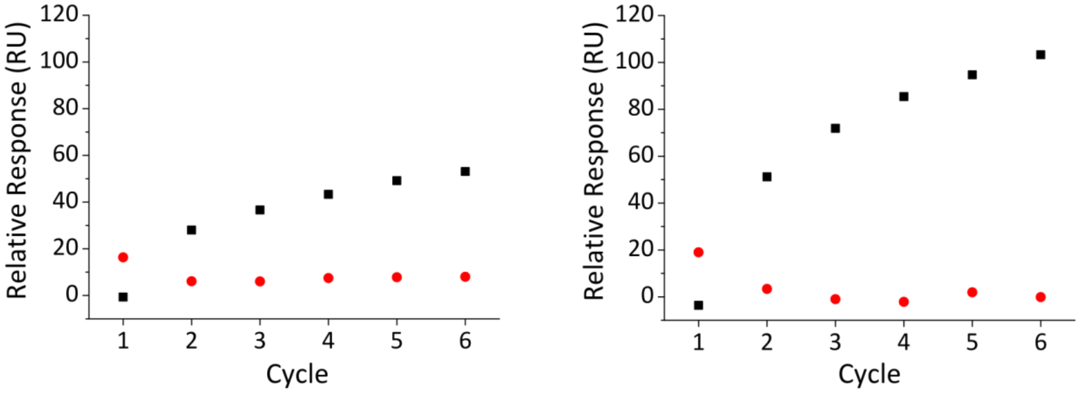

(c) Glycine-HCl pH 1.5

(d) 50 mM NaOH

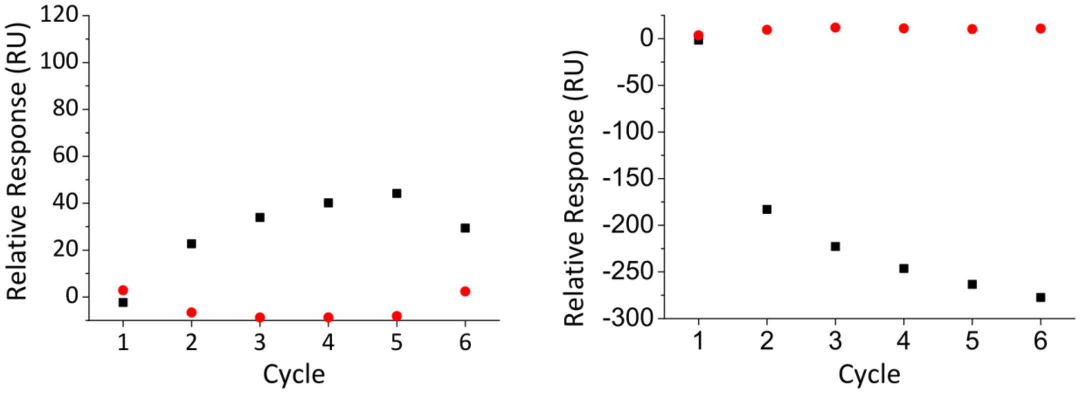

(e) 1 M NaCl

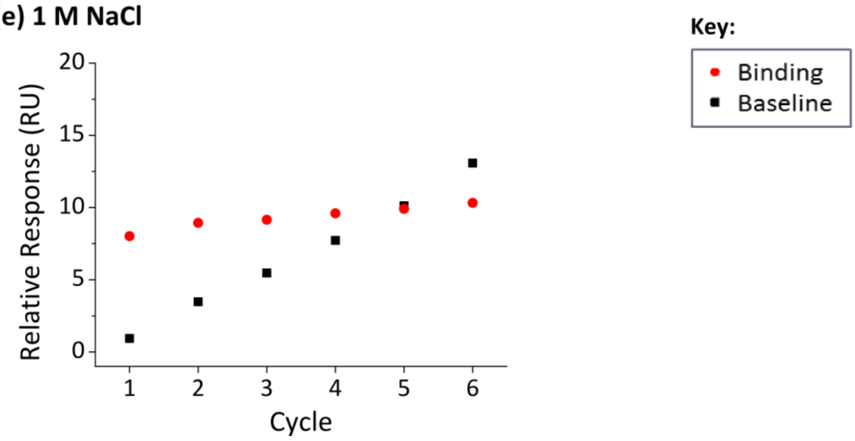

Figure 22. Regeneration conditions scouting. Binding and baseline levels of six samples monitored upon regeneration with (a) glycine – HCl pH 3; (b) glycine – HCl pH2; (c) glycine – HCl pH 1.5; (d) 50 mM NaOH; (e) 1M NaCl.

2.2.1.4. Binding interactions

Binding of natriuretic peptides

The kinetics of binding of CNP and ANP was determined using the single-cycle kinetics application of Biacore. A series of five injections of each peptide was performed at increasing concentrations (0.25, 0.50, 1, 2, and 4 nM) for 240 seconds each. Upon the last injection at 4 nM the binding had reached saturation and dissociation from the surface was monitored for 3600 seconds (Figure **23**). The association (k_a) and dissociation (k_d) rates were determined by the BIAevaluation software, using a 1:1 binding model, and the dissociation constant (K_D) was determined by dividing K_d by k_a(Table **3**). Affinity of the peptides to NPR-C measured by SPR is in the picomolar range, as expected considering the results previously obtained in cell measurements[97] and the main function of the receptor as a clearance receptor for natriuretic peptides, which upon binding leads to endocytosis.

Table 3. Kinetics of natriuretic peptides and antagonist binding to NPR-C. where K_a is association rate, k_d is the dissociation rate, K_D is the equilibrium binding constant, and SE is the standard error)

Compound	k_a (1/Ms)	SE (k_a)	k_d (1/s)	SE (k_d)	K_D (M)
CNP	4649089	28183.75	1.57E-05	6.68E-08	3.38E-12
ANP	18523324	321171.6	9.7E-05	1.4E-06	5.24E-12
M372049 (**15**)	6333821	96884.88	0.035691	0.000591	5.63E-09

(a) CNP

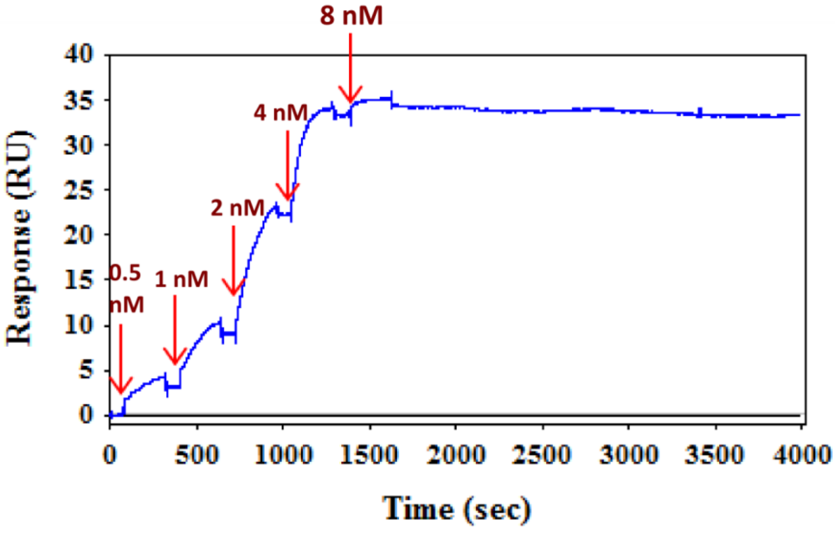

(b) ANP

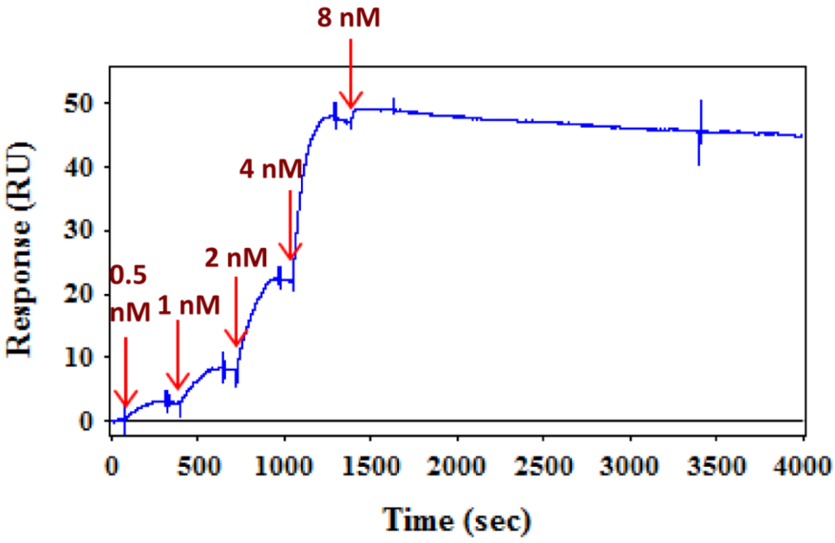

Figure 23. Single-cycle kinetics of CNP (a) and ANP (b). The arrows indicate the time points at which the peptide was injected into the flow cell and at which concentrations.

Binding of M372049 (15)

Having validated the SPR assay for binding of two of its biological ligands, the technique was tested for the binding of known antagonist M372049 (**15**), which inhibits NPR-C activity in nanomolar concentrations. Its binding to the receptor was measured as having an affinity in the range of 6 nM. At low concentrations (0.9 to 7.5 nM) association of the compound to the receptor was slow and did not reach equilibrium after 240 seconds, whilst at concentrations of 15 nM and higher binding equilibrium was observed after 60 seconds. Full dissociation of the compound was observed, as curves returned to baseline without the need for a regeneration solution (Figure **24b**).

The activity of M372049 (**15**) is thought to be due to competition with CNP for binding to NPR-C, which was confirmed in this assay. A simple competition experiment was performed in which the binding of the antagonist and the natriuretic peptide was measured separately as well as in a mixture sample. An overlay of the sensorgrams for binding of CNP at 15 nM, M372049 (**15**) at 30 nM, and a mixture of the two shows that when both compounds are present in solution, the resulting binding is less than the sum of the individual binding curves, indicating binding competition (Figure **24c**).

(a) Chemical structure of M372049

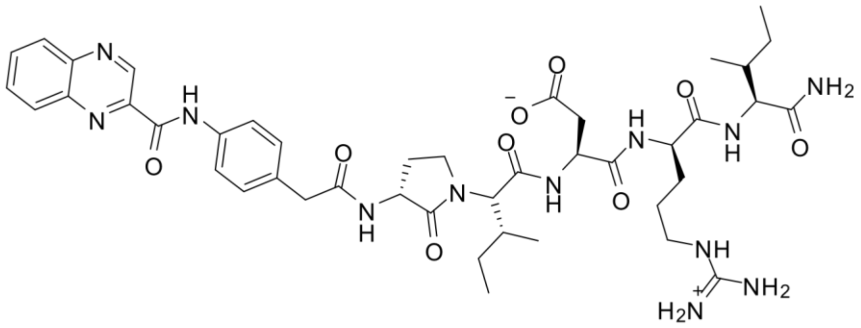

N
N
H
N
O
O
N
H
O
N
O
O
O
H
N
O
H
N
O
H
N
NH2
O
NH
NH2
H2N

(b) Binding of M372049

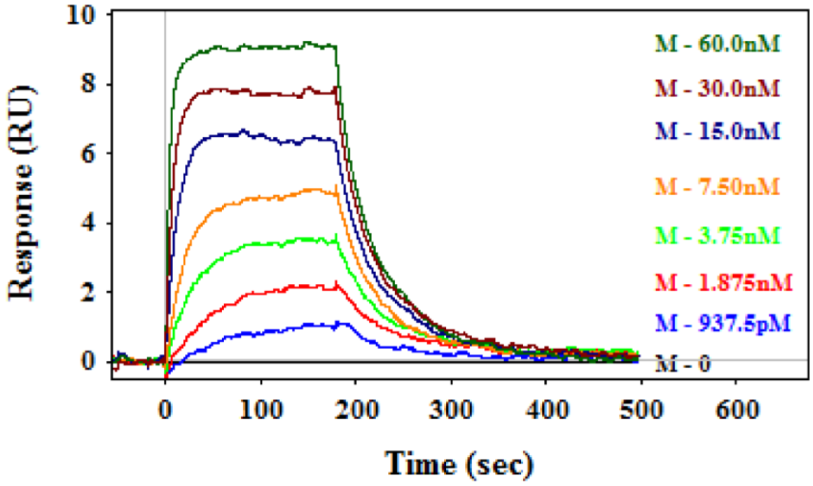

(c) M372047 and CNP competition

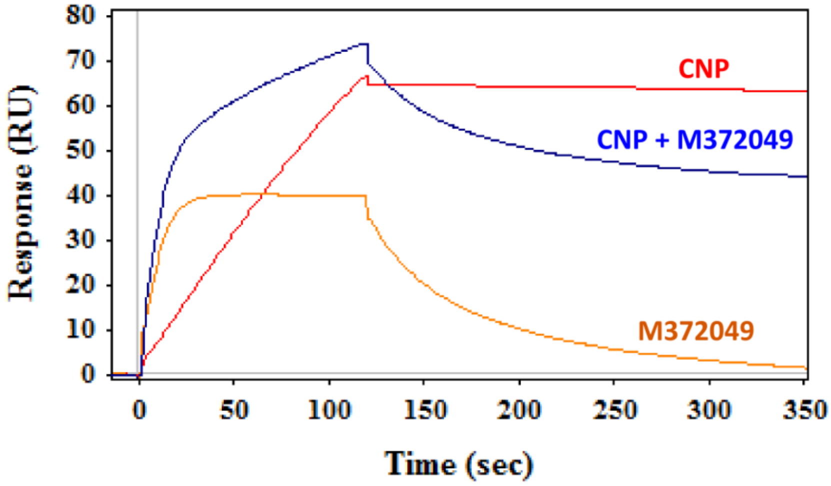

Figure 24. Sensorgrams of M372049 (15) binding to NPR-C. (a) Concentration-dependent binding (0.9 to 60 nM); (b) Binding competition between M372049 (**15**) (30 nM) and CNP (15 nM).

Binding of agonists

A subset of compounds was selected from a library designed and synthesised by former members of the Selwood group and their binding strength to NPR-C was tested (Table **4**). For binding rankings, stock solutions of 50 mM in DMSO were diluted to a final concentration of 5 % DMSO in assay buffer. These solutions were injected in triplicates for 30 seconds, allowing further 30 seconds of undisturbed dissociation. Steady-state binding signals were divided by the compounds molecular weight and multiplied by 100, to give a molecular weight normalised response. Average values from triplicate injections were ranked according to their normalised SPR signal (Figure **25**). Finally, the shape of each binding curve was examined as exemplified in Figure **26**.

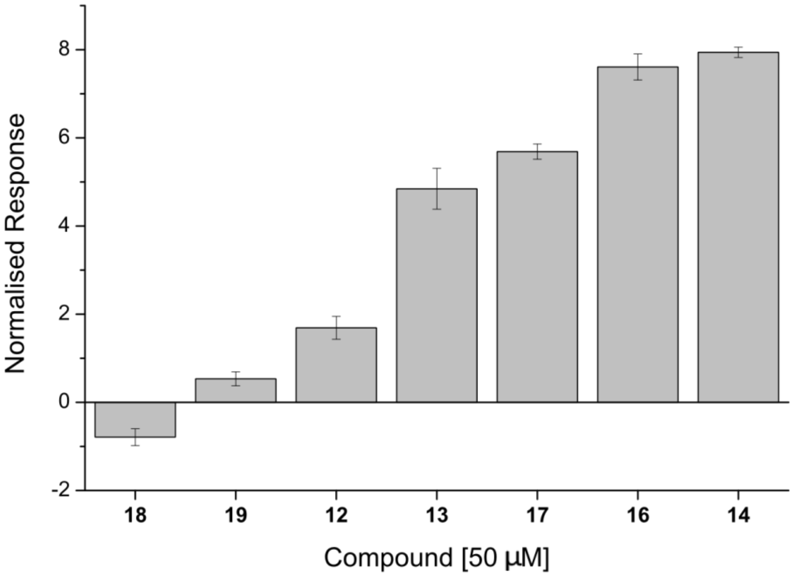

Figure 25. Ranking of NPR-C agonists binding to NPR-C.

Table 4. SAR of NPR-C small molecule agonists.

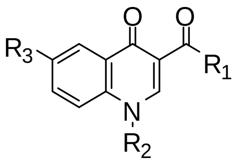

Compound	R1	R2	R3	% inhibition of Ang II-induced Ca^{2+} flux (compound [1μM])[*]
CNP	-	-	-	100 ± 0
12	Gly-OtBu	Bn	Br	100 ± 0
13	Gly	Bn	Br	95 ± 3
16	Gly	Bn	H	87 ± 4
17	Val	Bn	Br	80 ± 7
18	Val-OtBu	Bn	H	12 ± 4
19	Phe-OtBu	Bn	Br	27 ± 4

Compounds **18** and **19** showed mild or no activity as NPR-C agonists, and they also failed to bind significantly to the receptor (. The most active compounds **12** and **13** appear to show different binding behaviour, with **13** showing significantly higher binding strength. It was noticed however that compound **12** precipitated in solution, so the binding observed does not correspond to 50 μM. A follow-up study of the solubility of this compound can be found in section **2.2.2.**

Introduction of a valine residue in place of the glycine in R1 did not show significant changes in the binding of compound **17** in comparison to **13**, and causes only a small decrease in activity. Removal of the bromide in the R3 position gave compound **17**, which retains some activity as an NPR-C agonist and shows high binding to the receptor.

---

[*] Data obtained from Prof. Adrian Hobbs

Compound **14** showed apparent strong binding to the receptor. However, the binding did not reach equilibrium and the curve does not return to the baseline after dissociation. This behaviour is characteristic of non-specific binding and can be detected by observation of the binding sensorgrams (Figure **26b**).

The sensorgrams of compounds that bind to NPR-C show very fast association and dissociation, as represented by the curve given by compound **13** in Figure **26c**. Concentration-dependent binding was observed but binding saturation was not achieved when using concentrations up to 150 µM (Figure **27**). Thus, it was not possible to obtain association and dissociation kinetics or equilibrium binding affinity data.

(a) Compound 12

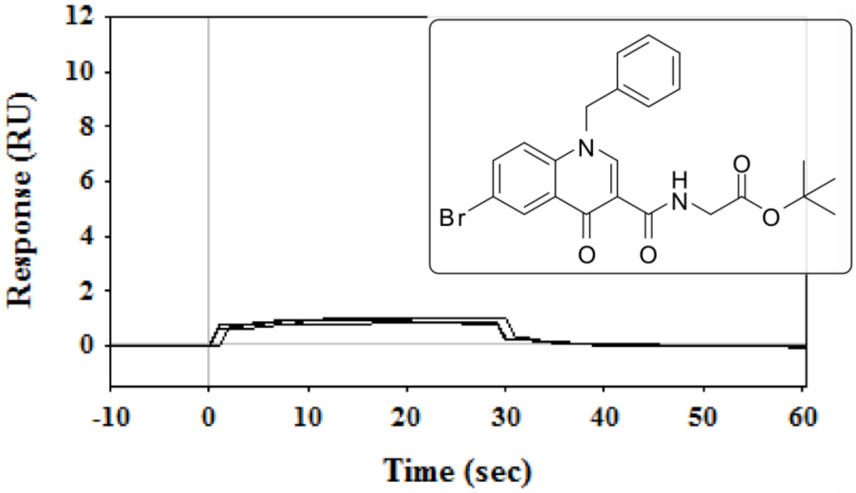

(b) Compound 14

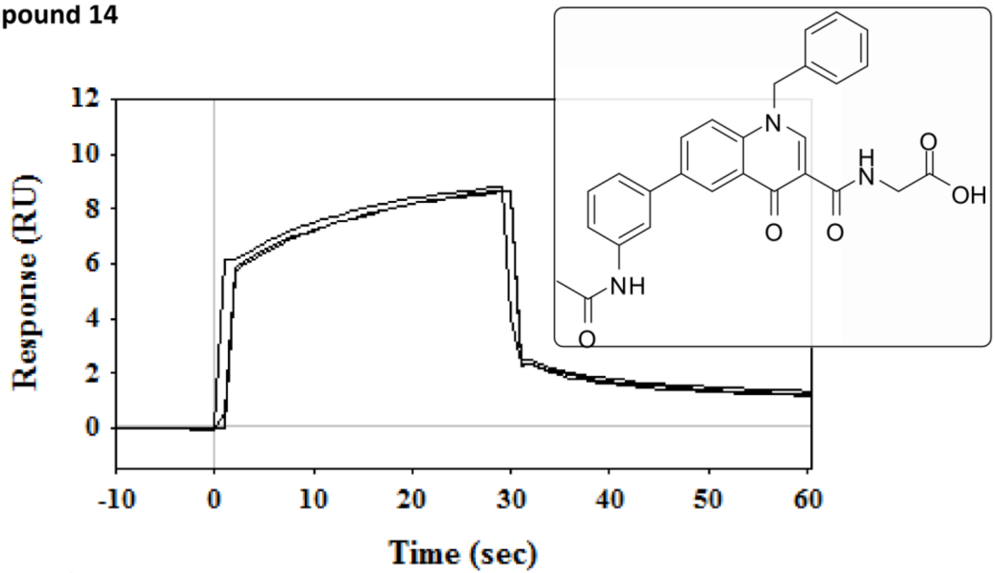

(c) Compound 13

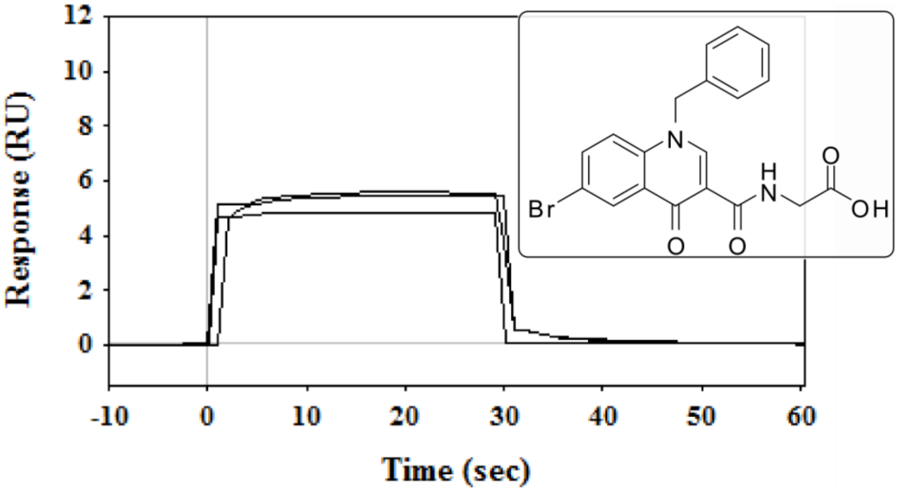

Figure 26. Examples of NPR-C agonist binding sensorgrams. Three categories of binding can be distinguished: (a) no binding – compound **12**; (b) binding plus non-specific binding – compound **14**; (c) specific binding – compound **13**.

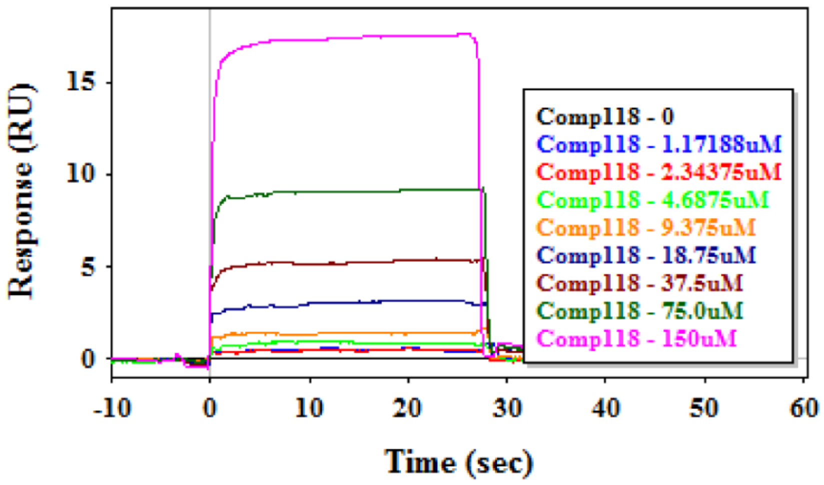

Figure 27. Sensorgram of concentration-dependent (1.2 to 150 µM) binding of compound 13.

DMSO correction

The antagonist M372049 (**15**) and the small molecule agonists were obtained in stock solutions in 100 % DMSO, and diluted to a final concentration of 5 % DMSO in buffer, in order to match the concentration of DMSO present in the instrument buffer used. However, small differences in DMSO concentration between samples can cause huge changes in the bulk signal intensity, therefore compromising the accuracy of the data obtained. In order to account for these differences in signal, a calibration procedure can be performed by measuring the binding of standard solutions of a range of DMSO concentrations, and then plotting the difference in signals between active and reference cell against the signal on the reference cell, fitting the data using linear regression. This function is already incorporated in both Srubber and BIAevaluation softwares. Sensorgrams and binding data presented here were therefore obtained after applying DMSO corrections.

2.2.2. Solubility Measurements

Some compounds showed poor solubility in the assay buffer, even in the presence of 5 % DMSO and detergent, and solid could be seen at the bottom of the wells in the assay plates after the experiments. This behaviour not only limits the characterisation of these compounds in the presented assay but also indicates their poor solubility may limit their use in further drug development.

The phosphodiesterase 5 (PDE5) inhibitor sildenafil **20** is only slightly soluble in water, has high membrane permeability and relatively low bioavailability after oral administration. It has been developed as a salt form such as sildenafil citrate, which improves solubility but still has a relatively low absolute bioavailability of about 40 % and late onset of action.[99] sildenafil citrate was used in this experiment so that the NPR-C agonists can be compared to a drug of known low solubility.

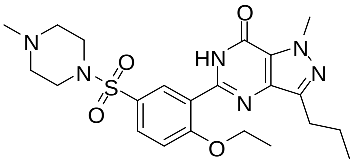

Sildenafil

20

Figure 28. Chemical structure of sildenafil 20.

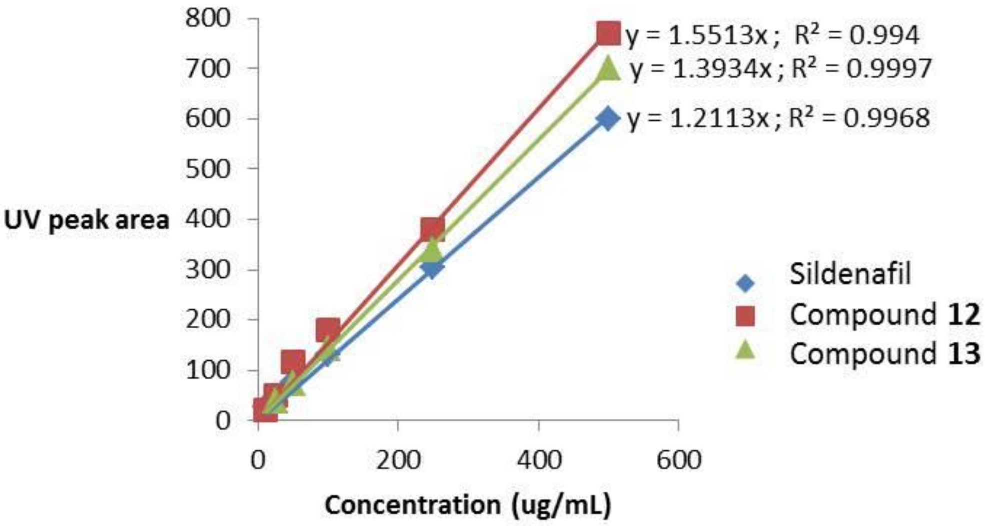

Figure 29. Solubility calibration curves for sildenafil 20 and compounds 12 and 13.

The solubilities of sildenafil **20** and compounds **12** and **13** were measured in aqueous buffer. Standard calibration curves were obtained (Figure **29**) and the solubility of the compounds measured in 10 mM PBS at pH 7.4. The solubility of sildenafil **20** in 10 mM PBS pH 7.4 was determined as 25.9 µg/mL, which puts it in the category of practically insoluble (PI). The solubility of compound **12** is below the lower limit of detection and could not be measured – by visual inspection, the compound remains in suspension in buffer throughout the 24h shaking process. In comparison, the solubility of the acid analogue **13** was calculated as 491.6 µg/mL, putting it one grade above sildenafil in qualitative terms, as very slightly insoluble.

Table 5. Calculated solubility of sildenafil 20 and compounds 12 and 13.

Compound	UV peak area	Solubility (µg/mL)	Solubility (µM)
Sildenafil	31.4	25.9	0.04
12	Not detected	<10.0	<0.02
13	685	491.6	1.18

2.3. Summary

NPR-C signalling through CNP binding has been shown to regulate vascular homeostasis, which can be inhibited by M372049 (**15**), an NPR-C antagonist. The Selwood group has developed a series of drug-like small molecules which mimic CNP activity and serve as NPR-C agonists in the absence of CNP. An SPR assay was developed in which the extracellular domain of NPR-C can be immobilised onto a CM5 sensor chip though amine coupling. The system has been validated by analysing the binding behaviour of natriuretic peptides type-C and type-A to the receptor, as well as its known antagonist. Their binding kinetics and affinity were determined and binding competition was observed between CNP and M372049 (**15**), confirming the activity of the antagonist is through binding to the CNP site, as originally designed. Binding of a subset of NPR-C agonists was measured as well, and observation of the sensorgrams allows the characterisation of these compounds as binding, non-binding, and binding non-specifically. Some compounds showed poor solubility in the assay buffer, limiting their characterisation in this assay. Equilibrium solubility of compounds **12** and **13** was determined alongside sildenafil **20**, a PDE5 inhibitor with poor solubility and bioavailability. It was not possible to determine the solubility of compound **12** as it was below the lower limit of the detection of the LC-MS instrument used. Compound **13** showed better solubility and should consequently be the agonist used for follow-up studies.

The SPR assay developed in this chapter provided data which is comparable to literature information about NPR-C behaviour. Thus, the experiments presented serve to validate the SPR instrument and methodology employed in the assay design.

Chapter 3: Discovery and characterisation of drug-like sGC activators

3. Discovery and characterisation of drug-like sGC activators

3.1. Introduction

3.1.1. The binding mode of sGC activators

There are currently two compound classes known to activate sGC by different mechanisms, one that acts in the absence of NO by replacing the heme moiety, such as cinaciguat **6** and a second class of compounds such as the benzylindazole derivative YC-1 (**5**) which is thought to bind to an allosteric site and act synergistically with NO to increase cGMP production.[91] YC-1 (**5**) is also capable of inhibiting sodium channels in a voltage-dependent manner, and it was used as the starting point for the design of a library of sodium channel modulators.[82, 100-101] Thus, cross-screening of this library of compounds against sGC was performed.

The mechanisms by which small molecules activate enzymes differ in many ways from those that apply to inhibitors and it can be challenging not only to discover activators but also to understand their mode of action. Activators commonly bind to an allosteric binding site and require lower doses than inhibitors to cause an effect.[102] Current biochemical characterisation of sGC modulation by small molecules is performed by measuring cGMP levels by radioimmunoassays and biophysical characterisation of the enzyme can also be performed using spectroscopic methods such as Raman spectroscopy and electron paramagnetic resonance.[73, 103] These methods provide a great deal of information regarding the activity of the enzyme in the presence and absence of small molecules, but give limited evidence about the binding strength and binding sites of these molecules. A biophysical method such as surface plasmon resonance would allow the detection of direct binding of small molecules to sGC and would complement the biochemical characterisation of such compounds.

3.1.2. SPR assay design

The large heterodimeric structure of sGC can make it particularly challenging to detect binding of low molecular weight compounds using SPR. Whilst higher concentrations of protein on the sensor chip provide a higher signal to noise ratio, a denser surface is also prone to higher non-specific binding and hindrance of the binding site. We evaluated if a construct of the α1β1 catalytic domain of sGC could be used as a model for the detection of binding to sGC. The catalytic domain of sGC (sGCcat) is easier to manipulate in an SPR assay as its smaller size (~50 kDa) allows the use of a less dense surface (lower immobilisation level), which reduces steric effects and non-specific electrostatic binding whilst still providing a high enough signal to noise ratio. Furthermore, comparison of binding between full-length and sGCcat would allow the determination of the domain to which the compounds are binding.

The assay development steps were similar to the ones described in chapter **2**, section **2.1.2**. Validation of the assay could be performed using ATP and GTP, and the use of both protein constructs would confirm whether the compounds are binding to the catalytic domain of the enzyme or not.

3.2. Results and Discussion

3.2.1. Screening for sGC activators

The screening of the library of YC-1 (**5**) analogues took place in two phases: the library was firstly virtually screened for compounds with certain substructures; followed by a biochemical evaluation of their activity.

3.2.1.1. Virtual screening

Virtual screening was performed using Pipeline Pilot, a program that allows the search, analysis and generation of data in numeric, textual, chemical, or biological formats using a range of scripts and filters, and integrating various other programs. This allows data to be input into a pipeline in a certain format and retrieved in another format of choice. The protocol used in this screening is shown in Figure **30**. A small database of 41 compounds was input into the pipeline and compounds that did not pass the Lipinski's rule of five were filtered out. Three substructure searches were followed.

Some compounds virtually selected were not physically available. Those available were subsequently evaluated for biological activity. The core structure of these compounds is made of an indazole substituted in the 3-position with a 1,2,4-oxadiazole. The main variations in the selected compounds were the substituent groups in the N1 and N2 positions of the indazole (R1) and the groups in the 3-position of the oxadiazole. The first substructure search retrieved compounds which had a free amine group in the 3-position of the oxadiazole and a benzyl group in the N1 position of the indazole. This search resulted in compounds **21**, **23**, and **25**, which vary only in the groups and positions of substituents in the benzyl group. The second search retained the free amine group in the oxadiazole and allowed a greater variation at N1 and N2 of the indazole, resulting in compounds **22**, **24**, **26**, **27**, and **28**. Finally, more diversity was allowed by selecting compounds with a tert-butyl carbamate group in the 3-position of the indazole and further substituents in the benzyl group at N1 of the indazole, of which compounds **29** and **30** were available.

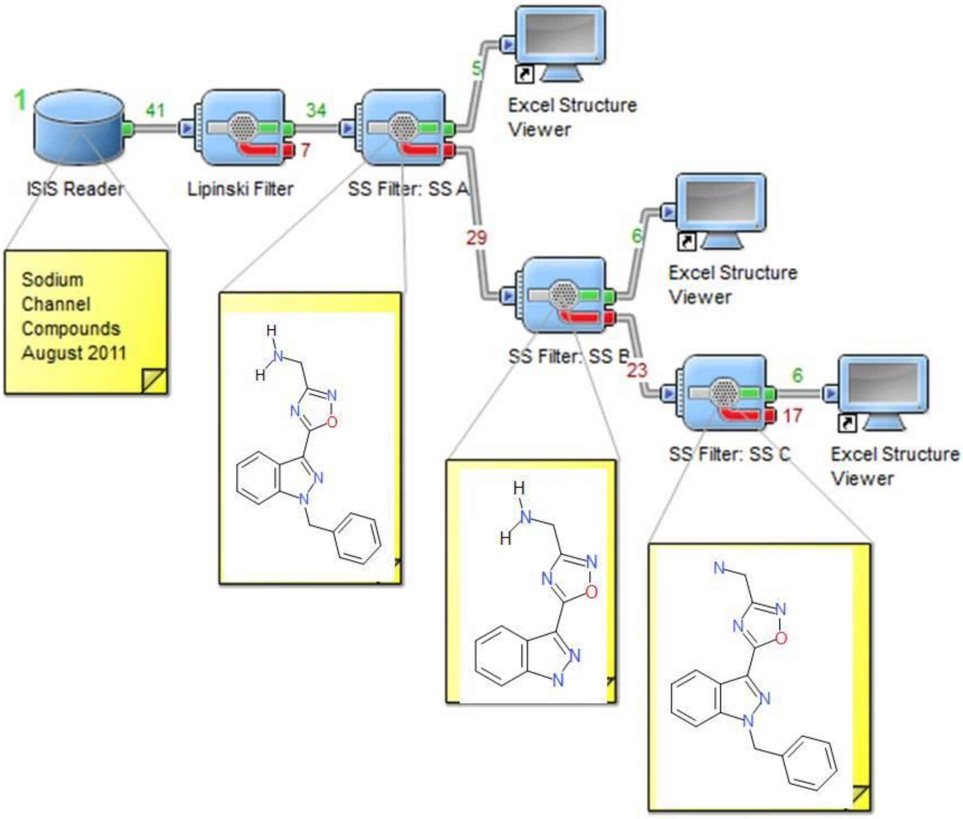
1
41
ISIS Reader
Sodium Channel Compounds August 2011
34
7
Lipinski Filter
5
Excel Structure Viewer
SS Filter: SS A
29
6
Excel Structure Viewer
SS Filter: SS B
23
6
17
SS Filter: SS C
Excel Structure Viewer
H
N
H
N
O
N
N
N

Figure 30. Pipeline Pilot protocol. A compound library of 41 compounds was filtered to keep only those which pass Lipinski's rule of five, keeping 34 compounds. Three substructures were searched and selected compounds were further evaluated.

Table 6. Chemical structures of sGC activators.

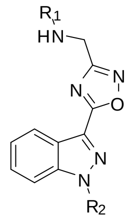

Compound	R1	R2
21	H	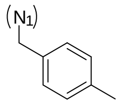
23	H	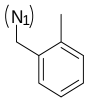
25	H	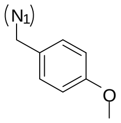
27	H	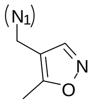
28	H	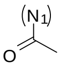
29	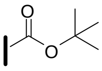	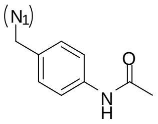
30	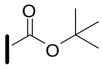	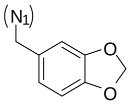

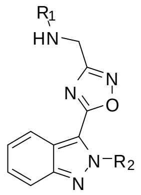

Compound	R1	R2
22	H	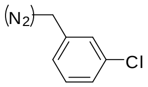
24	H	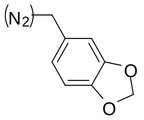
26	H	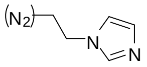

3.2.1.2. Biochemical evaluation

The activity of the selected compounds was evaluated using a radioimmunoassay which measures the amount of cGMP produced. Evaluation was performed using the well characterised bovine lung sGC as well as human recombinant protein. In this assay, the protein is treated with 1 mM MgGTP and 100 µM of compound. cGMP produced is solely due to the activation of the enzyme by the compound since no additional NO is included.

The results obtained with the different proteins show only small variations in activity. In the bovine lung sGC assay compounds **22**, **23**, **24**, **25**, **28**, and **29** do not produce more cGMP than a control sample containing no compound (~ 1 pmol/ng protein). Compounds **21**, **27**, and **30** successfully stimulated the enzyme to convert GTP into cGMP. Comparatively, the human recombinant protein showed increased activity and in addition to compounds **21**, **27**, and **30**, also compound **24** substantially activated the enzyme.

(a) Bovine lung sGC

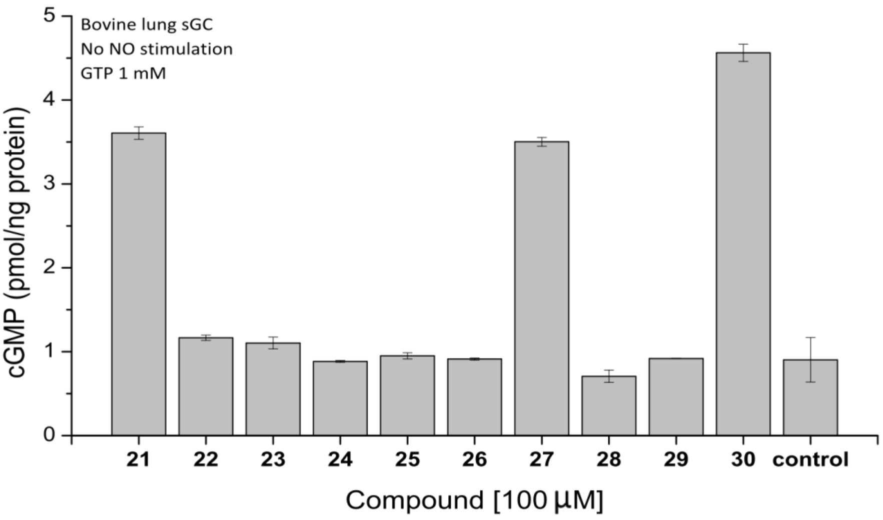

(b) Human recombinant sGC

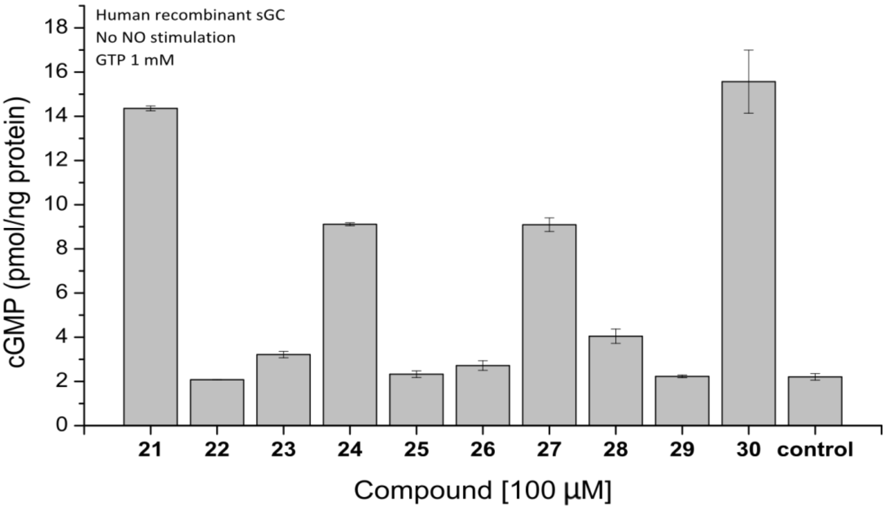

Figure 31. Biochemical activation of sGC by selected compounds. a) activation of bovine lung sGC; b) activation of human recombinant sGC. Assays performed in the presence of 1mM MgGTP and absence of added NO.

3.2.2. Biophysical assay development

3.2.2.1. Protein immobilisation

Immobilisation of sGC was performed using amine coupling through lysine residues as previously described. pH scouting was originally performed at different protein concentrations (Table **7**). This consisted of preconcentrating the protein on the sensor chip at concentration of 30, 50, and 200 µg/mL at pH 4, 4.5, 5, and 5.5. pH 5.5 worked well in all concentrations. In general, protein immobilisation was performed using 30 µg/mL sGCcat in 10 mM sodium acetate pH 5.5, except for experiments that required a high immobilisation level for which 200 µg/mL sGCcat in 10 mM sodium acetate pH 5.5 was used. Immobilisation was performed in the presence of MgATP and MgGTP, to protect binding sites so that lysines in these sites were not used for coupling to the dextran.

Immobilisation of full-length sGC was performed similarly to the catalytic domain of the enzyme. It required however a lower pH (4.5) of immobilisation buffer in order to achieve successful pre-concentration at the surface of the sensor chip.

Table 7. pH scouting for sGCcat immobilisation.

Protein concentration (ug/mL)	pH	Relative Response (RU)
30	5.5	8, 109
	5	5, 406
	4.5	6, 265
	4	-112
50	5.5	14, 748
	5	20, 964
	4.5	26, 681
	4	26, 700
200	5.5	56, 062
	5	33, 846
	4.5	24, 441
	4	16, 150

3.2.2.2. Buffer optimisation

Buffer scouting was performed in order to select the most appropriate buffer solution to use in experiments for nucleotide binding. The most commonly used buffers in Biacore assays are either HEPES (4-(2-hydroxyethyl)-1-piperazineethanesulfonic acid) based or PBS (phosphate buffer saline). HEPES was selected for this assay as it gave higher binding response with ATP than PBS. NaCl is present in the buffer to mimic physiological conditions and reduce nonspecific binding to the protein, and a small concentration of dithiothreitol (DTT) was also added to avoid oxidation of cysteine residues. Upon observation that

MgGTP shows higher binding that the nucleotide in the absence of cofactor Mg^{2+}, $MgCl_2$ was added to the running buffer at a concentration of 10 mM. Surfactant P20 was also included to reduce adsorption of hydrophilic molecules to the flow system surfaces. In experiments performed with the full length enzyme, NaCl was present in the buffer at a concentration of 300 mM, in order to reduce non-specific binding responses.

3.2.3. Binding of nucleotides

Binding of both nucleotide triphosphates (NTPs), ATP and GTP, to the immobilised proteins in the SPR assay was observed at physiological concentrations, whilst binding of cGMP only shifted from the baseline at concentrations higher than 1 mM (Figure **32**). Surface saturation could not be observed, as NTPs are known to aggregate at concentrations higher than 1 mM.[104] Moveover, ligands could be binding to a second site. Binding curves were fitted to a nonlinear curve model that considers binding plus linear non-specific binding. The fit was consistent with GTP binding to one binding site (n = 1) and ATP binding more than one site (n = 1.2) (Figure **33**). The K_D values obtained are only apparent and since ATP binds to both sites the value obtained is an apparent cumulative affinity, as determination of two separate binding affinities could not be achieved.

The conformation of the catalytic domain of sGC is thought to change significantly upon activation and “open” and “closed” states have been suggested. Although it is not possible to know in which conformation the protein was immobilised, binding of ATP and GTP shows that binding sites are accessible.

(a) ATP

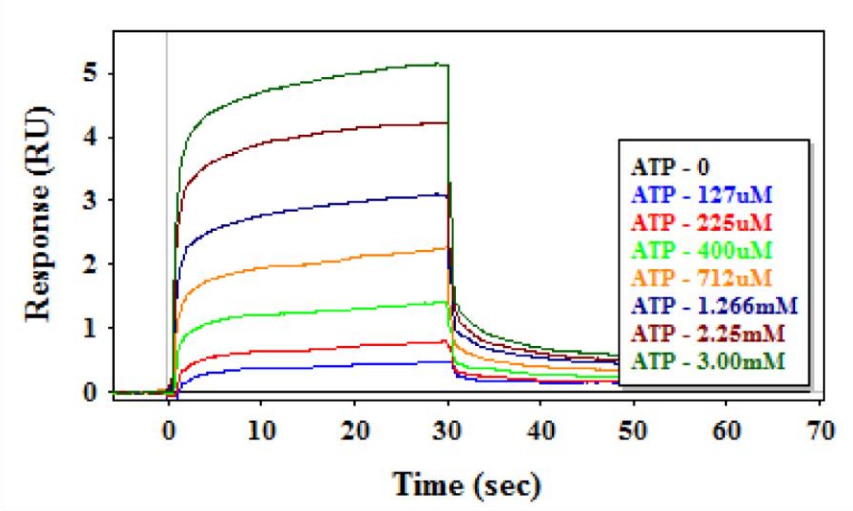

(b) GTP

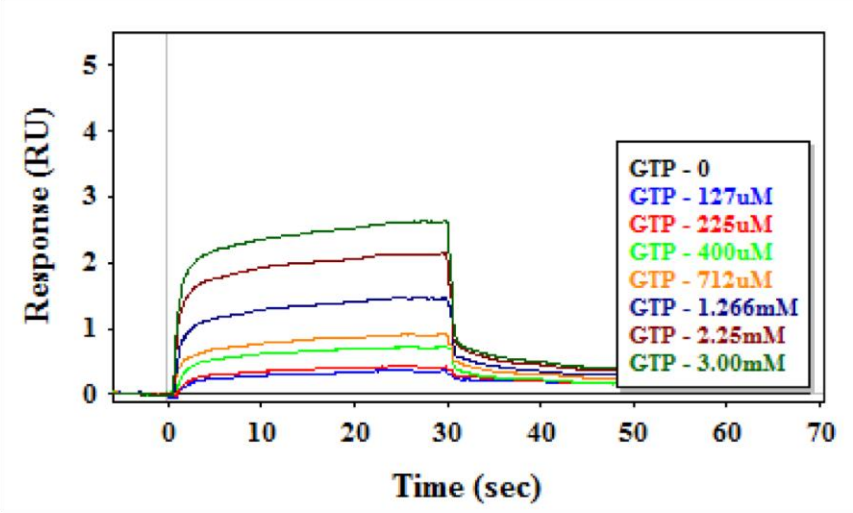

(c) cGMP

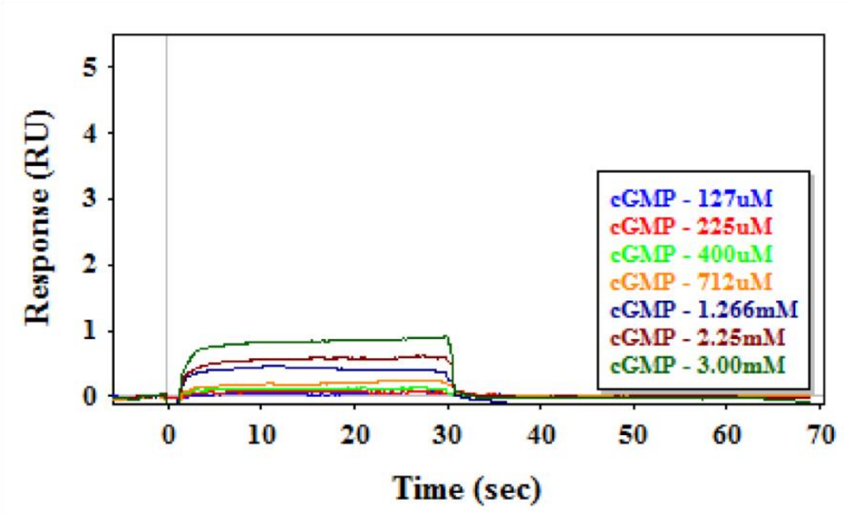

Figure 32. Sensorgrams of nucleotides binding to the catalytic domain of sGC. (a) ATP; (b) GTP; (c) cGMP.

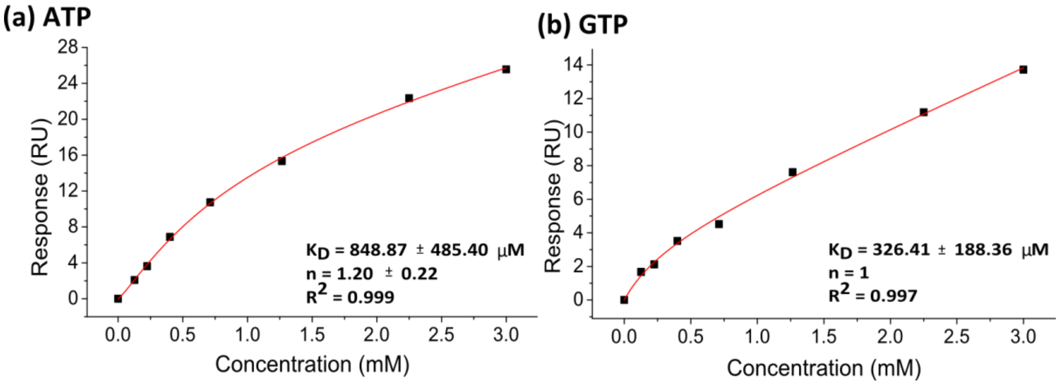

Figure 33. Fitting curves for ATP (a) and GTP (b) binding to the catalytic domain of sGC.

3.2.4. ATP and GTP binding site competition

ATP is known to regulate sGC activity and it has been hypothesised it does so through allosteric binding and/or competition with GTP. In order to confirm the immobilised protein could mimic its behaviour in functional assays, a competition assay was designed in which competition between ATP and GTP was assessed. In the SPR competition assay, the binding of the nucleotides was measured at five different concentrations, where the NTPs were present alone or in a mixture sample. If the two compounds were binding to separate sites, the response obtained with a mixture sample would be the same as the sum of binding responses when the NTPs are alone in solution (Figure **34 a – c**). However, it was observed that binding of the two NTPs injected in solution together is lower than the sum of their individual binding levels (Figure **35**). Thus, the information obtained in the competition assay, together with the observation that ATP binds more than one site in sGC, suggests the regulation of nucleotide binding to sGC involves the binding of ATP to the pseudosymmetric site of sGC's catalytic domain, combined with a competition between ATP and GTP to the catalytic site of the enzyme (Figure **34d**).

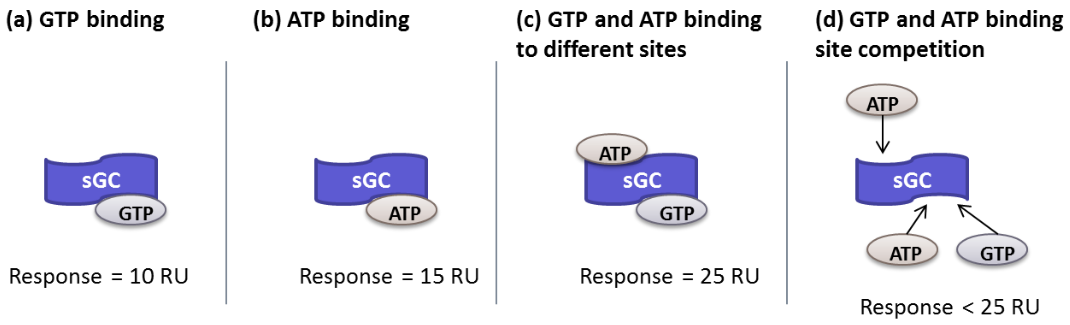
(a) GTP binding
sGC
GTP
Response = 10 RU
(b) ATP binding
sGC
ATP
Response = 15 RU
(c) GTP and ATP binding to different sites
ATP
sGC
GTP
Response = 25 RU
(d) GTP and ATP binding site competition
ATP
sGC
ATP
GTP
Response < 25 RU

Figure 34. Proposed mechanism for ATP and GTP competition measured by SPR. If GTP and ATP do not compete for a binding site the response obtained with both compounds in solution (c) will be the the sum of their individual binding responses (a) and (b); If the nucleotides compete for one or more binding sites the response obtained with both compounds in solution will be lower than the sum of their individual responses (d).

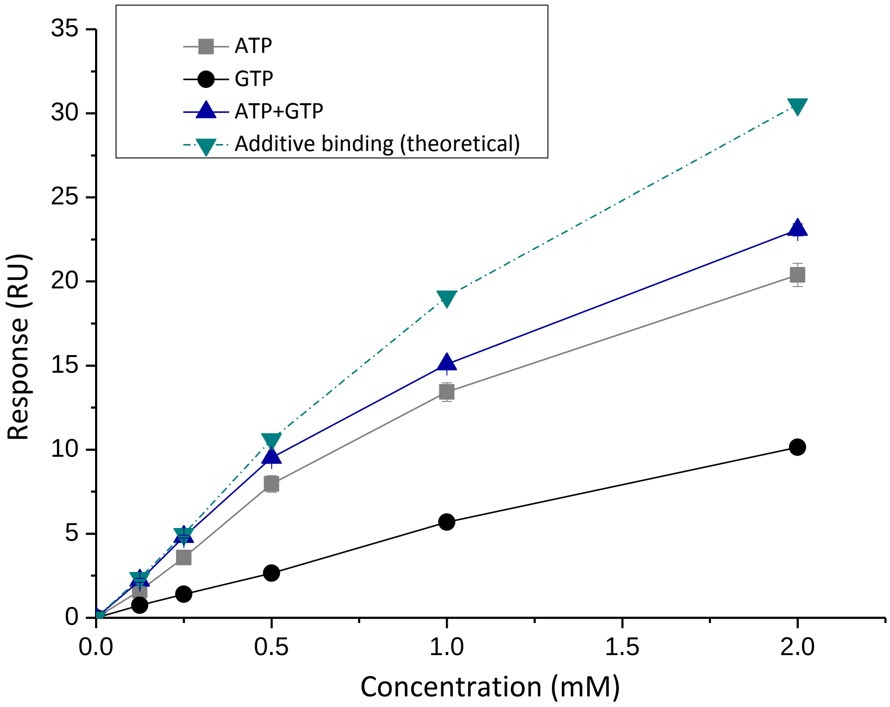

Figure 35. GTP and ATP competition assay

3.2.5. Binding of activators

Both proteins tolerated DMSO concentrations of up to 5 % which allowed binding of the small molecules to be evaluated using this system. The binding level of all compounds was measured at 100 µM (Figure **36**).

YC-1 (**5**) demonstrated strong binding to both proteins indicating that the YC-1 (**5**) binding site is located in the catalytic domain, consistent with previous investigations (Figure **37a** and **b**).[105] In contrast, the heme mimetic cinaciguat **6** which is known to bind to the H-NOX domain showed higher binding to the full length sGC than to the catalytic domain, appearing to bind to sGCcat non-specifically, as per analysis of the sensorgrams (Figure **37 c** and **d**).

Compounds **21** and **23** are close analogues, differing only in the position of a methyl group, and both give a high binding response to sGC in the SPR assay, similarly to YC-1 (**5**) itself. The 2-methylbenzyl-substituted indazole **23** does not activate the enzyme in the biochemical assay. Replacement of the methyl group in the 4-position of compound **21** by a methoxy group in compound **25** not only renders the compound inactive but also prevents it from binding to the enzyme in the SPR assay. Further variations at the N1 substituted indazole include a 5-methylisoxazole in compound **27** and an ethanone in compound **28**. The latter showed low binding to sGC and no activity in the biochemical assay. Compound **27** on the other hand, activated the enzyme and also showed binding in the SPR assay to a lower extent than compound **21**. The tert-butyl carbamate substituted (1,2,4-oxadiazol-3-yl)methanamines **29** and **30** vary in the substituents at the N1 of the indazole core. The 5-ethylbenzo[d][1,3]dioxole compound **30** is capable of activating sGC and shows significant binding to the enzyme, whilst the N-(4-ethylphenyl)acetamide compound **29**, despite showing higher binding than **30** is inactive in the biochemical assay. The acetamide group, which is both a hydrogen bond donor and acceptor, might contribute to a higher binding affinity, but this is not necessarily required for activity. Three compounds (**22**, **24**, and **26**) were selected in which the indazole core was substituted at the N2 position, and whilst compounds **22** and **24** showed strong binding to sGC they did not exhibit any biological activity.

(a) sGC catalytic domain

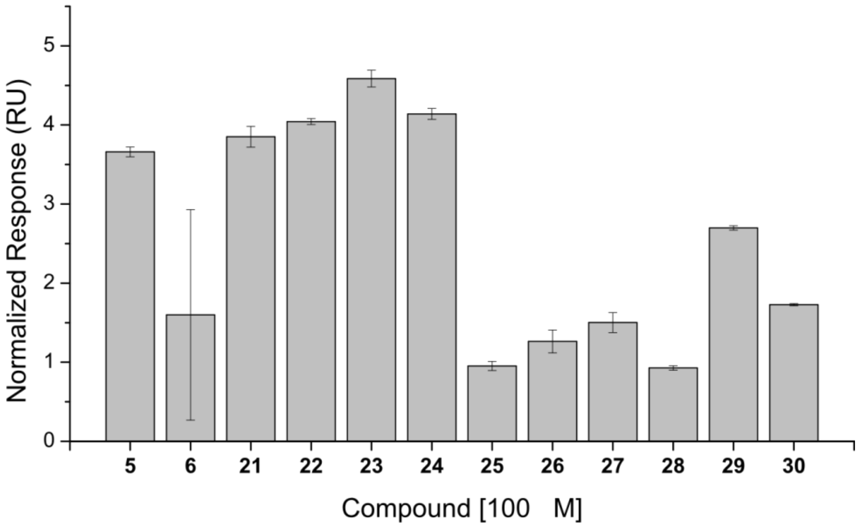

(b) Full length sGC

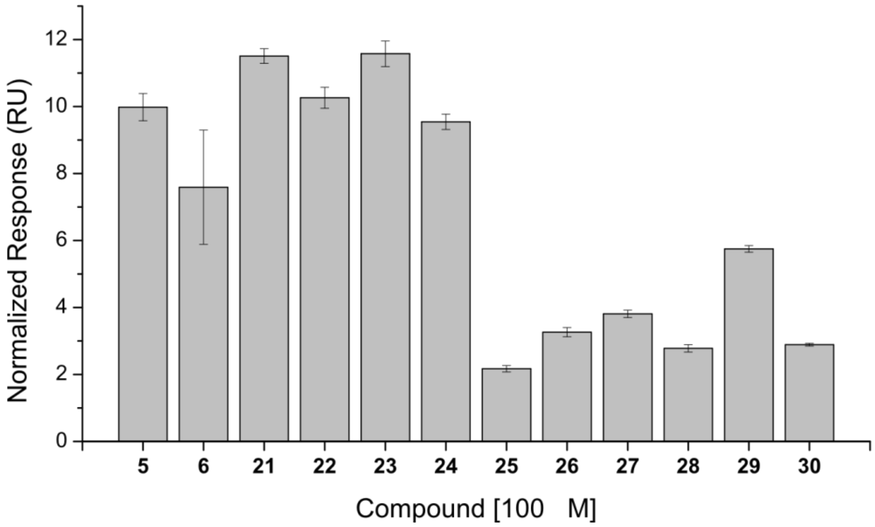

Figure 36. Binding response of selected compounds to sGC measured by SPR. a) Binding to the catalytic domain; b) Binding to full-length human recombinant sGC.

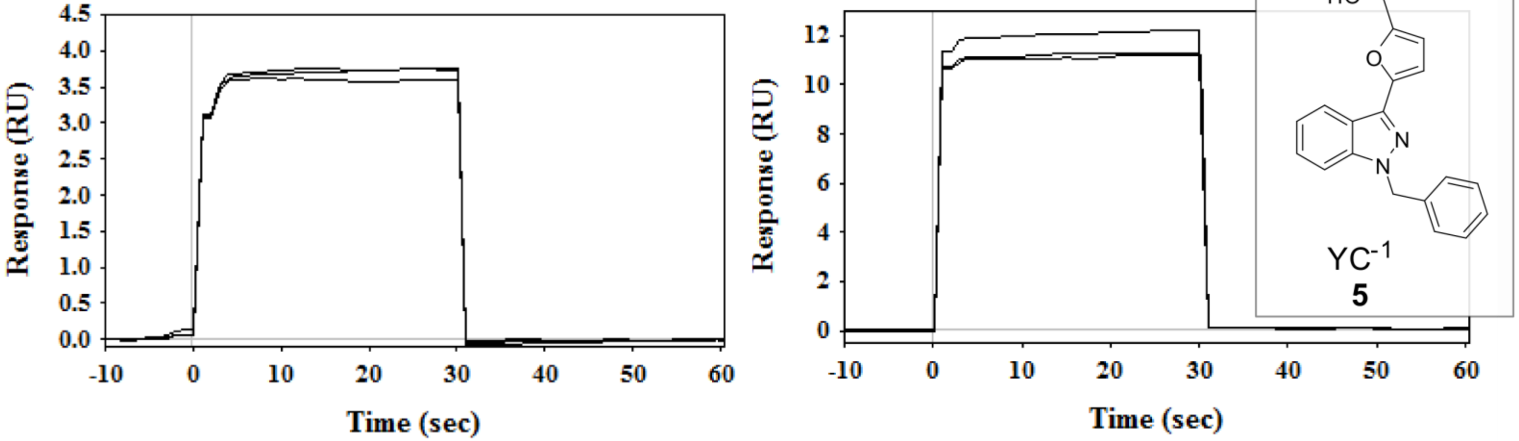
(a) sGCcat - YC-1

(b) sGC full length - YC-1

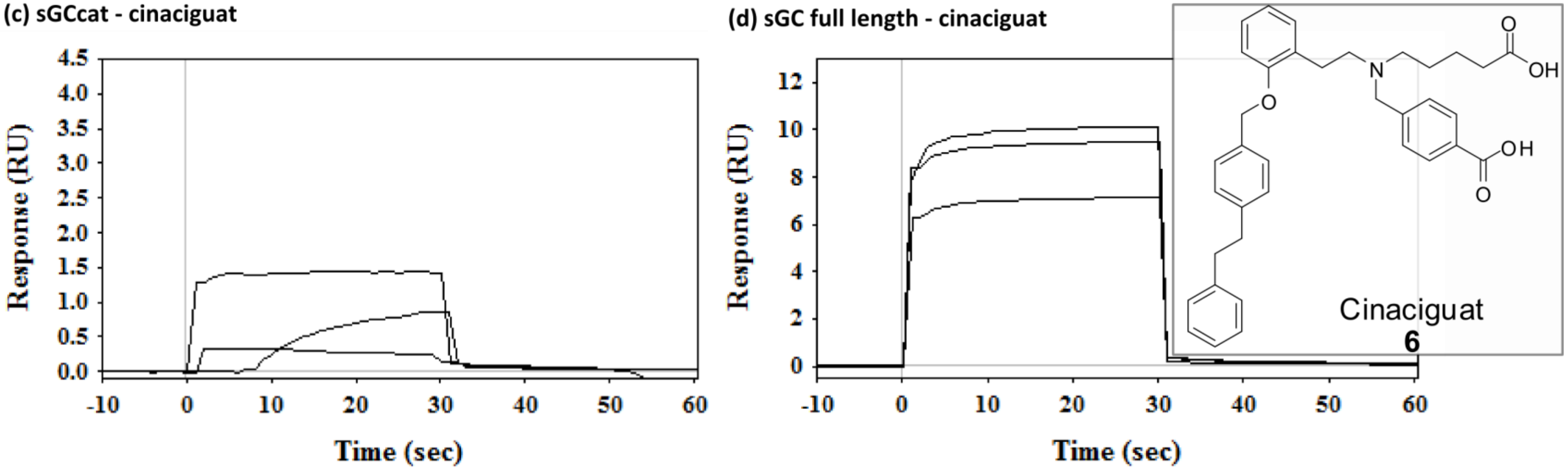
(c) sGCcat - cinaciguat

(d) sGC full length - cinaciguat

Figure 37. Sensorgrams for binding of YC-1 (5) (a, b) and cinaciguat 6 (c, d) to catalytic domain and full-length sGC, repectively.

The binding of the indazoleoxadiazole compounds to the full length sGC correlates with the binding to the catalytic domain construct, providing evidence that the binding site for this class of compounds is at the catalytic domain of sGC (Figure **38a**). This is most likely at the pseudosymmetric site, as previously suggested by structural models of YC-1 (**5**) interaction with the catalytic core of sGC.[105] No correlation was observed between binding level and lipophilicity (ClogP) of the compounds (Figure **38b**).

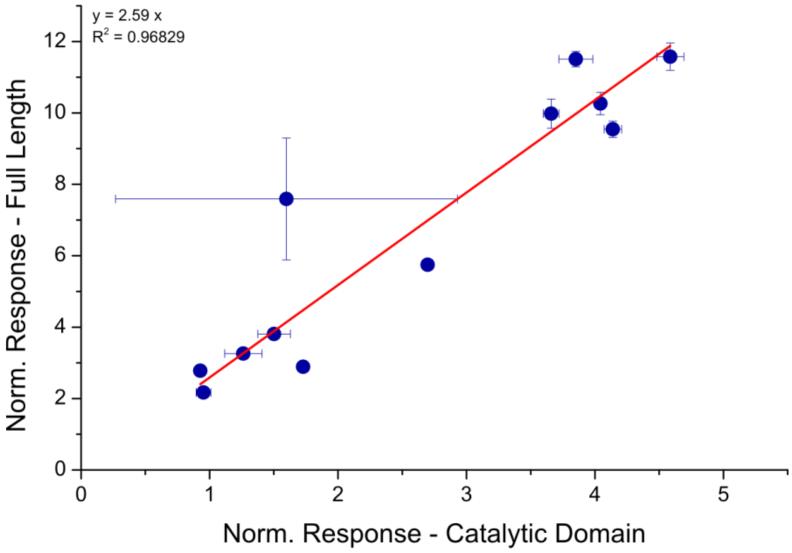
(a) Binding to full length vs binding to catalytic domain

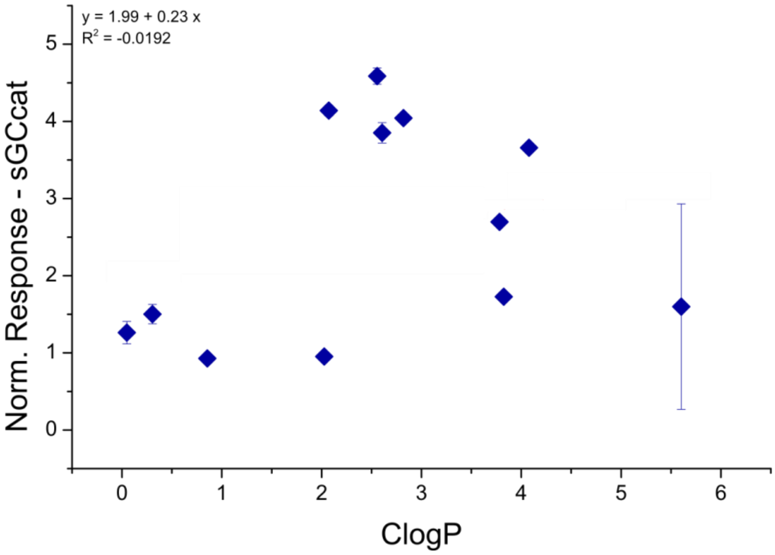
(b) Binding to catalytic domain vs clogP

Figure 38. Correlation between compound binding to full length and catalytic domain sGC (a) and between compound binding to catalytic domain and clogP (b).

3.3. Summary

An SPR assay was developed in which binding can be detected to two constructs of sGC, full length, and catalytic domain. The SPR assay detects binding alone and is not expected to correlate with biochemical activation and based on the data obtained this does not occur. However, binding may be a pre-requisite for activity and we did not observe biochemical activation without binding.

The results presented here provided further evidence that the so-called NO-independent sGC activators act through binding to an allosteric site on the catalytic domain of the enzyme. The assay was performed to evaluate a library of YC-1 (**5**) related compounds and discovered some new indazoleoxadiazole activators as a result. The α1β1 sGC catalytic domain construct used in this assay can therefore be used as a model for sGC binding in further SPR-based studies, which can provide a simple direct method to enable fragment-based drug design and inhibitor screening.

Chapter 4: Discovery and characterisation of small molecule inhibitors of sGC

4. Discovery and characterisation of small molecule inhibitors of sGC

4.1. Introduction

Inhibition of sGC activity can be attained by discrete mechanisms such as reduction of NO availability, and competition with NO or GTP for binding. Reduced availability of NO can be caused mainly by inhibition of nitric oxide synthase[106] or by reaction with radical species. In cells, the direct effects of NO are more than just interaction with metal complexes such as the heme in sGC. NO also plays a key role in response to oxidative stress, a hallmark of certain cardiovascular diseases which is characterised by excessive production of reactive oxygen species, such as superoxide ($O_2^{\cdot -}$). Superoxide can react with NO to form peroxynitrite (ONO_2^-), a powerful oxidant that may cause cell damage and death. This leads to a reduced bioavailability of NO, and superoxide is sometimes referred to as a sGC inhibitor.

Figure **39** shows small molecules that inhibit sGC activity, and the mechanisms by which these act are represented in Figure **40**.

The small molecule LY83583 (**31**) leads to inhibition of sGC activity by generating superoxide.[107] Scavenging of superoxide can be performed by superoxide dismutase (SOD), an enzyme that catalyses the dismutation of superoxide into oxygen (O_2) and hydrogen peroxide (H_2O_2), thus maintaining NO availability and sGC activity.[108-109]

Small molecules such as ODQ **4**, the 8-bromo analogue NS2028 (**32**), and related compounds are potent direct inhibitors of sGC which act through oxidation of the ferrous heme into ferric heme, thus preventing binding of NO.[110-112] However, such compounds lack *in vivo* selectivity, as they also oxidise other heme-containing proteins, such as haemoglobin.

Calmidazolium **33** has shown direct inhibition of isolated guanylate and adenylate cyclases by a mechanism that is not competitive with the natural ligands, ergo suggesting binding to allosteric sites. Calmidazolium **33** is a potent antagonist of calmodulin, a calcium-binding messenger protein which acts as a calcium sensor and signal transducer. Additionally, it has shown direct modulation of the Ca^{2+}/Mg^{2+}-ATPase and store-operated calcium channels.[113-114] This suggests calmidazolium **33** is a promiscuous inhibitor which may target several proteins.

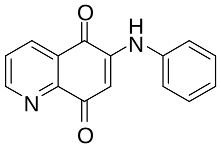
LY83583

31

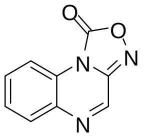
ODQ

4

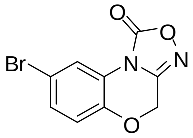
NS2028

32

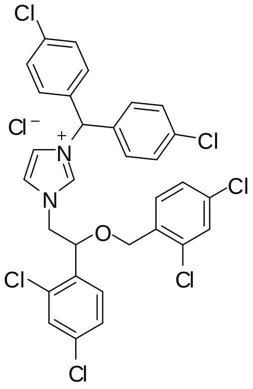
Calmidazolium

33

Figure 39. Chemical structures of inhibitors of sGC activity

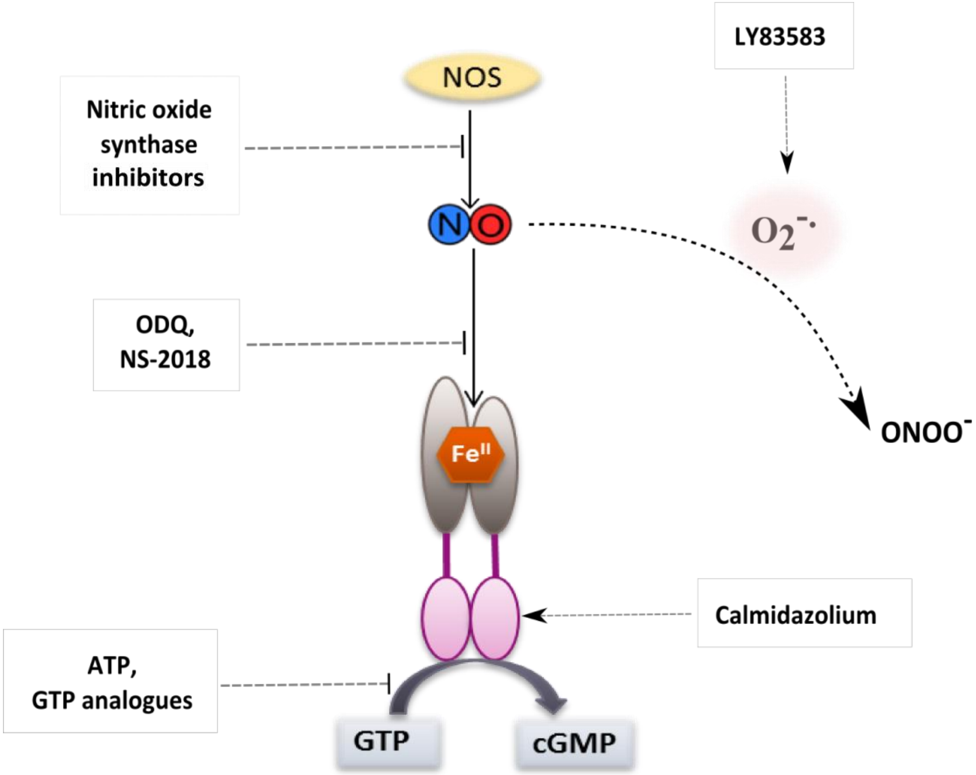
LY83583
NOS
Nitric oxide synthase inhibitors
NO
O2-•
ODQ, NS-2018
ONOO-
FeII
Calmidazolium
ATP, GTP analogues
GTP
cGMP

Figure 40. Schematic representation of different mechanisms for inhibition of sGC activity.

Since ATP and GTP analogues are known to compete with GTP for binding to sGC in addition to regulating enzyme activity through an allosteric site, these are also sometimes referred to as sGC inhibitors.[115-116]

This chapter will explore the search for a new direct inhibitor of sGC, which does not act through the formation of the superoxide radical, or oxidation of the heme, achieved by screening of commercial libraries of compounds. Moreover, the synthesis and biochemical and biophysical characterisation of a selected hit will also be investigated.

4.2. Results and discussion

4.2.1. Compound screening

N.B. *The results presented in section 4.2.1. took place before start of the PhD in the Selwood and Garthwaite labs. Virtual screening was performed by Dr. Paul Gane and Prof. David Selwood. Biochemical evaluation of all compounds reported in this thesis was performed by Prof. John Garthwaite and Kathryn Hampden-Smith (unless stated otherwise).*

Previous studies with the anti-convulsant drug lamotrigine **34** have shown increased NO-stimulated cGMP levels in cerebellar slides, suggesting a direct correlation with sGC.[117] Additional experiments with lamotrigine analogues **35** and **36** took place in the Garthwaite lab and it was discovered that contrary to lamotrigine **34**, the selected analogues **35** and **36** were mild inhibitors of sGC activity. Thus, these compounds were used as the starting point for the search of new inhibitors of sGC.

The core structure of lamotrigine **34** consists of a 6-phenyl-1,2,4-triazine ring system. In analogues **35** and **36** the 1,2,4-triazine ring is substituted by a pyrimidine, which was the ring used in the substructure searched (**A**).

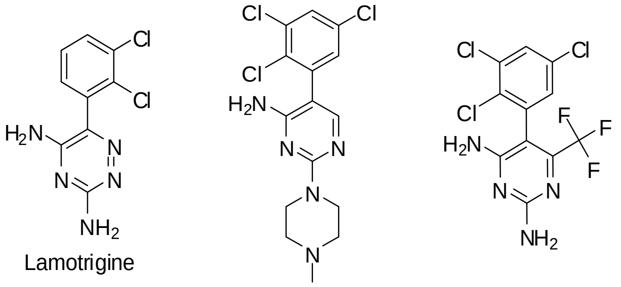

34 **35** **36**

Figure 41. Chemical structure of lamotrigine 34 and analogues 35 and 36.

Virtual screening was performed by similarity searches using MACCS fingerprints at 85 and 75 % Tanimoto of commercial libraries. Biochemical evaluation of selected compounds took place using purified rat lung guanylate cyclase (α1β1) and diethylamine NONOate (DEA/NO) **37** as the NO donor at 1 µM. DEA/NO spontaneously dissociates into NO in a pH-dependent process, with a half-life of 2 min at 37 °C pH 7.4. Enzyme activity was determined by measuring cGMP production using a standard cGMP [^{3}H] radioimmunoassay system.[118]

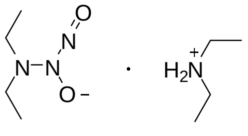

37

Figure 42. Chemical structure of diethylamine NONOate (DEA/NO).

The initial structure searched (structure **A**) resulted in circa 500 structures available, out of which 16 were selected by hand based upon diversity, molecular size, and availability. Compounds **38** and **42** showed inhibition of isolated enzyme activity by 51 %. A subsequent search was performed based on substructure **B**. Available compounds were filtered using PipelinePilot to select the 50 most diverse compounds. The symmetrical disubstituted [1,2,5]oxadiazolo[3,4-*b*]pyrazines compounds **39** and **43** were the most active of this library, with an sGC inhibition of 90 %. A search for substructure **C** resulted in the discovery of the symmetrical substituted quinoxaline compound **40** (73 % inhibition). A final library screening took place by searching for N^2,N^3-diphenylquinoxaline-2,3-diamines (substructure **D**), leading to the finding of compound **41**, which showed 99 % inhibition of sGC activity.

Further studies were conducted with compounds **40** and **41** which allowed the determination of their half-maximal inhibitory concentration (IC_{50}), summarised in Table **8**. In general, compound **41** was more potent than compound **40**. Both compounds also showed inhibition of sGC activity stimulated by the activator cinaciguat **6**, in the absence of added NO, proving they are not acting through competition with NO.

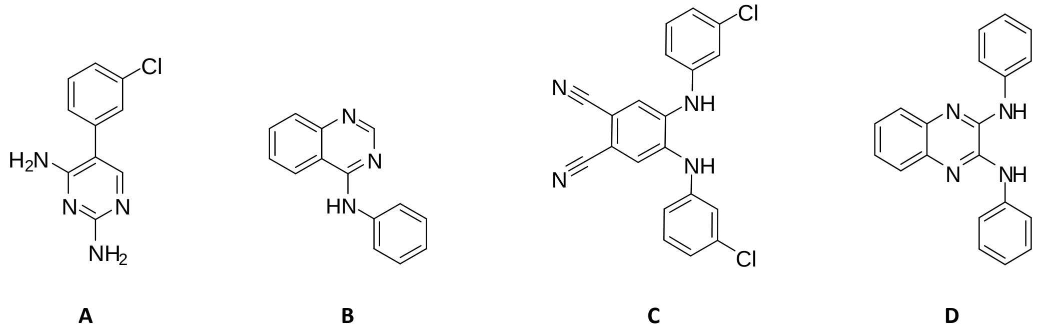

A **B** **C** **D**

Substructures

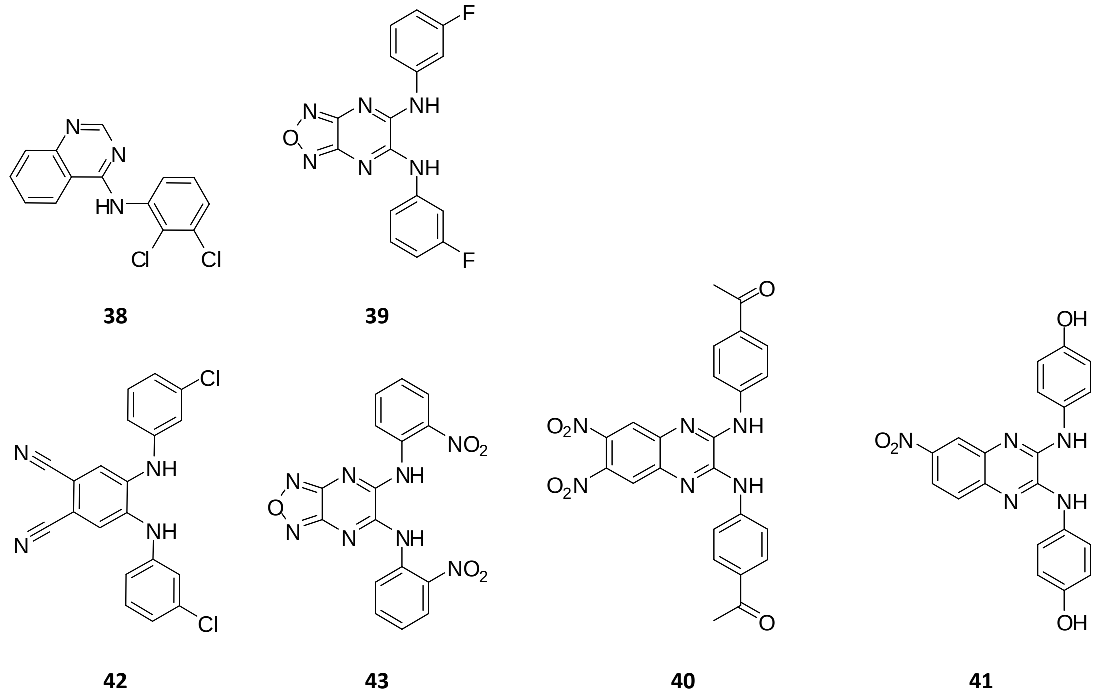

38 **39** **42** **43** **40** **41**

Hit Compounds

Figure 43. Chemical structures of virtually screened substructures and hit compounds.

Table 8. Biochemical activity of hit compounds 40 and 41.

GC activator		Compound 40 IC_{50} (µM) ± SE	Compound 41 IC_{50} (µM) ± SE
DEA/NO	10 nM	241.9 ± 21.3	24.3 ± 1.5
	0.3 nM	195.8 ± 11	25.7 ± 0.7
cinaciguat **6**	1 µM	79.8 ± 4.3	36.5 ± 39.5
	20 nM	64.4 ± 12.2	24.5 ± 4.2
ANP	1 µM	100.9 ± 10.6	24.6 ± 13.0
	10 nM	62.4 ± 10.2	20.7 ± 2.5
	basal	80.9 ± 15.0	14.5 ± 2.2

Most compounds had no effect on basal or forskolin-stimulated adenylyl cyclase (data not shown). The activity of compounds **40** and **41** was also tested on particulate GCs, using purified rat lung membranes in the presence of 10 µM ODQ **4** to inhibit NO-activated sGC. cGMP generation was measured after stimulation of pGC with ANP. The sGC inhibitors also showed inhibition of pGC-generated cGMP, indicating they are acting through the GC domain of the enzyme.

4.2.2. The synthesis of substituted quinoxalines

Some N^2,N^3-diphenylquinoxaline-2,3-diamines (substructure **D**) were reported as antimalarial agents in the late 1940's and their synthesis was based on the displacement of the chlorides in 2,3-dichloroquinoxalines with anilines at temperatures that ranged between 140 and 160°C for several hours. [119-120]

More recent literature has reported the synthesis of N^2,N^3-diphenylquinoxaline-2,3-diamines using microwave-assisted organic synthesis, which massively decreases reaction times, as shown in Scheme **1**, with the reaction between 2,3-dichloro-6-nitroquinoxaline **44** and (*E*)-3-(3-aminophenyl)acrylic acid **45** for 30 min at 160 °C, giving compound **46** with a 35 % yield (Scheme **1**).[121]

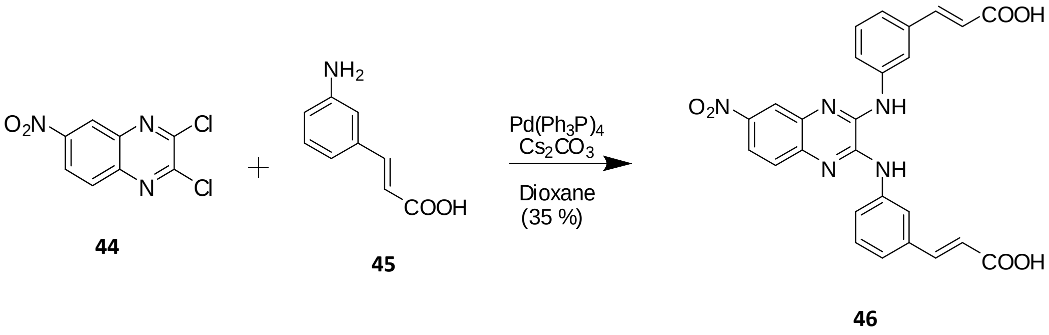

Scheme 1. Pd-catalysed synthesis of a substituted *N*^{2},*N*^{3}-diphenylquinoxaline-2,3-diamine.[121]

4.2.3. Synthesis of hit compound 41

The hit compound **41** was selected for further characterisation. Firstly, a synthetic route was desired that would allow a fast synthesis of compounds that could be obtained with high degrees of purity for biological analysis. The synthesis of compound **41** is not described in the literature. However, considering available literature of analogue compounds[122], it was proposed that it could be obtained by reaction of commercially available 2,3-dichloro-6-nitroquinoxaline **44** with 4-aminophenol **47.** Synthesis of compound **41** was not attempted using the Pd-catalysed synthesis described in Scheme **1** as it was initially performed before the publication of such method. Instead, a method was optimised for the synthesis of these compounds via nucleophilic aromatic substitution mechanism (S_NAr) (Scheme **2**)

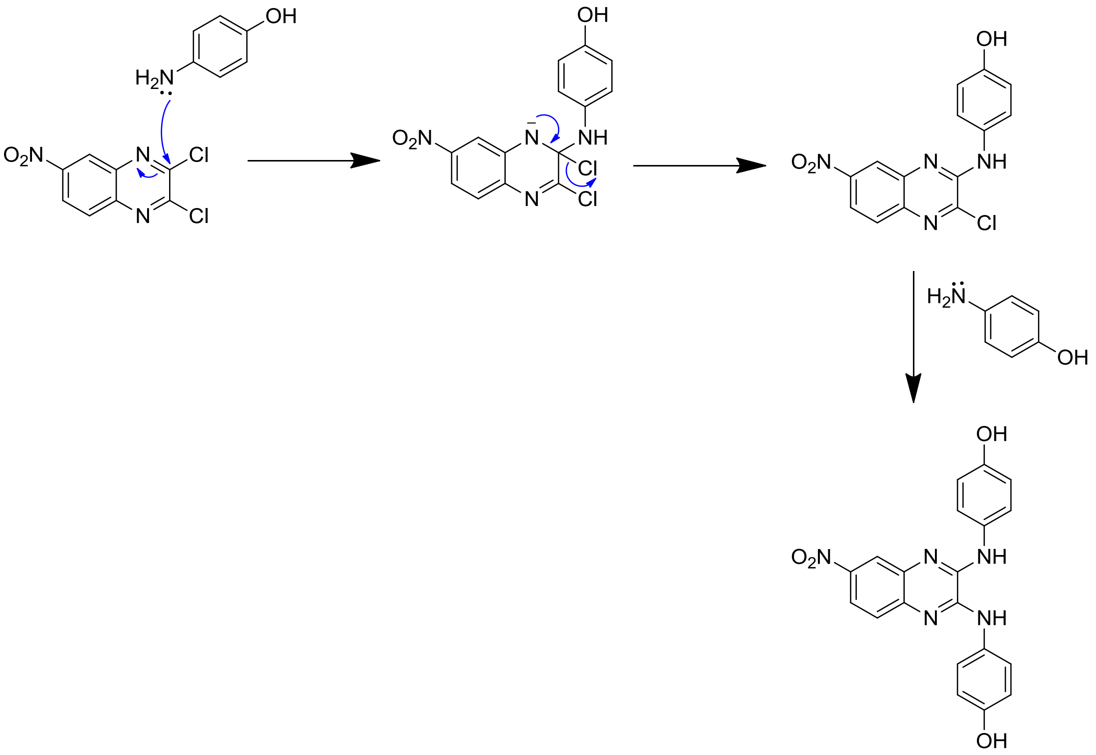

Scheme 2. S$_N$Ar mechanism for the synthesis of compound 41.

A small set of reaction conditions was tested (Table **9**) for the synthesis of compound **41**, using microwave irradiation at 150 Watt. The initial solvent chosen for this reaction was N-methyl-2-pyrrolidone (NMP). NMP is a polar aprotic solvent, a medium-absorber of microwave irradiation with a high boiling point of 215 °C, and dissolves most organic compounds, making it a preferred solvent in microwave synthesis. Reaction number 1 took place at 160 °C for 5 min. The microwave system did not take long to reach the set temperature (3:33 min). The presence of the desired product was shown by liquid chromatography-mass spectrometry (LC-MS) before aqueous work-up and the identity of the product was confirmed by NMR after purification by flash column chromatography. In order to optimize the reaction conditions, a few variables were changed. First, as the aqueous work-up initially used was long and the compound seemed to crystallize in water, crystallization and filtration were performed instead of an aqueous extraction. This was however not successful as NMP was not completely removed from the substance during the washes nor separated in the column. It was also noted that an increase in reaction time to 10 min did not improve the yields obtained. Replacement of the solvent NMP by acetonitrile (MeCN), another polar aprotic solvent and medium absorber was investigated.

The maximum temperature achieved with this solvent was 120 °C, and it took approximately 11 min to reach. Analysis of the crude compounds suggested the presence of a side product, possibly the mono-substituted compound, in small quantities, which did not occur with NMP. The experimental procedure followed in reaction 1 was the one which allowed a faster reaction and a more pure compound. In comparison to the microwave-assisted method described in the literature, the method presented here is faster, taking only 5 min whilst the Pd-catalysed method takes 30 min, and does not require the use of a catalyst, giving a much cleaner reaction.

Table 9. Reaction conditions for the synthesis of compound 41.

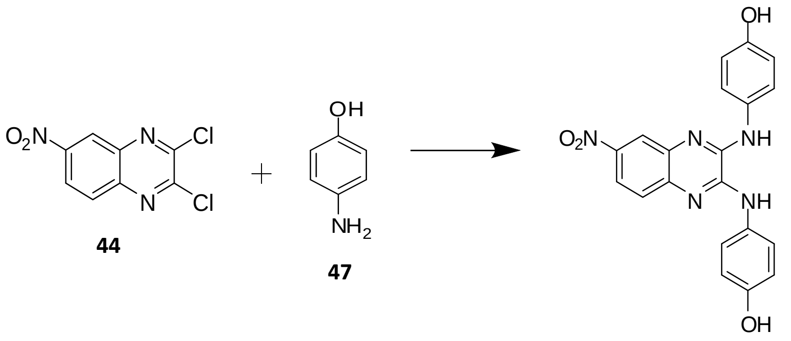

44 **47** **41**

Reaction number	Solvent	Temp. (° C)	Time[†] (min)	Workup	Result
1	NMP	160	5 (+ 3.33)	Aq. extraction	60 % yield
2	NMP	160	5 (+ 3.22)	Crystallisation	Impurities present
3	NMP	160	10 (+ 3.22)	Aq. extraction	60 % yield
4	MeCN	120	5 (+ 11:05)	Solvent evaporation	Longer reaction time; Possible side product with [M+H]+=317
5	MeCN	120	5 (+ 11:00)	Aq. extraction	

[†] Time in brackets corresponds to the time needed by the Microwave to reach the desired temperature.

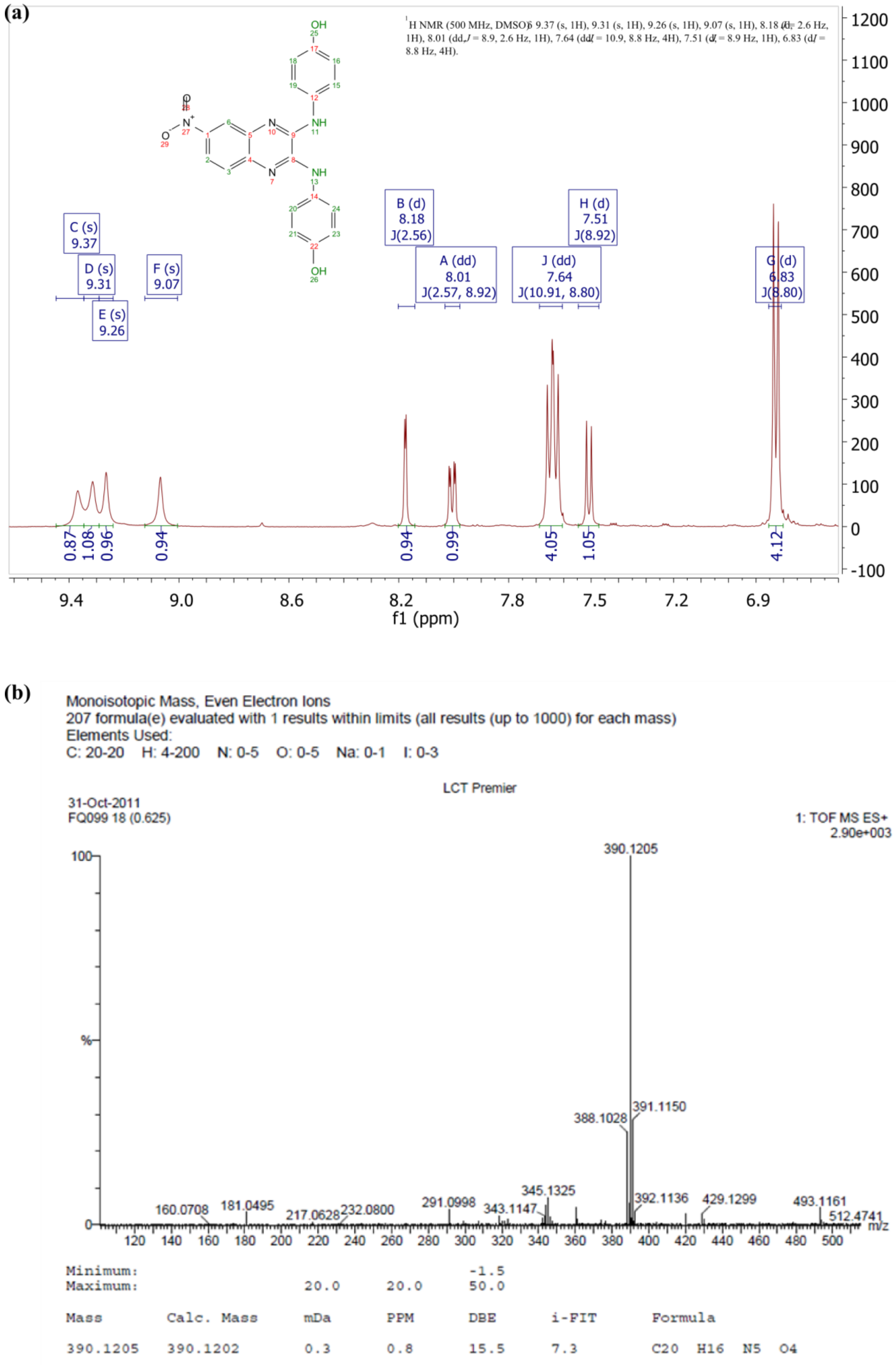

^{1}H NMR (500 MHz, DMSO) δ 9.37 (s, 1H), 9.31 (s, 1H), 9.26 (s, 1H), 9.07 (s, 1H), 8.18 (d, *J* = 2.6 Hz, 1H), 8.01 (dd, *J* = 8.9, 2.6 Hz, 1H), 7.64 (dd, *J* = 10.9, 8.8 Hz, 4H), 7.51 (d, *J* = 8.9 Hz, 1H), 6.83 (d, *J* = 8.8 Hz, 4H).

Monoisotopic Mass, Even Electron Ions
207 formula(e) evaluated with 1 results within limits (all results (up to 1000) for each mass)
Elements Used:
C: 20-20 H: 4-200 N: 0-5 O: 0-5 Na: 0-1 I: 0-3

31-Oct-2011
FQ099 18 (0.625)

```
Minimum:                                   -1.5
Maximum:                 20.0      20.0    50.0

Mass        Calc. Mass   mDa       PPM     DBE      i-FIT       Formula

390.1205    390.1202     0.3       0.8     15.5     7.3         C20  H16  N5  O4
```

Figure 44. Spectroscopic characterisation of compound 41. a) ^{1}H NMR: The four singlets between 9.0 and 9.4 ppm correspond to the two O*H* protons (two more downfield peaks) and the two N*H*s; the peak at 8.18 ppm correspond to the *H* in the carbon labelled as 6 in the quinoxaline ring, and it is coupled to the other *H* proximal to NO_2 at 8.01 ppm (*J* = 2.6 Hz). This is in turn coupled to the vicinal proton which resonates at 7.51 ppm (*J* = 8.9 Hz). The peak at 7.64 ppm integrates to 4 protons, the protons closer to the N*H*s in both phenol rings, and the remainder 4 protons closer to the OH groups appear at 6.83 ppm. b) High resolution mass spectrum: The major peak at *m/z* 390.1205 corresponds to $[M+H]^+$.

4.2.4. Biochemical characterisation of synthesised compound 41

The activity of the synthesised compound **41** was evaluated in a simplified assay using four concentration points (3, 10, 30, 100 µM). A new assay was employed using bovine lung purified sGC. The compounds were tested in the presence of 1 mM MgGTP and 30 nM DEA/NO for 2 min. Superoxide dismutase (SOD) was included in the assay at 1000 units/mL to account for possible enzyme inhibition due to superoxide radical. The synthesised compound showed an IC_{50} of 70 µM, only slightly more potent than the commercial compound (IC_{50} = 90 µM), possibly due to a higher degree of purity.

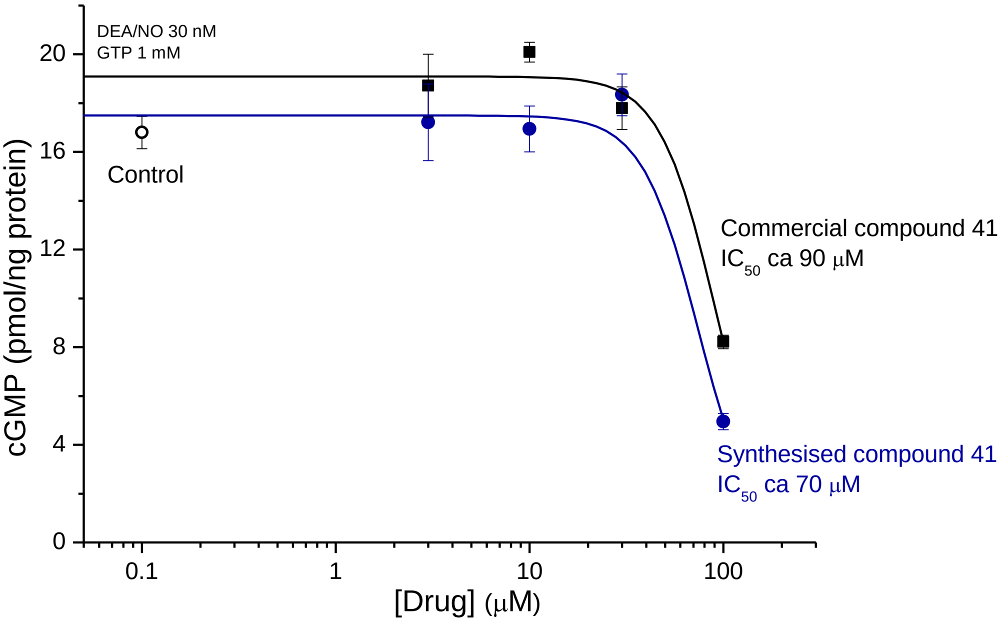

Figure 45. Comparison of biochemical activity between commercial and synthesised compounds 41.

4.2.5. Characterisation of the binding of compound 41 to sGC

The binding of compound **41** to sGC was characterised using SPR. The equilibrium affinities of the ligand to the full-length sGC and two constructs of the catalytic domain, a wild-type form and a mutant form, were compared. The mutated protein has the amino acid substitutions G476C and C541S in the β-subunit (GUCY1B3) and was generated to engineer a disulphide bond between the α and β subunits and prevent a disulphide bond between the β-subunits in order to preferentially obtain heterodimers, which allowed the generation of heterodimer crystals and subsequently the determination of their structure by x-ray crystallography.[71]

Binding of compound **41** was measured at six different concentrations and equilibrium dissociation constants (K_D) were obtained by fitting to a steady-state binding equation, considering one binding site (Equation **5**), or a model that takes into account non-stoichiometric binding (Equation **6**).

$$Resp = \frac{R_{max}(\frac{C}{K_D})}{1 + (\frac{C}{K_D})}$$

Equation 5. Model for one-to-one binding interaction. Where *Resp* corresponds to the response in RU obtained by SPR at a concentration *C*, R_{max} is the maximal response obtained and K_D is the equilibrium dissociation constant.

$$Resp = \left(R_{max}\frac{C^n}{K_D^n} + C^n\right) + kns^C$$

Equation 6. Model for non stoichiometric binding interaction. Where *Resp* corresponds to the response in RU obtained by SPR at a concentration *C*, R_{max} is the maximal response obtained, K_D is the equilibrium dissociation constant, *kns* is the dissociation constant for additional binding site, and *n* is the number of binding sites.

Two types of sensor chip were used in this experiment. GE Healthcare recommends the use of a CM7 chip to measure binding of small molecules. This chip has a higher degree of dextran carboxylation, allowing a higher degree of protein immobilisation at the surface which in turn is expected to give higher response levels and a greater signal to noise ratio. This chip was used to immobilise the wild type catalytic domain of sGC and the full length enzyme. The wild type sGCcat was also immobilised onto a CM5 chip, alongside the mutant sGCcat for comparison. Sensorgrams are shown in Figure **46**.

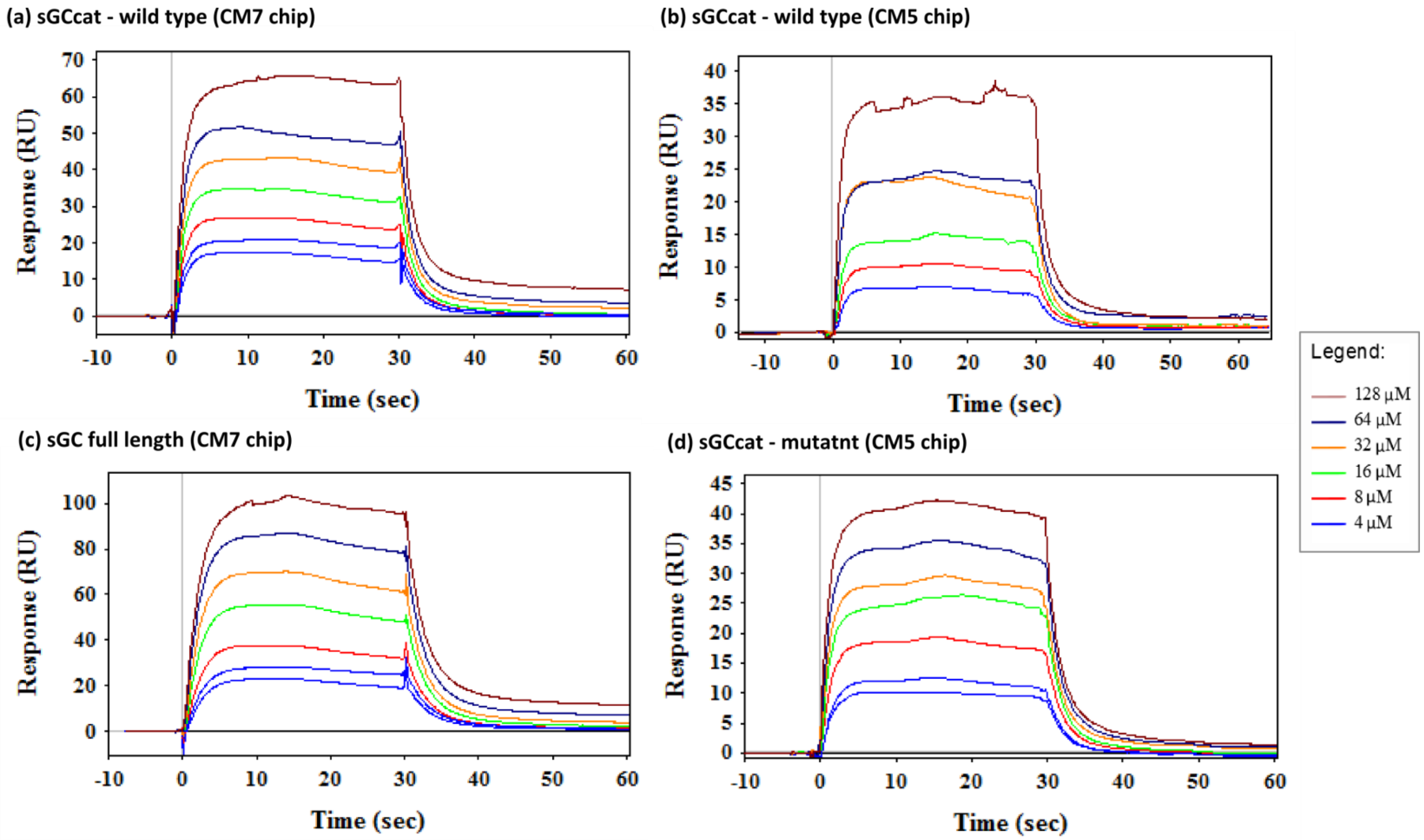

(a) sGCcat - wild type (CM7 chip)

(b) sGCcat - wild type (CM5 chip)

(c) sGC full length (CM7 chip)

(d) sGCcat - mutatnt (CM5 chip)

Figure 46. Sensorgrams of compound 44 binding to different immobilised constructs of sGC. a) wild-type sGCcat on a CM7 chip; b) wild-type sGC on a CM5 chip; c) full-length sGC on a CM7 chip; d) mutant sGCcat on a CM5 chip.

The equilibrium dissociation constant (K_D) of compound **41** was similar for all surfaces (ca 10 – 30 µM). Dose-response plots are shown in Figure **47** and calculated K_D summarised in Table **10**. At higher concentrations of compound **41**, the binding responses obtained in the full-length enzyme were higher than the theoretical maximal response (R_{max}) possible for one binding site, as calculated by Equation **5**. This may indicate that the compound is binding to a second site, possibly non-specifically. Non-specific binding had also been observed with nucleotides in chapter **2**, and it is possible that due to the high molecular weight of enzyme (~ 150 kDa) there may be other sites where small molecules could bind. Thus, a different model was employed to calculate the binding affinity of compound **41** to the full length enzyme, which takes into account non-specific binding (Equation **6**). Using this model, the R_{max} was fixed at 78 RU, the number of binding sites was determined as 1.3 and the calculated K_D was slightly smaller than that obtained when employing a one binding site model. Analysis of the sensorgrams obtained with the wild type sGCcat in the CM5 chip suggests binding saturation is achieved at 32 and 64 µM, but the response obtained at a concentration of 128 µM is again higher. Thus, the model for non-stoichiometric binding gives a better line fitting, with R_{max} fixed at 23 RU.

Table 10. Calculated equilibrium dissociation constants for compound 41.

Immobilised enzyme	R_{max}	One-to-one binding model K_D (µM)	Non-stoichiometric binding model	
			K_D (µM)	n
sGCcat – wild type (CM7 chip)	155	16.8 ± 3.9		
sGCcat – wild type (CM5 chip)	85	32.7 ± 10.1	11.5 ± 1.1	1.3 ± 0.1
sGC full length (CM7 chip)	78	19.4 ± 2.1	10.3 ± 0.7	1.3 ± 0.2
sGCcat – mutant (CM5 chip)	77	11.4 ± 1.8		

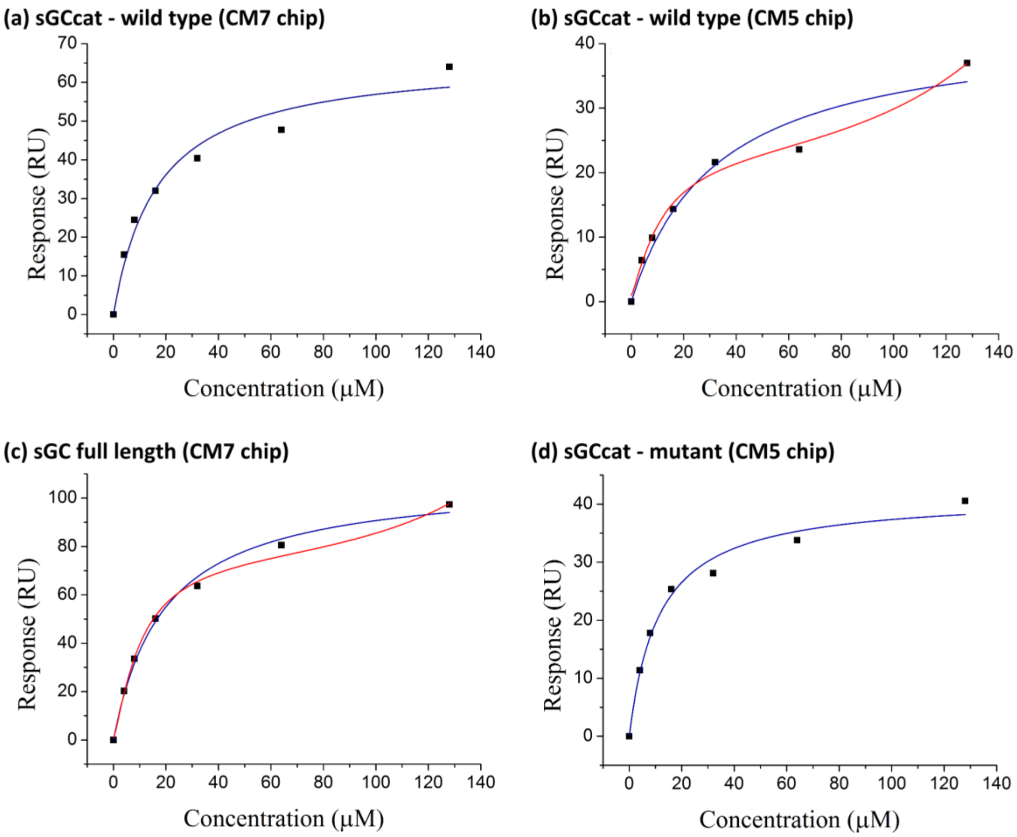

Figure 47. Dose-response plots of compound 41 binding to sGC. a) wild-type sGCcat on a CM7 chip; b) wild-type sGC on a CM5 chip; c) full-length sGC on a CM7 chip; d) mutant sGCcat on a CM5 chip. Lines in blue were fitted to a one-to-one binding model, whilst lines in red were fitted to a non-stoichimetric binding model.

4.2.6. Docking studies

Co-crystallisation of the catalytic domain of sGC with the inhibitor **41** has been attempted by Dr. Charles Allerston at the structural genomics consortium in Oxford, and the group of Dr. Alun Coker at the Royal Free in UCL. At the time of writing, co-crystals had been obtained but a high resolution structure had yet to be solved. Thus, a possible binding mode was investigated by molecular modelling, using the available crystal structure of a mutated catalytic domain of sGC. This mutated enzyme was used in the SPR studies reported in section **4.2.5**, and since the binding affinity of compound **41** to this enzyme was identical to the wild-type enzyme, it can be concluded that the mutated residues do not influence the binding of the inhibitor and the crystal structure can be used for docking purposes.

As discussed in chapter **3**, the catalytic domain of sGC shows two sites at the interface of the α- and β-subunits that can accommodate small molecules: the GTP binding site, and an allosteric regulatory binding site referred to as the pseudosymmetric site (Figure **48**). The two sites are different, and small molecules can bind to only one or both sites, thus showing a 1:1 or 1:2 binding ratio.

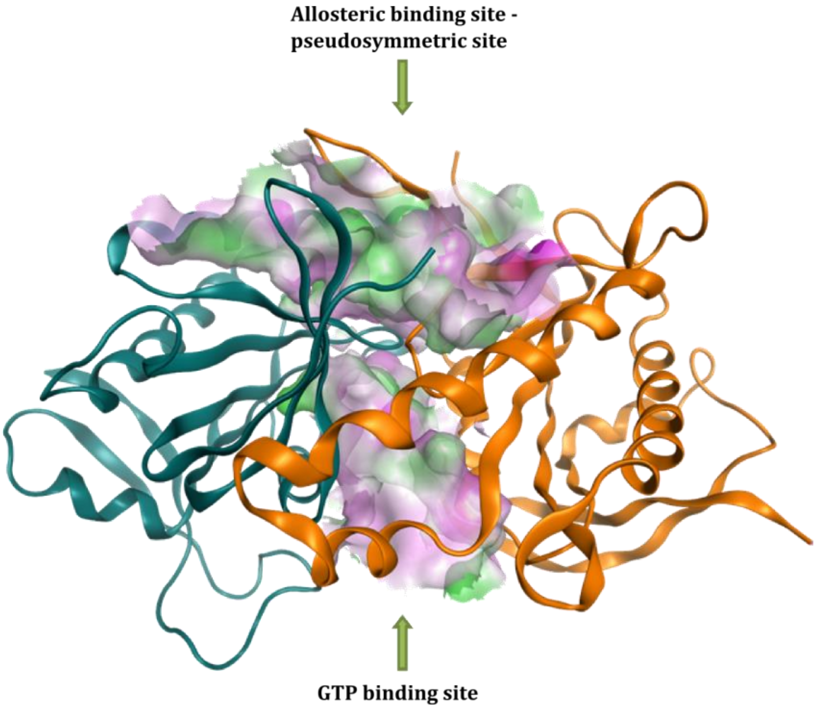

Figure 48. Cartoon representation of the catalytic domain of sGC (pdb entry 3uvj). Where the α-subunit is represented in green and the β-subunit in orange. The molecular surfaces depicted represent the GTP and pseudosymmetric binding sites, and are coloured according to lipophilicity, where the hydrophilic surface is coloured in pink, the lipophilic in bright green, and neutral in white.

Compound **41** was docked into the pseudosymmetric site of sGC and possible binding modes were analysed based on their Goldscore fitness. The Goldscore fitness function is a dimensionless score that gives an indication of how good the binding pose is, and is used as a comparative term. In general, the higher the score, the better the docking result is likely to be.

A superimposition of all the resulting binding modes obtained with the inhibitor shows that with the exception of one mode that is docked at a more exposed surface, most binding modes are similarly docked at buried pockets at the interface of the two subunits. Five out of nine binding poses show only slightly variances in the angle of the phenol rings and the nitro group (Figure **49**).

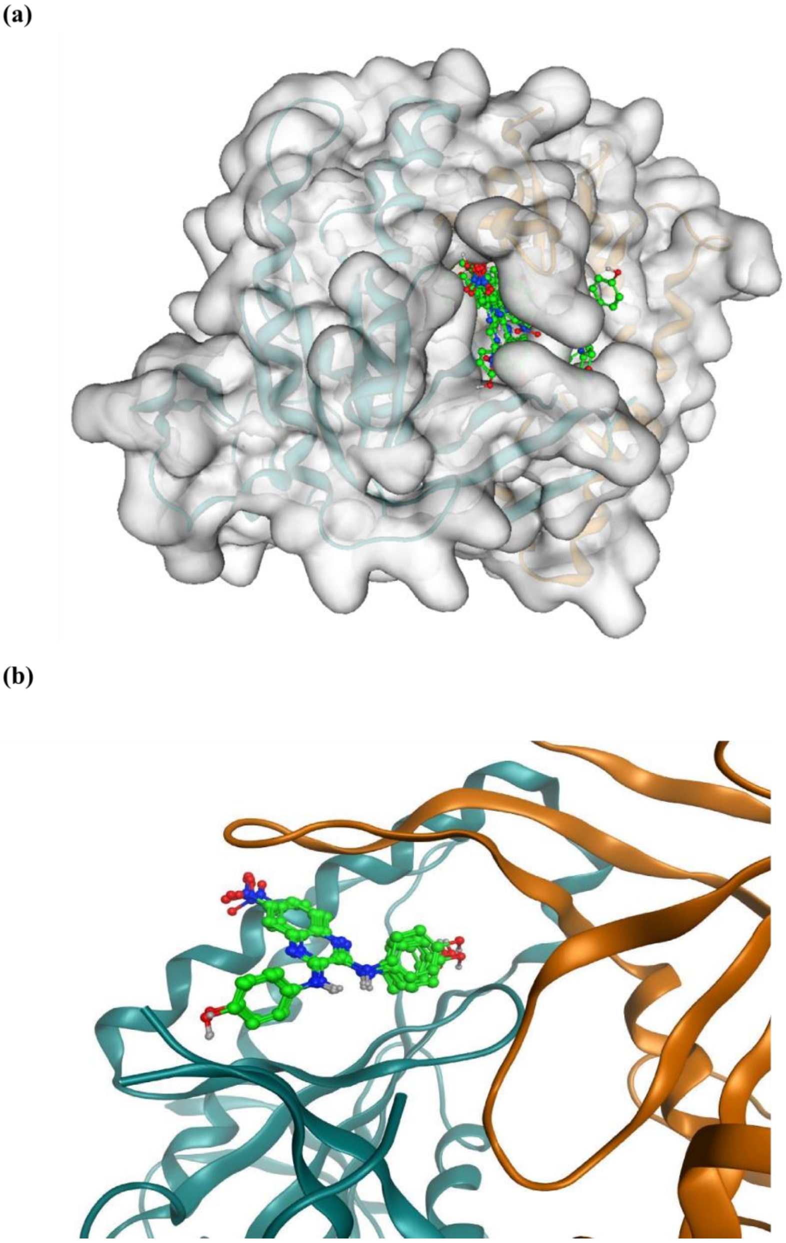

Figure 49. Superimposition of the binding poses of compound 41 in the pseudosymmetric site of sGC. a) All binding poses docked at pseudosymmetric site of sGC with protein suface; b) Zoomed image of five similar binding poses, without protein surface represented.

The binding pose with the highest Goldscore (57.86) shows four key interactions with the receptor: one oxygen of the nitro group may act as H-bond acceptor for two backbone NHs, being the only interaction with residues of the β-subunit; the two NH groups attached to the quinoxaline may act as H-bond donors for the side chain of a glutamic acid; one OH can act as a H-bond donor; and a π-cation interaction is suggested between a charged lysine and one of the aromatic rings (Figure **50** and Table **11**). In similar docking poses obtained with compound **41**, it is possible by small angle variations of the rotatable bonds that the other OH group would also act as H-bond donor to residues in proximity. In addition, the lysine and arginine residues present in the site could show π-cation interactions with other aromatic rings of the ligand.

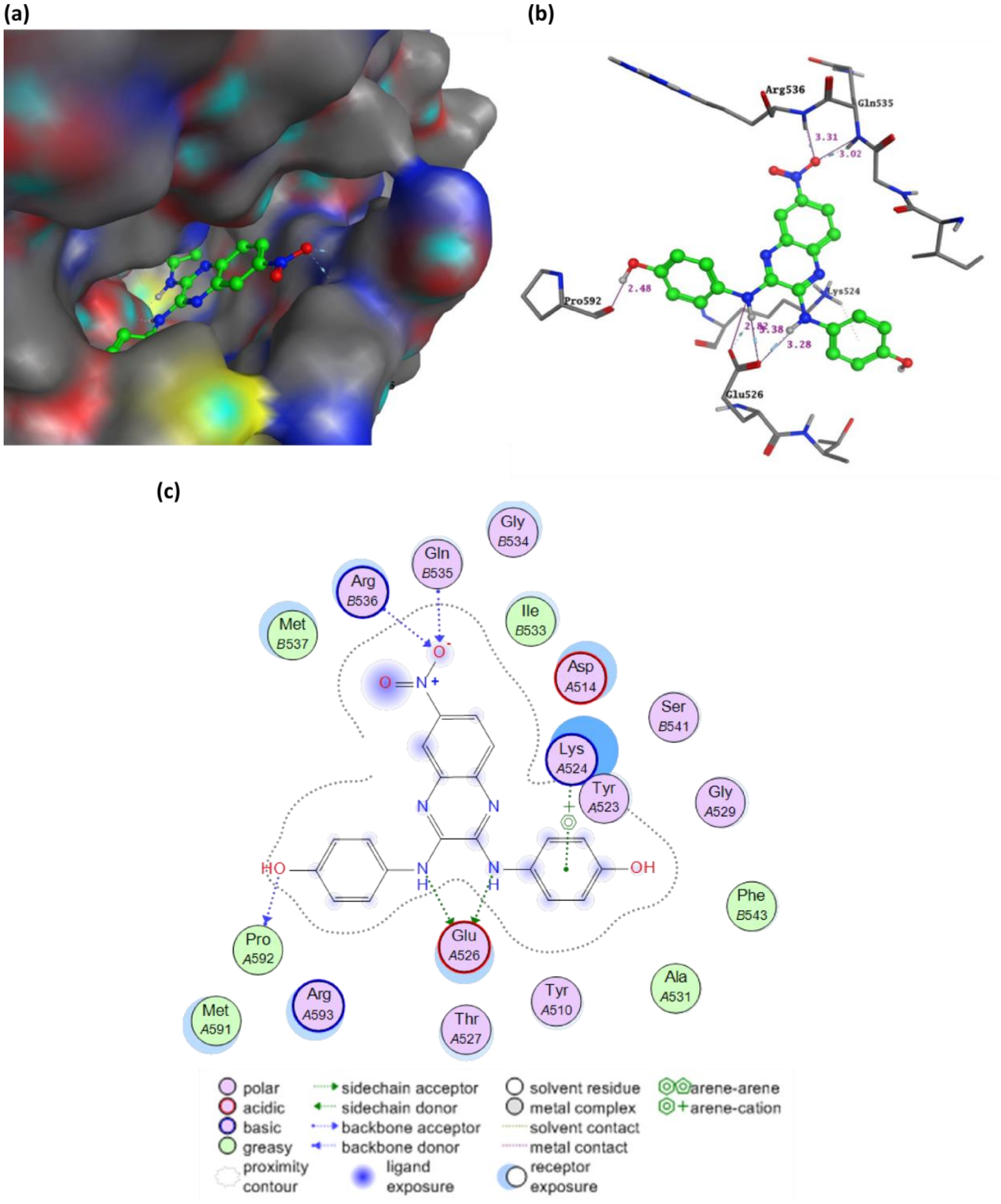
(a)
(b)
Arg536
Gln535
3.31
3.02
Pro592
2.48
Lys524
3.38
3.28
Glu526
(c)
Gly B534
Gln B535
Arg B536
Met B537
Ile B533
Asp A514
Ser B541
Lys A524
Tyr A523
Gly A529
Phe B543
Pro A592
Glu A526
Met A591
Arg A593
Thr A527
Tyr A510
Ala A531
HO
OH
N
H
polar
acidic
basic
greasy
proximity contour
sidechain acceptor
sidechain donor
backbone acceptor
backbone donor
ligand exposure
solvent residue
metal complex
solvent contact
metal contact
receptor exposure
arene-arene
arene-cation

Figure 50. Highest ranking docking pose of compound 41 into the pseudosymmetric site of sGC. a) and b) Cartoon representation of compound **41** docked into the pseudosymmetric site of sGC; b) 2D representation of the ligand interactions between the compound and the residues of sGC.

Table 11. Possible interactions between compound 41 and sGC and their respective distances obtained by docking.

Ligand	Receptor			Interaction	Distance (Å)
	Atom	Residue	Chain		
N 10	OE1	GLU526	A	H-donor	3.28
N 11	OE1	GLU526	A	H-donor	3.38
N 11	OE2	GLU526	A	H-donor	2.82
O 28	O	PRO592	A	H-donor	2.48
O 12	N	GLN535	B	H-acceptor	3.02
O 12	N	ARG536	B	H-acceptor	3.31
6-ring	NZ	LYS524	A	π-cation	3.63

4.3. Summary

sGC inhibitors currently used as biochemical tools to investigate the pathologies associated with sGC overactivity lack selectivity or bioavailability, limiting their use *in vivo* and further development as potential therapeutic agents. In this chapter, a new inhibitor of sGC has been presented. The small molecule, compound **41**, resulted from a series of screening experiments initially based on analogues of the anti-convulsing drug lamotrigine which showed mild sGC inhibition.

Compound **41** inhibits purified bovine lung sGC with an IC_{50} of 24 µM in the presence of 10 nM NO, and with an IC_{50} of 37 µM when the enzyme is stimulated with 1 µM cinaciguat **6**, in the absence of added NO. Inhibition of membrane-bound pGCs was also observed in purified rat lung membranes which had been treated with ODQ **4** to inhibit cGMP production by sGC. Compound **41** inhibited pGC activity with an IC_{50} value of 25 µM in the presence of 1 µM ANP. This indicates that the small molecule is not acting through oxidation of the heme, but rather targeting the catalytic domain of the enzyme.

Further characterisation of the binding of compound **41** was carried out using the SPR assay previously developed for the detection of binding of compound to sGC, described in chapter **3**. A comparison was performed between the binding of the inhibitor to the full-length enzyme, the wild type catalytic domain and the mutated catalytic domain whose crystal structure has been solved. An additional experiment was performed to compare the results obtained with the standard CM5 chip and the CM7 chip, which has a higher degree of carboxylation and allows higher immobilisation levels. In general, the binding affinity of compound **41** was similar for all immobilised proteins and chips (K_D = 11 – 33 µM). The CM7 chip gave slightly better sensorgrams with the wild type catalytic domain than the CM5 chip, with a lower degree of non-specific binding.

A simple route to the synthesis of the inhibitor **41** was developed using microware-assisted organic chemistry, which takes place through nucleophilic aromatic substitution in a polar aprotic solvent, without the need for the addition of catalysts or long reaction times. The synthesised compound showed similar activity to the commercially available material in a biochemical assay.

Co-crystallisation of sGC with a bound compound has yet to be achieved. In order to hypothesise a binding mode and consider the interactions that may take place between compound **41** and the receptor, docking studies were performed using the available crystal structure of a mutated catalytic domain of sGC, to which binding of the inhibitor had been observed by SPR. The inhibitor was successfully docked into the pseudosymmetric site of the receptor and it is possible that the interactions between the compound and the receptor include hydrogen bonds and π-cation interactions.

In summary, compound screening led to the identification of a new inhibitor of sGC which binds to the catalytic domain of the enzyme, possibly at the pseudosymmetric site, and may establish intermolecular interactions with both subunits of sGC.

Chapter 5: Design, synthesis and characterisation of small molecules as potential sGC inhibitors

5. Design, synthesis and characterisation of small molecules as potential sGC inhibitors

5.1. Introduction

In the previous chapter, the discovery of a new class of inhibitors of sGC was described, and the biochemical activity and biophysical binding of hit compound **41** was explored. Given that a crystal structure of the drug-target complex could not be obtained, it was necessary to synthesise and characterise a small library of analogues in order to explore the binding role of the different groups present in the molecule and seek more potent compounds. The activity of synthesised compounds was evaluated using a simple biochemical assay that allows the calculation of enzyme percent inhibition by selected compounds at 100 µM. Their binding to the catalytic domain was measured using SPR, also at a single concentration.

5.1.1. Design rationale for analogues of compound 41

In order to understand the functionality of the groups present in compound **41**, a series of analogues was designed and synthesised with small variations in their structure, as summarised in Figure **51**. Compound **41** is composed of a quinoxaline scaffold with a nitro group in the 6-position of the heterocycle and joined to two phenols via secondary amines which serve as linkers. Variations in this structure involved the replacement of *p*-phenols by *m*-phenols and other substituted benzenes (substructure **E**), replacement of the nitro group (substructure **F**), removal of the NH linker (substructure **G**), and reduced symmetry of the compounds by mono-substituted quinoxalines (substructure **H**).

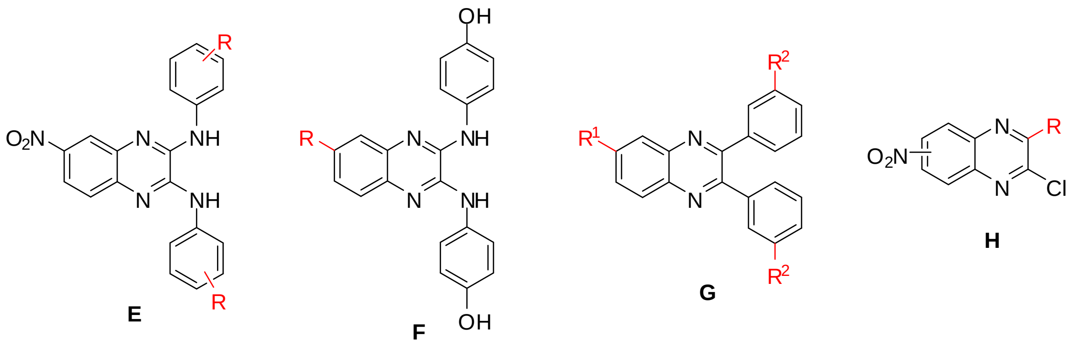

Figure 51. Substructures of compounds analogues of compound 41 to be synthesised.

5.2. Results and discussion

***N.B.** Compounds **53**, **60**, **61**, **70**, and **71** were synthesised by Revathy Selvarajah, at the time a MChem student from the Department of Chemistry.*

5.2.1. Replacement of phenols

A series of compounds was synthesised and tested in which the *p*-phenol rings were replaced by other substituted aromatic rings. Their structure, synthetic yield, percent inhibition, and binding response to sGCcat are summarised in Table **12**.

A common strategy in drug design is to change the position of substituents. In the case of compound **41** it would be possible that by changing the position of the hydroxyl group a stronger hydrogen bond could be formed by creating a more favourable contact with the receptor, thus increasing the activity of the inhibitor. Compound **48** was synthesized in which the hydroxyl group was in the meta-position. This compound also inhibits the activity of sGC and binds strongly to the receptor.

Hydroxyl groups are commonly encountered in drugs due to their involvement in hydrogen bonding: the oxygen atom can act as a H-bond acceptor and the hydrogen as a H-bond donor. Testing the activity of the methoxy analogue, compound **49**, could give some insight into the mechanism by which the compound is interacting with sGC. On one hand, if the proton of the original hydroxyl group is involved as a H-bond donor and is removed, the activity of the compound should be lowered. However, if the oxygen atom is acting as a H-bond acceptor, since it is still present in the methoxy analogue, the compound would remain active. Compound **49** showed no activity and no binding to sGC, confirming the hydroxyl group acts as H-bond donor and is required for activity. Removal of the hydroxyl group resulted in compound **50**, which also showed no activity or significant binding.

Many compounds in medicinal chemistry derive from peptides or polypeptides, and amide bonds are therefore present in the many lead compounds. Amides are likely to interact with binding sites through hydrogen bonding – primary and secondary amides have N-H groups that can act as H-bond donors, whilst the carbonyl oxygen atom can act as H-bond acceptor and has the potential to form two hydrogen bonds. Two acetamide analogues of compound **41** were synthesized: one in the para- position, compound **51**, and the other in the meta- position, compound **52**. Neither of the compounds showed activity or significant binding to sGC.

The insertion of fluorides in aromatic rings can lead to higher metabolic stability, when compared to hydroxyl groups. These are however not able to form halogen bonds, and the fluoride-containing compound **53** showed no significant binding or activity against sGC.

Indoles and indazoles are classical isosteres of phenol and have been shown not only to provide stronger interactions but also to improve metabolic stability.[123] In this case, replacement of the phenol by an indazole was preferred over indole, as its ClogP is lower, and compound **54** was synthesised. However, it showed no significant inhibition of sGC, and its binding to the enzyme could not be determined by SPR since the compound showed poor solubility in the assay buffer. Compound **54** cannot establish the same contacts as compound **41** when docked into the structure of sGC, and it generally docks into the opposite side of the pseudosymmetric binding site.

Table 12. SAR of compounds where p-phenols have been substituted.

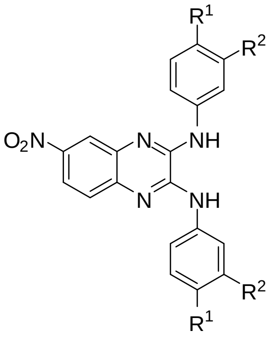

Compound number	R2	R2	% yield	sGC % inhibition	sGCcat binding Norm. Response (RU)
41	OH	H	60	56.2 ± 22.4	14.40 ± 1.72
48	H	OH	75	41.4	11.61 ± 0.76
49	OCH_3	H	40	0.8	0.99 ± 0.28
50	H	H	70	14.0	2.55 ± 0.21
51	$NHCOCH_3$	H	25	-8.7	0.84 ± 0.33
52	H	$NHCOCH_3$	50	9.0	2.99 ± 1.01
53	F	H	61	-41.0	1.88 ± 1.78
54	2-CHNNH-3		25	-12	-

5.2.2. Replacement of the nitro group

The electron-withdrawing nitro group commonly presents as a challenge in drug design. Nitro-aromatics are commonly associated with toxicity, but identifying suitable replacements has proven difficult. For example, in the development of the Bcl-XL inhibitor ABT-737 (**55**), an aromatic nitro group was replaced successfully by a trifluoromethylsulfone group; whilst in the development of inhibitors of the murine double minute 2 (MDM2)-p53 protein-protein interaction, the same replacement rendered the compound inactive.[124]

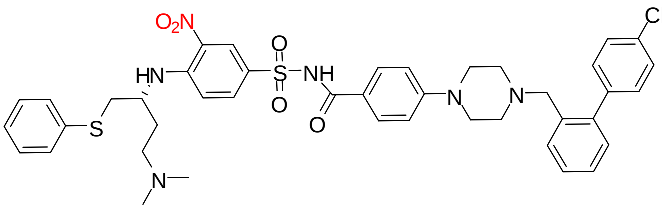

55

Figure 52. Chemical structure of the Bcl-XL inhibitor ABT-737.

The nitro group in compound **41** was replaced by a series of groups, their activity and binding was also investigated. A series of 6-substituted-2,3-dichloroquinoxalines was synthesised, since they were not commercially available. Further modifications included the reduction of the nitro to a primary amine, and the conversion of an acyl chloride into an amide.

5.2.2.1. Synthesis of 6-substituted-2,3-dichloroquinoxalines

2,3-dichloroquinoxalines (**57, 59, 61, 63**) were obtained by chlorination of 2,3-dihydroquinoxalines (**56, 58, 60, 62**) using thionyl chloride with a catalytic amount of dimethyl formamide (DMF). The precursor 2,3-dihydroquinoxalines were in turn obtained by condensation of 1,2-phenylenediamines with oxalic acid, following known protocols[125] (Scheme **3**).

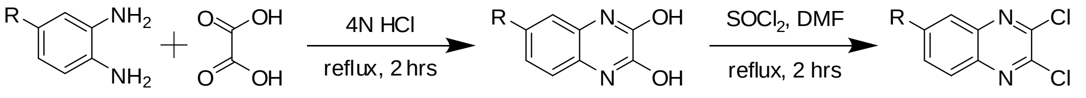

R =	CF_3	**56,**	50 %	R=	CF_3	**57,**	67 %
	CN	**58,**	59 %		CN	**59,**	67 %
	Cl	**60,**	85 %		Cl	**61,**	72 %
	COOH	**62,**	84 %		COCl	**63,**	66 %

Scheme 3. Synthesis of 2,3-dichloroquinoxalines.

The 2,3-dihydroquinoxalines are effectively chlorinated by the intermediate formidinium chloride salt , also known as the Vilsmeier reagent, which results from the reaction of DMF with thionyl chloride (Scheme **4**). In the first step, DMF attacks thionyl chloride, and the chloride ion leaves. The resulting cation undergoes nucleophilic attack by the chloride ion, forming a tetrahedral intermediate, whichintermediate collapses with the loss of sulphur dioxide and chloride ion. At this point, the Vilsmeier reagent forms an intermediate with the quinoxaline-2,3-diol by nucleophilic attack. Rearrangement of the intermetiade species leads to regeneration of DMF, which acts as a good leaving group, allowing for an efficient chlorination of the the quinoxaline.. The generated gases, SO_2 and HCl, leave the reaction vessel.

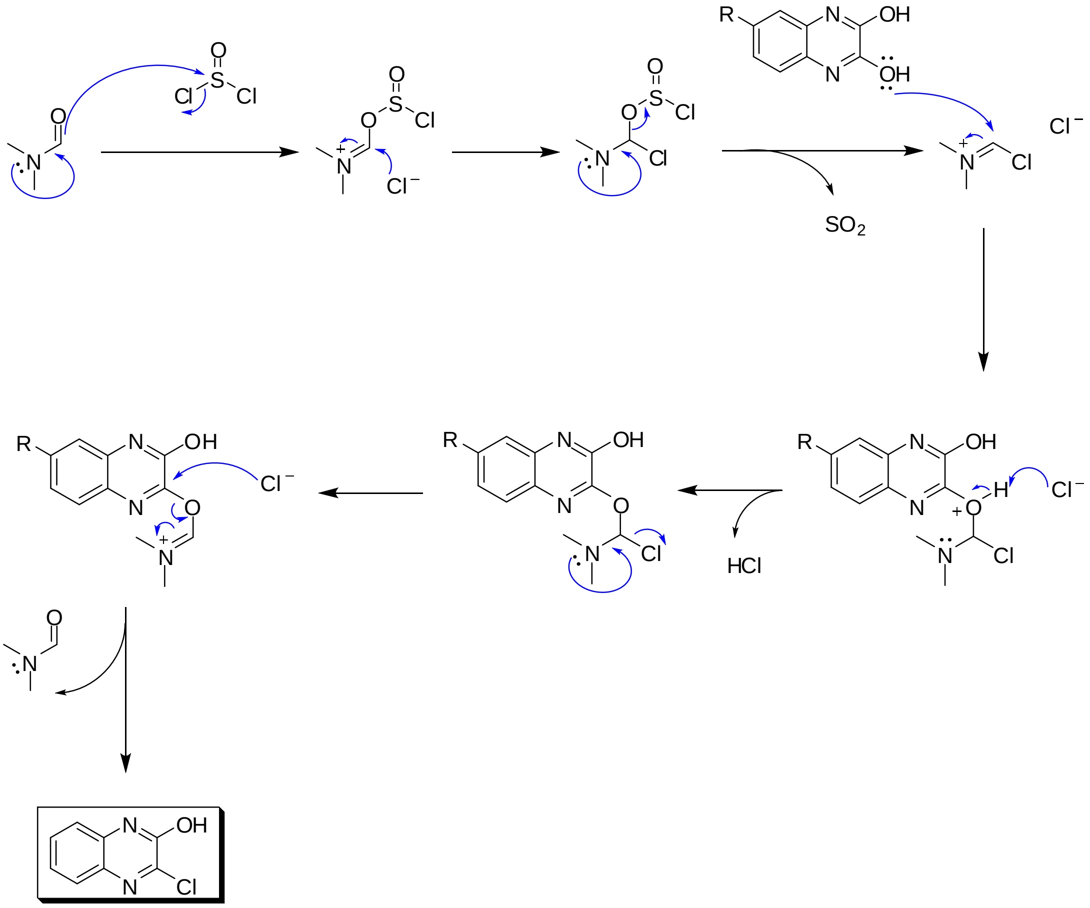

Scheme 4. Proposed mechanism for DMF catalysed chlorination with thionyl chloride.

5.2.2.2. Amide formation from acyl chloride

The acyl chloride **63,** was converted into a methylamide **64** by reaction with methylamine. Upon reaction with 3- and 4-aminophenols, the resulting analogues **73** and **74** were tested for sGC inhibition. It was proposed that if the nitro group is acting as a H-bond acceptor, its substitution by a carbonyl group could retain that interaction, which was observed in the docking studies. Although compound **74** showed strong binding to the receptor, neither of the compounds showed inhibition in the biochemical assay.

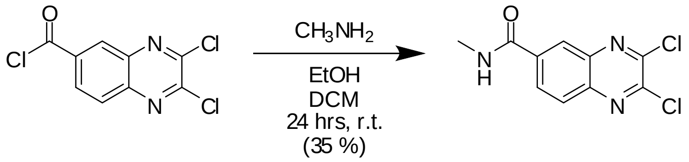

63 **64**

Scheme 5. Synthesis of 2,3-dichloro-N-methylquinoxaline-6-carboxamide 64.

5.2.2.3. Reduction of the nitro group

Reduction of nitro groups may take place under different mechanisms, including hydrogenation, electron transfer, and hydride reductions.

Reduction of aromatic nitro compounds by hydride is not straightforward Though aliphatic nitro compounds are relatively easy to reduce with lithium aluminium hydride ($LiAlH_4$), reduction of nitrobenzene gives the azo compound (Ph-N=N-Ph), not the aniline.[126-127] The most common metal counterion for hydride reducing agents are lithium and sodium. Nonetheless, alternative metal borohydrides can be generated with metals of higher ionic potential (such as Mg, Ca, Ba, and Sn) which may give better yields to the reduction of some functional groups.

Tin (II) chloride ($SnCl_2$) selectively reduces nitro groups into amines via a series of electron transfers.[128-129] In the Selwood lab, it has previously been found that a combination of $SnCl_2$ and sodium borohydride ($NaBH_4$) has given better results for the reduction of nitro groups than the use of $SnCl_2$ alone. $NaBH_4$ does not reduce nitro groups in aqueous or alcoholic solutions, but it has been found to do so in the presence of transition metals. For instance, reduction of 1-chloro-4-nitrobenzene takes place in the presence of copper (II) acetylacetonate and it has been proposed to follow the simple pathway benzene – nitrosobenzene – phenylhydroxylamine – aniline, rather than producing the condensation intermediates azoxy- and azo-benzene.[130] Reduction of the nitro group in compound **41** into an amine took place by reaction with tin (II) chloride dihydride and $NaBH_4$ in ethanol. In the proposed mechanism (Scheme **6**), Sn^{2+} coordinates with the nitro, allowing the first hydride attack to the nitrogen. Similarly to the copper (II) reaction described above, nitroso and hydroxylamine intermediates would be formed.

Formation of the amine (65 % yield) was confirmed by ^1H NMR, where the NH_2 broad peak can be seen at 5 ppm (Figure **53**).

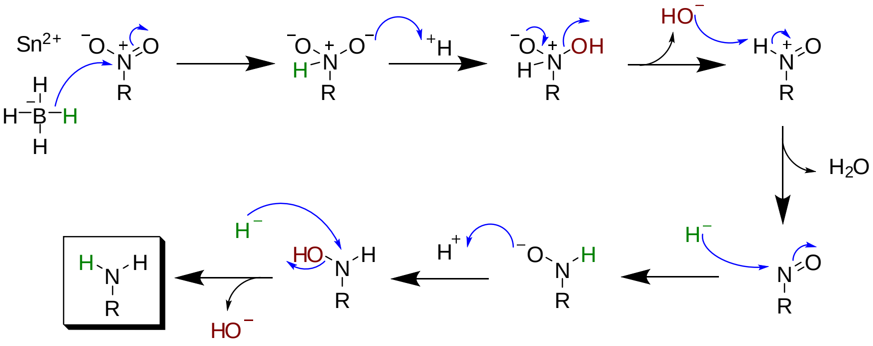

Scheme 6. Proposed mechanism for nitro reduction with $NaBH_4$ and $SnCl_2$.

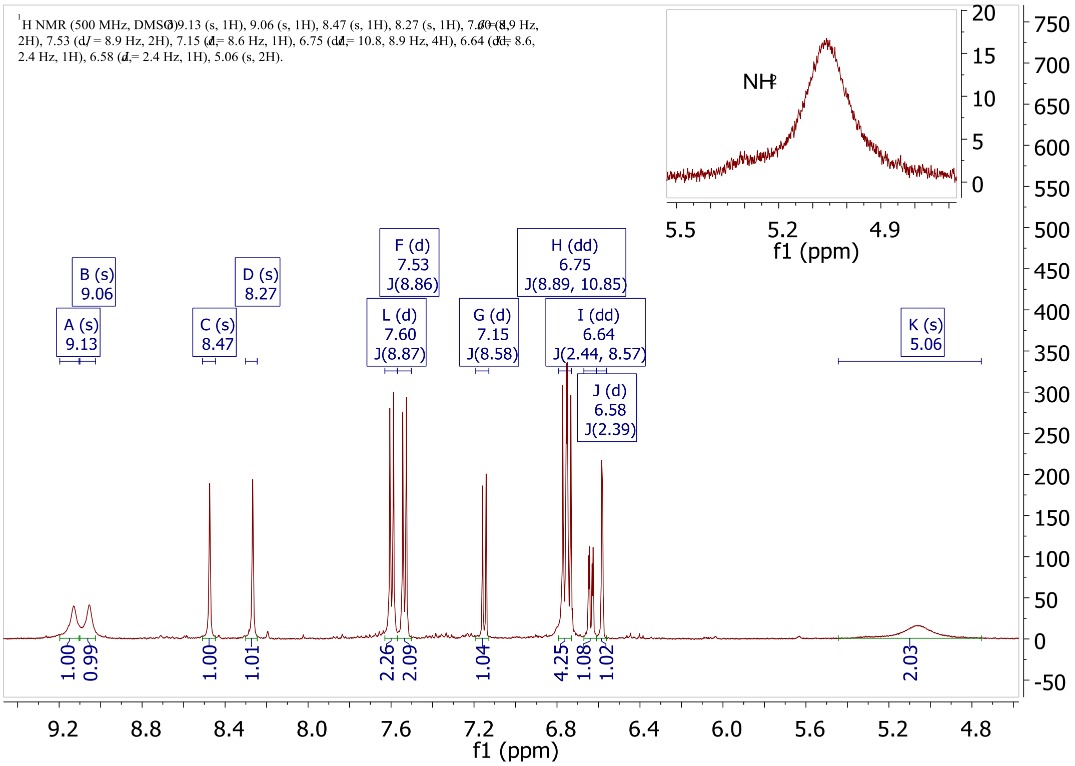

^{1}H NMR (500 MHz, DMSO) δ 9.13 (s, 1H), 9.06 (s, 1H), 8.47 (s, 1H), 8.27 (s, 1H), 7.60 (d, *J* = 8.9 Hz, 2H), 7.53 (d, *J* = 8.9 Hz, 2H), 7.15 (d, *J* = 8.6 Hz, 1H), 6.75 (dd, *J* = 10.8, 8.9 Hz, 4H), 6.64 (dd, *J* = 8.6, 2.4 Hz, 1H), 6.58 (d, *J* = 2.4 Hz, 1H), 5.06 (s, 2H).

Figure 53. ^{1}H NMR of compound 75. The broad peak at 5.06 ppm corresponds to the NH_2 in the 6-position of the quinoxaline, confirming successful reduction of the nitro groups. The NH_2 group also causes the quinoxaline protons to be more shielded thus appearing at lower ppm compared to compound **41**.

5.2.2.4. Characterisation of final compounds

The 6-substituted-2,3-dichloroquinoxalines described in sections **5.2.2.1** and **5.2.2.2** were reacted with 3-aminophenol and/or 4-aminophenol and the final compounds were tested for sGC binding and inhibition. Removal of the nitro group renders the compound inactive (compound **65**) although it still binds strongly to the receptor. This suggests the binding observed is not greatly influenced by the group in the 6-position of the quinoxaline, but it is however necessary for activity. Substitution of the nitro by other electron withdrawing groups gave similar results (Table **13**). Insertion of amine, chloro and nitrile groups also resulted in compounds which bind to the receptor but do not inhibit the enzyme activity. Conversely, insertion of a trifluoromethyl group resulted in active compounds (compounds **66** and **67**) that do not bind to the receptor so strongly.

The reaction of 2,3-dichloroquinoxaline-6-carbonyl chloride **63** with 3-aminophenol resulted in nucleophilic attack on the carbonyl as well, yielding the compound **72**, which did not show significant activity or binding.

Table 13. SAR of compounds where the nitro group has been substituted.

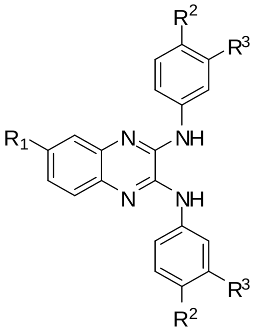

Compound number	R1	R2	R3	% yield	sGC % inhibition	sGCcat binding Norm. Resp. (RU)
41	NO_2	OH	H	60	56.2 ± 22.4	14.40 ± 1.72
65	H	OH	H	50	-28	12.43 ± 0.13
66	CF_3	OH	H	83	44.4	6.38 ± 0.47
67	CF_3	H	OH	83	21.1	2.96 ± 0.46
68	CN	OH	H	86	-31	4.46 ± 1.98
69	CN	H	OH	94	-57	10.46 ± 0.53
70	Cl	OH	H	79	-6	9.72 ± 0.49
71	Cl	H	OH	79	-11	9.01 ± 0.42
72	CONH-(3-OH)-Ph	OH	OH	31	16	3.96 ± 0.34
73	$CONHCH_3$	OH	H	72	-19	1.11 ± 0.30
74	$CONHCH_3$	H	OH	75	-54	9.58 ± 0.29
75	NH_2	OH	H	61	-24	9.85 ± 0.22

There is no clear correlation between binding and inhibition in this series of compounds. In general, removal of the nitro group or its substitution by other electron-withdrawing or carbonyl groups resulted in compounds which are still capable of binding the receptor, as observed by SPR, but only the trifluoromethyl-substituted compounds **66** and **67** were active in a functional assay. It is possible the inactive compounds are more stable at a conformation different from that of the active compounds, thus binding to the receptor in a different way, and docking of compounds shows it is possible for some compounds to fit at different ends of the binding site. Nonetheless, due to such a structural similarity between the compounds and their electronic behaviour, they would be expected to show similar binding behaviours.

5.2.2.5. Trifluoro-substituted inhibitors with reduced toxicity

As mentioned above, the use of nitro groups in drugs should be limited, as they are commonly associated with *in vivo* toxicity. Nitro-aromatic compounds can be metabolised into nitroso compounds and hydroxylamines, both of which present toxicity. Nitroso aromatics bind haemoglobin and can cause methemoglobinemia, whilst aromatic hydroxylamines may covalently modify DNA via electrophilic nitrinium formation.[131-132]

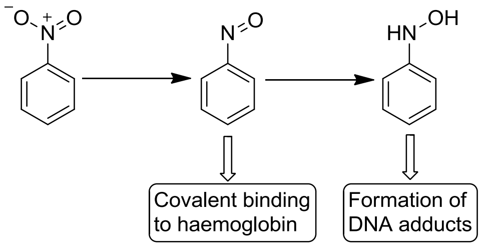

Figure 54. Reductive pathways involved in the metabolism of nitroaromatics. Addapted from Smith, G.[131]

The introduction of fluorides is common in medicinal chemistry since many approved pharmaceuticals are fluorinated. Fluorinated compounds may improve bioavailability by increasing stability to metabolism.[133] Thus, since the fluoromethylated compound **66** showed significant inhibition of sGC activity, this compound would be preferred for follow-up assays over the nitro compound **41**. Both compounds can be similarly docked into sGCcat. The stronger binding observed by SPR of compound **41** to the receptor may be due to a potential H-bond between the nitro group and backbone amines. This however does not seem to be necessary for activity (Figure **55**).

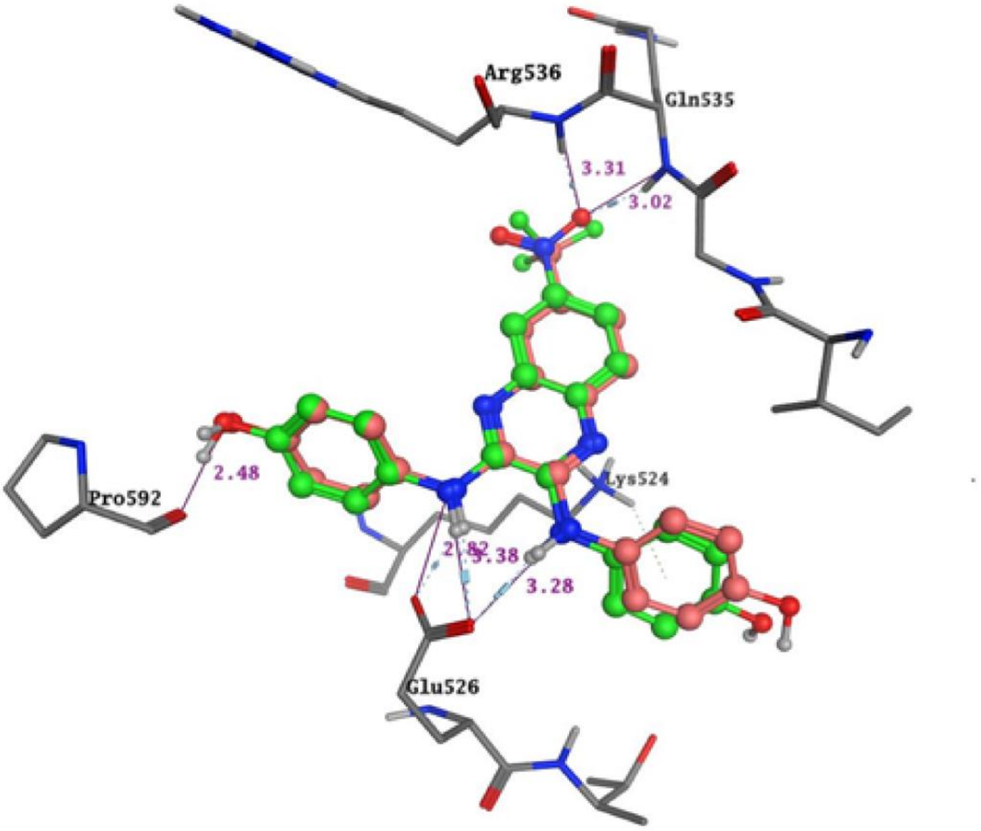
Arg536
Gln535
3.31
3.02
Pro592
2.48
Lys524
2.82
3.38
3.28
Glu526

Figure 55. Superimposition of compounds 41 and 66 binding to the pseudosymmetric site of sGC. Compound **41** (green) is docked with a Goldscore of 57.86 and the depicted pose for compound **66** (pink) has a Goldscore of 54.49.

5.2.3. Synthesis of mono-substituted quinoxalines

It was found that the reaction of 6-nitroquinoxaline **44** with *N*-(2-aminophenyl)acetamide **76** was unfavoured, as the *ortho*-substituted aniline is sterically hindered and prevents the displacement of a second chloride. The resulting compound is therefore mono-substituted and is obtained in very low yields (16 %). The reaction could result in two possible isoforms in which the nitro group of compound **78** could be in the 6- or 7- position of the quinoxaline. Analysis by LC-MS shoes only one major product with m/z $[M-H]^-$ = 356 and it is not possible to confirm which isoform was formed.

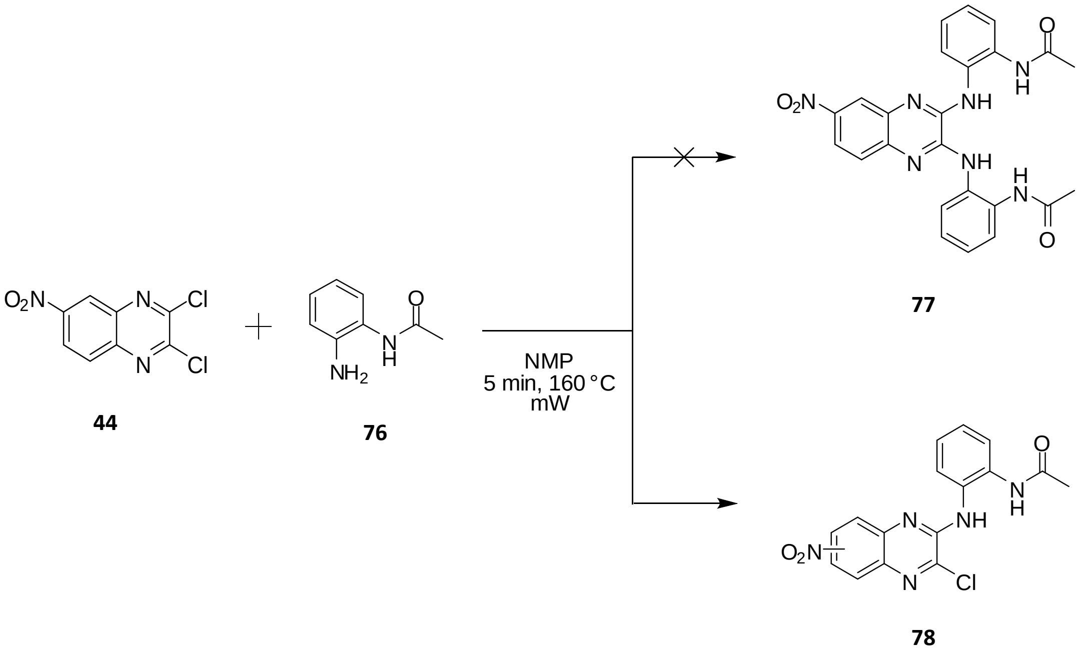

Scheme 7. Synthesis of compound 78.

(a) Chromatograph

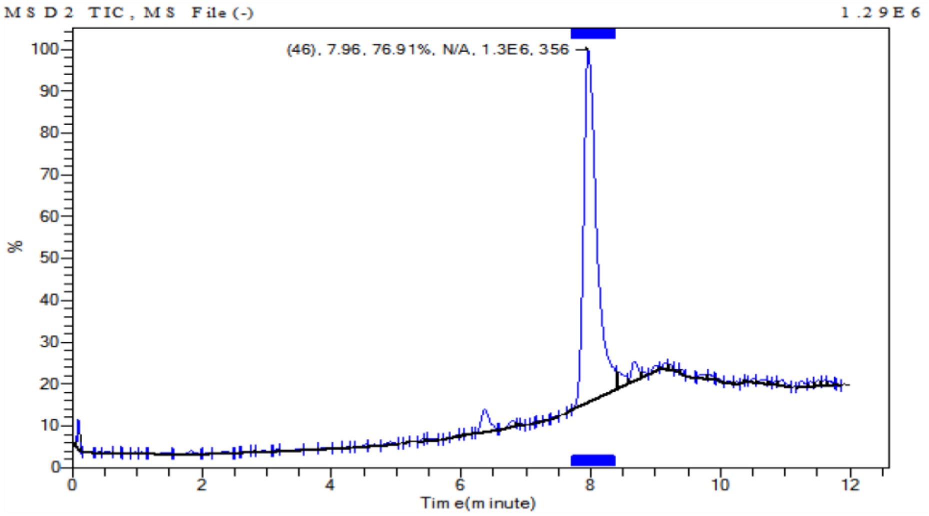

(b) Mass spectrum

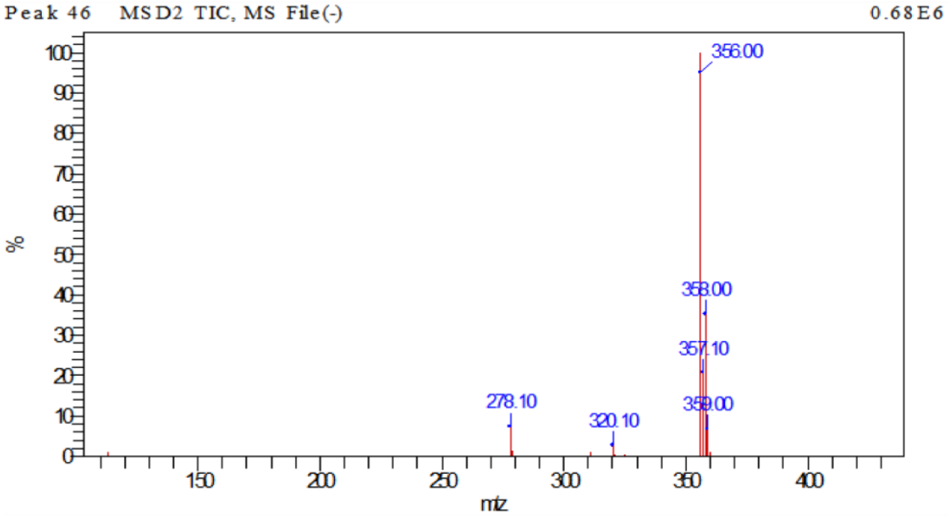

Figure 56. LC-MS spectrum of compound 78. (a) Chromatograph showing only one product with r.t. at 7.96 min; (b) Mass spectrum with $[M-H]^-$ (*m/z* 356.00) ion observed.

5.2.4. Improved synthesis of mono-substituted quinoxalines by Buchwald – Hartwig aryl amination

The Buchwald-Hartwig amination is a cross-coupling reaction of an aryl halide with an amine using a palladium catalyst, a ligand, and a strong base, to form a C – N bond.[134-135] This is a versatile technique as various palladium based catalysts are available and new ligands are constantly being developed to optimise the systems used for specific groups of organic molecules. A system using $Pd_2(dba)_3$ as precatalyst, the bidentate Xantphos as the ligand, and Cs_2CO_3 as base, has been widely used for coupling of aryl halides and amides.[136]

The method can also be applied under microwave conditions, which increase the rate of reaction and retains high yield.[137] It was investigated if this method could be employed to the coupling of 6-nitroquinoxaline **44** with the sterically hindered *N*-(2-aminophenyl)acetamide **76**. The reaction was carried out under microwave irradiation for 30 min at 120 °C, using dioxane as the solvent. The apparent yield of 40 % was indeed greater than the one obtained by nucleophilic aromatic substitution. In both cases however, it was not possible to obtain the desired compound with a great degree of purity. The use of the same conditions for the synthesis of compound **41** did not result in a greater yield (50 %) than that obtained by nucleophilic aromatic substitution (60 %).

The proposed mechanism for this cross-coupling reaction (Scheme **8**) starts with the oxidative addition (I) of 6-nitroquinoxaline **44** to the palladium catalyst generated by the precatalyst $Pd_2(dba)_3$ with the ligand Xantphos. Coordination (II) of the aniline to the catalyst takes place through its lone pair of electrons in the free amine. A base mediated palladium-amine bond formation (III) takes place, followed by reductive elimination (IV) in which the C-N bond is formed, to yield compound **78**.

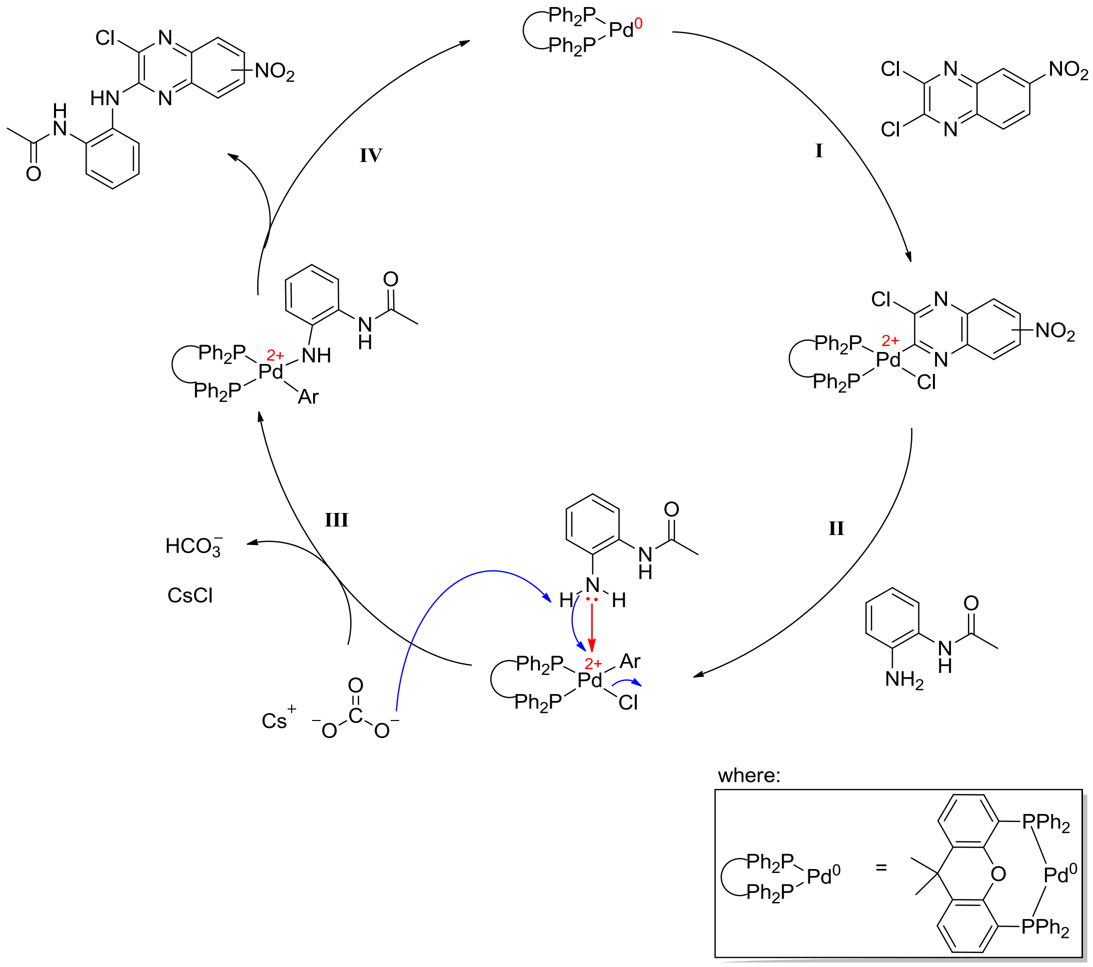

Scheme 8. Proposed mechanism for Buchwald-Hartwig cross-coupling reaction.

The addition of a methyl group in the 3-position of 4-aminophenol did not provide enough bulk for the reaction with 6-nitroquinoxaline **44** to result in a mono-substituted compound. Instead, compound **79** was obtained with 66 % yield. Surprisingly, the Buchwald-Hartwing cross-coupling proceeded via coupling of the quinoxaline with the hydroxyl group rather than the amine, possible because the amine was more hindered and the oxygen could coordinate with the catalyst more easily (Scheme **9**). This was confirmed by ^{1}H NMR, where the characteristic peak for a primary amine (4.92 ppm) can be observed (Figure **57**).

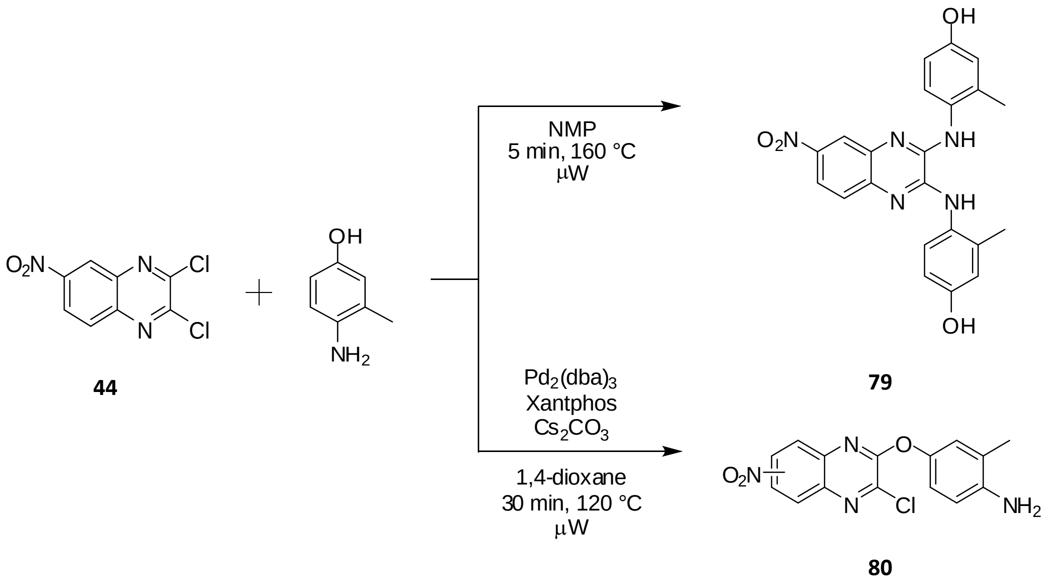
OH
O_2N
N
NH
N
NH
OH
O_2N
N
Cl
N
Cl
OH
NH_2
NMP
5 min, 160 °C
µW
44
79
$Pd_2(dba)_3$
Xantphos
Cs_2CO_3
1,4-dioxane
30 min, 120 °C
µW
O_2N
N
O
N
Cl
NH_2
80

Scheme 9. Synthesis of compounds 79 and 80.

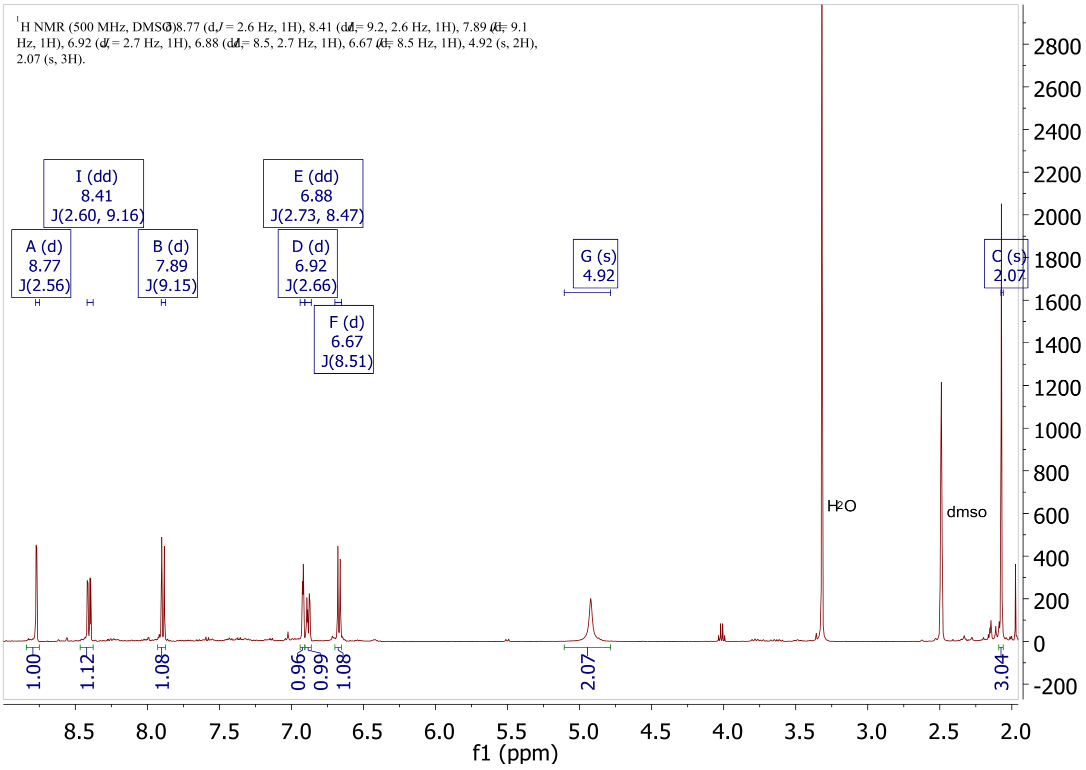

^{1}H NMR (500 MHz, DMSO) δ 8.77 (d, *J* = 2.6 Hz, 1H), 8.41 (dd, *J* = 9.2, 2.6 Hz, 1H), 7.89 (d, *J* = 9.1 Hz, 1H), 6.92 (d, *J* = 2.7 Hz, 1H), 6.88 (dd, *J* = 8.5, 2.7 Hz, 1H), 6.67 (d, *J* = 8.5 Hz, 1H), 4.92 (s, 2H), 2.07 (s, 3H).

Figure 57. ^{1}H NMR of compound 80. The peak at 8.77 ppm correspond to the *H* in the carbon in between the NO_2 and the pyrazine ring, and it is coupled to the other *H* proximal to NO_2 at 8.41 ppm (*J* = 2.6 Hz). This is in turn coupled to the vicinal proton which resonates at 7.89 ppm (*J* = 9.2 Hz). The peak at 6.92 ppm corresponds to the proton next to the methyl group and it is coupled to the *H* on the opposite side of the O at 6.88 ppm (*J* = 2.7 ppm), which is in turn coupled to the vicinal *H* at 6.67 ppm (*J* = 8.5 Hz). The NH_2 peak is seen at 4.92 ppm and the peak for the methyl group at 2.07 ppm.

The disubstituted analogue of compound **41**, compound **79**, bound strongly to the receptor but did not show enzyme inhibition. Neither of the mono-substituted compounds showed strong binding to sGC, but compound **80** inhibited its activity (Table **14**).

Table 14. Characterisation of compounds 78 - 80.

Compound number	% yield	sGC % inhibition	sGCcat binding Norm. Response (RU)
41	60	56.2 ± 22.4	14.40 ± 1.72
78	40	5	2.37 ± 0.60
79	66	-18	10.43 ± 0.08
80	26	41	2.86 ± 0.65

5.2.5. Asymmetrically substituted quinoxalines

The reaction of 2,3-dichloroquinoxalines with meta- or para-substituted anilines results in a bisubstitution of the quinoxaline by the aniline, giving compounds which are highly symmetrical. It is however possible that only one aminophenol in the active compounds (**41**, **66**, **67**) is required for activity, and that a different substitution on the vicinal carbon could take place, thus improving the activity or physico-chemical properties of the molecules.

Two asymmetrically substituted compounds were designed in which the solubilising groups piperazine and morpholine were introduced. The designed compounds would be expected to retain the key interactions with the receptor, whilst the reduced planarity and symmetry would be expected to increase their solubility.[138]

The quinoxaline was made symmetrical with the insertion of a second nitro group, in order to reduce the number of potential products. Nitration of 6-nitroquinoxaline-2,3-diol **81** was carried out in the presence of potassium nitrate and sulphuric acid. Formation of the nitric acid takes place by solvation of potassium nitrate in sulphuric acid. Subsequent reaction of nitric acid with sulphuric acid leads to the formation of the nitronium ion which is used in the electrophilic aromatic substitution of quinoxaline (Scheme **10**).

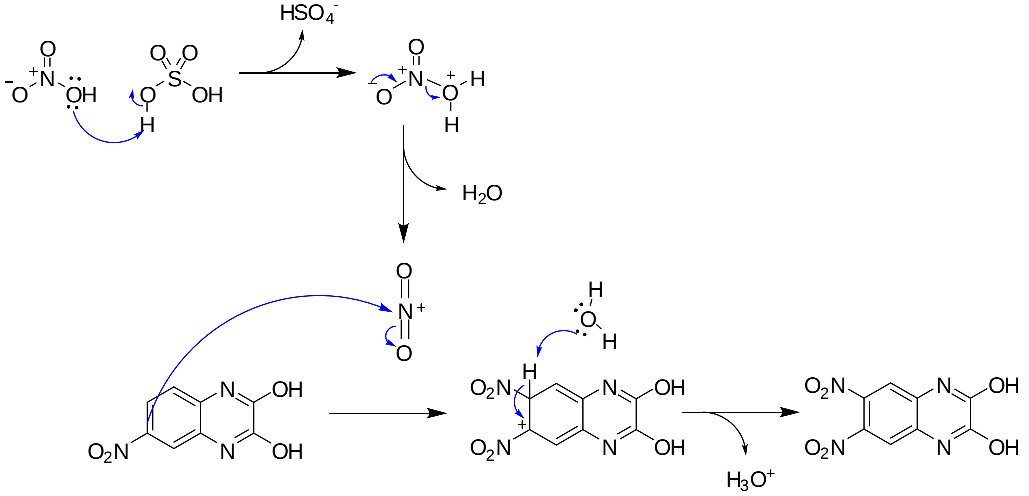
HSO4-
H2O
H3O+

Scheme 10. Proposed mechanism for the nitration of 2,3,-dichloro-6-nitroquinoxaline.

The progress of this reaction was monitored by LC-MS analysis, until consumption of the starting material was observed, after 48 hrs. The resulting 6,7-dinitroquinoxaline-2,3-diol **82** was then chlorinated to give 2,3-dichloro-6,7-dinitroquinoxaline **83** (Scheme 11).

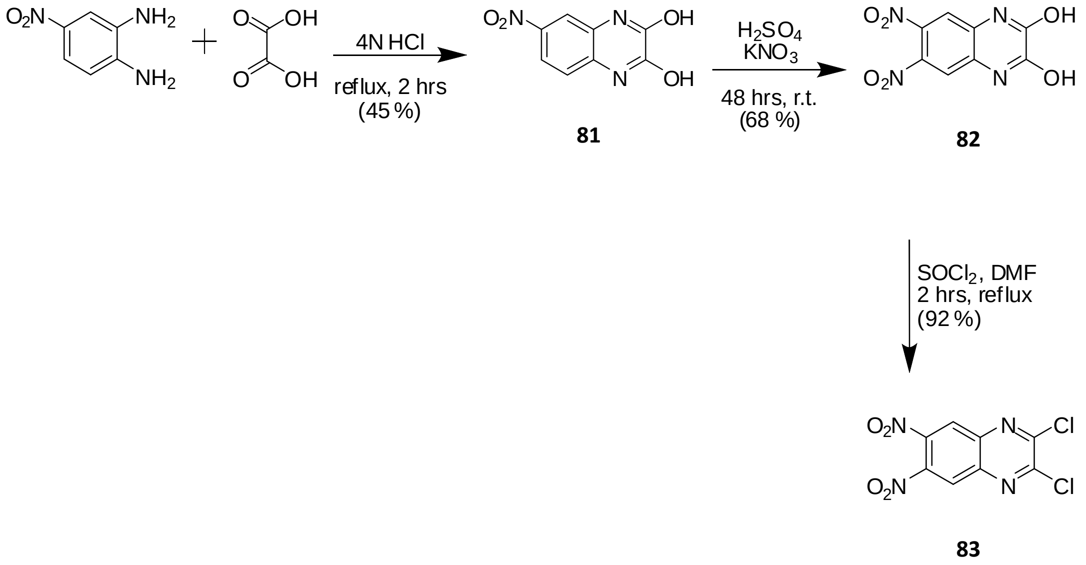
4N HCl
reflux, 2 hrs
(45 %)
81
H2SO4
KNO3
48 hrs, r.t.
(68 %)
82
SOCl2, DMF
2 hrs, reflux
(92 %)
83

Scheme 11. Synthesis of 2,3-dichloro-6,7-dinitroquinoxaline 83.

5.2.5.1. Synthesis of a piperazine-containing compound

Introduction of a piperazine in place of a hydroxyl group lead to compound **87**, which could potentially establish an additional H-bond since the piperazine would be protonated at neutral pH.

4-(4-methylpiperazin-1-yl)aniline **86** was obtained by a two-step process which started with the Eschweiler-Clarke methylation of 1-(4-nitrophenyl)piperazine **84** under microwave irradiation, using a literature method[139], followed by nitro reduction using sodium borohydride and tin (II) chloride. This methylation step took place to avoid reaction of the piperazine with the quinoxaline.

4-(4-methylpiperazin-1-yl)aniline **86** was reacted with 4-aminophenol and 2,3-dichloro-6,7-dinitroquinoxaline **83** and the resulting compound **87** was purified by reverse phase flash column chromatography (Scheme **12**). In addition to the desired asymmetrically substituted compound **87**, the reaction also proceeds via formation of symmetrically substituted compounds with both anilines used as starting material. Due to the similar polarity of the three compounds, it was not possible to successfully separate them by normal phase column chromatography, but separation was possible using C-18 columns and a water/methanol solution as the mobile phase.

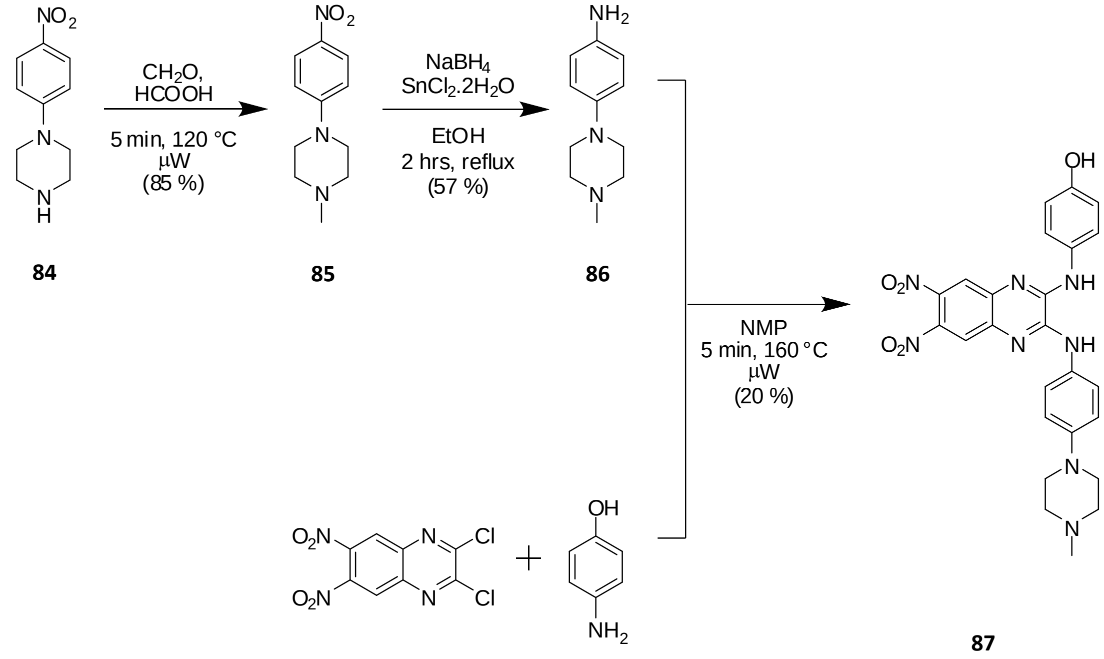

Scheme 12. Synthetic route to compound 87.

5.2.5.2. Synthesis of a morpholine-containing compound

A 4-phenylmorpholine was inserted instead of a second phenol (Scheme **13**). The purification of compound **89** was complex and required preparative HPLC purification after reverse phase flash column chromatography (Figure **58**). Preparative HPLC uses the same principle as analytical HPLC, except that in preparative HPLC the sample goes from the detector into a fraction collector, rather than into waste. This purification technique is considered lengthy and expensive when compared to traditional methods such as flash column chromatography and crystallisation and its use is therefore restricted for the separation of small quantities of compound. In this case, only 2 mg were obtained, which was enough for biological testing. NMR characterisation was not possible due to the small amount obtained, but compound identity was confirmed by accurate mass spectrometry.

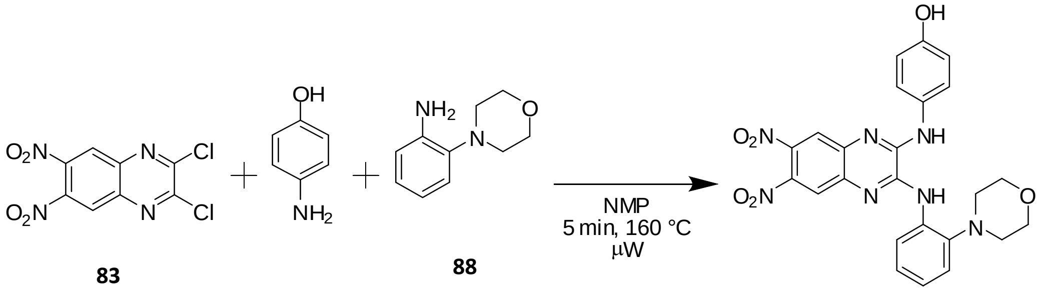

83

88

89

Scheme 13. Synthesis of 4-(3-(2-morpholinophenylamino)-6,7-dinitroquinoxalin-2-ylamino)phenol 89.

(a) Chromatograph of crude material

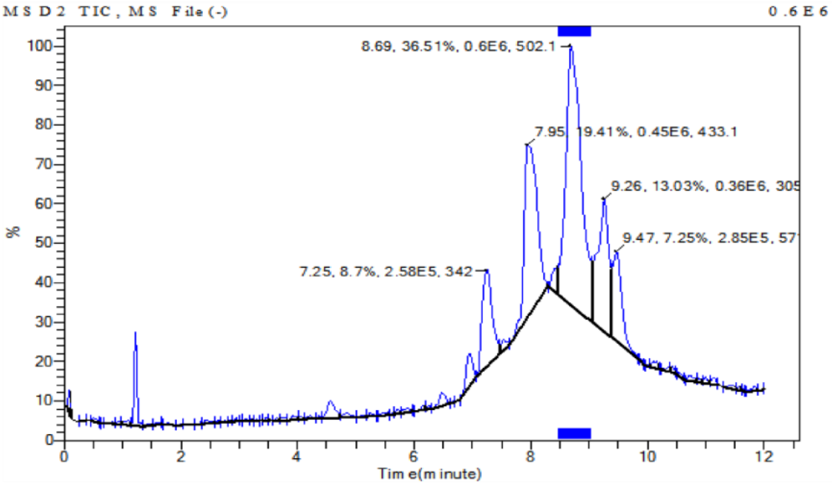

(b) Chromatograph after reverse phase column chromatography

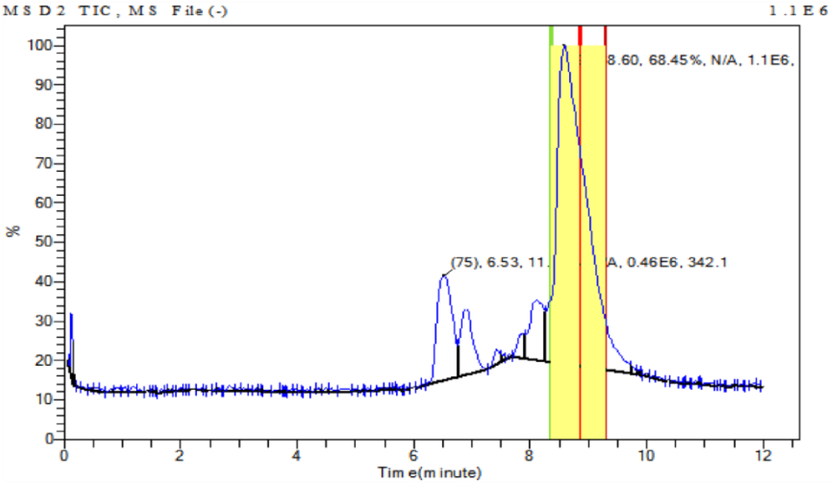

(c) Mass spectrum after purification

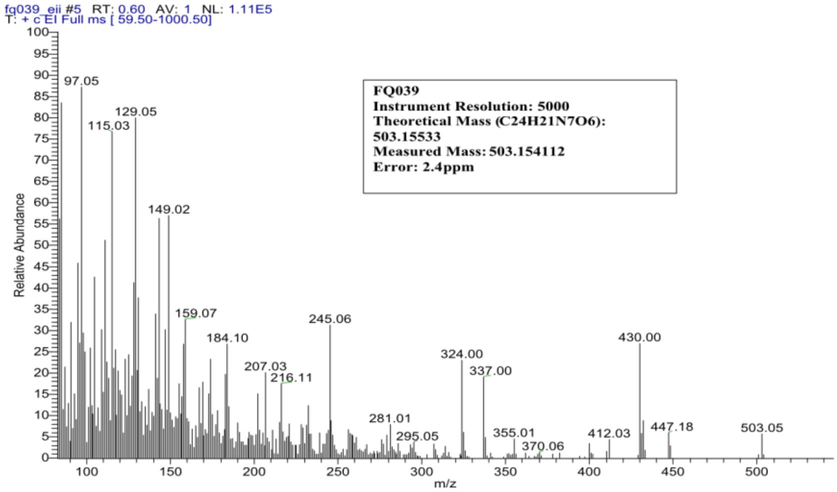
FQ039
Instrument Resolution: 5000
Theoretical Mass (C24H21N7O6):
503.15533
Measured Mass: 503.154112
Error: 2.4ppm

Figure 58. Monitoring the purification of compound 89 by liquid chromatography and mass spectrometry. (a) Chromatograph of the crude material, where the peat at r.t. 8.69 min corresponds to compound **89**; (b) Chromatograph obtained after reverse phase column chromatography, where the peak highlighted in yellow was recovered by preparative HPLC; (c) High resolution mass spectrum of compound **89** after purification. $[M+H]^+$ (*m/z* 503.15) ion observed.

5.2.6. Removal of the *NH* linker

A small set of compounds were obtained in which the *NH* linker was removed. These molecules are smaller and less flexible, and could potentially bind to deeper pockets in the receptor.

The available 4-substituted-1,2-diamines were condensed with commercially available 1,2-bis(3-methoxyphenyl)ethane-1,2-dione **90** and its demethylated analogue **91** using microwave irradiation. Demethylation of 1,2-bis(3-methoxyphenyl)ethane-1,2-dione **90** was achieved using HBr in AcOH, using a literature method (Scheme **14**). [140] [141]

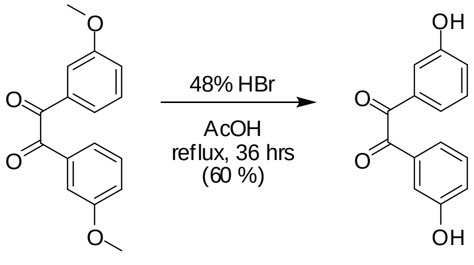

90 **91**

Scheme 14. Demethylation of 1,2-bis(3-methoxyphenyl)ethane-1,2-dione 91.

In general, hydroxyl-substituted compounds showed stronger binding to the receptor than the methoxy analogues. Conversely, methoxy analogues showed higher inhibition (Table **15**). Hydroxyl groups are strong H-bond donors, and may direct the compounds into a binding mode that is not favourable for inhibition. The methoxy analogues showed mild inhibition of sGC, and since they are very structurally different from the initial hit compound **41** they are expected to bind to the receptor in a different mode.

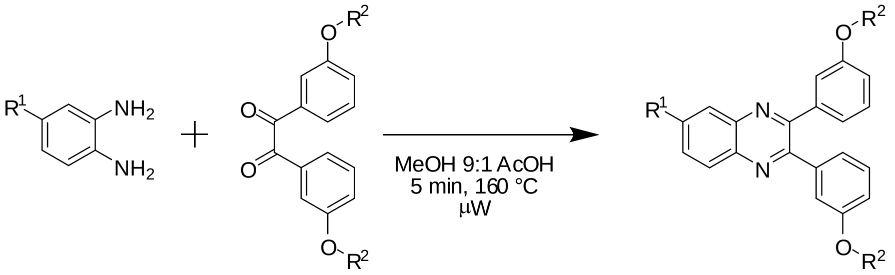

Scheme 15. Synthesis of 2,3-diphenylquinoxalines.

Table 15. SAR of2,3-diphenylquinoxalines.

Compound number	R1	R2	% yield	% inhibition	Norm. Response (RU)
41	-		60	56.2 ± 22.4	14.40 ± 1.72
92	CF_3	OCH_3	89	33	2.09 ± 0.21
93	CN	OCH_3	99	30	0.42 ± 0.25
94	Cl	OCH_3	99	38	-0.34 ± 0.54
95	F	OCH_3	89	39	1.09 ± 0.43
96	CF_3	OH	99	-46	10.95 ± 0.50
97	CN	OH	89	-21	8.44 ± 0.37
98	Cl	OH	99	-9	6.90 ± 0.46
99	F	OH	81	-36	5.52 ± 0.33

Docking of these compounds into the pseudosymmetric site of sGC suggests they are indeed binding to a deeper pocket of the pseudosymmetric site (Figure **59a**). The binding conformations of the two trifluoromethyl-substituted compounds **92** and **96** in the binding site show the trifluoromethyl groups at differents ends, and since **96** shows strong binding in the SPR assay but no activity, it is possible that as suggested, the strong H-bond possible between the hydroxyl groups is rendering the compound at a conformation that is not favourable for inhibition (Figure **59b**). On the other hand, compound **92** could be binding by structural complementarity, not necessarily establishing any strong H-bonds, but still inducing a conformational change that renders the enzyme inactive.

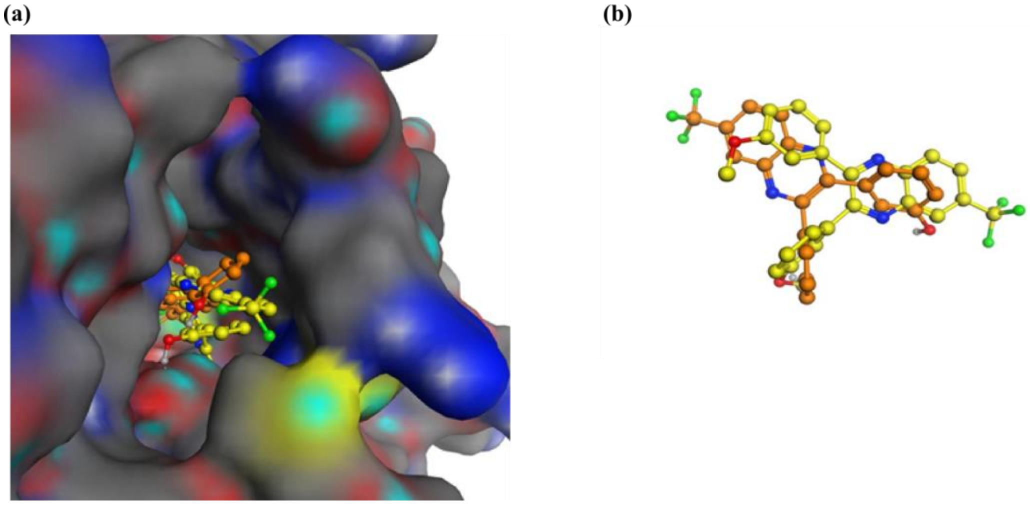

Figure 59. Docking of compounds 92 and 96 into the pseudosymmetric site of sGC. a) compounds **92** (yellow) and **96** (orange) bind to a deep pocket in the pseudosymmetric site of the enzyme; b) superimposion of the conformations with highest Goldscores of compounds **92** (yellow, goldscore 59.80) and **96** (orange, goldscore 54.73).

5.2.7. The role of superoxide dismutase in the biochemical assay

The biochemical assay used to test the activity of compounds reported in this chapter was developed and performed by the group of Prof. John Garthwaite (UCL). The assay used isolated purified bovine lung sGC, which was activated by the NO donor diethylamine NONOate, in the presence of GTP and the cofactor Mg^{2+}. Since some of the early reported inhibitors such as LY83583 (**31**) were found to inhibit enzyme activity by the formation of superoxide radicals, superoxide dismutase (SOD) was included in the assay buffer to prevent possible false positives that could result from the formation of superoxide. SOD is the general term given to metalloproteins which, as suggested by the name, dismutase superoxide into oxygen and peroxide. They are therefore considered antioxidants, and are commonly used in biochemical assays as radical scavengers. It was found that the activity of some initial hits reported in chapter **4** decreased in the presence of SOD, including that of compound **41** (data not shown).

Given that most analogues of compound **41** with at least one phenol ring showed binding to the enzyme in the biophysical assay it is surprising that only the trifluoromethyl substituted compounds showed significant inhibition of the enzyme. It should be noted that these compounds were only tested once. In addition, the activity of compound **41** varied significantly (56.2 ± 22.4 % inhibition) in the different assays performed, since the compounds were tested on different occasions, depending on their availability.

The last set of compounds tested were the *N*-methylquinoxaline-6-carboxamide derivatives **73** and **74**, and the asymmetrically substituted 6,7-dinitroquinoxalines **87** and **89**. The activity of the compounds was measured in the presence and absence of SOD. Additionally, basal activity was also assessed by measuring the production of cGMP in the absence of added NO (Figure **60**). [‡]

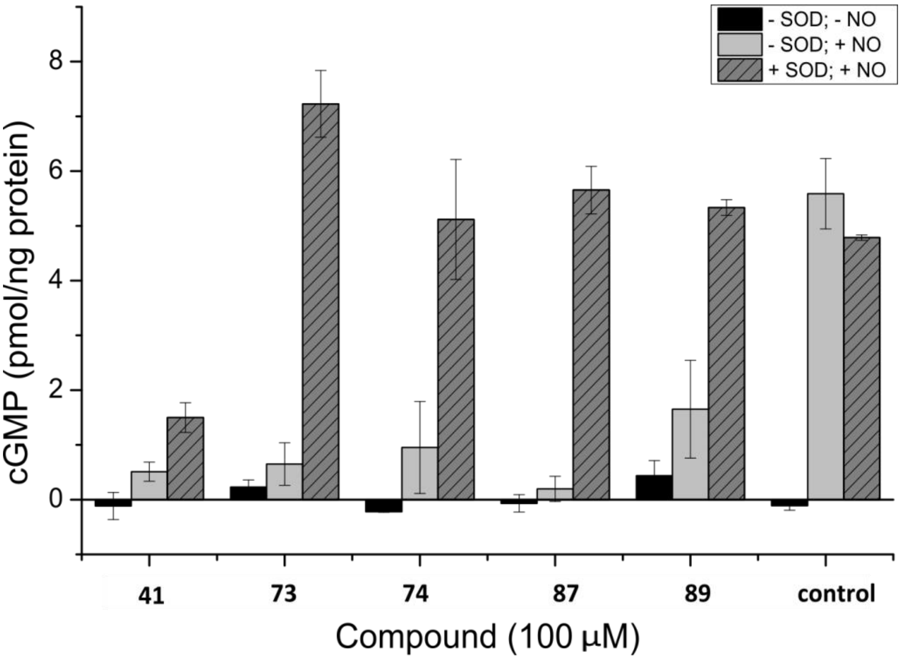

Figure 60. The activity of compounds 41, 73, 74, 87, and 89 in the presence and absence of SOD.

[‡] This set of experiments was performed by me and Prof. John Garthwaite.

It has been proposed that superoxide can be formed by reaction of DMSO and NaOH, both of which are present in the assay, with oxygen.[142] Yet, this has been controlled for as the compounds were tested alongside a control blank sample. No stimulation of sGC was observed in the absence of added NO. In the presence of 30 nM NO, cGMP production was observed in the presence and absence of SOD. All small molecules tested inhibited cGMP production to some extent in the absence of SOD, yet, when SOD was present only compound **41** showed enzyme inhibition.

SOD has a well-defined binding site formed at the dimer interface which has been shown to accommodate small molecules. [143-144] Moreover, SOD is a target for selective killing of cancer cells by oestrogen derivatives.[145]

This suggests the compounds reported here may be binding to SOD, which is present at high concentration in the assay buffer (0.1 mg/ mL), thus not acting on sGC. This could be investigated by a biophysical assay that would compare the affinity of the small molecules to SOD and sGC. Additionally, to confirm activity of the compounds, they could be tested in the presence of a different radical scavenger, such as the small molecule Tempol **100** (Figure **61**), which has been shown as effective as SOD in metabolising superoxide in cells.[146] At the time of writing this hypothesis had not been tested.

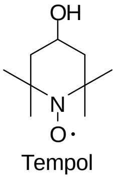

100

Figure 61. Chemical structure of the SOD mimetic Tempol 100.

5.3. Summary

In this chapter, the synthesis, biochemical activity and binding of a series of compounds based on compound **41** were described. Replacement of some of the functional groups present in the structure of the inhibitor has given useful information regarding its binding mode. One or both of the phenol rings are H-bond donors, and variations in these rings are not well tolerated. The position of the hydroxyl group can be changed whilst retaining binding strength and activity. However, other groups have rendered the compound inactive and reduced its binding strength.

Changes in the 6-position of the quinoxaline have resulted in compounds which have high affinity to the receptor, but only the trifluoromethyl compounds have shown significant inhibition of the enzyme. Nonetheless, the replacement of the nitro group by a trifluoromethyl would be very beneficial if the metabolism of the compounds is taken into consideration, since nitroaromatics are often metabolised into toxic compounds which may cause DNA damage.

The mono-substituted quinoxalines **78** and **80** showed only weak binding to the receptor but compound **80** showed mild inhibition of sGC, whilst the asymmetrically substituted compounds **87** and **89** inhibited sGC in the absence of SOD, but had no effect once SOD was included in the assay. A small set of 2,3-bis(3-methoxyphenyl)quinoxalines also presented mild inhibition of sGC activity.

It is possible that the inhibitors presented bind to the catalytic domain of sGC inducing a conformational change, or “locking” the enzyme in a basal conformation, that is not favourable to activation by NO or GTP binding. This hypothesis considers the simple model of sGC activation which consists of NO binding to the heme inducing a conformation change that leads to binding of GTP and its conversion into cGMP.

As discussed, the available biochemical assay used to assess the activity of the synthesised compounds is a highly artificial method, and it is proposed that a different functional assay could supplement the information reported here. A cell-based assay, if available, would provide a more accurate functional characterisation of this small library of compounds.

Chapter 6: General conclusions

6. General conclusions

Target-based drug discovery has the advantage of a known mechanism of drug action at a very early stage of development, ergo allowing the prediction of possible side effects and how to avoid them. If the exact binding mode of the drug to the target is known, by means of a crystal structure, it is often possible to improve drug-target interactions providing drugs with higher affinity to the target, potency and selectivity. Nonetheless, when a crystal structure is not available, it is still possible to obtain a great deal of information regarding binding affinity and the drug's binding site using other biophysical techniques.

Biophysical techniques such as SPR have in the past decade greatly facilitated target-based drug discovery. The technique can be used throughout the whole process of drug discovery from target identification to preclinical profiling. It has been extensively used in high throughput screening and structure-activity relationships.

In this thesis, information obtained from SPR experiments has been used in all results chapters (Chapters **2 – 5**). In chapter **2**, the technique was validated using the NPR-C as a target. Characterisation of the receptor interaction with its natural ligands, CNP and ANP, was consistent with the information available in the literature and the assay was optimised to allow the characterisation of binding of a peptide antagonist and a small set of small molecule agonists. Confirmation that the small molecules do in fact bind to this target has established NPR-C as a druggable target. In addition, further characterisation of the most potent compounds was carried out by analysis of their binding behaviour to the receptor and problems with aqueous solubility, allowing the selection of a lead compound for further drug development.

The main target of this thesis was sGC, a dimeric heme-containing enzyme which was already known to be druggable. Although small molecule activators of sGC have been known for over three decades, there have been no conclusive studies regarding their binding site, since a crystal structure is not available. Nonetheless, studies with mutated enzymes and molecular modelling had suggested different binding sites. The SPR assay presented here is to our knowledge the first SPR assay developed to detect binding to sGC, and it has provided further information to locate the binding site of these small molecules at the catalytic domain of the enzyme, possibly at an allosteric site, the pseudosymmetric binding site. Screening of a small library of compounds synthesised in the Selwood lab also resulted in the discovery of new enzyme activators.

Screening of commercially available compounds against sGC resulted in the discovery of the first class of compounds that inhibit the activity of the enzyme through allosteric regulation, rather than oxidation of the heme. The hit compound **41** was thoroughly characterised biochemically and biophysically, and it was observed that the small molecule binds to the catalytic domain of enzyme, preventing conversion of GTP into cGMP (Figure **62**). Activity of compound **41** was also observed in cells in the lab of Prof. Garthwaite (data not shown).

The synthesis of a small set of analogues was achieved using microwave-assisted organic synthesis, and the novel compounds were obtained using short synthetic routes with medium to high yields and high purity, suitable for biochemical evaluation. All compounds synthesised were ranked according to their binding strength, giving insight into the functional groups which are relevant for binding to the receptor.

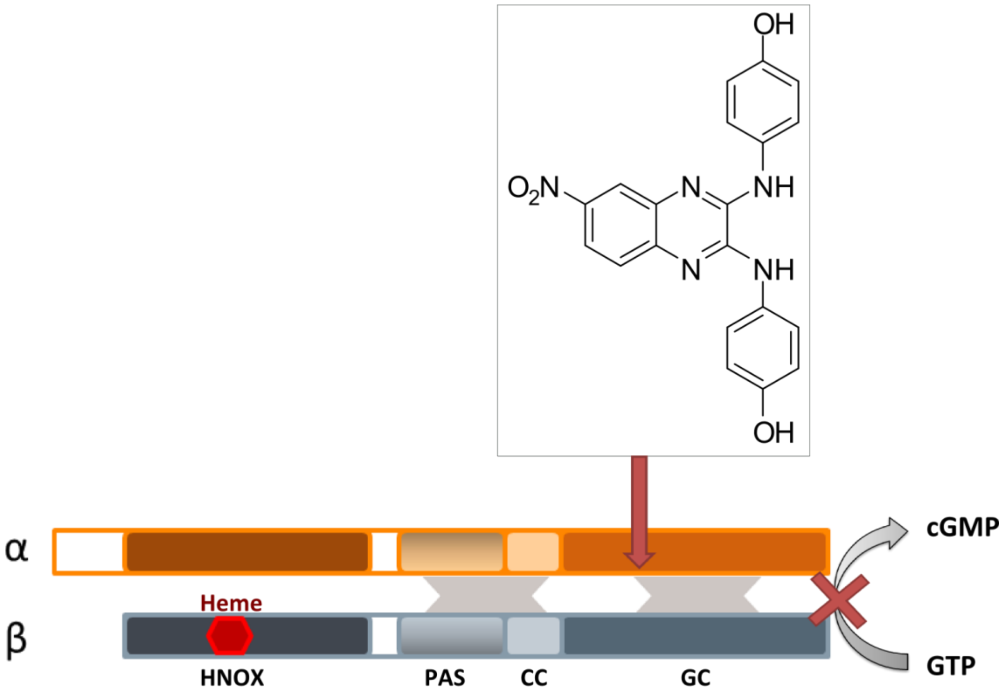

Figure 62.Schematic representation of the inhibition of sGC activity through binding of a small molecule to an allosteric site on the catalytic domain of the enzyme.

A radioimmunoassay was employed to assess the biochemical activity of sGC in the presence of all compounds and allowed the identification of compound **66** as an improved analogue of the hit compound **41**. The replacement of the nitro group by a trifluoromethyl group would have advantages in the metabolism of the small molecule, as metabolites of nitro-aromatics are known to be toxic.

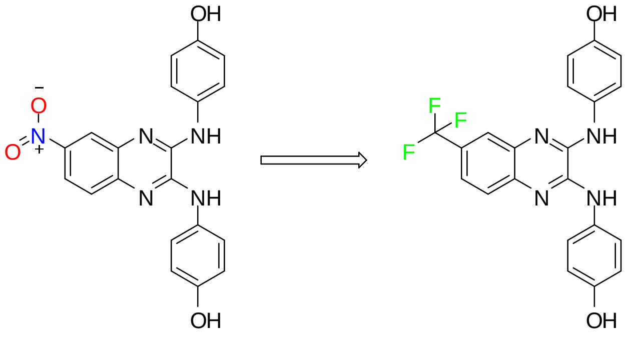

41 **66**

47 % sGC inhibition 44 % sGC inhibition

Figure 63. Chemical structures of most potent sGC inhibitors.

Compound **66** is hereby proposed as a useful tool to further elucidate the signalling pathways regulated by sGC. An inhibitor that targets the catalytic domain of the enzyme would have advantages over the use of heme-binders, which have already proven limitations such as lack of selectivity and bioavailability. A more suitable tool is required to study for example the role of sGC in Parkinson’s disease, as it has been proposed as an alternative target for the treatment of the condition.

6.1. Future work

The biochemical assay employed showed several limitations in the assessment of compound activity. A key point noted was that the activity of the hit compound varied significantly on different days. Moreover, the presence of SOD significantly decreased the activity of the compounds. Thus, a significant amount of work remains to be done to accurately assess the activity of the inhibitors synthesised. It would be interesting to re-test all compounds in the absence of SOD, as well as assess their effect on SOD, as it is possible the compounds are also binding to the metalloprotein and having an inhibitory/activating effect. A cell based assay would also complement this investigation.

The pseudosymmetric site of sGC was explored using molecular modelling software. It is a relatively large site at the dimer interface which can accommodate small molecules. Due to the large size of this site, it is possible that compounds bind to different ends or pockets of the site, which could lead to compounds binding but not having a biochemical effect. It is proposed that the binding of inhibitors would stabilise the enzyme into an inactive conformation, thus preventing cyclisation of GTP into cGMP. Collaborators at UCL are also interested in this regulatory site and will continue with the crystallisation studies aiming to obtain a high resolution structure of the compound bound to the enzyme. It has been determined by SPR that the inhibitors bind to the catalytic domain of the enzyme, and since conditions for crystallisation of this isolated domain are already known, it would theoretically be possible to obtain a co-crystal of the drug-protein. The crystal structure would therefore allow a structure-based drug design, which could ultimately lead to more potent compounds.

Further evaluation of compounds **41** and **66** in cell-based assay would be useful to assess the quality of these compounds as chemical probes.

Chapter 7: Experimental methods

7. Experimental methods

7.1. General methods

Human NPR-C was purchased from OriGene (Rockville, USA), CNP was purchased from Bachem (UK) Ltd. M372049 was a gift from AstraZeneca. NPR-C agonists were synthesised by the Selwood lab as reported in literature.[147] Full-length human recombinant guanylyl cyclase α1β1 (soluble) was obtained from Enzo lifesciences (catalogue number ALX-201-177). YC-1 (**5**) was purchased from Cayman Chemical. BAY 41-2272 (**7**) was purchased from Santa Cruz Biotechnology. Biacore consumables were purchased from GE Healthcare (UK), including buffer stock solutions. All other reagents used were obtained from Sigma.

7.1.1. SPR

Surface plasmon resonance (SPR) experiments were performed with a Biacore T200 instrument at 25 °C. Data processing and analysis were performed using BIAevaluation software and Scrubber2. All sensorgrams were double referenced by subtracting the response in a reference flowcell and a blank sample, and injection spikes were removed. Where specified, data obtained were corrected for molecular weight differences by dividing each relative response value by the molecular weight of the corresponding sample and multiplying it by 100 (Normalized Response = Relative Response/Molecular weight x 100).

7.1.1.1. SPR immobilisation via amine coupling

The carboxymethyl-modified dextran matrix of the chip was activated by injecting a solution containing 0.2 M (1-ethyl-3-(3-dimethylaminopropyl)-carbodiimide hydrochloride (EDC) and 50 mM N-hydroxysuccinimide (NHS) for 7 mins. The protein was injected in short pulses until the target level was reached and the surface free esters were blocked by injecting 1 M ethanolamine for 7 min. The upstream flowcell used as a reference was treated with EDC and NHS for 7min and blocked with ethanolamine for 7 min (blank immobilisation).

7.1.2. Biochemical assay for sGC activity

Briefly, soluble guanylate cyclase (5 ng/ml) was incubated with 50 mM Tris, 0.3 mM MgCl, 100 µM EGTA, 0.045 % BSA, and 1000 units/mL SOD at pH 7.4 and 1 mM MgGTP at 37 °C. Compounds were added at 100 µM prior to DEA/NO at 30nM when evaluating enzyme inhibition. To test for enzyme activation in the absence of NO, no DEA/NO was added. cGMP generation was allowed to proceed for two minutes, after which aliquots were withdrawn and inactivated by boiling in 50 mM Tris, 4 mM EDTA buffer. cGMP formation was measured by a standard radioimmunoassay.

7.1.3. Chemistry

Starting materials were either commercially available or synthesized according to methods reported in the literature. ^{1}H and ^{13}C NMR spectra were recorded on a Bruker AMX-300 or a Bruker AMX-500 spectrometer. Chemical shifts are reported as ppm relative to TMS internal standard. Mass spectra were recorded on a Fisons VG70-SE spectrometer (EI, FAB) or an Agilent 6100 Series LC-mass spectrometer using C-18 or C-4 columns. Microwave reactions were carried out using a CEM Discover microwave.

7.2. Chapter 2 methods

7.2.1. SPR

7.2.1.1. Buffer preparation

Running buffer for experiments without DMSO was prepared by diluting a 10x stock solution of HBS+ from GE Healthcare, to give a final composition of 10 mM HEPES, 150 mM NaCl, 0.05 % Surfactant P20.

To prepare running buffer with 5 % DMSO, firstly a 1.05x HBS+ buffer was prepared, followed by addition of DMSO to give a final composition of 10 mM HEPES, 150 mM NaCl, 0.05 % Surfactant P20, 5 % DMSO.

7.2.1.2. Immobilisation of NPR-C

NPR-C (25 µg/mL in 10 mM sodium acetate pH 4.5) was covalently attached to a CM5 chip via amine coupling. A surface density of 2700 RU was used for measurements with natriuretic peptides and the NPR-C antagonist M372049, and a density of 5200 RU for measurements with NPR-C agonists.

7.2.1.3. Antagonist and agonist sample preparation

Compounds were initially prepared as 50 mM stock solutions in DMSO. SPR samples were prepared by firstly diluting the DMSO samples with 20 parts of 1.05x HBS+. The correct concentration was then obtained by further dilution with 1x HBS, 5 % DMSO.

7.2.1.4. High-resolution CNP and ANP binding

Sequential injections of the natriuretic peptide at 0.25, 0.50, 1, 2, and 4 nM were performed at a flow rate of 30 µL/min for 240 sec each concentration, followed by a dissociation time of 3600 sec. Binding site saturation was observed and the surface was regenerated by two injections of 1M NaCl for 200 sec each. Kinetic parameters were calculated assuming a simple 1:1 (Langmuir) binding.

7.2.1.5. High-resolution binding of M372049 (15)

Binding of M372049 (**15**) was measured at 7 concentrations (0.94, 1.88, 3.75, 7.5, 15, 30, 60 nM) in duplicate. Injection time was of 120 sec followed by undisturbed dissociation for 600 sec, during which curves returned to baseline. A needle wash with 50 % DMSO was performed between each sample and a DMSO calibration cycle was performed to correct for variances in DMSO concentration between samples. Kinetic parameters were calculated assuming a simple 1:1 binding.

7.2.1.6. High resolution binding of agonist compound 13

Concentration dependent binding of compound **13** was measured at 8 concentrations (1.17, 2.34, 4.70, 9.38, 18.75, 37.50, 75, 150 µM) in duplicate. Injection time was of 30 sec followed by undisturbed dissociation for 30 sec, during which curves returned to baseline. A needle wash with 50 % DMSO was performed between each sample and a DMSO calibration cycle was performed to correct for variances in DMSO concentration between samples. Kinetic constants (rapid on/off rates) fall outside the instrument's limits of detection.

7.2.1.7. Binding of NPR-C agonists

Injections of compounds at 50 µM were performed in triplicate with an association time of 30 sec and dissociation of 30 sec, during which time curves returned to baseline. The surface was washed with running buffer and the needle washed with 50 % DMSO between samples. A DMSO calibration was performed to account for variations in DMSO concentration between samples and running buffer. Sensorgrams and all results were normalised for molecular weight variances by dividing the relative responses by the compound molecular weight and multiplying it by 100.

7.2.2. Solubility measurements

7.2.2.1. Generation of standard solubility curves

Stock solutions with a concentration of 1000 µg/mL were prepared by dissolving the solid compound in DMSO. The resulting solutions were dissolved with a mixture of water and methanol (1:1) to make up standard solutions of 500, 250, 100, 50, 25, and 10 µg/mL. The standard solutions were analysed by LC-MS and the concentration plotted against the peak area to obtain a calibration curve.

7.2.2.2. Measurement of compound solubility in buffer

Two solutions were prepared in which the solid compound (0.7 to 0.9 mg) was dissolved in 1 mL of 10 mM PBS pH 7.4 and shaken for 24 hrs. After 24 hrs, 500 µL were removed, filtered through 0.22 µm and analysed by LC-MS. The average area of the peak corresponding to the compound was fitted into the equation for the calibration curve and the concentration determined

7.3. Chapter 3 Methods

7.3.1. Protein expression and purification

sGCcat was a gift from Charles Allerston (Structural Genomics Consortium, Oxford). Protein expression and purification was performed as previously described except that the protein was finally buffer exchanged in to 50 mM HEPES, pH 7.5, 300 mM NaCl, 5 % glycerol, in order to make it ameanable to amine-coupling.[71]

7.3.2. SPR

7.3.2.1. Buffer preparation.

Running buffer for experiments without dmso was prepared by diluting a 10x stock solution of HBS-EP+ from GE Healthcare and adding DTT and $MgCl_2$, to give a final composition of 10 mM HEPES (pH 7.4), 150 mM NaCl, 3 mM EDTA, 0.05 % v/v Surfactant P20, 1 mM DTT, and 10 mM $MgCl_2$. To prepare running buffer with 5 % DMSO, the assay buffer was prepared as described above and 5 % DMSO was added. For experiments performed with full-length sGC, running buffer contained a concentration of 300 mM NaCl in its final composition.

7.3.2.2. Immobilisation of sGC α1β1 catalytic domain (sGCcat)

sGCcat (30 µg/mL in 10 mM sodium acetate buffer at pH 5.5 containing 1 mM DTT, 1 mM ATP, 1 mM GTP, and 3 mM $MgCl_2$) was covalently bound to a CM5 sensor chip via an amine coupling method

7.3.2.3. Immobilisation of full length human recombinant sGC

Full length enzyme (50 µg/mL in sodium acetate buffer at pH 4.5 containing 1 mM DTT, 2 mM ATP and 3 mM $MgCl_2$) was covalently bound to a CM5 sensor chip via an amine coupling method.

7.3.2.4. High-resolution binding of ATP, GTP, and cGMP

The equilibrium binding of nucleotides at 8 different concentrations (0.1 to 3 mM) was measured in duplicates using an injection and dissociation times of 30 sec each. The running buffer did not contain DMSO.

7.3.2.5. Binding of small molecules

Binding of compounds was measured at 100 µM. Injection time was for 30 sec followed by undisturbed dissociation for 30 sec were curves returned to baseline. A needle wash with 50 % DMSO was performed between each sample and a DMSO calibration cycle was performed to correct for variations in DMSO concentration between samples by a standard method.[148] Every sample was measured in triplicate.

7.4. Chapter 4 methods

7.4.1. Virtual screening

(Conducted by Paul Gane in the Selwood lab.)

Similarity searching using MACCS fingerprints at 85 and 75 % Tanimoto similarity was performed in 2007 using the following databases: Abinitio, Acros, Actimol, Akos/Akl, ,Akox/Akx, Akos/Owh, Asinex, Chembridge, Chemstar, LifeChemicals, MoscowMedChemLabs, Pharmeks, Sigma, SPECS, Vitas/Dah, Vitas/Stk. The available structures were selected by hand based upon diversity, molecular size, and apparent availability.

7.4.2. Particulate guanylate cyclase assay

(Conducted by the Garthwaite lab)

Purified rat lung membranes (20 µg protein/200 µL) were incubated in Tris buffer with 10 mM phosphocreatine, 10 units/mL creatine phosphokinase, and 10 µM ODQ to inhibit NO-activated GC. The reaction took place with 0.3 mM MgCl, 0.5 mM MgATP, and 1 mM MgGTP, at 37 °C. 1 µM ANP was added to activate pGC and cGMP penetration allowed to proceed for 10.5 – 12.5 min. Generated cGMP was measured by a standard radioimmunoassay.

7.4.3. Synthesis

4,4'-((6-nitroquinoxaline-2,3-diyl)bis(azanediyl))diphenol (41)

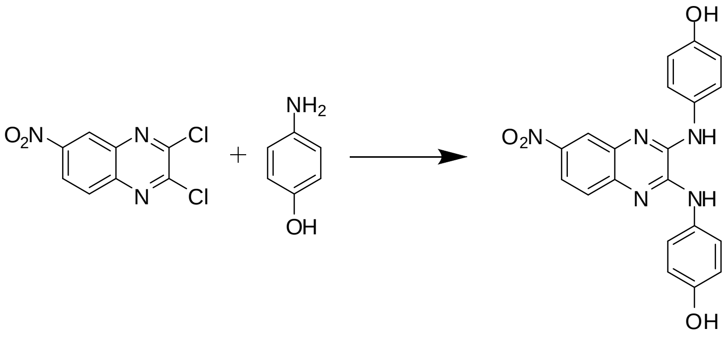

2,3-dichloro-6-nitroquinoxaline (24.4 mg, 0.10 mmol) and 4-aminophenol (43.6 mg, 0.40 mmol) were transferred into a 10 ml microwave vial containing a stirrer bar and NMP (1 mL). The mixture was stirred at 160°C for 5 min under microwave irradiation. The residue was taken up in water (5 mL) and extracted with ethyl acetate (3 x 5 mL). The organics were washed with water (3 x 5 mL) and brine (3 x 5 mL), dried over Mg_2SO_4, filtered and concentrated *in vacuo*. The crude material was purified by flash chromatography using a methanol gradient of 3 to 10 % in DCM to give the name compound as a red powder (24.0 mg, 60 %).

^{1}H NMR (500 MHz, d_6-DMSO) δ: 9.37 (s, 1H, O*H*), 9.31 (s, 1H, O*H*), 9.26 (s, 1H, N*H*), 9.07 (s, 1H, N*H*), 8.18 (d, *J* = 2.5 Hz, 1H, Ar*H*), 8.01 (dd, *J* = 8.9, 2.5 Hz, 1H, Ar*H*), 7.64 (dd, *J* = 10.9, 8.9 Hz, 4H, 4 x Ar*H*), 7.51 (d, *J* = 8.9 Hz, 1H, Ar*H*), 6.83 (d, *J* = 8.9 Hz, 4H, 4 x Ar*H*).

^{13}C NMR (126 MHz, d_6-DMSO) δ 154.2 (Ar*C*), 153.8 (Ar*C*), 143.2 (Ar*C*), 142.6 (Ar*C*), 141.5 (Ar*C*), 140.6 (Ar*C*), 135.3 (Ar*C*), 130.7 (Ar*C*), 130.3 (Ar*C*), 125.4 (Ar*C*H), 123.7 (Ar*C*H), 123.2 (Ar*C*H), 120.1 (Ar*C*H), 118.6 (Ar*C*H), 115.5 (Ar*C*H), 115.2 (Ar*C*H).

HRMS-ES (m/z): $[M + H]^+$ calculated for $C_{20}H_{16}N_5O_4$, 390.1202; found, 390.1205.

7.4.4. SPR

7.4.4.1. Immobilisation

The catalytic domain of sGC (sGCcat) and full-length enzyme were immobilised as described in section 3. The mutated catalytic domain sGC was immobilised using the same conditions as the wild type sGCcat.

The immobilisation level of sGCcat was 11386 RU on the CM5 chip and 20683 RU on the CM7 chip.

The immobilisation level of the mutated sGCcat on a CM5 chip was 10891 RU.

The immobilisation level of the full length sGC on a CM7 chip was 20683 RU.

7.4.4.2. High resolution binding of compound 41

Binding of compound **41** was measured at 6 concentrations (4, 8, 16, 32, 64, and 128 µM). Injection time was 30 sec followed by undisturbed dissociation for 60 sec, during which time curves returned to baseline. A needle wash with 50 % DMSO was performed between each sample. Kinetic parameters were calculated assuming a simple 1:1 binding model, and a binding model considering non-specific binding, where specified.

7.4.5. Molecular modelling

7.4.5.1. Small molecule preparation

3D coordinates were added to the 2D molecules by adding hydrogens and performing energy minimization using the force field MMFF94x in the MOE software. Files were saved as mol2 files.

7.4.5.2. Binding site mapping

The crystal structure of the catalytic domain of sGC (pdb entry 3uvj) was imported into the MOE software and binding sites were selected using the "site finder" functionality of the software. The two biggest sites (432 and 461 Å), corresponded to the GTP binding site and the pseudosymmetric site, respectively, as concluding by visualisation of the residues known to be involved in GTP binding.

7.4.5.3. Protein preparation

The pdb file was analysed and missing residue side chains were added to the structure.

7.4.5.4. Docking

Docking took place using Gold 5.1. Using the standard wizard setup, hydrogens were added. The binding site was selected by importing the list of residues obtained in **7.4.5.2**. The fitness function selected was GOLDSCORE and the genetic algorithm search was performed at medium speed.

7.5. Chapter 5 methods

7.5.1. General methods

7.5.1.1. Method A:

The quinoxaline and aniline (1:4) were transferred into a 10 mL microwave vial containing a stirrer bar and NMP (1 mL). The mixture was stirred at 160°C for 5 min under microwave irradiation. The residue was taken up in water (5 mL) and extracted with ethyl acetate (3 x 5 mL). The organics were washed with water (3 x 5 mL) and brine (3 x 5 mL), dried over Mg_2SO_4, filtered and concentrated *in vacuo*.

7.5.1.2. Method B

The 4-substituted-1,2-diamine and 1,2-bis(3-methoxyphenyl)ethane-1,2-dione (or 1,2-bis(3-hydroxyphenyl)ethane-1,2-dione) (1:1) were dissolved in 9:1 methanol-acetic acid (1.5 mL) and reacted under microwave irradiation for 5 min at 160 °C. Upon cooling, the solvent was evaporated under reduced pressure and the residue purified by flash column chromatography using a solvent gradient of 10-50 % ethyl acetate in cyclohexane.

7.5.1.3. Method C

A solution of oxalic acid in 4 N HCl (5 mL) was added to a stirring solution of the diamine (1 : 1) in 4N HCl (15 mL) and the reaction mixture was refluxed for 2hrs. The solution was cooled to room temperature and the precipitate filtered by suction, washed with water and freeze-dried.

7.5.1.4. Method D

N,N-dimethylformamide (0.01 eq.) was added to a solution of 2,3-dihydroxyquinoxaline-6-carbonitrile in thionyl choride (5 mL) and stirred under reflux for 2 hrs. The reaction mixture was cooled to room temperature and concentrated under vacuum. Water (10 mL) was added to the solid on an ice bath and the slurry was stirred for 30 min at room temperature, after which the solid was filtered and washed with water. The precipitate was taken up in a minimum amount of DCM and filtered through a silica column and eluted with DCM.

7.5.2. Synthesis[§]

3,3'-((6-nitroquinoxaline-2,3-diyl)bis(azanediyl))diphenol (48)

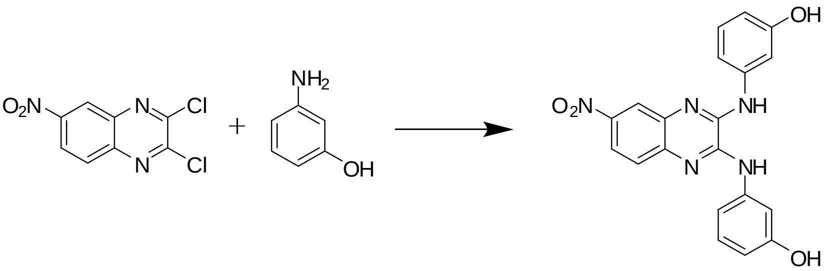

2,3-Dichloro-6-nitroquinoxaline (48.8 mg, 0.20 mmol) and 3-aminophenol (87.2 mg, 0.80 mmol) were reacted following method A. The crude material was purified by flash chromatography using ethyl acetate and cyclohexane (50 : 50) to give the named compound as a red powder (57.0 mg, 75 %).

^{1}H NMR (500 MHz, *d$_6$*-DMSO) δ: 9.50 (s, 1H, O*H*), 9.48 (s, 1H, O*H*), 9.41 (s, 1H, N*H*), 9.24 (s, 1H, N*H*), 8.32 (d, *J* = 2.6 Hz, 1H, Ar*H*), 8.11 (dd, *J* = 9.0, 2.6 Hz, 1H, Ar*H*), 7.66 (d, *J* = 2.0 Hz, 1H, Ar*H*), 7.64 (d, *J* = 9.0 Hz, 1H, Ar*H*), 7.51 (t, *J* = 7.3 Hz, 1H, Ar*H*), 7.27 (dd, *J* = 18.4, 8.0 Hz, 2H, 2 x Ar*H*), 7.22 – 7.16 (m, 2H, 2 x Ar*H*), 6.54 (ddd, *J* = 17.0, 8.0, 1.5 Hz, 2H, 2 x Ar*H*).

^{13}C NMR (126 MHz, *d$_6$*-DMSO) δ: 155.89, 155.55, 143.29, 143.23, 142.52, 141.43, 135.29, 132.27, 131.87, 125.53, 123.46, 122.95, 120.18, 118.80, 113.95, 55.25, 55.22.

HRMS-ES (m/z): [M + H]$^+$ calculated for $C_{22}H_{16}N_5O_4$, 390.1202; found, 390.1189.

[§] Compounds **53**, **60, 61, 70**, and **71** were synthesised by Revathy Selvarajah in the Selwood lab.

N2,N3-bis(4-methoxyphenyl)-6-nitroquinoxaline-2,3-diamine (49)

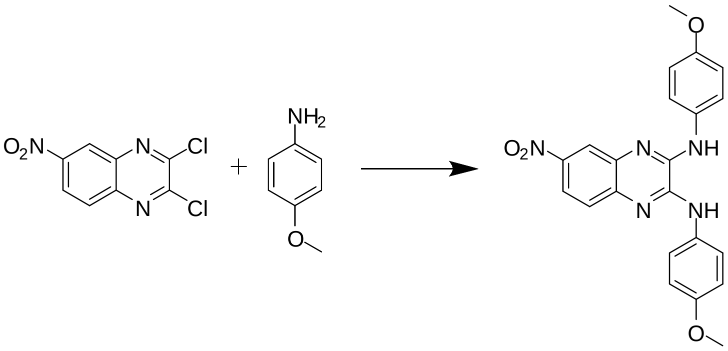

2,3-Dichloro-6-nitroquinoxaline (24.4 mg, 0.10 mmol) and 4-methoxyaniline (49.2 mg, 0.40 mmol) were reacted following method A. The crude material was purified by flash chromatography using an ethyl acetate gradient of 0 to 50 % in cyclohexane to give the named compound as a red powder (15.0 mg, 40 %).

^{1}H NMR (500 MHz, *d$_6$*-DMSO) δ: 9.39 (s, 1H, N*H*), 9.20 (s, 1H, N*H*), 8.21 (d, *J* = 2.6 Hz, 1H, Ar*H*), 8.04 (dd, *J* = 8.9, 2.6 Hz, 1H, Ar*H*), 7.82 – 7.74 (m, 4H, Ar*H*), 7.54 (d, *J* = 8.9 Hz, 1H, Ar*H*), 7.05 – 6.99 (m, 4H, Ar*H*), 3.78 (s, 6H, 2 x OCH_3).

^{13}C NMR (126 MHz, *d$_6$*-DMSO) δ 155.9 (Ar*C*), 155.6 (Ar*C*), 143.3 (Ar*C*), 143.2 (Ar*C*), 142.5 (Ar*C*), 141.4 (Ar*C*), 135.3 (Ar*C*), 132.3 (Ar*C*), 131.9 (Ar*C*), 125.5 (Ar*C*H), 123.5 (Ar*C*H), 122.9 (Ar*C*H), 120.2 (Ar*C*H), 118.8 (Ar*C*H), 113.9 (Ar*C*H), 55.3 (OCH_3), 55.2 (OCH_3).

HRMS-ES (m/z): $[M + H]^+$ calculated for $C_{22}H_{20}N_5O_4$, 418.1515; found, 418.1531.

6-nitro-N2,N3-diphenylquinoxaline-2,3-diamine (50)

Literature compound.[149]

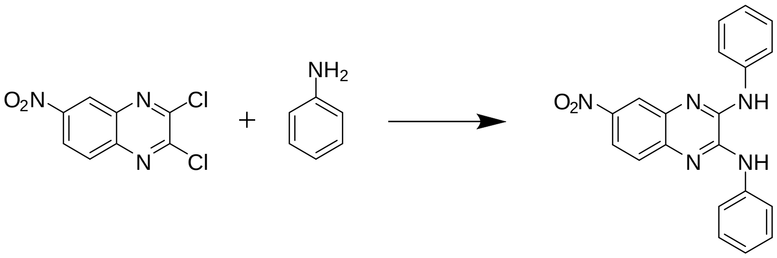

2,3-Dichloro-6-nitroquinoxaline (48.8 mg, 0.20 mmol) and aniline (74.4 mg, 0.80 mmol) was reacted using method A and purified by flash chromatography using an ethyl acetate gradient of 10 to 50 % in cyclohexane to give a yellow powder (49.0 mg, 70 %).

^{1}H NMR (500 MHz, d_6-DMSO) δ: 9.51 (s, 1H, N*H*), 9.34 (s, 1H, N*H*), 8.27 (d, *J* = 2.2 Hz, 1H, Ar*H*), 8.07 (dd, *J* = 8.8, 2.2 Hz, 1H, Ar*H*), 7.95 – 7.85 (m, 4H, 4 x Ar*H*), 7.62 (d, *J* = 8.8 Hz, 1H, Ar*H*), 7.47 – 7.39 (m, 4H, 4 x Ar*H*), 7.20 – 7.09 (m, 2H, 2x Ar*H*).

^{13}C NMR (126 MHz, d_6-DMSO) δ: 143.7 (Ar*C*), 143.1 (Ar*C*), 142.4 (Ar*C*), 141.2 (Ar*C*), 139.4 (Ar*C*), 139.1 (Ar*C*), 135.2 (Ar*C*), 128.8 (Ar*C*H), 125.9 (Ar*C*H), 123.9 (Ar*C*H), 123.4 (Ar*C*H), 121.6 (Ar*C*H), 121.1 (Ar*C*H), 120.5 (Ar*C*H), 119.2 (Ar*C*H).

HRMS-ES (m/z): $[M + H]^+$ calculated for $C_{20}H_{16}N_5O_2$, 358.1304; found, 358.1305.

N,N'-(((6-nitroquinoxaline-2,3-diyl)bis(azanediyl))bis(4,1-phenylene))diacetamide (51)

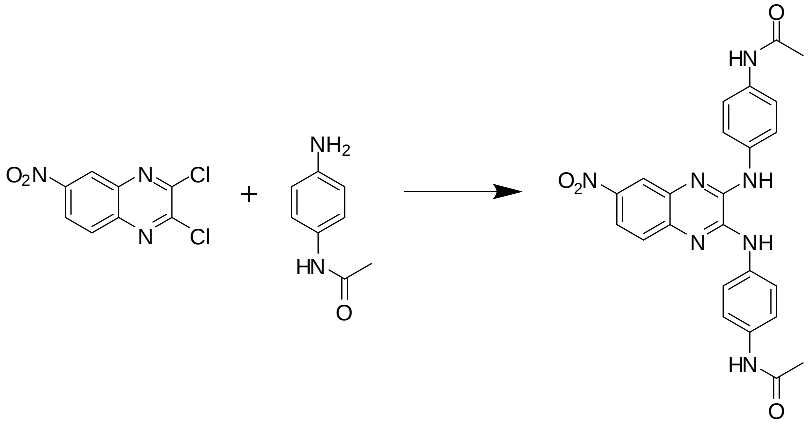

2,3-Dichloro-6-nitroquinoxaline (48.8 mg, 0.20 mmol) and N-(4-aminophenyl)acetamide (120 mg, 0.80 mmol) were reacted following method A. The crude material was purified by flash chromatography using a methanol gradient of 0 to 5 % in DCM to give the named compound as a red powder (23.0 mg, 25 %).

^{1}H NMR (500 MHz, *d$_6$*-DMSO) δ: 9.97 (s, 1H, N*H*), 9.96 (s, 1H, N*H*), 9.52 (s, 1H, N*H*), 9.33 (s, 1H, N*H*), 8.28 (d, *J* = 2.4 Hz, 1H, Ar*H*), 8.06 (dd, *J* = 8.9, 2.4 Hz, 1H, Ar*H*), 7.83 (dd, *J* = 13.6, 8.9 Hz, 4H, 4 x Ar*H*), 7.67 – 7.57 (m, 5H, 5 x Ar*H*), 2.05 (d, *J* = 4.9 Hz, 6H, 6 x Ar*H*).

^{13}C NMR (126 MHz, *d$_6$*-DMSO) δ: 168.1 (Ar-NH-*C*O-CH$_3$), 168.0 (Ar-NH-*C*O-CH$_3$), 143.5 (Ar*C*), 143.1 (Ar*C*), 142.3 (Ar*C*), 141.3 (Ar*C*), 135.5 (Ar*C*), 135.3 (Ar*C*), 134.5 (Ar*C*), 134.1 (Ar*C*), 125.7 (Ar*C*H), 122.1 (Ar*C*H), 121.6 (Ar*C*H), 120.4 (Ar*C*H), 119.4 (Ar*C*H), 119.3 (Ar*C*H), 118.9 (Ar*C*H), 23.9 (Ar-NH-CO-*C*H$_3$).

HRMS-ES (m/z): [M + H]$^+$ calculated for $C_{24}H_{22}N_7O_4$, 472.1733; found, 472.1750.

N,N'-(((6-nitroquinoxaline-2,3-diyl)bis(azanediyl))bis(3,1-phenylene))diacetamide (52)

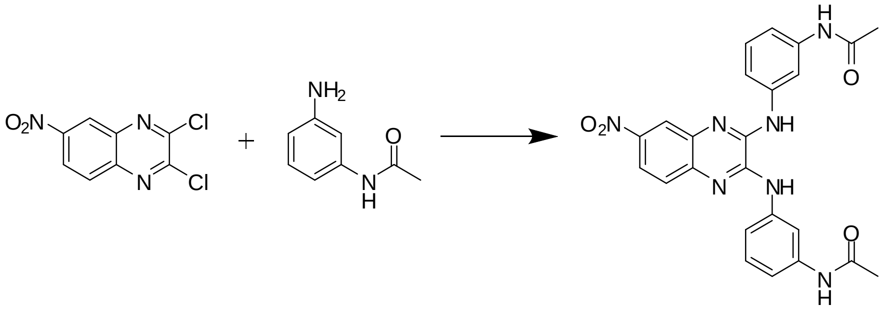

2,3-Dichloro-6-nitroquinoxaline (122 mg, 0.50 mmol) and N-(3-aminophenyl)acetamide (300 mg, 2.00 mmol) were reacted following method A. The crude material was purified by flash chromatography using ethyl acetate and cyclohexane (50 : 50) as eluent to give the name compound as a red powder (117.0 mg, 50 %).

^{1}H NMR (500 MHz, *d$_6$*-DMSO) δ 10.02 (s, 2H, 2 x N*H*), 9.62 (s, 1H, N*H*), 9.44 (s, 1H, N*H*), 8.46 – 8.32 (m, 3H, 3 x Ar*H*), 8.12 (dd, *J* = 8.8, 2.0 Hz, 1H, Ar*H*), 7.71 – 7.60 (m, 3H, Ar*H*), 7.36 – 7.25 (m, 5H, 5 x Ar*H*), 2.09 (s, 3H, CH_3), 2.08 (s, 3H, CH_3).

^{13}C NMR (126 MHz, *d$_6$*-DMSO) δ 168.4 (Ar-NH*C*OCH_3), 139.7 (Ar*C*), 135.1 (Ar*C*), 128.8 (Ar*C*H), 125.9 (Ar*C*H), 120.6 (Ar*C*), 119.2 (Ar*C*H), 116.3 (Ar*C*H), 115.8 (Ar*C*H), 114.5 (Ar*C*H), 114.1 (Ar*C*H), 112.2 (Ar*C*H), 111.6 (Ar*C*), 109.1 (Ar*C*), 24.1 (Ar-NHCO*C*H_3).

HRMS-ES (m/z): $[M + H]^+$ calculated for $C_{24}H_{22}N_7O_4$, 472.1733; found, 472.1733.

N2,N3-bis(4-fluorophenyl)-6-nitroquinoxaline-2,3-diamine (53)

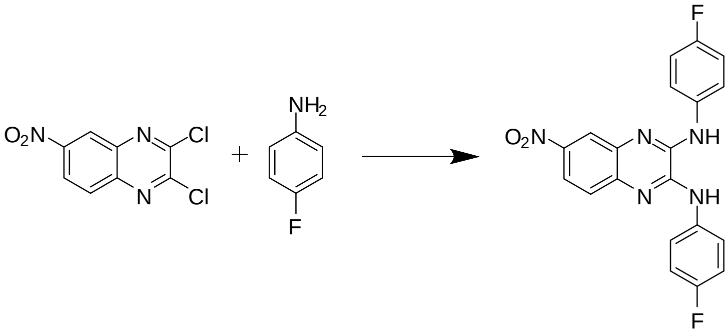

2,3-Dichloro-6-nitroquinoxaline (24.4 mg, 0.10 mmol) and 4-fluoroaniline (48.0 µl, 0.40 mmol) were reacted following method A. The crude material was purified by flash chromatography using a ethyl acetate gradient of 10 to 50 % in cyclohexane to give the named compound as an orange powder (24.0 mg, 61 %).

^{1}H NMR (500 MHz, *d$_6$*-DMSO) δ: 9.52 (s, 1H), 9.36 (s, 1H), 8.27 (d, *J* = 2.4 Hz, 1H), 8.07 (dd, *J* = 8.9, 2.4 Hz, 1H), 7.92 (ddd, *J* = 13.8, 8.9, 5.0 Hz, 4H), 7.60 (d, *J* = 8.9 Hz, 1H), 7.31 – 7.23 (m, 4H).

HRMS-ES (m/z): [M + H] calculated for $C_{20}H_{14}N_5O_3F_2$, 394.1116; found, 394.1123.

N2,N3-di(1H-indazol-6-yl)-6-nitroquinoxaline-2,3-diamine (54)

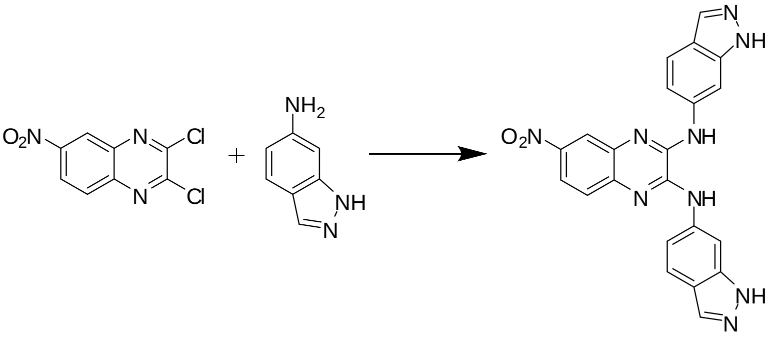

2,3-Dichloro-6-nitroquinoxaline (48.8 mg, 0.20 mmol) and 1H-indazol-6-amine (106.4 mg, 0.80 mmol) we reacted using method A and purified by flash chromatography using a methanol gradient of 0 to 10 % in DCM to give an orange powder (21.0 mg, 25 %).

^{1}H NMR (300 MHz, *d$_6$*-DMSO) δ: 13.04 (s, 1H, NN*H*), 12.98 (s, 1H, NN*H*), 9.78 (s, 1H, N*H*), 9.60 (s, 1H, N*H*), 8.68 (s, 1H, Ar*H*), 8.47 (s, 1H, Ar*H*), 8.36 (d, *J* = 2.6 Hz, 1H, Ar*H*), 8.17 (dd, *J* = 9.0, 2.6 Hz, 1H, Ar*H*), 8.03 (d, *J* = 5.4 Hz, 2H, 2 x Ar*H*), 7.79 (dd, *J* = 8.7, 4.4 Hz, 2H, 2 x Ar*H*), 7.66 (d, *J* = 9.0 Hz, 1H, Ar*H*), 7.51 – 7.39 (m, 2H, 2 x Ar*H*).

^{13}C NMR (126 MHz, *d$_6$*-DMSO) δ 143.7 (Ar*C*), 143.4 (Ar*C*), 142.6 (Ar*C*), 141.2 (Ar*C*), 140.5 (Ar*C*), 140.4 (Ar*C*), 137.7 (Ar*C*), 137.3 (Ar*C*), 135.2 (Ar*C*), 133.4 (Ar*C*), 133.4 (Ar*C*), 125.8 (Ar*C*H), 120.5 (Ar*C*H), 120.4 (Ar*C*H), 119.6 (Ar*C*H), 119.4 (Ar*C*H), 119.2 (Ar*C*H), 116.5 (Ar*C*H), 116.0 (Ar*C*H), 101.66 (Ar*C*H), 100.67 (Ar*C*H).

HRMS-ES (m/z): [M + H]$^+$ calculated for $C_{22}H_{16}N_9O_2$, 438.1427; found, 438.1425.

6-(trifluoromethyl)quinoxaline-2,3-diol (56)

Literature compound.[150]

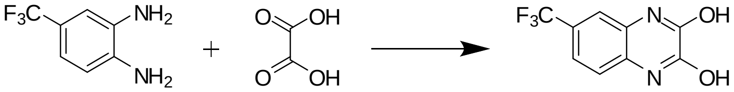

4-Trifluoromethyl-o-phenylenediamine (528 mg, 3.0 mmol) was reacted with oxalic acid (1.97 mg, 3.3. mmol) using method C to give the named compound as a brown powder (340 mg, 50 %).

^{1}H NMR (500 MHz, d_6-DMSO) δ: 12.17 (s, 1H, O*H*), 12.06 (s, 1H, O*H*), 7.41 (d, *J* = 8.3 Hz, 1H, Ar*H*), 7.38 (s, 1H, Ar*H*), 7.26 (d, *J* = 8.3 Hz, 1H, Ar*H*).

^{13}C NMR (126 MHz, d_6-DMSO) δ: 155.2 (Ar*C*), 154.9 (Ar*C*), 129.0 (Ar*C*), 126.1 (Ar*C*), 125.2 (Ar*C*H), 123.2-122.9 (m, Ar-*C*F$_3$), 119.7 (Ar*C*H), 115.8 (Ar*C*H), 111.8 (Ar*C*-CF$_3$).

MS-EI (m/z): [M]$^-$ calculated for $C_9H_4F_3N_2O_2$, 229.1363; found 229.00.

2,3-dichloro-6-(trifluoromethyl)quinoxaline (57)

Literature compound.[150]

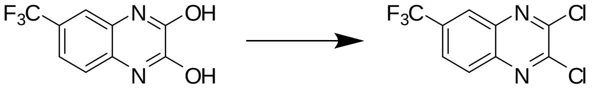

The reaction with 6-(trifluoromethyl)quinoxaline-2,3-diol (330 mg, 1.76 mmol) was carried out using method D to give the name compound as a white solid (268 mg, 67 %).

^{1}H NMR (500 MHz, d_6-DMSO) δ: 8.52 (d, *J* = 0.9 Hz, 1H, Ar*H*), 8.29 (d, *J* = 8.8 Hz, 1H, Ar*H*), 8.20 (dd, *J* = 8.8, 1.9 Hz, 1H, Ar*H*).

^{13}C NMR (126 MHz, d_6-DMSO) δ: 147.5 (Ar*C*), 146.7 (Ar*C*), 141.4 (Ar*C*), 139.2 (Ar*C*), 131.2 (Ar*C*-CF$_3$ or Ar-*C*F$_3$), 130.9 (Ar*C*-CF$_3$ or Ar-*C*F$_3$), 129.8 (Ar*C*H), 127.0 (Ar*C*H), 126.0 (Ar*C*H).

2,3-dihydroxyquinoxaline-6-carbonitrile (58)

Literature compound.[150]

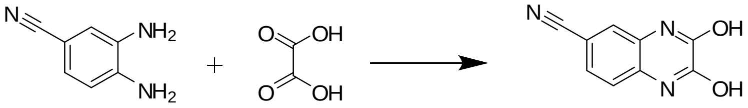

3,4-Diaminobenzonitrile (399 mg, 3 mmol) was reacted with oxalic acid (1.97 mg, 3.3. mmol) using method C to give the named compound as a purple powder (330 mg, 59 %)

^{1}H NMR (500 MHz, *d$_6$*-DMSO) δ: 12.21 (s, 1H, O*H*), 12.08 (s, 1H, O*H*), 7.50 (d, *J* = 8.2 Hz, 1H, Ar*H*), 7.39 (s, 1H, Ar*H*), 7.21 (d, *J* = 8.2 Hz, 1H, Ar*H*).

^{13}C NMR (126 MHz, *d$_6$*-DMSO) δ: 155.12 (Ar*C*), 154.76 (Ar*C*), 129.85 (Ar*C*), 126.85 (Ar*C*), 126.36 (Ar*C*H), 118.69 (Ar-*C*N), 118.28 (Ar*C*H), 115.99 (Ar*C*H), 104.54 (Ar*C*-CN).

MS-EI (m/z): $[M]^-$ calculated for C9H4N3O2, 186.1478; found 186.10.

2,3-dichloroquinoxaline-6-carbonitrile (59)

Literature compound.[150]

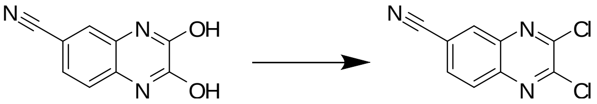

The reaction with 2,3-dihydroxyquinoxaline-6-carbonitrile (330 mg, 1.76 mmol) was carried out using method D to give the named compound as a white solid (264 mg, 67 %).

^{1}H NMR (500 MHz, *d$_6$*-DMSO) δ: 8.76 (s, 1H, Ar*H*), 8.25 (s, 2H, Ar*H*).

^{13}C NMR (126 MHz, *d$_6$*-DMSO) δ: 147.8 (Ar*C*), 146.9 (Ar*C*), 141.6 (Ar*C*), 139.2 (Ar*C*), 133.9 (Ar*C*H), 132.7 (Ar*C*H), 129.6 (Ar*C*H), 117.7 (Ar-*C*N), 113.7 (Ar*C*-CN).

MS-EI (m/z): $[M + Na^+]$ calculated for $C_9H_3C_{l2}N_3Na$, 247.0372; found 247.30.

6-chloroquinoxaline-2,3-diol (60)

Literature compound.[150]

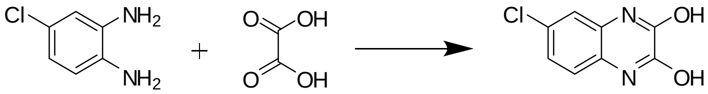

4-Chlorobenzene-1,2-diamine (570.36 mg, 4.0 mmol) was reacted with oxalic acid (396.18 mg, 4.4 mmol) using method C to give the named compound as a tan powder (668 mg, 85 %).

^{1}H NMR (500 MHz, d_6-DMSO) δ: 11.97 (s, 1H), 11.96 (s, 1H), 7.11 (s, 2H), 7.10 (s, 1H).

2,3,6-trichloroquinoxaline (61)

Literature compound.[150]

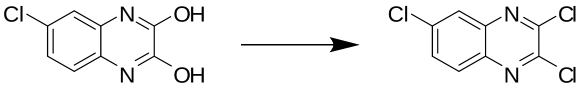

The reaction with 6-chloroquinoxaline-2,3-diol (658 mg, 3.3 mmol) was carried out using method D to give the named compound as a yellow solid (555 mg, 72 %).

^{1}H NMR (500 MHz, d_6-DMSO) δ: 8.21 (d, J = 2.3 Hz, 1H), 8.10 (d, J = 9.0 Hz, 1H), 7.96 (dd, J = 9.0, 2.3 Hz, 1H).

2,3-dihydroxyquinoxaline-6-carboxylic acid (62)

Literature compound.[151]

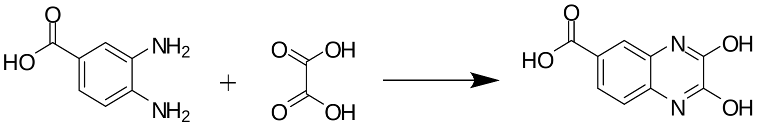

3,4-Diaminobenzoic acid (913 mg, 6.0 mmol) was reacted with oxalic acid (594 mg, 6.6 mmol) using method C to give the named compound as a pink powder (1.035 g, 84 %).

^{1}H NMR (500 MHz, d_6-DMSO) δ: 12.50 (s, 1H, O*H*), 12.39 (s, 1H, O*H*), 8.04 (s, 1H, Ar*H*), 7.97 (d, *J* = 6.5 Hz, 1H, Ar*H*), 7.51 (d, *J* = 6.5 Hz, 1H, Ar*H*).

^{13}C NMR (126 MHz, d_6-DMSO) δ: 166.7 (Ar-*C*OOH), 155.3 (Ar*C*), 155.0 (Ar*C*), 129.3 (Ar*C*), 125.4 (Ar*C*), 125.2 (Ar*C*), 124.4 (Ar*C*H), 116.4 (Ar*C*H), 115.2 (Ar*C*H).

MS-EI (m/z): [M - H]] calculated for $C_9H_5N_2O_4$, 205.1479; found 205.10.

2,3-dichloroquinoxaline-6-carbonyl chloride (63)

Literature compound.[152]

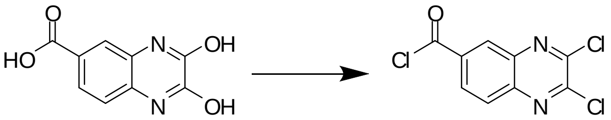

The reaction with 2,3-dihydroxyquinoxaline-6-carboxylic acid (1.0 g, 4.85 mmol) was carried out using method D to give the named compound as a white solid (841 mg, 66 %).

^{1}H NMR (500 MHz, d_6-DMSO) δ: 8.44 (dd, *J* = 2.6, 1.5 Hz, 1H, Ar*H*), 8.29 (dd, *J* = 8.7, 1.5 Hz, 1H, Ar*H*), 8.09 (d, *J* = 8.7 Hz, 1H, Ar*H*).

^{13}C NMR (126 MHz, d_6-DMSO) δ: 166.1 (Ar-*C*OOCl), 146.7 (Ar*C*), 145.9 (Ar*C*), 141.8 (Ar*C*), 139.3 (Ar*C*), 133.2 (Ar*C*), 130.8 (Ar*C*H), 129.3 (Ar*C*H), 128.4 (Ar*C*H).

MS-EI (m/z): [M + H]$^+$ calculated for $C_9H_3Cl_2N_2O_2$, 242.0396; found 242.90.

2,3-dichloro-N-methylquinoxaline-6-carboxamide (64)

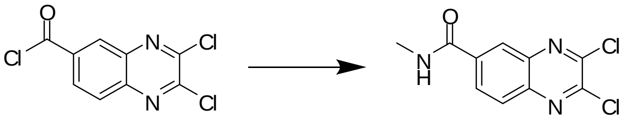

Methylamine solution (33 wt. % in absolute ethanol, 256 µL) was added to DCM (3 mL) on ice and the resulting mixture was added to a solution of 2,3-dichloroquinoxaline-6-carbonyl chloride **63,** (261 mg, 1 mmol) in DCM (3 mL) whilst stirring at room temperature. The mixture was stirred at room temperature overnight after which it was diluted with DCM (10 mL) and washed with saturated sodium bicarbonate (3 x 10 mL) and brine (3 x 10 mL). The organics were dried over $MgSO_4$, filtered, and the solved evaporated. The crude compound was purified by flash column chromatography using a gradient of 30 to 60 % ethyl acetate in cyclohexane to yield the named compound as a white powder (89 mg, 35 %).

^{1}H NMR (500 MHz, *d$_6$*-DMSO) δ: 8.84 (s, 1H, N*H*), 8.48 (s, 1H, Ar*H*), 8.29 (d, *J* = 8.6 Hz, 1H, Ar*H*), 8.14 (d, *J* = 8.6 Hz, 1H, Ar*H*), 2.85 (d, *J* = 3.7 Hz, 3H, C*H*$_3$).

^{13}C NMR (126 MHz, *d$_6$*-DMSO) δ: 165.0 (Ar*C*), 146.0 (Ar*C*), 145.6 (Ar*C*), 141.1 (Ar*C*), 139.6 (Ar*C*), 136.8 (Ar*C*), 129.9 (Ar*C*H), 128.1 (Ar*C*H), 126.6 (Ar*C*H), 26.5 (*C*H$_3$).

MS-EI (m/z): [M] calculated for $C_{10}H_7Cl_2N_3O$, 256.089; found 255.90.

4,4'-(quinoxaline-2,3-diylbis(azanediyl))diphenol (65)

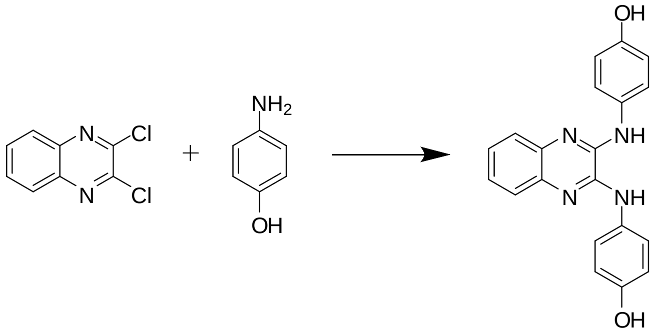

2,3-Dichloroquinoxaline (39.8 mg, 0.20 mmol) and 4-aminophenol (87.2 mg, 0.80 mmol) were reacted following method A and purified by flash column chromatography using an ethyl acetate gradient of 10 to 50 % to give the named compound as a yellow powder (35.0 mg, 50 %).

^{1}H NMR (500 MHz, d_6-DMSO) δ 9.21 (s, 2H, 2 x O*H*), 8.71 (s, 2H, 2 x N*H*), 7.61 (d, *J* = 8.7 Hz, 4H, 4 x Ar*H*), 7.42 (dt, *J* = 7.3, 3.4 Hz, 2H, 2 x Ar*H*), 7.23 (dd, *J* = 6.1, 3.4 Hz, 2H, 2 x Ar*H*), 6.79 (d, *J* = 8.7 Hz, 4H, 4 x Ar*H*).

^{13}C NMR (126 MHz, d_6-DMSO) δ 153.2 (Ar*C*), 141.4(Ar*C*), 136.2(Ar*C*), 131.5(Ar*C*), 125.0 (Ar*C*H), 124.4(Ar*C*H), 122.8(Ar*C*H), 115.1(Ar*C*H).

HRMS-ES (m/z): $[M + H]^+$ calculated for $C_{20}H_{17}N_4O_2$, 345.1352; found, 345.1347.

4,4'-((6-(trifluoromethyl)quinoxaline-2,3-diyl)bis(azanediyl))diphenol (66)

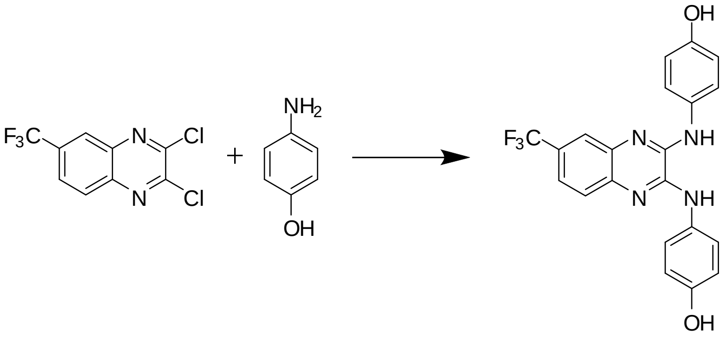

2,3-Dichloro-6-(trifluoromethyl)quinoxaline (52.8 mg, 0.20 mmol) and 4-aminophenol (87.2 mg, 0.80 mmol) were reacted following method A. The crude material was purified by flash chromatography using an ethyl acetate gradient of 30 to 70 % in cyclohexane to give the named compound as a red powder (68.0 mg, 83 %).

^{1}H NMR (500 MHz, *d*$_6$-DMSO) δ: 9.34 (s, 1H, O*H*), 9.32 (s, 1H, O*H*), 9.03 (s, 1H, N*H*), 8.96 (s, 1H, N*H*), 7.68 (s, 1H, Ar*H*), 7.65 – 7.59 (m, 4H, 4 x Ar*H*), 7.55 (d, *J* = 8.5 Hz, 1H, Ar*H*), 7.47 (dd, *J* = 8.5, 1.8 Hz, 1H, Ar*H*), 6.84 – 6.78 (m, 4H, 4 x Ar*H*).

^{13}C NMR (126 MHz, *d*$_6$-DMSO) δ: 170.3 (Ar*C*), 153.8 (Ar*C*), 153.6 (Ar*C*), 142.8 (Ar*C*), 142.3 (Ar*C*), 138.7 (Ar*C*), 135.7 (Ar*C*), 131.0 (Ar*C*), 130.8 (Ar*C*), 125.8 (Ar*C*H), 123.4 (Ar*C*H), 123.2 (Ar*C*H), 121.9 (Ar*C*H), 119.9 (Ar*C*H), 115.2 (Ar*C*H).

HRMS-CI (m/z): [M+H]$^+$ calculated for $C_{21}H_{16}F_3N_4O_2$, 413.12199; found, 413.120133.

3,3'-((6-(trifluoromethyl)quinoxaline-2,3-diyl)bis(azanediyl))diphenol (67)

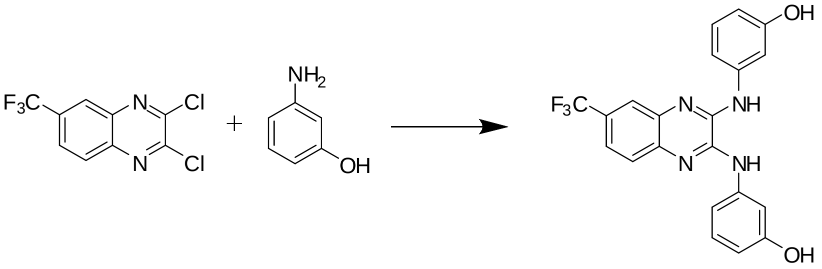

2,3-Dichloro-6-(trifluoromethyl)quinoxaline (52.8 mg, 0.20 mmol) and 3-aminophenol (87.2 mg, 0.20 mmol) were reacted following method A. The crude material was purified by flash chromatography using a ethyl acetate gradient of 30 to 70 % in cyclohexane to give the named compound as a red powder (68.0 mg, 83 %).

^{1}H NMR (500 MHz, d_6-DMSO) δ: 9.49 (s, 1H, O*H*), 9.46 (s, 1H, O*H*), 9.18 (s, 1H, N*H*), 9.12 (s, 1H, N*H*), 7.81 (s, 1H, Ar*H*), 7.67 (d, *J* = 8.4 Hz, 1H, Ar*H*), 7.61 – 7.56 (m, 2H, 2 x Ar*H*), 7.50 (d, *J* = 2.5 Hz, 1H, Ar*H*), 7.26 (dd, *J* = 11.6, 9.0 Hz, 2H, 2 x Ar*H*), 7.18 (td, *J* = 8.4, 2.5 Hz, 2H, 2 x Ar*H*), 6.57 – 6.46 (m, 2H, 2 x Ar*H*).

^{13}C NMR (126 MHz, d_6-DMSO) δ: 157.6 (Ar*C*), 142.5 (Ar*C*), 142.0 (Ar*C*), 140.7 (Ar*C*), 138.5 (Ar*C*), 135.5 (Ar*C*), 129.3 (Ar*C*H), 126.2 (Ar*C*H), 123.5 (Ar*C*), 122.3 (Ar*C*H), 120.6 (Ar*C*), 112.0 (Ar*C*H), 111.7 (Ar*C*H), 110.5 (Ar*C*H), 110.2 (Ar*C*H), 108.3 (Ar*C*H), 108.0 (Ar*C*H).

HRMS-CI (m/z): $[M + H]^+$ calculated for $C_{21}H_{16}F_3N_4O_2$, 413.12199; found, 413.121732.

2,3-bis((4-hydroxyphenyl)amino)quinoxaline-6-carbonitrile (68)

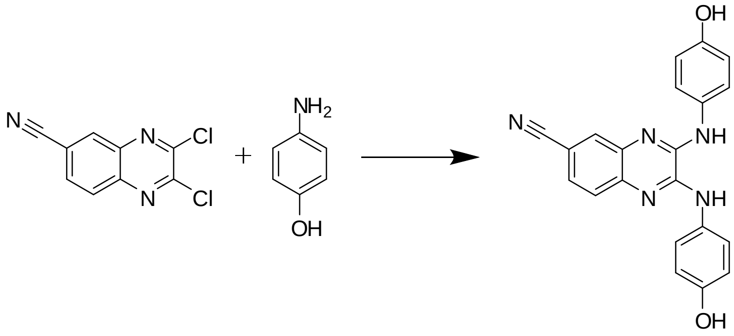

2,3-Dichloroquinoxaline-6-carbonitrile (112 mg, 0.50 mmol) and 4-aminophenol (218 mg, 1.20 mmol) were reacted following method A. The crude material was purified by flash chromatography using a ethyl acetate gradient of 30 to 70 % in cyclohexane to give the named compound as a red powder (158.0 mg, 86 %).

^{1}H NMR (500 MHz, d_6-DMSO) δ: 9.76 (s, 1H, O*H*), 9.73 (s, 1H, O*H*), 9.56 (s, 1H, N*H*), 9.43 (s, 1H, N*H*), 8.25 (s, 1H, Ar*H*), 8.04 (dt, *J* = 8.8, 3.2 Hz, 4H, 4 x Ar*H*), 7.93 (ddd, *J* = 11.1, 8.3, 2.3 Hz, 2H, 2 x Ar*H*), 7.24 (dt, *J* = 8.8, 3.2 Hz, 4H, 4 x Ar*H*).

^{13}C NMR (126 MHz, d_6-DMSO) δ: 153.9 (Ar*C*), 153.7 (Ar*C*), 142.9 (Ar*C*), 142.3 (Ar*C*), 139.6 (Ar*C*), 136.0 (Ar*C*), 130.8 (Ar*C*), 130.5 (Ar*C*), 129.3 (Ar*C*H), 126.5 (Ar*C*H), 125.9 (Ar*C*H), 123.6 (Ar*C*H), 123.2 (Ar*C*H), 119.5 (ArC-*C*N), 115.19 (Ar*C*H), 115.17 (Ar*C*H), 105.6 (ArC-*C*N).

HRMS-CI (m/z): [M + H]$^+$ calculated for $C_{21}H_{16}N_5O_2$, 370.13040; found, 370.129541.

2,3-bis((3-hydroxyphenyl)amino)quinoxaline-6-carbonitrile (69)

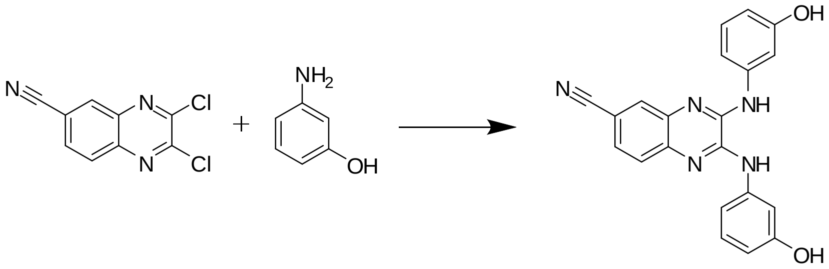

2,3-Dichloroquinoxaline-6-carbonitrile (67.2 mg, 0.30 mmol) and 3-aminophenol (130.8 mg, 1.20 mmol) were reacted following method A. The crude material was purified by flash chromatography using a ethyl acetate gradient of 30 to 70 % in cyclohexane to give the named compound as a red powder (104.0 mg, 94 %).

^{1}H NMR (500 MHz, d_6-DMSO) δ: 9.47 (s, 1H, O*H*), 9.42 (s, 1H, O*H*), 9.27 (s, 1H, N*H*), 9.16 (s, 1H, N*H*), 7.93 (d, *J* = 1.7 Hz, 1H, Ar*H*), 7.66 – 7.57 (m, 2H, 2 x Ar*H*), 7.53 (s, 1H, Ar*H*), 7.49 (s, 1H, Ar*H*), 7.30 – 7.24 (m, 2H, 2 x Ar*H*), 7.18 (dd, *J* = 14.3, 8.0 Hz, 2H, 2 x Ar*H*), 6.57 – 6.47 (m, 2H, 2 x Ar*H*).

^{13}C NMR (126 MHz, d_6-DMSO) δ: 157.6 (Ar*C*), 142.6 (Ar*C*), 142.0 (Ar*C*), 140.6 (Ar*C*), 140.3 (Ar*C*), 139.3 (Ar*C*), 135.8 (Ar*C*), 129.7 (Ar*C*H), 129.3 (Ar*C*H), 127.0 (Ar*C*H), 126.3 (Ar*C*H), 119.3 (Ar-*C*), 112.1 (Ar*C*H), 111.8 (Ar*C*H), 110.8 (Ar*C*H), 110.4 (Ar*C*H), 108.4 (Ar*C*H), 108.1 (Ar*C*H), 106.4 (ArC-*C*N).

HRMS-CI (m/z): $[M + H]^+$ calculated for $C_{21}H_{16}N_5O_2$, 370.13040; found, 370.129114.

4,4'-((6-chloroquinoxaline-2,3-diyl)bis(azanediyl))diphenol (70)

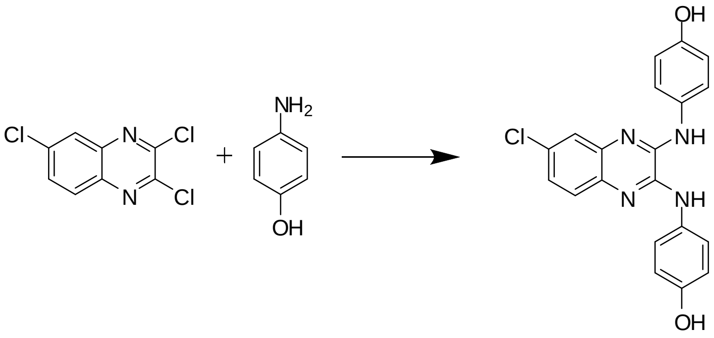

2,3,6-Trichloroquinoxaline (46.7 mg, 0.20 mmol) and 4-aminophenol (87.3 mg, 0.80 mmol) were reacted following method A. The crude material was purified by flash chromatography using an ethyl acetate gradient of 0 to 50 % in cyclohexane to give the named compound as a yellow powder (30.0 mg, 79 %).

^{1}H NMR (500 MHz, *d$_6$*-DMSO) δ: 9.24 (s, 1H), 9.23 (s, 1H), 8.87 (s, 1H), 8.81 (s, 1H), 7.65 – 7.55 (m, 4H), 7.45 – 7.37 (m, 2H), 7.22 (dt, *J* = 8.6, 2.1 Hz, 1H), 6.83 – 6.76 (m, 4H).

^{13}C NMR (126 MHz, *d$_6$*-DMSO) δ: 153.51 (Ar*C*), 153.45 (Ar*C*), 141.97 (Ar*C*), 141.61 (Ar*C*), 137.03 (Ar*C*), 134.97 (Ar*C*), 131.18 (Ar*C*), 131.09 (Ar*C*), 128.04 (Ar*C*), 126.35 (Ar*C*H), 124.25 (Ar*C*H), 123.73 (Ar*C*H), 123.07 (Ar*C*H), 123.04 (Ar*C*H), 115.14 (Ar*C*H).

HRMS-ES (m/z): [M + H] calculated for $C_{20}H_{16}N_4O_2Cl$, 379.0962; found, 379.0927.

3,3'-((6-chloroquinoxaline-2,3-diyl)bis(azanediyl))diphenol (71)

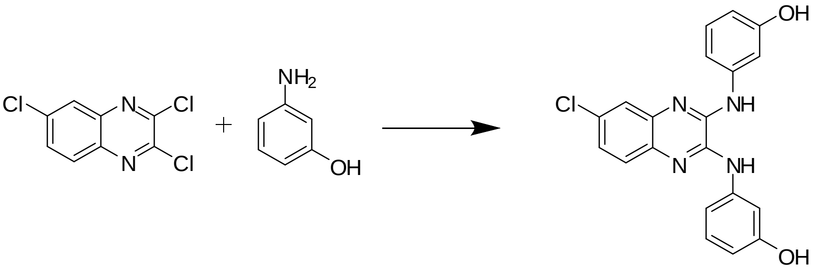

2,3,6-Trichloroquinoxaline (46.7 mg, 0.20 mmol) and 3-aminophenol (87.3 mg, 0.80 mmol) were reacted following method A. The crude material was purified by flash chromatography using an ethyl acetate gradient of 0 to 60 % in cyclohexane to give the named compound as a yellow powder (30.0 mg, 79 %).

^{1}H NMR (500 MHz, *d$_6$*-DMSO) δ: 9.39 (s, 2H), 9.03 (s, 1H), 8.98 (s, 1H), 7.58 – 7.49 (m, 3H), 7.48 (s, 1H), 7.33 (dd, *J* = 8.7, 2.3 Hz, 1H), 7.23 (s, 2H), 7.16 (td, *J* = 8.0, 1.7 Hz, 2H), 6.50 (d, *J* = 8.0 Hz, 2H).

^{13}C NMR (126 MHz, *d$_6$*-DMSO) δ: 157.58 (Ar*C*), 141.66 (Ar*C*), 141.25 (Ar*C*), 140.92 (Ar*C*), 140.83 (Ar*C*), 136.82 (Ar*C*), 134.79 (Ar*C*), 129.22 (Ar*C*H), 128.78 (Ar*C*), 126.72 (Ar*C*H), 125.03 (Ar*C*H), 124.05 (Ar*C*H), 111.55 (Ar*C*H), 110.06 (Ar*C*H), 107.83 (Ar*C*H).

HRMS-ES (m/z): [M + H] calculated for $C_{20}H_{16}N_4O_2Cl$, 379.0962; found, 379.0940.

N-(3-hydroxyphenyl)-2,3-bis((3-hydroxyphenyl)amino)quinoxaline-6-carboxamide (72)

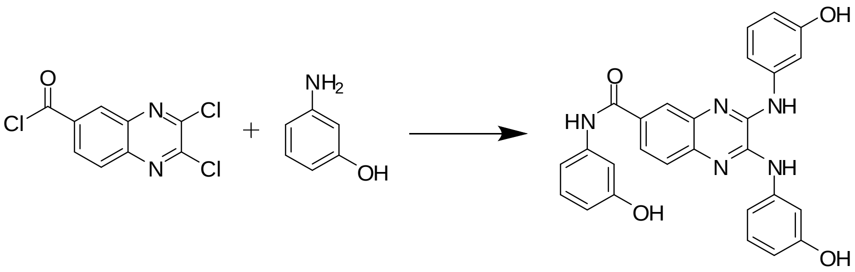

2,3-Dichloroquinoxaline-6-carboxylic acid (243 mg, 1.0 mmol) and 3-aminophenol (436 mg, 4.0 mmol) were reacted following method A. The crude material was purified by flash chromatography using a ethyl acetate gradient of 30 to 70 % in cyclohexane containing 1 % acetic acid to give the named compound as a red powder (148.0 mg, 31 %).

^{1}H NMR (500 MHz, $CDCl_3$) δ: 10.19 (s, 1H, Ar-CON*H-Ar*), 9.12 (s, 1H, N*H*), 9.04 (s, 1H, N*H*), 8.15 (d, *J* = 1.9 Hz, 1H, Ar*H*), 7.87 (dd, *J* = 8.5, 1.9 Hz, 1H, Ar*H*), 7.60 (d, *J* = 8.5 Hz, 1H, Ar*H*), 7.51 (dt, *J* = 8.5, 1.9 Hz, 2H, 2 x Ar*H*), 7.33 (t, *J* = 1.9 Hz, 1H, Ar*H*), 7.29 – 7.23 (m, 2H, 2 x Ar*H*), 7.20 – 7.09 (m, 4H, 4 x Ar*H*), 6.56 – 6.48 (m, 3H, 3 x , Ar*H*).

^{13}C NMR (126 MHz, d_6-DMSO) δ: 172.5 (Ar-*C*ONH-Ar), 165.5 (Ar*C*), 157.5 (Ar*C*), 157.3 (Ar*C*), 142.0 (Ar*C*), 141.6 (Ar*C*), 140.9 (Ar*C*), 140.7 (Ar*C*), 140.2 (Ar*C*), 138.3 (Ar*C*), 135.2 (Ar*C*), 131.0 (Ar*C*), 129.4 (Ar*C*H), 129.3 (Ar*C*H), 125.1 (Ar*C*H), 124.9 (Ar*C*H), 124.2 (Ar*C*H), 111.9 (Ar*C*H), 111.8 (Ar*C*H), 111.4 (Ar*C*H), 110.8 (Ar*C*H), 110.4 (Ar*C*H), 110.2 (Ar*C*H), 108.1 (Ar*C*H), 108.0 (Ar*C*H), 107.7 (Ar*C*H).

HRMS-EI (m/z): [M] calculated for $C_{27}H_{21}N_5O_4$, 479.1588; found, 479.1600.

2,3-bis((4-hydroxyphenyl)amino)-N-methylquinoxaline-6-carboxamide (73)

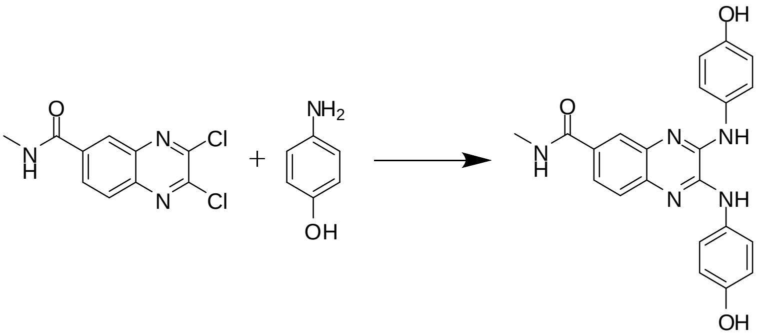

2,3-Dichloro-N-methylquinoxaline-6-carboxamide (25.7 mg, 0.10 mmol) and 4-aminophenol (43.6 mg, 0.40 mmol) were reacted following method A. The crude material was purified by flash chromatography using an ethyl acetate gradient of 20 to 70 % in cyclohexane to give the named compound as a yellow powder (29.0 mg, 72 %).

^{1}H NMR (500 MHz, *d$_6$*-DMSO) δ 9.26 (s, 1H, O*H*), 9.25 (s, 1H, O*H*), 8.89 (s, 1H, Ar-N*H*), 8.82 (s, 1H, Ar-N*H*), 8.44 (q, *J* = 4.5 Hz, 1H, Ar-CON*H*CH$_3$), 7.94 (d, *J* = 2.0 Hz, 1H, Ar*H*), 7.71 (dd, *J* = 8.4, 2.0 Hz, 1H, Ar*H*), 7.63 (d, *J* = 8.4 Hz, 4H, 4 x Ar*H*), 7.43 (d, *J* = 8.4 Hz, 1H, Ar*H*), 6.86 – 6.77 (m, 4H, 4 x Ar*H*), 2.77 (d, *J* = 4.5 Hz, 3H, Ar-CONHC*H*$_3$).

^{13}C NMR (126 MHz, *d$_6$*-DMSO) δ 166.5 (Ar-*C*ONHCH$_3$), 153.5 (Ar*C*), 153.4 (Ar*C*), 142.2 (Ar*C*), 141.9 (Ar*C*), 138.2 (Ar*C*), 137.2 (Ar*C*), 135.4 (Ar*C*), 131.3 (Ar*C*), 131.1 (Ar*C*), 130.0 (Ar*C*H), 124.6 (Ar*C*H), 123.8 (Ar*C*H), 123.1 (Ar*C*H), 115.1 (Ar*C*H), 26.3 (Ar-CONH*C*H$_3$).

HRMS-EI (m/z): [M] calculated for $C_{22}H_{19}N_5O_3$, 401.1488; found, 401.1481.

6,7-bis((3-hydroxyphenyl)amino)-N-methyl-2-naphthamide (74)

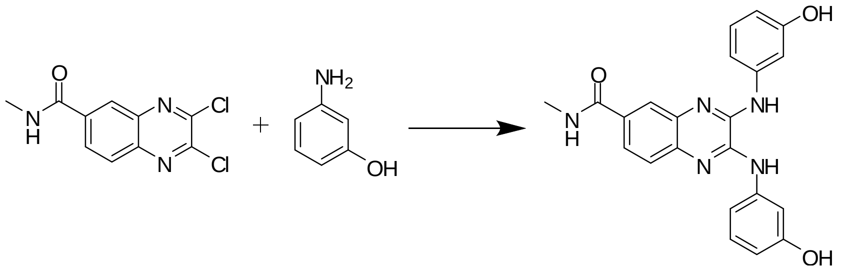

2,3-Dichloro-N-methylquinoxaline-6-carboxamide (25.7 mg, 0.10 mmol) and 3-aminophenol (43.6 mg, 0.40 mmol) were reacted following method A. The crude material was purified by flash chromatography using an ethyl acetate gradient of 20 to 70 % in cyclohexane to give the named compound as a yellow powder (30.0 mg, 75 %).

^{1}H NMR (500 MHz, *d$_6$*-DMSO) δ 9.42 (s, 1H, O*H*), 9.41 (s, 1H, O*H*), 9.04 (s, 1H, N*H*), 8.98 (s, 1H, N*H*), 8.51 (d, *J* = 4.4 Hz, 1H, Ar-CON*H*CH$_3$), 8.06 (s, 1H, ArC*H*), 7.80 (d, *J* = 8.4 Hz, 1H, ArC*H*), 7.55 (d, *J* = 8.4 Hz, 1H, ArC*H*), 7.50 (d, *J* = 12.0 Hz, 2H, 2 x ArC*H*), 7.28 (d, *J* = 8.0 Hz, 2H, 2 x ArC*H*), 7.17 (t, *J* = 8.0 Hz, 2H, 2 x ArC*H*), 6.50 (d, *J* = 8.0 Hz, 2H, 2 x ArC*H*), 2.80 (d, *J* = 4.4 Hz, 3H, Ar-CONHC*H*$_3$).

^{13}C NMR (126 MHz, *d$_6$*-DMSO) δ 166.5 (Ar-*C*ONHCH$_3$), 157.6 (Ar*C*), 157.6 (Ar*C*), 141.9 (Ar*C*), 141.6 (Ar*C*), 141.0 (Ar*C*), 140.9 (Ar*C*), 137.9 (Ar*C*), 135.3 (Ar*C*), 130.8 (Ar*C*H), 129.22 (Ar*C*H), 129.19 (Ar*C*H), 124.9 (Ar*C*), 124.3 (Ar*C*), 123.7 (Ar*C*), 111.7 (Ar*C*H), 111.6 (Ar*C*H), 110.2 (Ar*C*H), 110.0 (Ar*C*H), 108.0 (Ar*C*H), 107.9 (Ar*C*H), 26.3 (Ar-CONH*C*H$_3$).

HRMS-EI (m/z): [M] calculated for $C_{22}H_{19}N_5O_3$, 401.1488; found, 401.1479.

4,4'-((6-aminoquinoxaline-2,3-diyl)bis(azanediyl))diphenol (75)

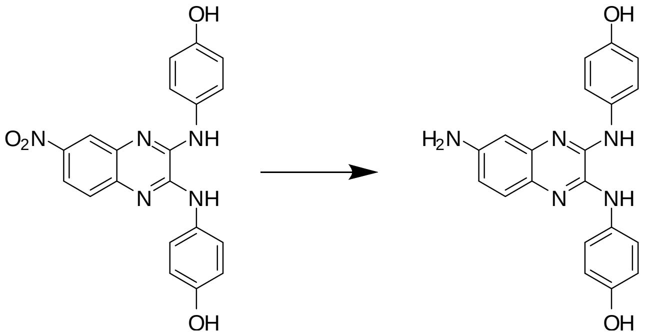

Tin (II) chloride dihydrate (112.5 mg, 0.5 mmol) was added to a solution of 4,4'-((6-nitroquinoxaline-2,3-diyl)bis(azanediyl))diphenol (39 mg, 0.1 mmol) in ethanol (15 mL) and the resulting mixture was brought to boil. A solution of sodium borohydride (18.9 mg, 0.5 mmol) in ethanol (5 mL) was added to the boiling mixture dropwise and refluxed for 1.5 hrs. Upon cooling, water (10 mL) was added. Sodium hydroxide was added until neutralisation of the solution. The ethanol was evaporated from the mixture and an extraction with ethyl acetate (20 mL) was performed. The organics were washed with brine (3 x 10 mL) and dried over magnesium sulphate, filtered and the solvent evaporated under reduced pressure. The crude material was purified by flash column chromatography using a gradient of 50 to 80 % ethyl acetate in cyclohexane to give the named compound (22.0 mg, 61 %).

^{1}H NMR (500 MHz, d_6-DMSO) δ: 9.13 (s, 1H, O*H*), 9.06 (s, 1H, O*H*), 8.47 (s, 1H, N*H*), 8.23 (s, 1H, N*H*), 7.60 (d, *J* = 8.9 Hz, 2H, 2 x Ar*H*), 7.53 (d, *J* = 8.9 Hz, 2H, 2 x Ar*H*), 7.15 (d, *J* = 8.6 Hz, 1H, Ar*H*), 6.75 (dd, *J* = 10.8, 8.9 Hz, 4H, 4 x Ar*H*), 6.64 (dd, *J* = 8.6, 2.4 Hz, 1H, Ar*H*), 6.58 (d, *J* = 2.4 Hz, 1H, Ar*H*), 5.06 (s, 2H, NH_2).

^{13}C NMR (126 MHz, d_6-DMSO) δ: 152.8 (Ar*C*), 152.4 (Ar*C*), 146.3 (Ar*C*), 141.4 (Ar*C*), 138.5 (Ar*C*), 137.6 (Ar*C*), 132.5 (Ar*C*), 132.0 (Ar*C*), 128.4 (Ar*C*), 125.4 (Ar*C*H), 122.4 (Ar*C*H), 121.8 (Ar*C*H), 115.0 (Ar*C*H), 114.99 (Ar*C*H), 114.8 (Ar*C*H), 106.5 (Ar*C*H).

HRMS-CI (m/z): $[M + H]^+$ calculated for $C_{20}H_{18}N_5O_2$, 360.1460; found, 360.1451.

N-(2-(3-chloro-7-nitroquinoxalin-2-ylamino)phenyl)acetamide or N-(2-(3-chloro-6-nitroquinoxalin-2-ylamino)phenyl)acetamide (78)

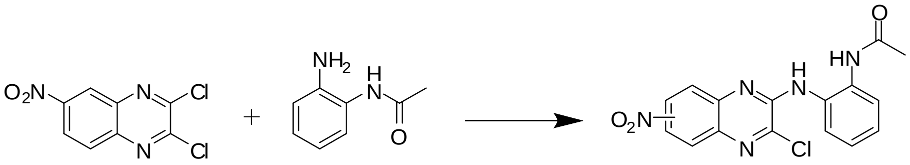

A mixture containing the 2,3-dichloro-6-nitroquinoxaline (48.8 mg, 0.20 mmol), N-(2-aminophenyl)acetamide (27 mg, 0.22 mmol), cesium carbonate (84.7 mg, 0.22 mmol), 4,5-Bis(diphenylphosphino)-9,9-dimethylxanthene (11.6 mg, 0.02 mmol) and $Pd_2(dba)_3$ (18.3 mg, 0.02 mmol) was made up in dioxane (6 mL) and allowed to react under microwave for 5 min at 120 °C. The solvent was then evaporated under reduced pressure and the residue was taken up in ethyl acetate (30 mL) and washed with H_2O (3 x 15 mL). The organic solution was dried over Na_2SO_4, filtered and the solvent removed under reduced pressure. The crude material was purified by flash column chromatography using a gradient of 20 to 60% ethyl acetate in cyclohexane to give a yellow powder (29 mg, 40 %).

^{1}H NMR (500 MHz, d_6-DMSO) δ: 9.86 (s, 1H, Ar-N*H*COCH$_3$), 9.45 (s, 1H, N*H*), 8.61 (d, *J* = 1.9 Hz, 1H, Ar*H*), 8.33 (dd, *J* = 9.1, 1.9 Hz, 1H, Ar*H*), 7.80 – 7.73 (m, 1H, Ar*H*), 7.65 (d, *J* = 9.1 Hz, 1H, Ar*H*), 7.56 – 7.49 (m, 1H, Ar*H*), 7.31 – 7.24 (m, 2H, Ar*H*), 2.04 (s, 3H, C*H*$_3$).

^{13}C NMR (126 MHz, d_6-DMSO) δ: 169.6 (NH*C*OCH$_3$), 148.2 (Ar*C*), 144.4 (Ar*C*), 143.7 (Ar*C*), 134.7 (Ar*C*), 132.4 (Ar*C*), 130.2 (Ar*C*), 126.9 (Ar*C*H), 126.5 (Ar*C*H), 126.2 (Ar*C*H), 125.0 (Ar*C*H), 124.4 (Ar*C*H), 124.1 (Ar*C*H), 123.4 (Ar*C*H), 23.3(NHCO*C*H$_3$).

HRMS-EI (m/z): [M] calculated for $C_{16}H_{12}N_5O_3$, 357.0629; found, 357.0632.

4,4'-((6-nitroquinoxaline-2,3-diyl)bis(azanediyl))bis(3-methylphenol) (79)

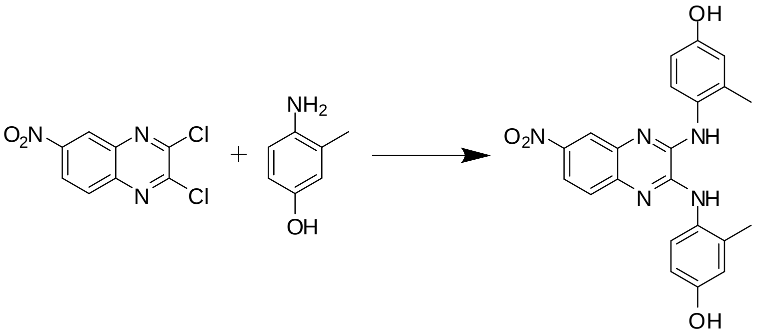

2,3-Dichloro-6-nitroquinoxaline (48.8 mg, 0.20 mmol) and 4-amino-3-methylphenol (98.4 mg, 0.80 mmol) were reacted following method A. The crude material was purified by flash chromatography using an ethyl acetate gradient of 20 to 50 % in cyclohexane to give the name compound as a red powder (55.0 mg, 66 %).

^{1}H NMR (500 MHz, d_6-DMSO) δ: 9.39 (s, 1H, O*H*), 9.36 (s, 1H, O*H*), 8.90 (s, 1H, N*H*), 8.66 (s, 1H, N*H*), 8.00 (d, *J* = 2.5 Hz, 1H, Ar*H*), 7.92 (dd, *J* = 8.9, 2.5 Hz, 1H, Ar*H*), 7.37 (d, *J* = 8.9 Hz, 1H, Ar*H*), 7.20 (dd, *J* = 8.4, 2.2 Hz, 2H, 2x Ar*H*), 6.73 (s, 2H, 2 x Ar*H*), 6.67 (d, *J* = 8.4 Hz, 2H, 2 x Ar*H*), 2.13 (d, *J* = 3.6 Hz, 6H, 2 x CH_3).

^{13}C NMR (126 MHz, d_6-DMSO) δ: 155.73 (Ar*C*), 155.56 (Ar*C*), 144.67 (Ar*C*), 142.90 (Ar*C*), 141.93 (Ar*C*), 135.66 (Ar*C*), 135.47 (Ar*C*), 135.38 (Ar*C*), 128.21 (Ar*C*H), 128.09 (Ar*C*H), 127.76 (Ar*C*), 125.28 (Ar*C*), 119.91 (Ar*C*H), 118.22 (Ar*C*), 116.95 (Ar*C*H), 113.11 (Ar*C*H), 113.07 (Ar*C*H), 18.14(Ar$C\mathrm{H}_3$).

HRMS-EI (m/z): [M] calculated for $C_{22}H_{19}N_5O_4$, 417.14.316; found, 417.143144.

4-(3-chloro-7-nitroquinoxalin-2-yloxy)-2-methylaniline or 4-(3-chloro-6-nitroquinoxalin-2-yloxy)-2-methylaniline (80)

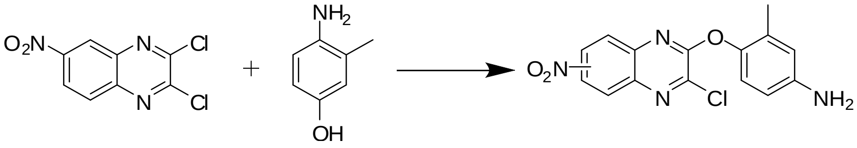

A mixture containing the 2,3-dichloro-6-nitroquinoxaline (48.8 mg, 0.20 mmol), 4-amino-3-methylphenol (27 mg, 0.22 mmol), cesium carbonate (84.7 mg, 0.22 mmol), 4,5-Bis(diphenylphosphino)-9,9-dimethylxanthene (11.6 mg, 0.02 mmol) and $Pd_2(dba)_3$ (18.3 mg, 0.02 mmol) was made up in dioxane (6 mL) and allowed to react under microwave for 5 min at 120°C. The solvent was then evaporated under reduced pressure and the residue was taken up in ethyl acetate (30 mL) and washed with H_2O (3 x 15 mL). The organic solution was dried over Na_2SO_4, filtered and the solvent removed under reduced pressure. The crude material was purified by flash column chromatography using a gradient of 20 to 50 % ethyl acetate in cyclohexane to give a yellow powder (17 mg, 26 %).

^{1}H NMR (500 MHz, d_6-DMSO) δ: 8.77 (d, *J* = 2.6 Hz, 1H, Ar*H*), 8.41 (dd, *J* = 9.2, 2.6 Hz, 1H, Ar*H*), 7.89 (d, *J* = 9.2 Hz, 1H, Ar*H*), 6.92 (d, *J* = 2.6 Hz, 1H, Ar*H*), 6.88 (dd, *J* = 8.5, 2.6 Hz, 1H, Ar*H*), 6.67 (d, *J* = 8.5 Hz, 1H, Ar*H*), 4.92 (s, 2H, N*H*2), 2.07 (s, 3H, CH_3).

^{13}C NMR (126 MHz, d_6-DMSO) δ: 155.3 (Ar*C*), 145.9 (Ar*C*), 144.9 (Ar*C*), 142.7 (Ar*C*), 142.3 (Ar*C*), 142.1 (Ar*C*), 137.0 (Ar*C*), 128.3 (Ar*C*H), 124.1 (Ar*C*H), 123.4 (Ar*C*H), 122.4 (Ar*C*H), 122.2 (Ar*C*H), 119.2 (Ar*C*H), 114.2 (Ar*C*H), 17.5 (*C*H_3).

HRMS-EI (m/z): [M] calculated for $C_{15}H_{11}N_4O_3$, 330.05142; found, 330.051748.

6-nitroquinoxaline-2,3-diol (81)

Literature compound.[150]

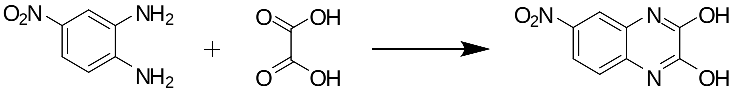

4-Nitrobenzene-1,2-diamine (3.06 g, 20 mmol) was reacted with oxalic acid (1.980 g, 22 mmol) using method C to give the named compound as a tan powder (1.870 g, 45 %).

^{1}H NMR (500 MHz, *d$_6$*-DMSO) δ: 12.36 (s, 1H, O*H*), 12.16 (s, 1H, O*H*), 8.00 – 7.84 (peak overlapped, 2H, 2 x Ar*H*), 7.24 (d, *J* = 8.6 Hz, 1H, Ar*H*).

^{13}C NMR (126 MHz, *d$_6$*-DMSO) δ: 155.1 (Ar*C*), 154.7 (Ar*C*), 142.1 (Ar*C*), 131.6 (Ar*C*), 126.1 (Ar*C*), 118.6 (Ar*C*), 115.5 (Ar*C*), 110.3 (Ar*C*).

MS-EI (m/z): [M - H] calculated for $C_8H_4N_3O_4$, 206.1359; found 206.00.

6,7-dinitroquinoxaline-2,3-diol (82)

Literature compound.[150]

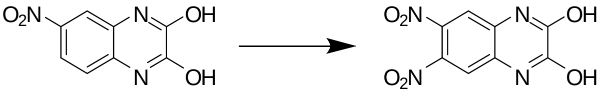

A solution of 6-nitroquinoxaline-2,3-diol **81** (1.0 g, 4.8 mmol) was made up in sulphuric acid (15 mL) at 0 °C and potassium nitrate (727 mg, 7.2 mmol) was added in several portions. The resulting solution was allowed to warm to room temperature and stirred for 48 hrs, until consumption of the starting material was observed by LC-MS. The mixture was carefully poured into 50 mL of ice/water and stirred for 30 min, filtered, washed with water, and dried to give the named compound (822 mg, 68 % recovery).

^{1}H NMR (500 MHz, *d$_6$*-DMSO) δ: 12.47 (s, 2H, 2 x O*H*), 7.71 (s, 2H, 2 x Ar*H*).

^{13}C NMR (126 MHz, *d$_6$*-DMSO) δ: 154.7 (Ar*C*), 136.9 (Ar*C*), 129.6 (Ar*C*), 111.8 (ArCH).

MS-EI (m/z): [M - H] calculated for $C_8H_3N_4O_6$, 251.1335; found 250.90.

2,3-dichloro-6,7-dinitroquinoxaline (83)

Literature compound.[150]

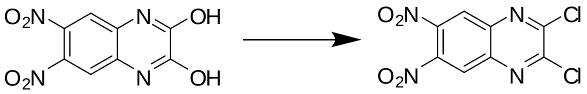

The reaction with 6,7-dinitroquinoxaline-2,3-diol (378 mg, 1.5 mmol) was carried out using method D to give the named compound as a red solid (400 mg, 92 %).

^{1}H NMR (500 MHz, d_6-DMSO) δ 9.06 (s, 2H, 2 x Ar*H*).

^{13}C NMR (126 MHz, d_6-DMSO) δ 150.3 (Ar*C*), 142.2 (Ar*C*), 140.8 (Ar*C*), 126.5 (Ar*C*H).

1-methyl-4-(4-nitrophenyl)piperazine (85)

Literature compound.[139]

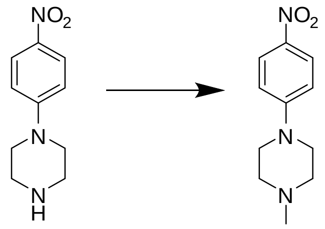

1-(4-nitrophenyl)piperazine (1.0 g, 4.8 mmol) was reacted with formic acid (2 mL, 48 mmol) and 40 % formaldehyde (3.6 mL, 48 mmol) under microwave irradiation at 120 °C for 5 minutes. Upon cooling, the mixture was added to ethyl acetate (100 mL) and 2M NaOH (70 mL) and the layers were separated. The organic layer was washed with brine (50 mL) after which the brine layer was further extracted with ethyl acetate (50 mL). The organics were combined and dried over Mg_2SO_4, filtered and concentrated under vacuum to give the named compound (897 mg, 85% yield). Analysis of the compound showed no traces of starting material and it was used without further purification.

^{1}H NMR (500 MHz, $CDCl_3$) δ: 8.14 – 8.08 (m, 2H, 2 x Ar*H*), 6.84 – 6.78 (m, 1H, 2 x Ar*H*), 3.45 – 3.40 (m, 4H, 2 x C*H*$_2$), 2.58 – 2.51 (m, 4H, 2 x C*H*$_2$), 2.35 (s, 3H).

^{13}C NMR (126 MHz, $CDCl_3$) δ: 154.9 (Ar*C*), 138.5 (Ar*C*), 126.0 (Ar*C*H), 112.8 (Ar*C*H), 54.6 (*C*H$_2$), 47.1 (*C*H$_2$), 46.1(*C*H$_3$).

MS-EI (m/z): $[M + H]^+$ calculated for $C_{11}H_{16}N_3O_2$, 222.2648; found 222.00.

4-(4-methylpiperazin-1-yl)aniline (86)

Literature compound.[153]

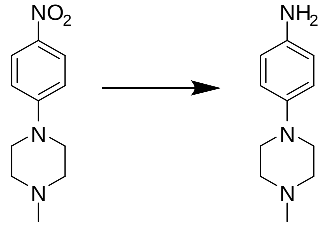

Tin (II) chloride dihydrate (2.250 g, 10 mmol) was added to a solution of **85** (442 mg, 2 mmol) in ethanol (250 mL) and the mixture was brought to boil. Sodium borohydride (378 mg, 10 mmol) in ethanol (50 mL) was added to the boiling solution dropwise after which the resulting mixture was kept under reflux for 2.5 hrs until disappearance of starting material was observed by TLC. Upon cooling, sodium hydroxide was added until neutralisation of the solution was obtained. The ethanol was evaporated under reduced pressure and the compound extracted with ethyl acetate (3 x 100 mL). The organics were washed with brine and dried over Mg_2SO_4, filtered and concentrated under vacuum, to yield the name compound (216 mg, 57 % recovery).

^{1}H NMR (500 MHz, d_6-DMSO) δ: 6.68 – 6.62 (m, 2H, 2 x Ar*H*), 6.51 – 6.45 (m, 1H, 2 x Ar*H*), 4.57 (s, 2H, N*H*$_2$), 2.90 – 2.85 (m, 4H, 2 x C*H*$_2$), 2.43 – 2.38 (m, 2H, 2 x C*H*$_2$), 2.19 (s, 3H, C*H*$_3$).

^{13}C NMR (126 MHz, d_6-DMSO) δ: 142.4 (Ar*C*), 142.1 (Ar*C*), 117.8 (Ar*C*H), 114.7 (Ar*C*H), 54.9 (C*H*$_2$), 50.2 (C*H*$_2$), 45.9 (C*H*$_3$).

MS-EI (m/z): $[M + H]^+$ calculated for $C_{11}H_{18}N_3$, 192.2818; found 192.10.

4-((3-((4-(4-methylpiperazin-1-yl)phenyl)amino)-6,7-dinitroquinoxalin-2-yl)amino)phenol (87)

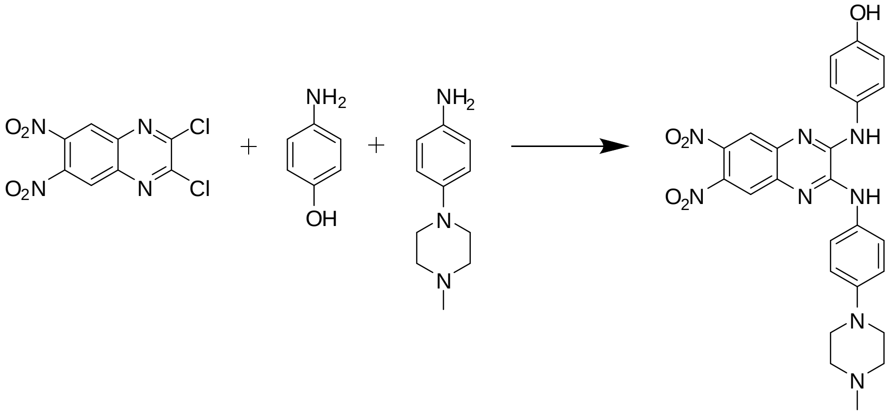

To a microwave vial containing a magnetic stirrer bar was added 2,3-dichloro-6,7-dinitroquinoxaline (289 mg, 1 mmol), 4-(4-methylpiperazin-1-yl)aniline **86** (191 mg, 1 mmol), 4-aminophenol (109 mg, 1 mmol) and NMP (5 mL). The mixture was reacted under microwave irradiation for 5 min at 160 °C in a closed vial. Upon cooling, the mixture was added to saturated sodium bicarbonate (50 mL) and extracted with ethyl acetate (3 x 50 mL). The organics were washed with brine and the solvent evaporated under reduced pressure. Purification was carried on by reverse phase column chromatography, using a gradient of 0 to 100 % methanol in water containing 0.1 % formic acid, to obtain the name compound as a red powder (100 mg, 20 % yield).

^{1}H NMR (600 MHz, d_6-DMSO) δ: 9.57 (s, 1H, O*H*), 8.24 (s, 2H, 2 x N*H*), 7.94 (s, 1H, Ar*H*), 7.94 (s, 1H, Ar*H*), 7.69 (d, *J* = 8.7 Hz, 2H, 2 x Ar*H*), 7.60 (d, *J* = 8.6 Hz, 2H, 2 x Ar*H*), 6.99 (d, *J* = 9.0 Hz, 2H, 2 x Ar*H*), 6.82 (d, *J* = 8.8 Hz, 2H, 2 x Ar*H*), 3.22 – 3.19 (m, 4H, 2 x CH_2), 2.77 – 2.73 (m, 4H, 2 x CH_2), 2.41 (s, 3H, N-CH_3).

^{13}C NMR (151 MHz, d_6-DMSO) δ: 207.9 (Ar*C*), 164.9 (Ar*C*H), 154.3 (Ar*C*), 147.4 (Ar*C*), 137.9 (Ar*C*), 137.8 (Ar*C*), 123.9 (Ar*C*H), 123.0 (Ar*C*H), 121.5 (Ar*C*H), 115.8 (Ar*C*H), 115.3 (Ar*C*H), 53.7 (CH_2), 47.4 (CH_2), 44.4 (CH_3).

HRMS-ES (m/z): [M + H] calculated for $C_{25}H_{25}N_8O_5$, 517.1948; found, 517.1948.

4-(3-(2-morpholinophenylamino)-6,7-dinitroquinoxalin-2-ylamino)phenol (89)

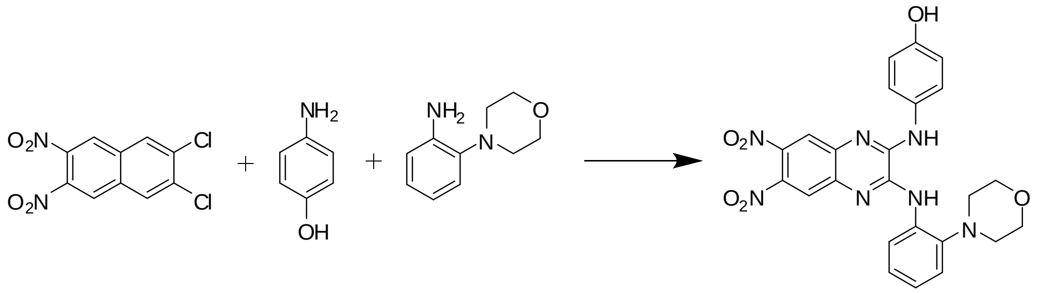

To a microwave vial containing a magnetic stirrer bar was added 2,3-dichloro-6,7-dinitroquinoxaline (289 mg, 1 mmol), 2-morpholinoaniline (178 mg, 1 mmol), 4-aminophenol (109 mg, 1 mmol) and N-methyl-2-pyrrolidone (5 mL). The mixture was reacted under microwave irradiation for 5 min at 160 °C in a closed vial. Upon cooling, the mixture was added to saturated sodium bicarbonate (50 mL) and extracted with ethyl acetate (3 x 50 mL). The organics were washed with brine and the solvent evaporated under reduced pressure. Purification was carried on by reverse phase column chromatography, using a gradient of 0 to 100 % methanol in water containing 0.1 % formic acid, followed by preparative HPLC to give the named compound.

HRMS-EI (m/z): $[M+H]^+$ calculated for $C_{24}H_{21}N_7O_6$, 503.15533; found, 503.154112.

1,2-bis(3-hydroxyphenyl)ethane-1,2-dione (91)

Literature compound.[141]

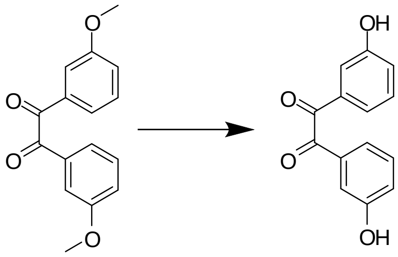

1,2-Bis(3-methoxyphenyl)ethane-1,2-dione (500 mg, 1.85 mmol) was taken up in 48 % HBr in Acetic acid (20 mL) and refluxed for 36hrs. Upon cooling, the mixture was poured into water (20 mL) and extracted with ethyl acetate (20 mL). The organic layer was washed with water (20 mL), dried over Mg_2SO_4, filtered and the solvent removed under reduced pressure. The crude material was purified by flash column chromatography using a solvent gradient of 10 to 50 % ethyl acetate in cyclohexane to give the named compound in 60 % yield.

^{1}H NMR (500 MHz, *d$_6$*-DMSO) δ 10.06 (s, 2H, 2 x Ar-O*H*), 7.44 – 7.38 (m, 2H, 2 x Ar*H*), 7.30 – 7.26 (m, 2H, 2 x Ar*H*), 7.26 – 7.24 (m, 2H, 2 x Ar*H*), 7.16 (ddd, *J* = 8.1, 2.5, 0.9 Hz, 2H, 2 x Ar*H*).

^{13}C NMR (126 MHz, *d$_6$*-DMSO) δ 195.1 (*C*O), 158.1 (Ar*C*), 133.5 (Ar*C*), 130.8 (Ar*C*H), 122.8 (Ar*C*H), 120.6 (Ar*C*H), 114.9 (Ar*C*H).

MS-EI (m/z): $[M + Na]^+$ calculated for $C_{14}H_{10}O_4Na$, 265.2179; found 265.00.

2,3-bis(3-methoxyphenyl)-6-(trifluoromethyl)quinoxaline (92)

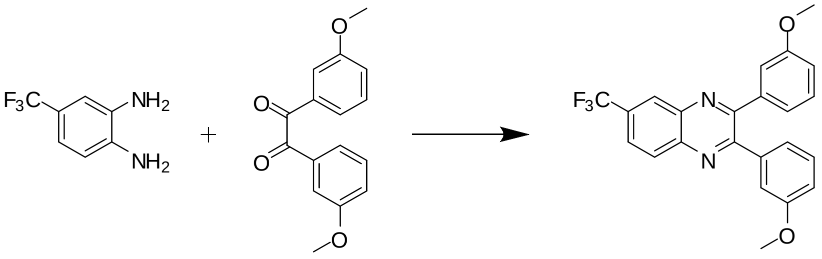

4-(Trifluoromethyl)benzene-1,2-diamine (35.2 mg, 0.20 mmol) and 1,2-bis(3-methoxyphenyl)ethane-1,2-dione (54 mg, 0.20 mmol) were reacted using method B to give the name compound as a white powder (73 mg, 89 %).

^{1}H NMR (500 MHz, CDCl$_3$) δ: 8.50 (s, 1H, Ar*H*), 8.29 (d, *J* = 8.8 Hz, 1H, Ar*H*), 7.94 (dd, *J* = 8.8, 1.9 Hz, 1H, Ar*H*), 7.26 (td, *J* = 7.8, 1.5 Hz, 2H, 2 x Ar*H*), 7.13 – 7.07 (m, 4H, 4 x Ar*H*), 6.97 – 6.93 (m, 2H, 2 x Ar*H*), 3.73 (s, 6H, 2 x C*H*$_3$).

^{13}C NMR (126 MHz, CDCl$_3$) δ: 159.60 (Ar*C*-OCH$_3$), 155.28 (Ar*C*), 154.72 (Ar*C*), 142.25 (Ar*C*), 140.21 (Ar*C*), 139.75 (Ar*C*), 139.71 (Ar*C*), 131.82 (Ar*C*-CF$_3$ or *C*F$_3$), 131.55 (Ar*C*-CF$_3$ or *C*F$_3$), 130.48 (Ar*C*H), 129.53 (Ar*C*H), 129.51 (Ar*C*H), 127.34 (Ar*C*H), 125.67 (Ar*C*H), 122.39 (Ar*C*H), 122.36 (Ar*C*H), 115.76 (Ar*C*H), 115.73 (Ar*C*H), 114.85 (Ar*C*H), 114.79 (Ar*C*H), 55.37 (O*C*H$_3$).

HRMS-CI (m/z): [M+H]$^+$ calculated for $C_{23}H_{18}F_3N_2O_2$, 411.13149; found, 411.130521.

2,3-bis(3-methoxyphenyl)quinoxaline-6-carbonitrile (93)

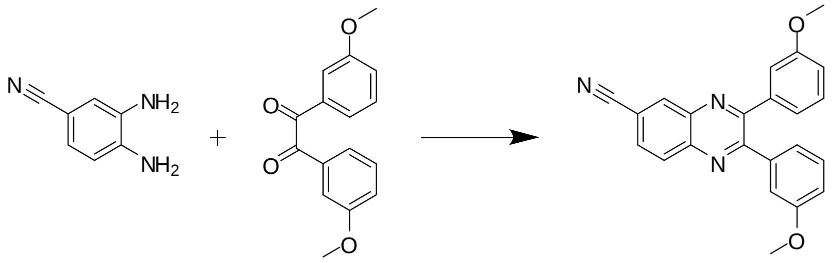

3,4-Diaminobenzonitrile (26.6 mg, 0.20 mmol) and 1,2-bis(3-methoxyphenyl)ethane-1,2-dione (54 mg, 0.20 mmol) were reacted using method B to give the named compound as a white powder (73 mg, 99 %).

^{1}H NMR (500 MHz, $CDCl_3$) δ: 8.54 (dd, *J* = 1.8, 0.5 Hz, 1H, Ar*H*), 8.25 (dd, *J* = 8.6, 0.5 Hz, 1H, Ar*H*), 7.91 (dd, *J* = 8.6, 1.8 Hz, 1H, Ar*H*), 7.29 – 7.24 (m, 2H, 2 x Ar*H*), 7.13 – 7.06 (m, 4H, 4 x Ar*H*), 6.98 – 6.94 (m, 2H, 2 x Ar*H*), 3.73 (s, 3H, C*H*$_3$), 3.72 (s, 3H, C*H*$_3$).

^{13}C NMR (126 MHz, $CDCl_3$) δ: 159.6 (Ar*C*-OCH_3), 159.6(Ar*C*-OCH_3), 155.8(Ar*C*), 155.2(Ar*C*), 142.6(Ar*C*), 140.3(Ar*C*), 139.5(Ar*C*), 139.4(Ar*C*), 135.2(Ar*C*-CN), 130.8(Ar*C*H), 130.8(Ar*C*H), 129.6(Ar*C*H), 122.4(Ar*C*H), 122.4(Ar*C*H), 118.2(Ar*C*H), 116.0(Ar*C*H), 115.9(Ar*C*H), 114.9(Ar*C*H), 114.8(Ar*C*H), 113.4 (Ar-*C*N), 55.4 (O*C*H$_3$).

HRMS-CI (m/z): $[M + H]^+$ calculated for $C_{23}H_{18}F_3N_3O_2$, 368.1394; found, 368.1388.

6-chloro-2,3-bis(3-methoxyphenyl)quinoxaline (94)

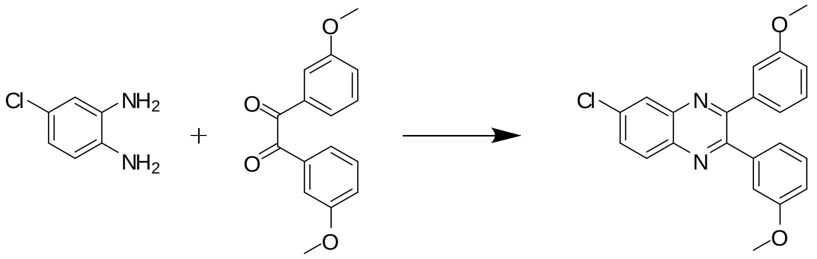

4-Chlorobenzene-1,2-diamine (28.4 mg, 0.20 mmol) and 1,2-bis(3-methoxyphenyl)ethane-1,2-dione (54 mg, 0.20 mmol) were reacted using method B to give the named compound as a white powder (75 mg, 99 %).

^{1}H NMR (500 MHz, $CDCl_3$) δ: 8.17 (d, *J* = 2.3 Hz, 1H, Ar*H*), 8.10 (d, *J* = 8.9 Hz, 1H, Ar*H*), 7.71 (dd, *J* = 8.9, 2.3 Hz, 1H, Ar*H*), 7.30 – 7.18 (m, 2H, 2 x Ar*H*), 7.14 – 7.02 (m, 4H, 4 x Ar*H*), 6.96 – 6.86 (m, 2H, 2 x Ar*H*), 3.71 (s, 6H, 2 x CH_3).

^{13}C NMR (126 MHz, $CDCl_3$) δ: 159.6(Ar*C*-OCH_3), 154.2(Ar*C*), 153.5(Ar*C*), 141.5(Ar*C*), 140.0(Ar*C*), 139.9(Ar*C*), 139.8(Ar*C*), 135.8 (Ar*C*-Cl), 131.1(Ar*C*H), 130.5(Ar*C*H), 129.5(Ar*C*H), 129.4(Ar*C*H), 128.2(Ar*C*H), 122.4(Ar*C*H), 122.4(Ar*C*H), 115.6(Ar*C*H), 115.5(Ar*C*H), 114.8(Ar*C*H), 114.8(Ar*C*H), 55.4(OCH_3).

HRMS-CI (m/z): $[M + H]^+$ calculated for $C_{22}H_{18}ClN_2O_2$, 377.1051; found, 377.1049.

6-fluoro-2,3-bis(3-methoxyphenyl)quinoxaline (95)

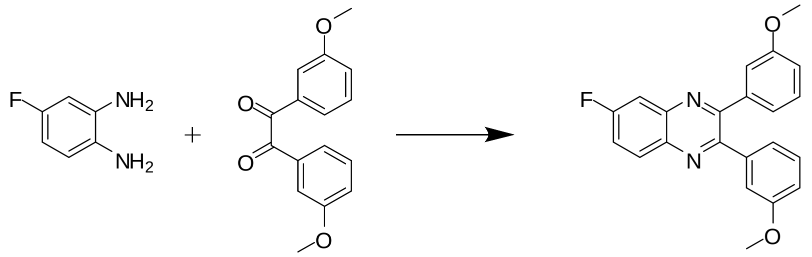

4-Fluorobenzene-1,2-diamine (25.2 mg, 0.20 mmol) and 1,2-bis(3-methoxyphenyl)ethane-1,2-dione (54 mg, 0.20 mmol) were reacted using method B to give the named compound as a white powder (64 mg, 89 %).

^{1}H NMR (500 MHz, *d$_6$*-DMSO) δ: 8.23 (ddd, *J* = 10.4, 7.4, 3.1 Hz, 1H), 7.98 – 7.90 (m, 1H), 7.81 (ddd, *J* = 10.4, 4.7, 2.3 Hz, 1H), 7.27 (td, *J* = 8.2, 2.0 Hz, 2H), 7.03 (s, 4H), 6.99 – 6.91 (m, 2H), 3.65 (s, 6H).

^{13}C NMR (126 MHz, *d$_6$*-DMSO) δ: 163.3 (Ar*C*), 161.4 (Ar*C*), 158.8 (Ar*C*), 153.7 (Ar*C*), 152.4 (Ar*C*), 141.1 (Ar*C*), 139.9 (Ar*C*), 139.8 (Ar*C*), 137.8 (Ar*C*), 131.4 (Ar*C*H), 129.2 (Ar*C*H), 122.0 (Ar*C*H), 121.9 (Ar*C*H), 120.7 (Ar*C*H), 120.5 (Ar*C*H), 115.1 (Ar*C*H), 114.8 (Ar*C*H), 114.6 (Ar*C*H), 112.4 (Ar*C*H), 112.2 (Ar*C*H), 55.1 Ar-O*C*H$_3$).

HRMS-CI (m/z): [M + H]$^+$ calculated for $C_{22}H_{18}FN_2O_2$, 361.1347; found, 361.1339.

3,3'-(6-(trifluoromethyl)quinoxaline-2,3-diyl)diphenol (96)

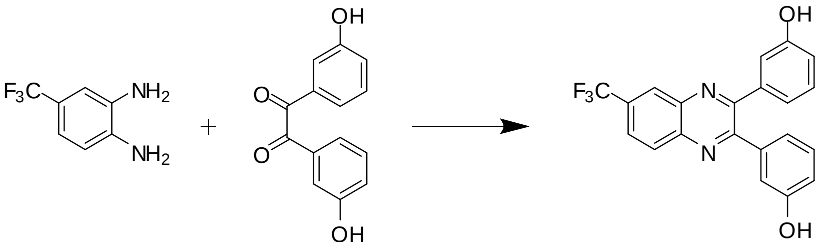

4-(Trifluoromethyl)benzene-1,2-diamine (17.6 mg, 0.10 mmol) and 1,2-bis(3-hydroxyphenyl)ethane-1,2-dione (24.2 mg, 0.10 mmol) were reacted using method B to give the named compound as a white powder (40 mg, 99 %).

^{1}H NMR (500 MHz, d_6-DMSO) δ: 9.58 (s, 2H, 2 x O*H*), 8.50 (s, 1H, Ar*H*), 8.33 (d, *J* = 8.7 Hz, 1H, Ar*H*), 8.11 (dd, *J* = 8.7, 2.0 Hz, 1H, Ar*H*), 7.14 (t, *J* = 7.9 Hz, 2H, 2 x Ar*H*), 7.02 – 6.98 (m, 2H, 2 x Ar*H*), 6.86 (d, *J* = 7.9 Hz, 2H, 2 x Ar*H*), 6.82 – 6.78 (m, 2H, 2 x Ar*H*).

^{13}C NMR (126 MHz, d_6-DMSO) δ: 157.1 (Ar*C*-OH), 155.3 (Ar*C*), 154.7(Ar*C*), 141.6(Ar*C*), 139.5 (Ar*C*), 139.5 (Ar*C*), 139.3 (Ar*C*), 130.7 (Ar*C*-CF_3 or *C*F_3), 130.6 (Ar*C*-CF_3 or *C*F_3), 129.1 (Ar*C*H), 126.7 (Ar*C*H), 126.7 (Ar*C*H), 125.5 (Ar*C*H), 120.4 (Ar*C*H), 116.4 (Ar*C*H), 116.3 (Ar*C*H), 116.2 (Ar*C*H).

HRMS-EI (m/z): [M] calculated for $C_{21}H_{13}F_3N_2O_2$, 382.0936; found, 382.0924.

2,3-bis(3-hydroxyphenyl)quinoxaline-6-carbonitrile(97)

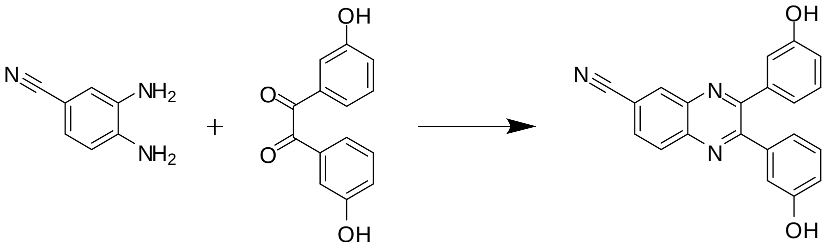

3,4-diaminobenzonitrile (13.3 mg, 0.10 mmol) and 1,2-bis(3-hydroxyphenyl)ethane-1,2-dione (24.2 mg, 0.10 mmol) were reacted using method B to give the named compound as a white powder (31 mg, 89 %).

^{1}H NMR (500 MHz, d_6-DMSO) δ: 9.59 (s, 1H, O*H*), 9.58 (s, 1H, O*H*), 8.73 (d, *J* = 1.4 Hz, 1H, Ar*H*), 8.27 (d, *J* = 8.6 Hz, 1H, Ar*H*), 8.15 (dd, *J* = 8.6, 1.8 Hz, 1H, Ar*H*), 7.17 – 7.11 (m, 2H, 2 x Ar*H*), 7.01 – 6.98 (m, 2H, 2 x Ar*H*), 6.89 – 6.82 (m, 2H, 2 x Ar*H*), 6.82 – 6.76 (m, 2H, 2 x Ar*H*).

^{13}C NMR (126 MHz, d_6-DMSO) δ: 157.1 (Ar*C*), 155.5 (Ar*C*), 154.8 (Ar*C*), 141.9 (Ar*C*), 139.5 (Ar*C*), 139.4 (Ar*C*), 134.9 (Ar*C*H), 131.1 (Ar*C*H), 130.5 (Ar*C*H), 129.1 (Ar*C*H), 120.5 (Ar*C*H), 120.4 (Ar*C*H), 118.2(Ar*C*), 116.4 (Ar*C*H), 116.4 (Ar*C*H), 116.3 (Ar*C*H), 112.4 (Ar-*C*N).

HRMS-EI (m/z): [M] calculated for $C_{21}H_{13}N_3O_2$, 339.1008; found, 339.1002.

3,3'-(6-chloroquinoxaline-2,3-diyl)diphenol (98)

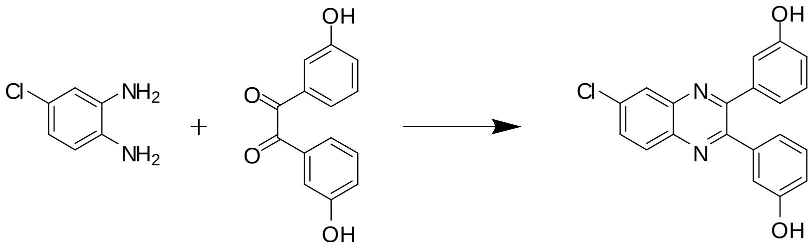

4-Chlorobenzene-1,2-diamine (14.2 mg, 0.10 mmol) and 1,2-bis(3-hydroxyphenyl)ethane-1,2-dione (24.2 mg, 0.10 mmol) were reacted using method B to give the named compound as a white powder (35 mg, 99 %).

^{1}H NMR (500 MHz, d_6-DMSO) δ: 9.54 (d, *J* = 6.6 Hz, 2H, O*H*), 8.20 (d, *J* = 2.2 Hz, 1H), 8.14 (d, *J* = 9.0 Hz, 1H), 7.88 (dd, *J* = 9.0, 2.2 Hz, 1H), 7.13 (td, *J* = 7.9, 1.9 Hz, 2H), 6.98 – 6.95 (m, 2H), 6.82 (ddd, *J* = 7.9, 4.9, 3.7 Hz, 2H), 6.80 – 6.76 (m, 2H).

^{13}C NMR (126 MHz, d_6-DMSO) δ: 157.0 (Ar*C*-OH), 154.0 (Ar*C*), 153.4 (Ar*C*), 140.7 (Ar*C*), 139.7 (Ar*C*), 139.7 (Ar*C*), 139.0 (Ar*C*), 134.5 (Ar*C*-Cl), 130.9 (Ar*C*H), 130.6 (Ar*C*H), 129.0 (Ar*C*H), 127.5 (Ar*C*H), 120.5 (Ar*C*H), 120.4 (Ar*C*H), 116.37 (Ar*C*H), 116.36 (Ar*C*H), 116.1 (Ar*C*H), 116.0 (Ar*C*H).

HRMS-EI (m/z): [M] calculated for $C_{20}H_{13}ClN_2O_2$, 348.0666; found, 348.0666.

3,3'-(6-fluoroquinoxaline-2,3-diyl)diphenol (99)

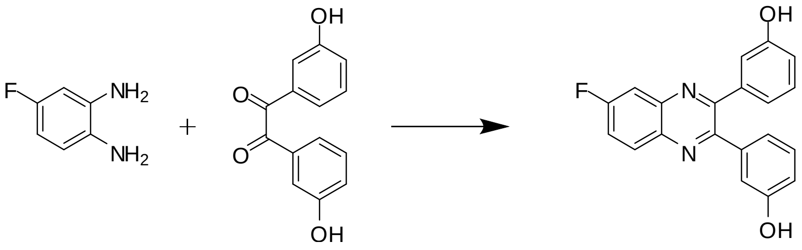

4-Fluorobenzene-1,2-diamine (12.6 mg, 0.10 mmol) and 1,2-bis(3-hydroxyphenyl)ethane-1,2-dione (24.2 mg, 0.10 mmol) were reacted using method B to give the named compound as a white powder (27 mg, 81 %).

^{1}H NMR (500 MHz, *d$_6$*-DMSO) δ: 9.54 (s, 2H, 2 x O*H*), 8.20 (dd, *J* = 9.2, 5.9 Hz, 1H, Ar*H*), 7.90 (dd, *J* = 9.2, 2.8 Hz, 1H, Ar*H*), 7.79 (td, *J* = 8.9, 2.8 Hz, 1H, Ar*H*), 7.12 (td, *J* = 8.0, 1.2 Hz, 2H, 2 x Ar*H*), 7.00 – 6.93 (m, 2H, 2 x Ar*H*), 6.87 – 6.81 (m, 2H, 2 x Ar*H*), 6.81 – 6.74 (m, 2H, 2 Ar*H*).

^{13}C NMR (126 MHz, *d$_6$*-DMSO) δ: 157.0 (Ar*C*), 153.8 (Ar*C*), 152.5 (Ar*C*), 141.1 (Ar*C*), 139.9 (Ar*C*), 139.8 (Ar*C*), 137.7 (Ar*C*), 131.4 (Ar*C*H), 131.3 (Ar*C*H), 130.8 (Ar*C*), 129.0 (Ar*C*H), 120.4 (Ar*C*H), 120.4 (Ar*C*H), 116.4 (Ar*C*H), 116.3 (Ar*C*H), 116.0 (Ar*C*H), 115.9 (Ar*C*H), 114.9 (Ar*C*H), 112.3 (Ar*C*H), 112.1 (Ar*C*H).

HRMS-EI (m/z): [M] calculated for $C_{20}H_{13}FN_2O_2$, 332.09611; found, 332.097001.

Bibliography

Bibliography

1. Hopkins, A. L.; Groom, C. R., The druggable genome. *Nature Reviews Drug Discovery* **2002,** *1* (9), 727-730.

2. Drews, J., Genomic sciences and the medicine of tomorrow. *Nature biotechnology* **1996,** *14* (11), 1516-1518.

3. Drews, J.; Ryser, S., Drug Development: The role of innovation in drug development. *Nature biotechnology* **1997,** *15* (13), 1318-1319.

4. Imming, P.; Sinning, C.; Meyer, A., Drugs, their targets and the nature and number of drug targets. *Nature Reviews Drug Discovery* **2006,** *5* (10), 821-834.

5. Overington, J. P.; Al-Lazikani, B.; Hopkins, A. L., How many drug targets are there? *Nature Reviews Drug Discovery* **2006,** *5* (12), 993-996.

6. Makley, L. N.; Gestwicki, J. E., Expanding the Number of 'Druggable'Targets: Non-Enzymes and Protein–Protein Interactions. *Chemical Biology & Drug Design* **2013,** *81* (1), 22-32.

7. Druker, B. J.; Tamura, S.; Buchdunger, E.; Ohno, S.; Segal, G. M.; Fanning, S.; Zimmermann, J. r.; Lydon, N. B., Effects of a selective inhibitor of the Abl tyrosine kinase on the growth of Bcr-Abl positive cells. *Nature Medicine* **1996,** *2* (5), 561-566.

8. Lipinski, C. A.; Lombardo, F.; Dominy, B. W.; Feeney, P. J., Experimental and computational approaches to estimate solubility and permeability in drug discovery and development settings. *Advanced Drug Delivery Reviews* **1997,** *23* (1), 3-25.

9. Veber, D. F.; Johnson, S. R.; Cheng, H.-Y.; Smith, B. R.; Ward, K. W.; Kopple, K. D., Molecular properties that influence the oral bioavailability of drug candidates. *Journal of Medicinal Chemistry* **2002,** *45* (12), 2615-2623.

10. Walters, W. P.; Green, J.; Weiss, J. R.; Murcko, M. A., What do medicinal chemists actually make? A 50-year retrospective. *Journal of Medicinal Chemistry* **2011,** *54* (19), 6405-6416.

11. Frye, S. V., The art of the chemical probe. *Nature Chemical Biology* **2010,** *6* (3), 159-161.

12. Gosling, J. P., A decade of development in immunoassay methodology. *Clinical Chemistry* **1990,** *36* (8), 1408-27.

13. Jelesarov, I.; Bosshard, H. R., Isothermal titration calorimetry and differential scanning calorimetry as complementary tools to investigate the energetics of biomolecular recognition. *Journal of Molecular Recognition* **1999,** *12* (1), 3-18.

14. Quinteiro, G. F.; Fernandez-Rossier, J.; Piermarocchi, C., Long-range spin-qubit interaction mediated by microcavity polaritons. *Physical Review Letters* **2006,** *97* (9), 097401.

15. Vanwetswinkel, S.; Heetebrij, R. J.; van Duynhoven, J.; Hollander, J. G.; Filippov, D. V.; Hajduk, P. J.; Siegal, G., TINS, target immobilized NMR screening: an efficient and sensitive method for ligand discovery. *Chemistry & Biology* **2005,** *12* (2), 207-216.

16. Nordin, H.; Jungnelius, M.; Karlsson, R.; Karlsson, O. P., Kinetic studies of small molecule interactions with protein kinases using biosensor technology. *Analytical Biochemistry* **2005,** *340* (2), 359-368.

17. Stenlund, P.; Frostell-Karlsson, Å.; Karlsson, O. P., Studies of small molecule interactions with protein phosphatases using biosensor technology. *Analytical Biochemistry* **2006,** *353* (2), 217-225.

18. Navratilova, I.; Besnard, J.; Hopkins, A. L., Screening for GPCR ligands using surface plasmon resonance. *ACS Medicinal Chemistry Letters* **2011,** *2* (7), 549-554.

19. Perspicace, S.; Banner, D.; Benz, J.; Müller, F.; Schlatter, D.; Huber, W., Fragment-Based Screening Using Surface Plasmon Resonance Technology. *Journal of Biomolecular Screening* **2009,** *14* (4), 337-349.

20. Jönsson, U.; Fägerstam, L.; Ivarsson, B.; Johnsson, B.; Karlsson, R.; Lundh, K.; Löfås, S.; Persson, B.; Roos, H.; Rönnberg, I., Real-time biospecific interaction analysis using surface plasmon resonance and a sensor chip technology. *Biotechniques* **1991,** *11* (5), 620-627.

21. Stenberg, E.; Persson, B.; Roos, H.; Urbaniczky, C., Quantitative determination of surface concentration of protein with surface plasmon resonance using radiolabeled proteins. *Journal of Colloid and Interface Science* **1991,** *143* (2), 513-526.

22. Navratilova, I.; Papalia, G. A.; Rich, R. L.; Bedinger, D.; Brophy, S.; Condon, B.; Deng, T.; Emerick, A. W.; Guan, H.-W.; Hayden, T., Thermodynamic benchmark study using Biacore technology. *Analytical Biochemistry* **2007,** *364* (1), 67-77.

23. Karlsson, R.; Roos, H.; Fägerstam, L.; Persson, B., Kinetic and concentration analysis using BIA technology. *Methods* **1994,** *6* (2), 99-110.

24. GE-Healthcare, *Biacore Sensor Surface Handbook*. BR-1005-71 Edition AB ed.

25. O'Shannessy, D. J.; Brigham-Burke, M.; Peck, K., Immobilization chemistries suitable for use in the BIAcore surface plasmon resonance detector. *Analytical Biochemistry* **1992,** *205* (1), 132-136.

26. GE Healthcare Life Sciences, Biacore T200, data file 20-9794-15AB, Ed.2013

27. Willett, P.; Barnard, J. M.; Downs, G. M., Chemical Similarity Searching. *Journal of Chemical Information and Computer Sciences* **1998,** *38* (6), 983-996.

28. Ganellin, C.; Lindberg, P.; Mitscher, L., Glossary of terms used in medicinal chemistry. **1998**.

29. Loupy, A., *Microwaves in organic synthesis*. Wiley-VCH: 2002.

30. Hayes, B. L., *Microwave synthesis: chemistry at the speed of light*. CEM publising: 2002.

31. Zhou, P.; Huang, J.; Tian, F., Specific Noncovalent Interactions at Protein-Ligand Interface: Implications for Rational Drug Design. *Current Medicinal Chemistry* **2012,** *19* (2), 226-238.

32. Patrick, G. L., *An introduction to medicinal chemistry*. Oxford University Press: 2013.

33. Bissantz, C.; Kuhn, B.; Stahl, M., A medicinal chemist’s guide to molecular interactions. *Journal of Medicinal Chemistry* **2010,** *53* (14), 5061-5084.

34. Cowan-Jacob, S. W.; Fendrich, G.; Floersheimer, A.; Furet, P.; Liebetanz, J.; Rummel, G.; Rheinberger, P.; Centeleghe, M.; Fabbro, D.; Manley, P. W., Structural biology contributions to the discovery of drugs to treat chronic myelogenous leukaemia. *Acta Crystallographica Section D* **2007,** *63* (1), 80-93.

35. Böhm, H.-J.; Klebe, G., What Can We Learn from Molecular Recognition in Protein–Ligand Complexes for the Design of New Drugs? *Angewandte Chemie International Edition in English* **1996,** *35* (22), 2588-2614.

36. Gallivan, J. P.; Dougherty, D. A., A Computational Study of Cation−π Interactions vs Salt Bridges in Aqueous Media: Implications for Protein Engineering. *Journal of the American Chemical Society* **2000,** *122* (5), 870-874.

37. Kitchen, D.; Decornez, H.; Furr, J.; Bajorath, J., Docking and scoring in virtual screening for drug discovery: methods and applications. *Nature Reviews Drug discovery* **2004,** *3* (11), 935-49.

38. GOLD user guide & tutorials - v5.1.0. centre, T. C. c. d., Ed. 2013.

39. Liao, C.; Sitzmann, M.; Pugliese, A.; Nicklaus, M. C., Software and resources for computational medicinal chemistry. *Future Medicinal Chemistry* **2011,** *3* (8), 1057-1085.

40. Labute, P., An integrated application in MOE for the visualization and analysis of protein active sites with molecular surfaces, contact statistics and electrostatic maps. *Journal of Chemical Computing Group [Online]* **2006**.

41. Labute, P.; Santavy, M., Locating binding sites in protein structures. *Journal of Chemical Computing Group* **2007**.

42. Clark, A. M.; Labute, P., 2D depiction of protein-ligand complexes. *Journal of Chemical Information and Modeling* **2007,** *47* (5), 1933-1944.

43. Lucas, K. A.; Pitari, G. M.; Kazerounian, S.; Ruiz-Stewart, I.; Park, J.; Schulz, S.; Chepenik, K. P.; Waldman, S. A., Guanylyl Cyclases and Signaling by Cyclic GMP. *Pharmacological Reviews* **2000,** *52* (3), 375-414.

44. Senter, P. D.; Eckstein, F.; Mülsch, A.; Böhme, E., The stereochemical course of the reaction catalyzed by soluble bovine lung guanylate cyclase. *Journal of Biological Chemistry* **1983,** *258* (11), 6741-6745.

45. Potter, L. R.; Yoder, A. R.; Flora, D. R.; Antos, L. K.; Dickey, D. M., Natriuretic peptides: their structures, receptors, physiologic functions and therapeutic applications. In *cGMP: Generators, Effectors and Therapeutic Implications*, Springer: 2009; pp 341-366.

46. Derbyshire, E. R.; Marletta, M. A., Structure and regulation of soluble guanylate cyclase. *Annual Review of Biochemistry* **2012,** *81*, 533-559.

47. Hofmann, F.; Ammendola, A.; Schlossmann, J., Rising behind NO: cGMP-dependent protein kinases. *Journal of Cell Science* **2000,** *113* (10), 1671-1676.

48. Francis, S. H.; Busch, J. L.; Corbin, J. D., cGMP-dependent protein kinases and cGMP phosphodiesterases in nitric oxide and cGMP action. *Pharmacological Reviews* **2010,** *62* (3), 525-563.

49. Hsu, Y.-T.; Molday, R. S., Modulation of the cGMP-gated channel of rod photoreceptor cells by calmodulin. *Letters to Nature* **1993,** *361*, 76-79.

50. Hamet, P.; Tremblay, J.; Pang, S. C.; Garcia, R.; Thibault, G.; Gutkowska, J.; Cantin, M.; Genest, J., Effect of native and synthetic atrial natriuretic factor on cyclic GMP. *Biochemical and Biophysical Research Communications* **1984,** *123* (2), 515-527.

51. Chien, K., *Molecular Basis of Cardiovascular Disease (Second Edition)*. **2004**.

52. Martel, G.; Hamet, P.; Tremblay, J., Central role of guanylyl cyclase in natriuretic peptide signaling in hypertension and metabolic syndrome. *Molecular and Celular Biochemistry.* **2010,** *334* (1-2), 53-65.

53. Chauhan, S. D.; Hobbs, A. J.; Ahluwalia, A., C-type natriuretic peptide: new candidate for endothelium-derived hyperpolarising factor. *International Journal of Biochemistry & Cell Bioogy.* **2004,** *36* (10), 1878-1881.

54. Rose, R. A.; Giles, W. R., Natriuretic peptide C receptor signalling in the heart and vasculature. *The Journal of Physiology* **2008,** *586* (2), 353-366.

55. Ahluwalia, A.; Hobbs, A. J., Endothelium-derived C-type natriuretic peptide: more than just a hyperpolarizing factor. *Trends in Pharmacological Sciences* **2005,** *26* (3), 162-167.

56. Villar, I. C.; Panayiotou, C. M.; Sheraz, A.; Madhani, M.; Scotland, R. S.; Nobles, M.; Kemp-Harper, B.; Ahluwalia, A.; Hobbs, A. J., Definitive role for natriuretic peptide receptor-C in mediating the vasorelaxant activity of C-type natriuretic peptide and endothelium-derived hyperpolarising factor. *Cardiovascular Research* **2007,** *74* (3), 515-525.

57. Iyer, L. M.; Anantharaman, V.; Aravind, L., Ancient conserved domains shared by animal soluble guanylyl cyclases and bacterial signaling proteins. *BMC genomics* **2003,** *4* (1), 5.

58. Garthwaite, J.; Charles, S. L.; Chess-Williams, R., Endothelium-derived relaxing factor release on activation of NMDA receptors suggests role as intercellular messenger in the brain. *Nature* **1988,** *336* (6197), 385-388.

59. Derbyshire, E.; Marletta, M., Biochemistry of soluble guanylate cyclase. *Handbook of Experimental Pharmacoogyl* **2009,** *191*, 17 - 31.

60. Evgenov, O. V.; Pacher, P.; Schmidt, P. M.; Hasko, G.; Schmidt, H. H. H. W.; Stasch, J.-P., NO-independent stimulators and activators of soluble guanylate cyclase: discovery and therapeutic potential. *Nature Reviews Drug Discovery* **2006,** *5* (9), 755-768.

61. Moncada, S.; Higgs, E. A., Nitric oxide and the vascular endothelium. In *Vascular Endothelium I*, Moncada, S.; Higgs, A., Eds. Springer-Verlag Berlin, Heidelberger Platz 3, D-14197 Berlin, Germany: **2006**; Vol. 176, pp 213-254.

62. Madhani, M.; Okorie, M.; Hobbs, A.; MacAllister, R., Reciprocal regulation of human soluble and particulate guanylate cyclases in vivo. *British Journal of Pharmacology* **2006,** *149* (6), 797-801.

63. Kemp-Harper, B.; Schmidt, H. H. H. W., cGMP in the Vasculature. In *Handbook of Experimental Pharmacology*, Schmidt, H.; Hofmann, F.; Stasch, J. P., Eds. Springer-Verlag Berlin, Heidelberger Platz 3, D-14197 Berlin, Germany: **2009**; Vol. 191, pp 447-467.

64. Garthwaite, J.; Bellamy, T. C.; Wood, J.; Goodwin, D. A., Rapid desensitization of the nitric oxide receptor, soluble guanylyl cyclase, underlies diversity of cellular cGMP responses. *Proceedings of the National Academy of Sciences of the United States of America* **2000,** *97* (6), 2928-2933.

65. Koesling, D.; Neitz, A.; Mittmann, T.; Mergia, E., NO signalling in synaptic transmission. *BMC Pharmacology* **2011,** *11* (Suppl 1), O21.

66. Gómez-Pinedo, U.; Rodrigo, R.; Cauli, O.; Herraiz, S.; Garcia-Verdugo, J.-M.; Pellicer, B.; Pellicer, A.; Felipo, V., cGMP modulates stem cells differentiation to neurons in brain *in vivo*. *Neuroscience* **2010,** *165* (4), 1275-1283.

67. Zhang, L.; Dawson, V. L.; Dawson, T. M., Role of nitric oxide in Parkinson's disease. *Pharmacology & Therapeutics* **2006,** *109* (1), 33-41.

68. Tseng, K. Y.; Caballero, A.; Dec, A.; Cass, D. K.; Simak, N.; Sunu, E.; Park, M. J.; Blume, S. R.; Sammut, S.; Park, D. J., Inhibition of striatal soluble guanylyl cyclase-cGMP signaling reverses basal ganglia dysfunction and akinesia in experimental parkinsonism. *PloS one* **2011,** *6* (11), e27187.

69. Brichta, L.; Greengard, P.; Flajolet, M., Advances in the pharmacological treatment of Parkinson's disease: targeting neurotransmitter systems. *Trends in Neurosciences* **2013,** *36* (9), 543-554.

70. Cary, S. P. L.; Winger, J. A.; Derbyshire, E. R.; Marletta, M. A., Nitric oxide signaling: no longer simply on or off. *Trends in Biochemical Sciences* **2006,** *31* (4), 231-239.

71. Allerston, C. K.; von Delft, F.; Gileadi, O., Crystal structures of the catalytic domain of human soluble guanylate cyclase. *PloS one* **2013,** *8* (3), e57644.

72. Friebe, A.; Wedel, B.; Harteneck, C.; Foerster, J.; Schultz, G.; Koesling, D., Functions of conserved cysteines of soluble guanylyl cyclase. *Biochemistry* **1997,** *36* (6), 1194-1198.

73. Babcock, G. T.; Schelvis, J. P. M.; Zhao, Y.; Marletta, M. A., Resonance Raman characterization of the heme domain of soluble guanylate cyclase. *Biochemistry* **1998,** *37* (46), 16289-16297.

74. Marletta, M. A.; Stone, J. R., Synergistic activation of soluble guanylate cyclase by YC-1 and carbon monoxide: implications for the role of cleavage of the iron-histidine bond during activation by nitric oxide. *Chemistry & Biology* **1998,** *5* (5), 255-261.

75. Underbakke, E. S.; Iavarone, A. T.; Marletta, M. A., Higher-order interactions bridge the nitric oxide receptor and catalytic domains of soluble guanylate cyclase. *Proceedings of the National Academy of Sciences* **2013,** *110* (17), 6777-6782.

76. Winger, J. A.; Derbyshire, E. R.; Lamers, M. H.; Marletta, M. A.; Kuriyan, J., The crystal structure of the catalytic domain of a eukaryotic guanylate cyclase. *BMC Structural Biology* **2008,** *8*, 42.

77. Zhang, G.; Liu, Y.; Qin, J.; Vo, B.; Tang, W. J.; Ruoho, A. E.; Hurley, J. H., Characterization and crystallization of a minimal catalytic core domain from mammalian type II adenylyl cyclase. *Protein science* **1997,** *6* (4), 903-908.

78. Beste, K. Y.; Burhenne, H.; Kaever, V.; Stasch, J.-P.; Seifert, R., Nucleotidyl cyclase activity of soluble guanylyl cyclase α1β1. *Biochemistry* **2011,** *51* (1), 194-204.

79. Ruiz-Stewart, I.; Tiyyagura, S.; Lin, J.; Kazerounian, S.; Pitari, G.; Schulz, S.; Martin, E.; Murad, F.; Waldman, S., Guanylyl cyclase is an ATP sensor coupling nitric oxide signaling to cell metabolism. *Proceedings of the National Academy of Sciences* **2004,** *101* (1), 37-42.

80. Martin, F.; Baskaran, P.; Ma, X.; Dunten, P. W.; Schaefer, M.; Stasch, J.-P.; Beuve, A.; van den Akker, F., Structure of cinaciguat (BAY 58–2667) bound to Nostoc H-NOX domain reveals insights into heme-mimetic activation of the soluble guanylyl cyclase. *Journal of Biological Chemistry* **2010,** *285* (29), 22651-22657.

81. Follmann, M.; Griebenow, N.; Hahn, M. G.; Hartung, I.; Mais, F. J.; Mittendorf, J.; Schäfer, M.; Schirok, H.; Stasch, J. P.; Stoll, F., The chemistry and biology of soluble guanylate cyclase stimulators and activators. *Angewandte Chemie International Edition* **2013,** *52* (36), 9442-9462.

82. Wu, C. C.; Ko, F. N.; Kuo, S. C.; Lee, F. Y.; Teng, C. M., Yc-1 Inhibited Human Platelet-Aggregation through NO-Independent Activation of Soluble Guanylate-Cyclase. *British Journal of Pharmacology* **1995,** *116* (3), 1973-1978.

83. Mulsch, A.; Bauersachs, J.; Schafer, A.; Stasch, J. P.; Kast, R.; Busse, R., Effect of YC-1, an NO-independent, superoxide-sensitive stimulator of soluble guanylyl cyclase, on smooth muscle responsiveness to nitrovasodilators. *British Journal of Pharmacology* **1997,** *120* (4), 681-689.

84. Koesling, D.; Friebe, A., Mechanism of YC-1-induced activation of soluble guanylyl cyclase. *Molecular Pharmacology* **1998,** *53* (1), 123-127.

85. Hoenicka, M.; Becker, E. M.; Apeler, H.; Sirichoke, T.; Schroder, H.; Gerzer, R.; Stasch, J. P., Purified soluble guanylyl cyclase expressed in a baculovirus/Sf9 system: stimulation by YC-1, nitric oxide, and carbon monoxide. *Journal of Molecular Medicine-Jmm* **1999,** *77* (1), 14-23.

86. Schmidt, H. H. H. W.; Galle, J.; Zabel, U.; Hubner, U.; Hatzelmann, A.; Wagner, B.; Wanner, C., Effects of the soluble guanylyl cyclase activator, YC-1, on vascular tone, cyclic GMP levels and phosphodiesterase activity. *British Journal of Pharmacology* **1999,** *127* (1), 195-203.

87. Sheng-Chung, T.; Jin-Cherng, L.; Che-Ming, T.; Sheng-Chu, K., Synthesis and antiplatelet activity of 1-substituted benzyl-2-(5-hydroxymethyl-2-furyl)benzimidazoles. *Chinese Pharmaceutical Journal (Taipei)* **2000,** *52* (2), 79-90.

88. Stasch, J. P.; Becker, E. M.; Alonso-Alija, C.; Apeler, H.; Dembowsky, K.; Feurer, A.; Gerzer, R.; Minuth, T.; Perzborn, E.; Pleiss, U.; Schroder, H.; Schroeder, W.; Stahl, E.; Steinke, W.; Straub, A.; Schramm, M., NO-independent regulatory site on soluble guanylate cyclase. *Nature* **2001,** *410* (6825), 212-215.

89. Straub, A.; Stasch, J. P.; Alonso-Alija, C.; Benet-Buchholz, J.; Ducke, B.; Feurer, A.; Furstner, C., NO-independent stimulators of soluble guanylate cyclase. *Bioorganic & Medicinal Chemistry Letters* **2001,** *11* (6), 781-784.

90. Behr, J., New clinical results with sGC stimulators. *BMC Pharmacology* **2011,** *11* (Suppl 1), O2.

91. Martin, F.; Baskaran, P.; Ma, X.; Dunten, P. W.; Schaefer, M.; Stasch, J.-P.; Beuve, A.; van den Akker, F., Structure of Cinaciguat (BAY 58-2667) Bound to Nostoc H-NOX

Domain Reveals Insights into Heme-mimetic Activation of the Soluble Guanylyl Cyclase. *Journal of Biological Chemistry* ***2010**, 285* (29), 22651-22657.

92. Gheorghiade, M.; Greene, S. J.; Filippatos, G.; Erdmann, E.; Ferrari, R.; Levy, P. D.; Maggioni, A.; Nowack, C.; Mebazaa, A.; Investigators, o. b. o. t. C.; Coordinators, Cinaciguat, a soluble guanylate cyclase activator: results from the randomized, controlled, phase IIb COMPOSE programme in acute heart failure syndromes. *European Journal of Heart Failure* **2012,** *14* (9), 1056-1066.

93. Babcock, G. T.; Zhao, Y. D.; Brandish, P. E.; DiValentin, M.; Schelvis, J. P. M.; Marletta, M. A., Inhibition of soluble guanylate cyclase by ODQ. *Biochemistry* **2000,** *39* (35), 10848-10854.

94. Zhao, Y. D.; Brandish, P. E.; DiValentin, M.; Schelvis, J. P. M.; Babcock, G. T.; Marletta, M. A., Inhibition of soluble guanylate cyclase by ODQ. *Biochemistry* **2000,** *39* (35), 10848-10854.

95. Ahluwalia, A.; Hobbs, A., Endothelium-derived C-type natriuretic peptide: more than just a hyperpolarizing factor. *Trends in Pharmacological Sciences* **2005,** *26*, 162 - 167.

96. Quinteiro, F. M.; Gane, P.; Rebstock, A.-S.; Worthington, R.; Simone, M.; Djordevic, S.; Hobbs, A.; Selwood, D., Design and development of novel non-peptide agonists at NPR-C. *BMC Pharmacology* **2011,** *11* (Suppl 1), P54.

97. He, X. L.; Dukkipati, A.; Garcia, K. C., Structural determinants of natriuretic peptide receptor specificity and degeneracy. *Journal of Molecular Biology* **2006,** *361* (4), 698-714.

98. Stegemann, S.; Leveiller, F.; Franchi, D.; de Jong, H.; Linden, H., When poor solubility becomes an issue: From early stage to proof of concept. *European Journal of Pharmaceutical Sciences* **2007,** *31* (5), 249-261.

99. Jung, S.-Y.; Seo, Y.-G.; Kim, G. K.; Woo, J. S.; Yong, C. S.; Choi, H.-G., Comparison of the solubility and pharmacokinetics of sildenafil salts. *Archives of Pharmacal research* **2011,** *34* (3), 451-454.

100. Garthwaite, G.; Goodwin, D. A.; Neale, S.; Riddall, D.; Garthwaite, J., Soluble Guanylyl Cyclase Activator YC-1 Protects White Matter Axons from Nitric Oxide Toxicity and

Metabolic Stress, Probably through Na+ Channel Inhibition. *Molecular Pharmacology* **2002,** *61* (1), 97-104.

101. Selwood, D. L.; Clutterbuck, L. A.; Posada, C. G.; Visintin, C.; Riddall, D. R.; Lancaster, B.; Gane, P. J.; Garthwaite, J., Oxadiazolylindazole Sodium Channel Modulators are Neuroprotective toward Hippocampal Neurones. *Journal of Medicinal Chemistry* **2009,** *52* (9), 2694-2707.

102. Zorn, J. A.; Wells, J. A., Turning enzymes ON with small molecules. *Nature Chemical Biology* **2010,** *6* (3), 179-188.

103. Griffiths, C.; Wykes, V.; Bellamy, T. C.; Garthwaite, J., A New and Simple Method for Delivering Clamped Nitric Oxide Concentrations in the Physiological Range: Application to Activation of Guanylyl Cyclase-Coupled Nitric Oxide Receptors. *Molecular Pharmacology* **2003,** *64* (6), 1349-1356.

104. Sigel, H.; Griesser, R., Nucleoside 5′-triphosphates: self-association, acid–base, and metal ion-binding properties in solution. *Chemical Society Reviews* **2005,** *34* (10), 875-900.

105. Lamothe, M.; Chang, F.-J.; Balashova, N.; Shirokov, R.; Beuve, A., Functional Characterization of Nitric Oxide and YC-1 Activation of Soluble Guanylyl Cyclase: Structural Implication for the YC-1 Binding Site? *Biochemistry* **2004,** *43* (11), 3039-3048.

106. Hobbs, A. J.; Higgs, A.; Moncada, S., Inhibition of nitric oxide synthase as a potential therapeutic target. *Annual Review of Pharmacology and Toxicology* **1999,** *39* (1), 191-220.

107. Kumagai, Y.; Midorikawa, K.; Nakai, Y.; Yoshikawa, T.; Kushida, K.; Homma-Takeda, S.; Shimojo, N., Inhibition of nitric oxide formation and superoxide generation during reduction of LY83583 by neuronal nitric oxide synthase. *European Journal of Pharmacology* **1998,** *360* (2), 213-218.

108. Mittal, C. K.; Murad, F., Activation of guanylate cyclase by superoxide dismutase and hydroxyl radical: a physiological regulator of guanosine 3', 5'-monophosphate formation. *Proceedings of the National Academy of Sciences* **1977,** *74* (10), 4360-4364.

109. Brune, B.; Schmidt, K.-U.; Ullrich, V., Activation of soluble guanylate cyclase by carbon monoxide and inhibition by superoxide anion. *European Journal of Biochemistry* **1990,** *192* (3), 683-688.

110. Garthwaite, J.; Southam, E.; Boulton, C. L.; Nielsen, E. B.; Schmidt, K.; Mayer, B., Potent and selective inhibition of nitric oxide-sensitive guanylyl cyclase by 1H-[1,2,4]oxadiazolo[4,3-a]quinoxalin-1-one. *Molecular Pharmacology* **1995,** *48* (2), 184-188.

111. Spyridonidou, K.; Fousteris, M.; Antonia, M.; Chatzianastasiou, A.; Papapetropoulos, A.; Nikolaropoulos, S., Tricyclic indole and dihydroindole derivatives as new inhibitors of soluble guanylate cyclase. *Bioorganic & Medicinal Chemistry Letters* **2009,** *19* (16), 4810-4813.

112. Schrammel, A.; Behrends, S.; Schmidt, K.; Koesling, D.; Mayer, B., Characterization of 1H-[1,2,4]oxadiazolo[4,3-a]quinoxalin-1-one as a heme-site inhibitor of nitric oxide-sensitive guanylyl cyclase. *Molecular Pharmacology* **1996,** *50* (1), 1-5.

113. Haunsø, A.; Simpson, J.; Antoni, F. A., Small Ligands Modulating the Activity of Mammalian Adenylyl Cyclases: A Novel Mode of Inhibition by Calmidazolium. *Molecular Pharmacology* **2003,** *63* (3), 624-631.

114. James, L. R.; Griffiths, C. H.; Garthwaite, J.; Bellamy, T. C., Inhibition of nitric oxide-activated guanylyl cyclase by calmodulin antagonists. *British Journal of Pharmacology* **2009,** *158* (6), 1454-1464.

115. Brandwein, H. J.; Lewicki, J. A.; Waldman, S. A.; Murad, F., Effect of Gtp Analogs on Purified Soluble Guanylate-Cyclase. *Journal of Biological Chemistry* **1982,** *257* (3), 1309-1311.

116. Chang, F.-J.; Lemme, S.; Sun, Q.; Sunahara, R. K.; Beuve, A., Nitric Oxide-dependent Allosteric Inhibitory Role of a Second Nucleotide Binding Site in Soluble Guanylyl Cyclase. *Journal of Biological Chemistry* **2005,** *280* (12), 11513-11519.

117. Balkan, S.; Ozben, T.; Balkan, E.; Oguz, N.; Serteser, M.; Gumuslu, S., Effects of Lamotrigine on brain nitrite and cGMP levels during focal cerebral ischemia in rats. *Acta Neurologica Scandinavica* **1997,** *95* (3), 140-146.

118. Wood, P.; Marks, V., Direct measurement of cGMP in blood plasma and urine by radioimmunoassay. *Annals of Clinical Biochemistry* **1978,** *15* (1), 25.

119. Carter, S. D.; Cheeseman, G. W. H., Quinoxalines and related compounds--X : The formation of indolo[2,3-b]quinoxalines and 2-p-aminophenyl-3-anilinoquinoxalines from 2-anilinoquinoxalines. *Tetrahedron* **1978,** *34* (7), 981-988.

120. Haworth, R. D.; Robinson, S., 157. Synthetic antimalarials. Part XXVII. Some derivatives of phthalazine, quinoxaline, and isoquinoline. *Journal of the Chemical Society (Resumed)* **1948**, 777-782.

121. Deng, J.; Feng, E.; Ma, S.; Zhang, Y.; Liu, X.; Li, H.; Huang, H.; Zhu, J.; Zhu, W.; Shen, X., Design and synthesis of small molecule RhoA inhibitors: a new promising therapy for cardiovascular diseases? *Journal of Medicinal Chemistry* **2011,** *54* (13), 4508-4522.

122. Ammar, Y. A.; Al-Sehemi, A. G.; El-Sharief, A. M. S.; El-Gaby, M. S. A., Chemistry of 2,3-Dichloroquinoxalines. *Phosphorus, Sulfur, and Silicon and the Related Elements* **2009,** *184* (3), 660-698.

123. Wu, W.-L.; Burnett, D. A.; Spring, R.; Greenlee, W. J.; Smith, M.; Favreau, L.; Fawzi, A.; Zhang, H.; Lachowicz, J. E., Dopamine D1/D5 receptor antagonists with improved pharmacokinetics: design, synthesis, and biological evaluation of phenol bioisosteric analogues of benzazepine D1/D5 antagonists. *Journal of Medicinal Chemistry* **2005,** *48* (3), 680-693.

124. Meanwell, N. A., Synopsis of Some Recent Tactical Application of Bioisosteres in Drug Design. *Journal of Medicinal Chemistry* **2011,** *54* (8), 2529-2591.

125. Romer, D. R., Synthesis of 2,3-dichloroquinoxalines via Vilsmeier reagent chlorination. John Wiley & Sons, Inc.: **2009**; Vol. 46, pp 317-319.

126. Hart, M. E.; Suchland, K. L.; Miyakawa, M.; Bunzow, J. R.; Grandy, D. K.; Scanlan, T. S., Trace Amine-Associated Receptor Agonists: Synthesis and Evaluation of Thyronamines and Related Analogues. *Journal of Medicinal Chemistry* **2006,** *49* (3), 1101-1112.

127. Nystrom, R. F.; Brown, W. G., Reduction of Organic Compounds by Lithium Aluminum Hydride. III. Halides, Quinones, Miscellaneous Nitrogen Compounds1. *Journal of the American Chemical Society* **1948,** *70* (11), 3738-3740.

128. Faul, M. M.; Thiel, O. R., Tin(II) Chloride. In *Encyclopedia of Reagents for Organic Synthesis*, John Wiley & Sons, Ltd: **2001**.

129. Bellamy, F. D.; Ou, K., Selective reduction of aromatic nitro compounds with stannous chloride in non acidic and non aqueous medium. *Tetrahedron Letters.* **1984,** *25* (8), 839-842.

130. Hanaya, K.; Muramatsu, T.; Kudo, H.; Chow, Y. L., Reduction of aromatic nitro-compounds to amines with sodium borohydride–copper (II) acetylacetonate. *Journal of the Chemical Society, Perkin Transactions 1* **1979**, 2409-2410.

131. Smith, G. F., 1 Designing Drugs to Avoid Toxicity. *Progress in Medicinal Chemistry* **2011,** *50*, 1.

132. Purohit, V.; Basu, A. K., Mutagenicity of Nitroaromatic Compounds. *Chemical Research in Toxicology* **2000,** *13* (8), 673-692.

133. Hagmann, W. K., The Many Roles for Fluorine in Medicinal Chemistry. *Journal of Medicinal Chemistry* **2008,** *51* (15), 4359-4369.

134. Guram, A. S.; Buchwald, S. L., Palladium-Catalyzed Aromatic Aminations with in situ Generated Aminostannanes. *Journal of the American Chemical Society* **1994,** *116* (17), 7901-7902.

135. Paul, F.; Patt, J.; Hartwig, J. F., Palladium-catalyzed formation of carbon-nitrogen bonds. Reaction intermediates and catalyst improvements in the hetero cross-coupling of aryl halides and tin amides. *Journal of the American Chemical Society* **1994,** *116* (13), 5969-5970.

136. Yin, J.; Buchwald, S. L., Pd-catalyzed intermolecular amidation of aryl halides: the discovery that xantphos can be trans-chelating in a palladium complex. *Journal of the American Chemical Society* **2002,** *124* (21), 6043-6048.

137. Obermayer, D.; Glasnov, T. N.; Kappe, C. O., Microwave-assisted and continuous flow multistep synthesis of 4-(pyrazol-1-yl) carboxanilides. *The Journal of Organic Chemistry* **2011,** *76* (16), 6657-6669.

138. Ishikawa, M.; Hashimoto, Y., Improvement in aqueous solubility in small molecule drug discovery programs by disruption of molecular planarity and symmetry. *Journal of Medicinal Chemistry* **2011,** *54* (6), 1539-1554.

139. FAK INHIBITORS. WO2012/110773, **2012**.

140. Zhao, Z.; Wisnoski, D. D.; Wolkenberg, S. E.; Leister, W. H.; Wang, Y.; Lindsley, C. W., General microwave-assisted protocols for the expedient synthesis of quinoxalines and heterocyclic pyrazines. *Tetrahedron Letters* **2004,** *45* (25), 4873-4876.

141. You, L.; Cho, E. J.; Leavitt, J.; Ma, L.-C.; Montelione, G. T.; Anslyn, E. V.; Krug, R. M.; Ellington, A.; Robertus, J. D., Synthesis and evaluation of quinoxaline derivatives as potential influenza NS1A protein inhibitors. *Bioorganic & Medicinal Chemistry Letters* **2011,** *21* (10), 3007-3011.

142. Qiao, X.; Chen, S.; Tan, L.; Zheng, H.; Ding, Y.; Ping, Z., Investigation of formation of superoxide anion radical in DMSO by ESR: Part 1. Influence of Fe2+ and Cu2+. *Magnetic Resonance in Chemistry* **2001,** *39* (4), 207-211.

143. Prasanth, G. K.; Divya, L.; Sadasivan, C., Effects of mono and di (n-butyl) phthalate on superoxide dismutase. *Toxicology* **2009,** *262* (1), 38-42.

144. Ray, S. S.; Nowak, R. J.; Brown, R. H.; Lansbury, P. T., Small-molecule-mediated stabilization of familial amyotrophic lateral sclerosis-linked superoxide dismutase mutants against unfolding and aggregation. *Proceedings of the National Academy of Sciences of the United States of America* **2005,** *102* (10), 3639-3644.

145. Huang, P.; Feng, L.; Oldham, E. A.; Keating, M. J.; Plunkett, W., Superoxide dismutase as a target for the selective killing of cancer cells. *Nature* **2000,** *407* (6802), 390-395.

146. Luo, Z.; Chen, Y.; Chen, S.; Welch, W.; Andresen, B.; Jose, P.; Wilcox, C., Comparison of inhibitors of superoxide generation in vascular smooth muscle cells. *British journal of pharmacology* **2009,** *157* (6), 935-943.

147. Clutterbuck, L. A.; Posada, C. G.; Visintin, C.; Riddall, D. R.; Lancaster, B.; Gane, P. J.; Garthwaite, J.; Selwood, D. L., Oxadiazolylindazole Sodium Channel Modulators are Neuroprotective toward Hippocampal Neurones. *Journal of Medicinal Chemistry* **2009,** *52* (9), 2694-2707.

148. Frostell-Karlsson, Å.; Remaeus, A.; Roos, H.; Andersson, K.; Borg, P.; Hämäläinen, M.; Karlsson, R., Biosensor Analysis of the Interaction between Immobilized Human Serum Albumin and Drug Compounds for Prediction of Human Serum Albumin Binding Levels. *Journal of Medicinal Chemistry* **2000,** *43* (10), 1986-1992.

149. Beckert; Kapplinger; Lindauer; Waisser; Walther, A novel synthesis for 2,3-diamino substituted quinoxalines. *Pharmazie* **1997,** *52* (8), 638 - 639.

150. Romer, D. R., Synthesis of 2,3-dichloroquinoxalines via Vilsmeier reagent chlorination. John Wiley & Sons, Inc.: 2009; pp 317-319.

151. Gilbert, E. E., *Journal of Heterocyclic Chemistry* **1969,** *6*, 483 - 490.

152. Rebek Jr, J.; Renslo, A. R.; Rudkevich, D. M.; Tucci, F. C., Synthesis and assembly of self-complementary cavitands. *Journal of the American Chemical Society* **2000,** *122* (19), 4573 - 4582.

153. Lee, R. E.; Lee, R. E.; Tangallapally, R. P.; Yendapally, R.; Lenaerts, A. J. M., Synthesis and evaluation of cyclic secondary amine substituted phenyl and benzyl nitrofuranyl amides as novel antituberculosis agents. *Journal of Medicinal Chemistry* **2005,** *48* (26), 8261 - 8269.

Appendix I: Publications

Quinteiro *et al. BMC Pharmacology* 2011, **11**(Suppl 1):P54
http://www.biomedcentral.com/1471-2210/11/S1/P54

BMC
Pharmacology

POSTER PRESENTATION Open Access

Design and development of novel non-peptide agonists at NPR-C

Filipa Mota Quinteiro[1*], Paul Gane[1], Anne-Sophie Rebstock[1], Roberta Worthington[1], Michela Simone[1], Snezana Djordevic[2], Adrian Hobbs[3], David Selwood[1]

From 5th International Conference on cGMP: Generators, Effectors and Therapeutic Implications
Halle, Germany. 24-26 June 2011

Background

Endothelium-derived C-type natriuretic peptide (CNP) possesses cytoprotective and anti-atherogenic functions that regulate vascular tone and smooth-muscle relaxation and might be key in protecting against ischaemia-reperfusion injury [1]. The finding that many of the vasoprotective effects of CNP are mediated by the natriuretic peptide receptor type-C (NPR-C) suggests that this receptor might represent a novel therapeutic target for the treatment of cardiovascular diseases. Thus, we have designed and developed small molecule drug-like mimetics of CNP agonists at NPRC.

Methods and results

We employ a multi-disciplinary approach that comprises molecular modelling, chemical synthesis and biological and functional assays. The crystal structure of NPR-C was used as the starting point for the design of peptidic and subsequently non-peptidic ligands to the receptor [2]. We have determined which fragments of CNP are crucial for binding to NPR-C and modified the NPR-C antagonist AP-811 using pharmacophore searches to replace the peptide component, which led to the design of a library of compounds that were subsequently synthesised, tested and optimised [3].

Conclusion

Novel and selective non-peptide NPR-C agonists have been identified that relax rat isolated mesenteric arteries in vitro. We foresee that such molecules will facilitate the development of potential therapeutic agents for cardiovascular diseases.

---

* Correspondence: filipa.quinteiro.10@wibr.ucl.ac.uk
[1]Wolfson Institute for Biomedical Research, University College London, London, WC1E 6BT, UK
Full list of author information is available at the end of the article

Author details

[1]Wolfson Institute for Biomedical Research, University College London, London, WC1E 6BT, UK. [2]Institute for Structural and Molecular Biology, University College London, London WC1E 6BT, UK. [3]Neuroscience, Physiology & Pharmacology, University College London, London, WC1E 6BT, UK.

Published: 1 August 2011

References

1. Ahluwalia A, Hobbs AJ: **Endothelium-derived C-type natriuretic peptide: more than just a hyperpolarizing factor.** *Trends Pharmacol Sci* 2005, **26**:162-167.
2. He XL, Chow DC, Martick MM, Garcia KC: **Allosteric activation of a spring-loaded natriuretic peptide receptor dimer by hormone.** *Science* 2001, **293**:1657-1662.
3. Veale CA, Alford VC, Aharony D, Banville DL, Bialecki RA, Brown FJ, Damewood JR, Dantzman CL, Edwards PD, Jacobs RT, Mauger RC, Murphy MM, Palmer WE, Pine KK, Rumsey WL, Garcia-Davenport LE, Shaw A, Steelman GB, Surian JM, Vacek EP: **The discovery of non-basic atrial natriuretic peptide clearance receptor antagonists.** *Bioorg Med Chem Lett* 2000, **10**:1949-1952, Part 1.

doi:10.1186/1471-2210-11-S1-P54
Cite this article as: Quinteiro *et al.*: Design and development of novel non-peptide agonists at NPR-C. *BMC Pharmacology* 2011 **11**(Suppl 1):P54.

Submit your next manuscript to BioMed Central and take full advantage of:

- **Convenient online submission**
- **Thorough peer review**
- **No space constraints or color figure charges**
- **Immediate publication on acceptance**
- **Inclusion in PubMed, CAS, Scopus and Google Scholar**
- **Research which is freely available for redistribution**

Submit your manuscript at
www.biomedcentral.com/submit

BioMed Central

BioMed Central

© 2011 Quinteiro et al; licensee BioMed Central Ltd. This is an open access article distributed under the terms of the Creative Commons Attribution License (http://creativecommons.org/licenses/by/2.0), which permits unrestricted use, distribution, and reproduction in any medium, provided the original work is properly cited.